Chemical Proteomic Strategies to Probe Novel Kinase and Serine Hydrolase Function in Native Biological Systems

Caroline Elise Franks
Hebron, Maryland

B.S. with Honors in Chemistry, University of North Carolina at Wilmington, 2014

A Dissertation presented to the Graduate Faculty of the University of Virginia in Candidacy for the Degree of Doctor of Philosophy

Department of Chemistry

University of Virginia

May 2019

Abstract

Chemical proteomic profiling is a powerful chemical tool that enables the analysis of protein *activity* in native biological systems. This strategy can be tailored to access diverse enzyme classes to aid in the: (1) identification of novel protein targets; (2) discovery of novel pharmacological compounds; and (3) characterization of enzyme active sites. The work contained in this dissertation exploits current chemical probe technologies to reveal new insights in enzyme function and novel applications for existing small molecule inhibitors.

In Chapters 2 and 3, we utilize ATP acyl phosphate probes to characterize lipid enzyme diacylglycerol kinase (DGK) and reported type 1 DGKα inhibitor ritanserin. We define, for the first time, the unique regions responsible for ATP and ligand binding in all five DGK subtypes and discover multiple protein kinase off-targets of ritanserin. We also use fragment-based inhibitor discovery to profile the unique activities of distinct structural regions of ritanserin.

In Chapters 4 and 5, we utilize chemical proteomic profiling to discover novel clinical applications for existing small molecule inhibitors. We discover a new ritanserin-dependent kinase network that broadly kills lung tumor cell types, and identify c-RAF as a target of ritanserin that may be a key target mediating its anticancer activity. Additionally, we identify a serine hydrolase inhibitor capable of enhancing $CD4^+$ T cell function that could potentially be utilized to enhance current cancer immunotherapy strategies.

Acknowledgements

To my PI and mentor, Dr. Ken Hsu, thank you for always pushing and encouraging me to reach my fullest potential. The past five years of achievement would be not have been possible without your continued support and guidance.

To the many faculty members and staff I have had the pleasure of working with during my time at UVa, thank you for the endless help and advice. To Dr. Thurl Harris, and Dr. Benjamin Purow, thank you for collaborating with us on the DGK project, assisting with experiments, and sharing your expertise. And thank you also to Dr. Harris for always supporting my science endeavors in the form of conversations, letters of recommendation, and so much more. To Dr. Timothy Bullock and the Bullock lab, thank you for taking the time to teach and train me in basic immunology. To my thesis committee, thank you for taking the time to participate in this huge final step of my graduate career. I appreciate your feedback and encouragement. I want to extend my utmost thanks to the Department of Chemistry for believing in and supporting my work, and for providing countless scientific development and outreach opportunities. Thank you to Michael Birckhead, Debbie Scott and Danny Via for taking care of all of our last minute ordering requests for those must-have experiments and always brightening my day with kindness. Thank you to Cecelia Cropley for your assistance in preparing grant applications and making sure they get submitted on time (even though we love pushing deadlines). Thank you to Seth Matula for keeping my finances straight and always taking the time for a great hallway conversation, and to Susie Marshall for answering all of my questions about thesis submission, travel grants, and everything grad school related.

To my lab mates, thank you for the constant help and collaboration, and thank you for always encouraging me to get out lab to have fun (even if I am a flake). Especially to Shin and Emmanuel, thank you for being the best teammates and friends I could have ever hoped for in my graduate career. You are constant sources of support and encouragement, and the greatest listeners for all of my grad school complaints. I truly would not have been able to complete these past five years without you both.

To my family, thank you for the nonstop reminders of how proud of me you are. To my mom and dad, thank you for always encouraging my love of science and teaching me the value of endurance and hard work from an early age. And to the Nottinghams, thank you for generously welcoming me into your home for much-needed weekend getaways and helping to celebrate my every little success.

Finally, to my boyfriend Trueman. Words cannot describe how grateful I am to have had your support and encouragement throughout my time in grad school. You are my happy when I am sad, my strength when I feel as if I cannot continue working another day, and always my greatest source of laughter and fun. Thank you for always sticking by my side and riding out this crazy life with me.

Table of Contents

Abstract ii
Acknowledgements iii
Table of Contents vi
Chapter 1: Introduction 1
1.1 Overview of Diacylglycerol Kinases 1
1.1.1 *A History of the Diacylglycerol Kinase Superfamily* 2
1.1.2 *Common Structural Features of Diacylglycerol Kinases* 3
1.1.3 *The Diacylglycerol Kinase Subtypes* 4
1.1.4 *Physiological Role of Diacylglycerol Kinases* 6
1.1.4.a Immune Function 6
1.1.4.b Cancer 7
1.1.4.c Neurological Disorders 8
1.1.5 *Pharmacological Targeting of Diacylglycerol Kinases* 9
1.1.6 *Repurposing Ritanserin as a DGKα Inhibitor* 13
1.2 Methods to Evaluate Enzyme Function 15
1.2.1 *Kinases* 15
1.2.1.a Kinase Enzyme Assays 16
1.2.1.b Competitive Labeling Assays 17
1.2.1.c Comparison of Kinase Assay Methodologies 19
1.2.2 *Serine Hydrolases* 22
1.2.2.a Activity-Based Protein Profiling (ABPP) 23
1.2.2.b Serine Hydrolase Chemical Probes. 24
1.2.2.c Triazole Ureas as a Privileged Serine Hydrolase Inhibitor Scaffold 25
1.2.3 *Limitations of ABPP Methodologies* 26

Chapter 2: Discovery of the Diacylglycerol Kinase ATP and Ligand Binding Regions 32
2.1 Abstract 32
2.2 Introduction 33
2.3 Materials and Methods 36
2.4 Results 47
2.4.1 *ATP Acyl Phosphate Functions as Activity-Based Probe for DGKa* 47
2.4.2 *Mapping the ATP Binding Site of DGKa Using Quantitative Chemical Proteomics* 49
2.4.3 *Chemical Proteomic Profiling of the DGK Superfamily Using an ATP Acyl Phosphate Probe* 51
2.4.4 *Inhibitor Profiling to Determine Ritanserin Binding Mode and Selectivity* 54

2.4.5 *Discovery of a Lead Fragment Inhibitor of DGKα by Ritanserin Deconstruction* 56
2.5 Discussion 59
2.6 Acknowledgements 81

Chapter 3: Identification of the Structural Region of Ritanserin Mediating Off-Target Activity 82
3.1 Abstract 82
3.2 Introduction 83
3.3 Materials and Methods 86
3.4 Results 91
3.4.1 *Fragment Based Deconstruction of Ritanserin Yields RLM001* . . . 91
3.4.2 *Chemical Proteomics Reveals RLM001 Site of Binding* 91
3.4.3 *RLM001 Functions as a General Ligand for ATP-Binding Pockets* 95
3.5 Discussion 97
3.6 Acknowledgements 113

Chapter 4: Chemoproteomic Discovery of a Ritanserin-Targeted Kinase Network Mediating Apoptotic Cell Death of Lung Tumor Cells 114
4.1 Abstract 114
4.2 Introduction 115
4.3 Materials and Methods 117
4.4 Results 121
4.4.1 *Ritanserin Shows Serotonin-Independent Cytotoxic Activity in Lung Tumor Cells* 121
4.4.2 *Ritanserin Activates Apoptotic Cell Death of Broad Lung Tumor Cell Types* 122
4.4.3 *Chemoproteomic Kinome Profiling of Ritanserin Action in Lung Tumor Cell Proteomes* 123
4.4.4 *Chemoproteomic Profiling Reveals c-RAF as a Principal Target of Ritanserin in SCLC Proteomes* 125
4.4.5 *Ritanserin Block c-RAF But Not B-RAF Activation of MEK Signaling in Live Cells* 127
4.5 Discussion 129
4.6 Acknowledgements 165

Chapter 5: Identification of a Key Serine Hydrolase Enzyme Mediating the Induction of T cell Anergy 166
5.1 Abstract 166
5.2 Introduction 167
5.3 Materials and Methods 169
5.4 Results 173
5.4.1 *APEH Inhibition Enhances IL-2 Production in $CD4^+$ T cells* 173

5.4.2 *Inhibition of APEH by AA741 Enhances Cytokine Production and Diminishes NDRG1 Expression in Anergic T cells* 174
5.4.3 *Chemical Proteomic Profiling of AA741* 177
5.5 Discussion 178
5.6 Acknowledgements 187

Chapter 6: Conclusions and Future Directions 188
6.1 Conclusions and Significance 188
6.2 Future Directions 191

Chapter 7: Publications Resulting From This Work 193

Chapter 1: Introduction

1.1 Overview of Diacylglycerol Kinases

Diacylglycerol kinases (DGKs) are lipid kinases with diverse roles in cellular signaling. This enzyme family catalyzes the phosphorylation of diacylglycerol (DAG) to generate phosphatidic acid (PA) (1-3) (Figure 1.1). This reaction leads to attenuation of DAG lipids (2), which regulate intracellular proteins including protein kinase C (PKC), chimerins, Unc-1, and Ras guanyl nucleotide-releasing protein (RasGRP) by serving as a chemical signal to activate or recruit proteins to the membrane (1, 3, 4). The production of PA also activates key signaling proteins such as mammalian target of rapamycin (mTOR) and isoforms of PKC, and serves as a vital lipid intermediate (1, 3, 4). Thus, DGKs serve as important metabolic hubs to coordinate several bioactive lipid-signaling pathways by regulating the balance between lipid messengers DAG and PA. However, the molecular principles guiding specificity of DGK substrate and ligand binding remains ill defined. Chapters 2 and 3 of this dissertation will present the work we have completed to try to further elucidate the substrate and ligand binding regions of DGK active sites, which I will describe further in Chapter 1.1.1-1.1.6.

1.1.1 *A History of the Diacylglycerol Kinase Superfamily*

Earliest identification of DGKs from the late 1950's report diglyceride phosphokinase in deoxycholate extracts of brain microsomes responsible for the generation of PA upon addition of various DAG lipid substrate species (Scheme 1) (5).

$$ATP + diglyceride \xrightarrow{diglyceride\ phosphokinase} phosphatidic\ acid + ADP \quad (1)$$

Now recognized as DGKs, the enzymes were early characterized as exhibiting substrate-dependent enzyme activity, generating differential amounts of PA depending on the DAG substrate composition (5-7). Efforts to purify the DGK enzyme from E. coli to further characterize its functionality quickly followed and were quite successful (8-11). Analyses of bacterial DGK revealed that it absolutely requires Mg^{+2} for catalytic activity and broadly catalyzes the phosphorylation of many lipid types, yet still displays substrate preference that is dependent on lipid fluidity and polarity (10, 12). Similar findings were obtained from analyses of a purified porcine ~80kDA DGK enzyme (found to be structurally distinct from bacterial DGKs) which has since been annotated as DGKα (13, 14).

In the late 1980's porcine studies of DGK enzymes progressed into analyses of distinct cell types where it was discovered that pig tissues contain at least three distinct DGK isozymes with different functions under different control mechanisms (15, 16). Over the next 15 years identification and characterization of these isozymes ensued, and it is now widely established that there are 10 unique mammalian DGK isoforms (α, β, γ,

δ, ε, ζ, η, θ, ι, and κ) each with distinct tissue localization, cellular expression and function (3).

1.1.2 *Common Structural Features of Diacylglycerol Kinases*

Most organisms that have been studied actually contain DGKs, and they become more specialized as the species become more complex (4). For example, bacteria contain a single DGK isoform, which does not possess the structural elements that are needed for regulation of activity (4). Yeast also contains a single DGK isoform, DGK1, and unlike DGKs from bacteria and animals, it consumes cytidine triphosphate (CTP) as opposed to ATP (17). There are 10 identified mammalian DGK isoforms, which can be subdivided based upon structural features deduce from primary protein sequences into five subtypes (I, II, III, IV, and V) (Figure 1.2). Despite differences in regulatory domains, all DGKs contain at least two cysteine-rich C1 domains (C1A and C1B) and a catalytic domain.

The cysteine-rich C1 domain is a feature of all DAG-binding proteins possessing zinc- and hydrophobic lipid-binding regions (18, 19). They can be classified as either typical (bind and respond to DAG/phorbol ester) or atypical (do not bind and respond to DAG/phorbol ester) (19). The homology between DGK C1 domains and the phorbol ester/DAG binding C1 domains of protein kinase C leads to the assumption that they are responsible for DAG binding and/or localizing enzymes to accumulations of DAG pools (4, 18, 20). However, sequence analysis indicates that the DGK C1 (C1A and C1B) domains lack key residues (with the exception of DGKβ and DGKγ) to be classified as canonical C1 binding domains (20). Therefore DGK C1 domains are classified as

atypical (DGKs happen to be the largest family of enzymes with two atypical C1 domains), with much debate surrounding the actual role of DGK C1 domains. DGKs also contain an extended region of 15 amino acids in the C1B domain not present in C1 domains of other proteins (4). Some reports indicate that mutations of this region significantly reduce kinase activity, while others found that the C1 domains are not necessary for DAG phosphorylation activity (4, 18).

The DGK catalytic domain, which presumably houses the ATP-binding pocket, can be divided into two distinct regions: the catalytic and accessory subunits. These regions are typically linked as one large unit, however for the type II DGKs (ζ, η, and κ) the regions are disjointed by a long peptide that lacks any known function (4, 21). The catalytic subunit contains a conserved GGDG*XX*GG sequence motif essential for kinase catalytic activity in all 10 mammalian DGK isoforms (20). The catalytic function of this subunit has been validated by glycine to aspartate or alanine mutation studies wherein the DGK kinase activity was rendered catalytically inactive (4, 22-24). Studies also suggest that the catalytic subunit may require other motifs for maximal kinase activity. When expressed as isolated subunits, the catalytic subunits of DGKs δ, ε, and θ express little DGK activity and DGKα retains about 1/3 of its activity (4).

1.1.3 *The Diacylglycerol Kinase Subtypes*

In addition to the common C1 and catalytic structural motifs, each DGK subtype contains distinct regulatory motifs. Currently, our knowledge of these features is limited to the primary sequences of the enzymes, as the three-dimensional structures of

mammalian DGKs remain elusive. Type I DGKs (α, β, and γ) possess an N-terminal recoverin homology domain (RVH; related to the N termini of the recoverin family of neuronal calcium sensors) and EF-hands motifs (responsible for calcium binding) that increase enzyme activity in the presence of calcium (3, 25). Mutational studies of DGKα show that when the calcium is bound to the EF-hands, a conformational change then induces membrane association and activation (4). Deletion of the RVH domain in DGKα results in loss of calcium-dependent activation, and further deletion of the EF-hands motifs results in a constitutively active enzyme (25). This suggests that these sequences are required for enzyme autoinhibition (25).

Type II DGKs δ, η, and κ contain an N-terminal pleckstrin homology (PH) domain. These domains are best known for their capability to bind phosphoinositides but <10% of all PH domains share this ability; it is more likely that they represent conservation of structural fold rather than function (26). DGKδ and η also contain a C-terminal sterile alpha motif (SAM) that is predicted to impact localization and induce oligomerization (3). The SAM domains of DGKδ bind zinc at multiple sites, and mutational studies containing a SAM domain refractory to zinc binding displays impaired localization to the cytoplasm and enhanced localization to the plasma membrane (4).

Type III DGKε is the only DGK isoform contains an identifiable hydrophobic domain, predicted to form a transmembrane helix, in addition to the C1 and catalytic domains (27). Interestingly, it is the only DGK isoform that displays specificity for acyl chains of DAG, preferring 2-arachidonoyl-DAG which is the major species of DAG released from phosphatidylinositols (PIs) by phospholipase C (3, 4).

Type IV DGKs ζ and ι contain a myristolated alanine-rich C kinase substrate (MARCKS) domain that is enriched in lysine and arginine residues (4). This acts as a nuclear localization signal and acts as a substrate for protein kinase C; phosphorylation of this domain limits nuclear localization of the enzymes (4). These enzymes also contain C-terminal Ankyrin repeats, one of the most common protein motifs that functions as a mediator of protein-protein interactions (28).

Type V DGKθ is characterized by an N-terminal proline-rich region, three C1 domains (instead of two) and a PH domain (3, 4, 29). While the precise function of the proline-rich region remains undefined, studies have shown that the C1 domains of DGKθ do not bind phorbol esters but may bind other lipids or participate in protein-protein interactions (29).

1.1.4 *Physiological Role of Diacylglycerol Kinases*

Diacylglycerol kinases have been well characterized in a variety of physiological contexts. They regulate immune function, cell proliferation, brain and cardiac function, contribute to glucose homeostasis and vision, and much more (4).

1.1.4.a Immune Function

DGKα and ζ are highly expressed in immune cells and organs (thymus and peripheral T cells and the spleen). This abundance is especially relevant given the requirement for DAG in the onset of proper T cell activation. Upon recognition of antigen and co-stimulatory signals (CD28/IL2R) by the T cell receptor (TCR) the TCR

activates tyrosine kinases leading to PLCγ1 activation, which then generates DAG to recruit and activate RasGRP1 (30). Ras GRP1 is required for T cell development and imperative for selection of thymocytes that express weakly selecting TCRs (31). DGKα and ζ function as negative regulators of DAG TCR signaling by phosphorylation of DAG to form PA (32).

T cell anergy is a form of tolerance that aids in prevention of autoimmunity. Induction of anergy occurs when a T cell recognizes self-antigen in the absence of co-stimulatory signals, which renders the T cell functionally inactive (31). Previous studies have shown that anergic T cells express increased levels of DGKα, and increased or no change in DGKζ (31). Overexpression of DGKα during T cell anergy up-regulates the hyporesponsive state, and pharmacological inhibition of DGKα in DGKζ deficient T cells restores cytokine production and activation, and promotes resistance to T cell anergy (4, 33). T cells lacking DGKα or ζ display increased diacylglycerol-dependent T cell receptor signaling when stimulated in anergy-inducing conditions, and proliferate and produce interleukin 2 (34). In DGKα knockout mice, T cells exhibit impaired induction of anergy (34). These results suggest that a DGK-α and/or -ζ inhibitor could be a promising clinical candidate to target immune dysfunction.

1.1.4.b Cancer

Normally, DGKα is expressed only in the brain, kidney, and T cells (35). However, expression of DGKα is upregulated in tumors cells such as melanomas, hepatocarcinomas, and glioblastomas (30). Knockdown and inhibition of DGKα in

human glioblastoma cell lines led to induction of apoptosis, while overexpression of DGKα increased cell number *in vitro* (36). The enzyme mediates cancer cell progression mechanisms including tumor cell survival, migration, and invasion (30, 37). These studies suggest that DGKα may provide a survival advantage and contribute to drug resistance (30), however further studies are required to determine the precise roles of DGKs in cancer.

1.1.4.c Neurological Disorders

Bipolar disorder is a heritable neuropsychiatric disorder that impacts approximately 4% of the United States population, and poses a signification mortality risk (approximately 25% of patients attempt suicide and 11% complete) (38, 39). It is characterized by extreme swings from depressive to manic behavior. DGKβ expression is not limited to brain tissue, however it is expressed specifically in areas that are vital for cognitive and emotional processes in the central nervous system (4). DGKβ-KO mice display a phenotype representative of bipolar disorder, with hyperactivity, lowered anxiety, and reduced depression that is attenuated by the common bipolar treatment, lithium (1, 4). Genome wide association studies have also identified DGKη as a novel genetic candidate as a target for treatment, with strong association between bipolar disorder and three SNPs (rs9315885, rs1012053, and rs1170191) (1, 39). Generation of DGKη-KO mice has only been accomplished recently. Their phenotype exhibits increased behavioral switching activity, lower anxiety, and lower depressive states and,

quite interestingly, were also sensitive to the common bipolar disorder treatment, lithium (39).

Parkinson's is the second most common chronic neurodegenerative disease, and thus has been studied extensively. Five gene mutations (PARK2, PARK7, PINK1, SNCA, LRRK2) have been identified to influence risk of Parkinson's and accepted as clinical markers. However, two additional SNPs (rs1564282 and rs 11248060) in the *GAK* (cyclin G associated kinase)/DGKθ region (DGKθ is expressed highly in the brain) have been also reported to be associated with Parkinson's, which suggests it may be utilized as a new susceptibility allele (39).

Other studies have associated DGKε with seizure, as its signaling is required for the regulation of epilepsy-induced genes, expression of DGKδ and ε with protection against cardiac dysfunction, and low DGKδ expression with glucose intolerance and obesity. It is clear that DGKs pose a significant role in mammalian biology and are a promising potential therapeutic drug target.

1.1.5 *Pharmacological Targeting of Diacylglycerol Kinases*

Despite overwhelming clinical precedence for targeting the DGK superfamily, development of DGK inhibitors has been limited by compounds with low potency, lack of selectivity, and poor pharmacokinetics, which prevent their utilization in the clinic. Contributing to this slow development is the fact that no crystal structure information exists for any of the ten mammalian DGK isoforms. The few identified DGK inhibitors

can be divided into three groups: 1) allosteric inhibitors, 2) DAG analogues and 3) ATP competitive inhibitors (Figure 1.3) (40).

The first reported inhibitor targeting DGK enzymes came approximately 15 years after the discovery of DGKs; novel compound R59-022 (or 6-[2-[4-[(4-fluorophenyl) phenylmethylene)-1-piperidinyl]ethyl]-7-methyl-5H-thiazolo[3,2-alpha] pyrimidin-5-one) was discovered to inhibit diacylglycerol kinase in human red blood cell membranes with a reported IC50 of 3.8 μM (41). R59-949 (or 3-[2-[4-[bis(4-fluorophenyl)methylene]-1-piperidinyl]ethyl]-2,3- dihydro-2-thioxo-4(1H)-quinazolinone) was reported shortly thereafter to inhibit diacylglycerol kinase in isolated platelet membranes with an IC50 (concentration where 50% blockade of activity is observed) of 0.3 μM (42). In addition to their role as DGK inhibitors, R59-022 and R59-949 also function as serotonin receptor antagonists (43). Interestingly, both demonstrate selectivity for type 1 DGKs among the five mammalian DGK isotypes, although reports have been conflicting (43). As such, they have been vital pharmacological tools to understand the biological function of type 1 DGKs and other DGK isozymes (29, 44, 45). The mechanism of action by which inhibitors bind and inactivate enzymes is fundamental to understanding enzyme function and can aid in the development of optimized inhibitors. Studies concluded that R59-949 binds to the catalytic domain of DGKα in cooperation with Mg-ATP without disrupting DAG binding, and in theory does so by binding in proximity to the catalytic site or by inducing a conformational change that exposes the catalytic and R59-949 binding sites; kinetic studies of R59949 suggest noncompetitive inhibition that supports this hypothesis of allosteric inhibition (44). Most

recently, AMB639572 was identified as a DGKα inhibitor from *in silico* studies using R59-022 and R59-949 as template scaffolds (40). Although the IC50 of AMB63972 is comparable (IC50 = 4.3 ± 0.6 μM) to either R59 compound, it inhibits DGKα without affecting serotonin signaling; thus it may be a promising scaffold for lead optimization efforts (40). In cell-based assays AMB639572 is highly active with negligible cytotoxicity and restored the induction of key pro-apoptotic molecules NUR77 and NOR1 in SAP-deficient cells, indicating a potential therapeutic application for the treatment of X-linked lymphoproliferative disease 1 (XLP-1; a rare genetic disorder with deregeulated DGKα activity) (40).

Fungal metabolites calphostin C and stemphone have also been reported as *in vitro* allosteric DGK inhibitors (40). Calphostin C, an anti-tumor agent that binds to the regulatory domain of protein kinase C (PKC), inhibits DGK activity with an IC50 of 40 μM and binds competitively with respect to DAG (46). These findings indicate similarities between the DAG binding sites of DGK and PKC, and direct comparison of the structures of calphostin C, phorbol dibutyrate (PKC substrate) and DAG revealed similar free hydroxyl moieties between the three compounds that may aid in the development of DGK/PKC specific inhibitors (46). Stemphone (cochlioquinone A), isolated from *Drechslera sacchari*, inhibits DGKs in competition with ATP and non-competitively with DAG with an IC50 of 3.1 μM (47). In studies of vascular reactivity stemphone has been shown to suppress U46619 (thromboxane A_2 analog) -induced endothelial cell layer permeability through DGK inhibition, suggesting that it may be used to improve vascular endothelial dysfunction in diabetic hyperglycemia or

inflammatory conditions (48). It has been hypothesized that stemphone inhibits Ca^{2+}-independent DGK isoforms selectively however, stemphone-mediated DGK inhibition remains to be characterized (49). Neither compound has translated to the clinic.

The utilization of DAG analogues as *in vitro* DGK inhibitors has been attempted with the goal of determining the substrate specificity of DGK enzymes. These compounds possess the lowest potency among the groups of DGK inhibitors (40). Dioctanoylethylene glycol (K_i = 58 μM) inhibits diacylglycerol phosphorylation in platelets (70-100% at 100 μM), leading to increased DAG signaling (50). Treatment with 1-monooleoylglycerol (K_i = 91 μM) leads to elevated diacylglycerol levels in unstimulated and thrombin-stimulated platelets, up to 4-fold and 10-fold increases, respectively (50). Inhibition with both DAG analogues was equivalent between 0.1 - 0.5 mM phosphatidyl serine (PS) suggesting that the analogues were interacting directly with the kinase.

The distinguishing feature of all kinase enzymes (protein and lipid) is an ATP binding domain that catalyzes enzyme activity. Design and development of drugs to target and inactivate this site is theoretically the most efficient and prosperous method, and has proven to be quite successful in regards to protein kinase drugs. In fact, out of the 48 small molecule protein kinase inhibitors approved by the US FDA, 45 interact directly with the protein kinase domain (51). However, there are a number of problems with targeting this ubiquitous domain. To highlight the most obvious issue, promiscuity with other kinases possessing the same ATP binding domain structure can lead to poor drug selectivity. In regards to DGKs, the ATP binding domain has a different structure

compared to serine/threonine and tyrosine kinases and lipid kinases such as PI3Ks (40). This is exemplified by the pan-kinase inhibitor staurosporine, which has no impact on the activity of DGKs (40). Recently, a DGKα selective inhibitor CU-3 was identified from a high-throughput screen with an IC50 of 0.6 μM in Cos-7 cells expressing recombinant DGKα (52). A distinguishing feature of CU-3 is its ability to reduce the affinity of DGKα for ATP while having no impact on DAG or PS (40, 52). CU-3 induces apoptosis in HepG2 hepatocellular carcinoma and HeLa cervical cancer cells, while also enhancing IL-2 production in Jurkat T cells (52). These results suggest that CU-3 is an ideal anti-cancer drug candidate, as it attenuates cancer cell proliferation while simultaneously boosting immune response (52).

1.1.6 *Repurposing Ritanserin as a DGKα Inhibitor*

Based on structural similarities to R59022, serotonin receptor antagonist ritanserin was recently identified as a potential DGKα inhibitor (Figure 1.4) (37, 43). This compound was previously tested in human trials for schizophrenia, alcoholism, and insomnia, and displayed no clinically relevant negative effects, which could result in rapid drug repurposing to target DGKα-associated conditions (37, 53). Ritanserin was found to potently inhibit DGKα activity (IC50 = 15 μM), and, similarly to R59-022 and R59-949, prefers binding to an ATP-enzyme complex with no impact on DAG binding affinity (43). Selectivity studies indicate that ritanserin attenuates DGKα activity with no impact on other DGK isoforms, and treatment of HeLa and U87, but not U251 (cell line has a low relative mRNA expression of DGKα), glioblastoma cells resulted in a significant

increase in PKC substrates as compared to untreated cells; this data supports that ritanserin functions as a DGKα inhibitor (43). Treatment with single-agent ritanserin in intracranial glioblastoma and melanoma xenograft models resulted in increased mouse survival (up to 30%; $P < 0.05$), but low potency and promiscuity of ritanserin suggest that these findings may not translate to the clinic as straightforwardly as hoped (37).

1.2 Methods to Evaluate Enzyme Function

Enzymes act as catalysts to increase the rate of specific chemical reactions in cells and are important targets in developing drug candidates. Pharmacological inhibition of enzymes can modulate key metabolic and signaling functions in a biological system (54). The overarching theme of this dissertation is the utilization of chemoproteomic methodology to assess drug potency, selectivity, and mode of inhibition to target enzymes in broad biological contexts, which will be described further in Chapter 1.2.1-1.2.2. My work highlights the extensive capabilities of chemoproteomic profiling, especially in regards to its use as a drug candidate-screening platform.

1.2.1 *Kinases*

Human kinases have stood at the forefront of drug discovery efforts over the past 30 years; approximately 1/3 of all protein targets under investigation in the pharmaceutical industry are protein or lipid kinases (55). This family of 500+ protein enzymes catalyzes the transfer of a phosphate group (generally from adenosine triphosphate; ATP) to a specific substrate, a process known as phosphorylation. Phosphorylation is one of the most important posttranslational modifications and functions as a universal mechanism for cellular control and adaptation by impacting activity, localization, and reactivity of protein, lipid, and carbohydrate molecules (56, 57). Processes regulated by phosphorylation include metabolism, DNA transcription and replication, cellular transport, neurotransmitter biosynthesis, cell differentiation, and much more (55, 57);

therefore, kinases represent one of the most important target classes for treating human disease.

Although many studies have been performed to establish the regulation and function of protein kinases, resulting in over 40 FDA approved drugs targeting this enzyme class, much less is known regarding lipid kinases (51). As previously mentioned in Chapter 1.1, of particular interest to us when developing this project was the investigation of a class of lipid kinases known as DGKs. In order to further understand the functional role of this enzyme and profile potential pharmacological inhibitors, we adapted modern techniques for profiling protein kinases to investigate lipid kinases like DGKs. In Chapters 1.2.1.a - 1.2.1.c, I will describe historical and modern techniques used to assess kinase function that are of importance to this dissertation, and compare the benefits and detriments of each.

1.2.1.a Kinase Enzyme Assays

The most commonly used and widely available readouts of kinase enzymatic activity are kinase enzyme assays that detect the conversion of substrate by detecting the formation of phospho-product, disappearance of ATP, or formation of ADP (58). These assays require: 1) co-factors ATP and magnesium, 2) the kinase protein and 3) the substrate (58).

Radioactivity-based kinase assays are one of the first technologies reported as readouts of DGK enzyme activity (5). These traditional assays measure the transfer of the γ position ^{32}P from ATP to substrate, resulting in a ^{32}P-labeled phospho-product that can be captured, eluted, and radioactivity analyzed by scintillation counting (58, 59). Due to

modern safety and handling requirements regarding radioactive reagents and the development of safer, cheaper alternatives, the use of radioactive kinase assays is now much less frequent, but they are still considered the 'gold standard' by many (58).

Fluorescence-based kinase assays can be implemented in several readouts: fluorescence polarization (FP), time-resolved fluorescence energy transfer (or TR-FRET), immunosorbant assays, and others (58). The general principle behind all fluorescence-based kinase assays is the use of a fluorescent phosphopeptide antibody to detect phosphorylated products. Formation of phospho-product is then measured by a change in rotational velocity (by FP) (60, 61), change in emission energy of the fluorophore (TR-FRET) (62), or increase in total measured fluorescence (immunosorbant assay) (63).

Luciferase-based kinase assays (Promega ADP-Glo or Perkin-Elmer Easylite Kinase) take advantage of the high-energy bonds of ATP being converted to ADP (58, 64). These assays monitor depletion of ATP over time via phosphorescence of luciferase and luciferin. Luciferases use the high-energy bonds of ATP to convert luciferin to oxyluciferin, which then produces light (58, 64). Phosphorescence readout is then quantitated and directly proportional to kinase activity.

1.2.1.b Competitive Labeling Assays

Competitive labeling assays have been developed more recently and rely on chemical probes that react with active kinases. The probes contain moieties that covalently modify active kinases in cells or cell lysates for downstream enrichment/analysis, or catalyze energy transfer in live cells resulting in a fluorescent readout (65).

One of the first reported chemical probe-based methods for the detection of active kinases was the KiNativ platform by Patricelli et al. in 2007. This platform utilizes biotinylated ATP or ADP derivatives to covalently label a conserved lysine residue in proximity to the catalytic domain of active kinases via an electrophilic acyl phosphate group (66, 67). The labeled kinases are then enriched using streptavidin affinity chromatography, eluted, and analyzed by liquid chromatography-tandem MS (66, 67). When coupled with stable isotope labeling by amino acids in culture (SILAC), this platform provides a quantitative readout of native kinase activity present in cell proteomes (66, 67). Inhibitor potency and selectivity can be assessed by direct competition between the probes and inhibitors (66, 67).

Kinobeads were reported shortly thereafter and rely on on-bead immobilized mixed kinase-inhibitor matrices that enrich for kinases non-selectively from cell lysates (68). Bound proteins are then quantified by mass spectrometry to determine the protein-affinity profiles of kinase inhibitors in various cell and tissue types, as well as the differential drug-induced changes of phosphorylation events on the captured proteome (68, 69).

Recently, a covalent chemical probe that can label kinases in live cells has been reported that relies on an exclusive reaction between sulfonyl fluoride and a conserved lysine in the ATP binding site, named XO 44 (70). This probe is covalent, cell-permeant and contains a latent alkyne for coupling azido-reporter tags by click chemistry (71) for pull-down and subsequent MS-based analysis; XO44 was reported to covalently label up

to 133 endogenous kinases in live cells, even competing with high intracellular concentrations of ATP (70).

Another live cell method to measure kinase binding or enzymatic inhibition is the use of a bioluminescence resonance energy transfer technique called NanoBRET (72). In live cells, the target protein of interest is first expressed with a NanoLuc reporter tag, and then a cell-permeable fluorescent energy transfer probe is introduced into the culture medium (72). If the probe is able to bind to the target protein, fluorescence is produced that can be quantified by a luminometer (65). Compound binding results in displacement of the probe and a loss of energy transfer, and therefore fluorescence, in live cells (72). In order to access the broad kinome, probes were designed based on a diverse set of ATP-competitive kinase inhibitors (72).

1.2.1.c Comparison of Kinase Assay Methodologies

There are a number of benefits and detriments to using kinase enzyme assays or competitive labeling assays to profile potential kinase drug candidates. Care should be taken to determine which is most suitable for the experiment that you are designing. Some considerations for each method are described below.

Kinase enzyme assays have a few distinct advantages over any of the competitive labeling assays: they are cost effective, high throughput, and time efficient. There are three main 'ingredients' to these assays that are as representative as possible of native biological systems. This means that you can tailor concentrations and identities of co-factors and substrates to create a unique environment most susceptible to the activity of

your kinase of interest. However, each of these benefits may also be seen as a detriment. Recombinant proteins, buffer conditions, and precise concentrations do not always best reflect physiological conditions and may result in disconnect between compound activity in these assays versus live animal models, or even *in situ* live cell analyses. If the assay requires purified protein, then additional choices like substrate identity may impact the activity of the kinase and effects of drug treatment. The major disadvantage of kinase enzyme assays is that they lack the ability to profile selectivity of an inhibitor; results will simply indicate whether or not the drug interacts with the target kinase.

Readouts of kinase enzyme assays have unique advantages and disadvantages. Scintillation proximity assays rely on photon emission as the readout of radioactivity, and thus kinase activity. Using a radioactivity-based assay, there is no dependence on phospho-specific antibodies and little interference by light-absorbing compounds as the analyte detection is only performed at one emission, which makes the assay quite versatile (58). However, these assays require radioactive waste disposal, which may or may not be available depending on lab facilities (58).

Fluorescence-based assays, like FP, TR-FRET, and immunosorbant assays, have the distinct disadvantage of being susceptible to interference. Pre-treatment with drugs or protease inhibitors may shift fluorescent readout and negatively impact results. FP methods are versatile and do not require antibodies, however substrates are required to be quite small as to not interfere with rotational velocity (58). Immunosorbant assays may be used as a sensitive probe for cell lysates, however these have much lower throughput with multiple washing steps (58).

Kinase enzyme assays with luciferase-based readouts have the advantage of being versatile and non-radioactive. These assays may be tailored to evaluate purified protein or cell lysates. The assay readout relies on decrease of signal, the depletion of ATP, and is a secondary readout of activity. The assay is also susceptible to interferences with luciferase inhibitors (58).

All of the described competitive labeling assays have a few huge advantages that may outweigh the high throughput efficiency of kinase enzyme assays. They access the broad kinome and allow for analysis selectivity of a drug or compound, and they are all performed within a native biological context. The Kinativ platform is commercially available and can be performed on a variety of sample types: cell lysates or tissue lysates from in vivo studies (66, 67). Kinativ probes access any ATP-utilizing enzyme, which includes kinases and ATPases, broadening the selectivity profile for inhibitor analyses. However, the promiscuity of these probes could lead to interference with kinase detection due to highly abundant ATP binding proteins such as actin and heat shock proteins (66, 67). This assay is more expensive compared to most kinase enzyme assays and results may differ depending on kinase affinity for the ATP probe (65).

Kinobeads can also be utilized for a variety of sample types, including cell or tissue lysates and efficiently captures native kinases distributed across the kinome (68, 69). Selection of the most suitable probe and cell line combination is required to optimize studies of drug interactions with a particular kinome (69). A 96-well format of this assay has been designed to implement large scale, high throughput analyses, however each

sample still requires liquid chromatography-mass spectrometry (LC-MS) as the readout, which may limit throughput efficiency (69).

Probe XO44 is commercially available and optimized for in cell analyses; it may complement initial *in vitro* studies. This may be advantageous depending on the stage of the project; the probe can assess cellular target engagement and may paint a better picture of how an inhibitor works in live systems (70).

The NanoBRET assay is also designed live cell analyses, which permits analysis of kinase binding in a physiologically relevant environment. All of the reagents are commercially available and the probes have been validated for up to 178 kinases across the kinome (72). One severe limitation of this system is the requirement for tagging of proteins with NanoLuc. This may impact kinase activity and effect probe and/or inhibitor binding. The probes are ATP-site probes; therefore results can also be impacted by the affinity of different kinases for the probe (65). The readout is conducted in live cells using a luminometer. This may increase the efficiency of experiments, however interference of synthetic molecules on the energy relationships with transient protein interactions may negatively impact results (72).

In this dissertation, we chose to deploy the Kinativ platform to globally evaluate the potency and selectivity of inhibitor compounds against lipid and protein kinases in a variety of biological contexts. This will be further discussed in Chapters 2, 3, and 4.

1.2.2 *Serine Hydrolases*

The serine hydrolase superfamily is a diverse class of over 200 human enzymes, which includes lipases, esterases, thioesterases, amidases, peptidases, and proteases (73). These

enzymes are characterized by an active site serine nucleophile that is required for the hydrolysis of substrates (73). Serine hydrolases represent ~1% of the human proteome and are involved in numerous physiological processes: blood clotting, digestion, metabolism, neurotransmission, inflammation, cancer, bacterial infection and more (73, 74). As such, several drugs have been developed and approved targeting serine hydrolase enzymes including: orlistat for obesity targeting pancreatic/gastric lipases, dabigatran etexilate and argatroban for thrombosis targeting thrombin, rivaroxaban for thrombosis targeting factor Xa, and sivelestat for respiratory disease targeting human neutrophil elastase (74). Despite major (and many successful) efforts by researchers to characterize and drug this enzyme family, the majority of serine hydrolases remain poorly characterized and lack selective *in vivo*-active inhibitors (74).

In the Hsu lab, graduate students have access to the most up-to-date technology in regards to analyzing the enzymatic activity of the serine hydrolase superfamily: activity-based protein profiling. In Chapter 5 of this dissertation I employed fluorophosphonate (FP) activity-based probes FP-rhodamine and FP-biotin, which I will describe further in Chapter 1.2.2.a, to probe the involvement of a serine hydrolase enzyme in T cell function in order to assess the clinical relevance of an existing serine hydrolase drug candidate for potential cancer immunotherapy applications.

1.2.2.a Activity-Based Protein Profiling

Activity-based protein profiling (or ABPP) relies on the development of covalent chemical probes that access and modify enzyme active sites to provide a quantitative

readout of enzyme activity in relevant biological contexts (75). Chemical (or activity-based) probes can be designed and optimized to access broad (entire families) or specific (individual isoforms) enzyme classes and contain two general features: a reactive warhead and a reporter tag (75). The reactive warhead interacts with specific active site residues, at which point it then covalently modifies the target enzyme with the reporter tag (i.e. fluorophores, biotin, or azides) (75, 76). The covalent modification can then be resolved by gel electrophoresis followed by in-gel imaging, or by LC-MS (75). The former is suitable as a high throughput-screening platform to identify hit candidates/scaffolds for drug design, while the latter may be more suitable for detailed analyses of potency and selectivity of specific compounds of interest.

1.2.2.b Serine Hydrolase Chemical Probes

The shared feature of the serine hydrolase (SH) family is a catalytic triad of amino acid residues (typically serine, histidine, and aspartate or glutamate) that activates a serine nucleophile for hydrolysis of ester, thioester, and amide bonds (77). The serine nucleophile is activated and attacks the substrate the form an acyl-enzyme intermediate, followed by hydrolysis of the intermediate to liberate the final product (75, 77). The nucleophilicity of the catalytic serine residue renders it highly susceptible to covalent modification, which is exploited by activity-based probes (75).

Reporter-tagged fluorophosphonates (FPs) represent the most broadly reactive identified warhead that selectively targets SHs (75). Over 80 unique SHs have been identified as targets of FP probes in human and murine proteomes (75). Previous studies

have validated their use as SH activity-based probes, as they react with active enzymes but not inactive precursor or inhibitor- bound enzyme forms (75). This has enabled the analysis of SH enzyme activity, and the identification of potential SH inhibitors, in the context of numerous biological systems, including cancer, immune function, and nervous system signaling (75). In this dissertation, we use rhodamine-tagged FP to evaluate the potency of a SH inhibitor in T cell proteomes, and to broadly assess the changes in SH profiles of different T cell activation states. This will be further discussed in Chapter 5.

1.2.2.c Triazole Ureas as a Privileged Serine Hydrolase Inhibitor Scaffold

Previous reports suggest N-heterocyclic urea (NHU) scaffolds as optimal for the design of selective SH inhibitors (78-80). In particular, monocyclic 1,2,3-triazole ureas are uniquely structured to react with serine hydrolases due to their electrophilicity, which is sufficient for serine hydrolase reactivity, but not so much as to cross-react with other enzymes (78). It is a highly versatile scaffold, amenable cheaply and easily through simple click chemistry, and has the distinct advantage of inactivating SHs by a covalent, irreversible mechanism, which leads to long-term enzyme inactivation, an attractive feature for clinical applications (78). In Chapter 5, we implemented a screening assay using a 1,2,3-triazole urea compound library based on numerous previous studies identifying this scaffold as selective for serine hydrolase enzymes inactivation (78, 81, 82).

1.2.3 *Limitations of ABPP Methodologies*

Activity-based protein profiling (ABPP) is a powerful tool that is capable of generating data regarding potency of a drug against an enzyme target, selectivity of a drug against an entire enzyme family, and even evaluation of the compound site of binding. Previously, I described how ABPP could be exploited to evaluate both kinases and serine hydrolases. It is important to note, however, that limitations of this methodology may impact data collection and analyses.

ABPP relies on the availability of an enzyme active site as the sole readout of activity. For example, ATP acyl phosphate probes that evaluate kinase activity rely on the availability of the catalytic ATP binding pocket. There are many cases in which a false positive or negative readout of activity may occur due to this binding event. In cases where an inhibitor binds to a site that is distinct from the catalytic binding site (such as an allosteric inhibitor), the active binding site would still be available for probe binding, while substrate turnover activity of the protein is inactivated. This would result in a false positive readout for protein activity, as the probe could still bind to and covalently modify the protein even though the protein is not fully active. Activity of protein kinases is regulated by the phosphorylation of an activation loop positioned directly outside of the active binding site (83). Dephosphorylation of the activation loop site results in autoinhibition via physical blockade of the kinase active site, while phosphorylation releases the autoinhibitor resulting in catalysis (83). Kinase catalytic site availability is dynamic and may vary depending on the cellular state, resulting in a false negative readout of kinase activity in the evaluation of compound

potency and selectivity. Thus, probe binding may not always signify protein activity and a secondary method (such as a kinase activity assay) should always be used to validate any identified hit compounds.

A variety of chemical probes have been identified that evaluate enzyme activity *in vitro* (in cell lysates) and *in situ* (in live cells). Probes capable of performing *in vitro* studies are fantastic tools for initial compound studies, which allow assessment against all proteins present within a cell lysate. However, it is important to complement *in vitro* studies with *in situ* live cell analyses to ensure that a compound is capable of exhibiting the desired effects in a system where proteins may be differentially localized to subcellular compartments or membranes, or differentially active due to intact cellular signaling pathways. *In situ* analyses validate compound efficacy in a more representative biological system, and support future *in vivo* studies. The potential of chemical probes to be utilized for *in vitro* or *in situ* analyses depends on their chemical structure and the ability of cells to uptake the probe. For our studies, we chose to utilize the Kinativ platform, which uses a probe based on the structure of ATP. In previous studies (Unpublished, Hsu lab), we have found the probe to be incapable of live cell readouts, potentially due to the highly negative charges of the three phosphate groups. In order to complement the studies described in this dissertation with live cell analyses, we may consider utilizing a live cell probe such as XO44.

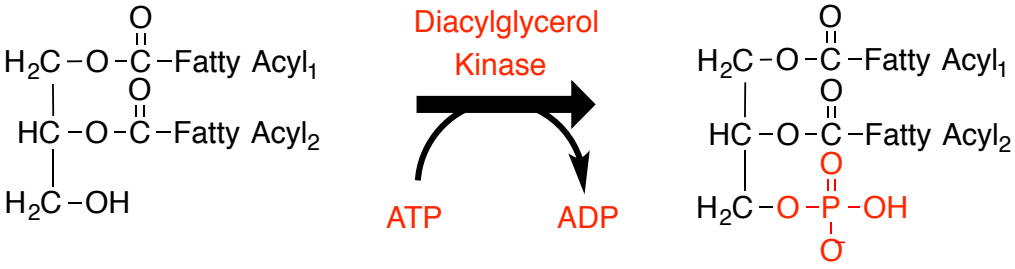

Figure 1.1. DGK catalyzes the phosphorylation of diacylglycerol to produce phosphatidic acid.

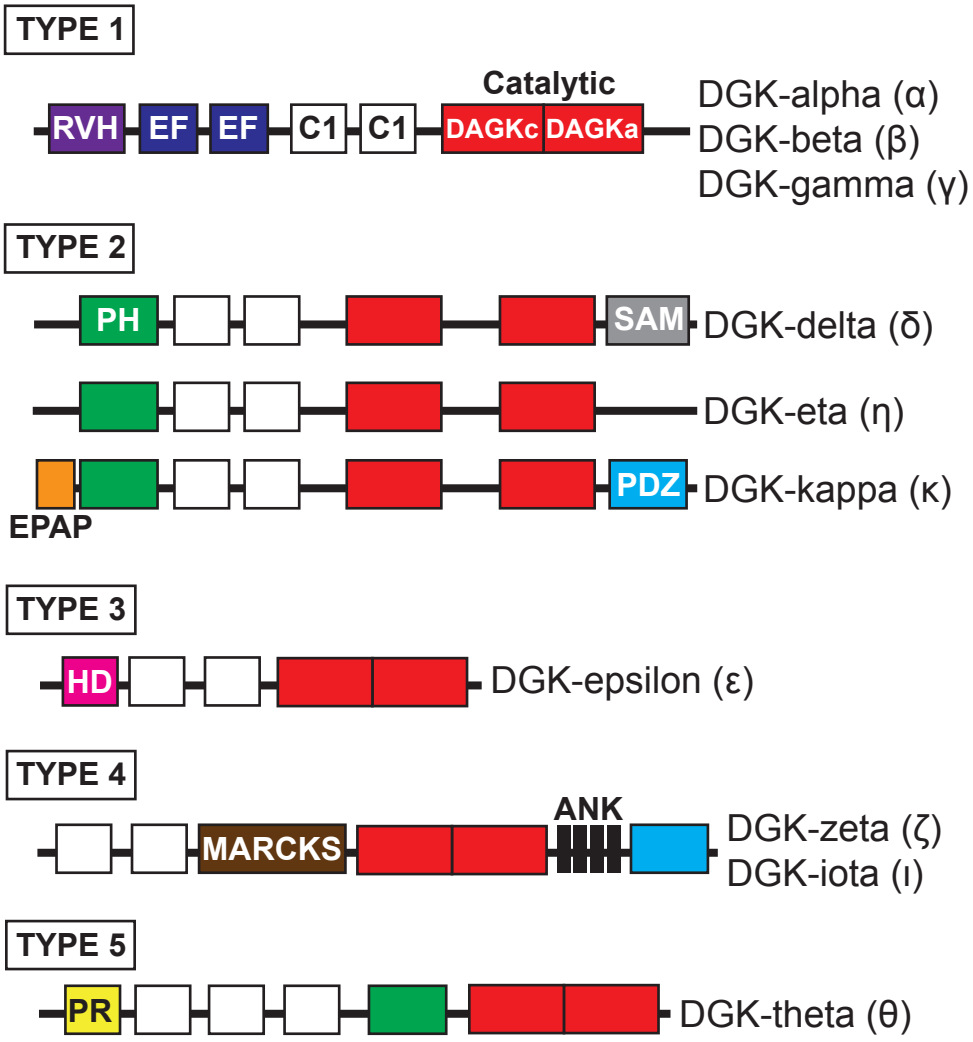

Figure 1.2 Structure of mammalian DGK isoforms. The ten mammalian DGK isoforms are grouped by sequence homology into five subtypes. The structural motifs common to several DGKs are shown.

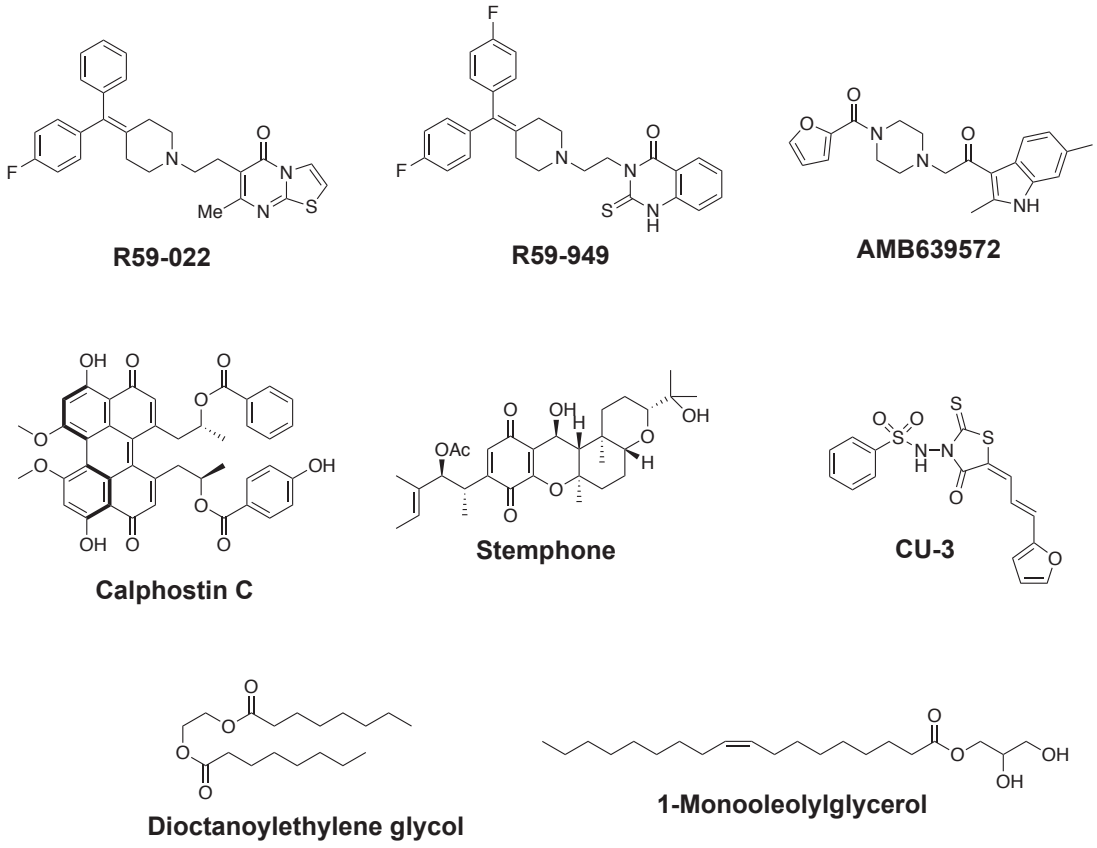

Figure 1.3 Structures of various diacylglycerol kinase inhibitors.

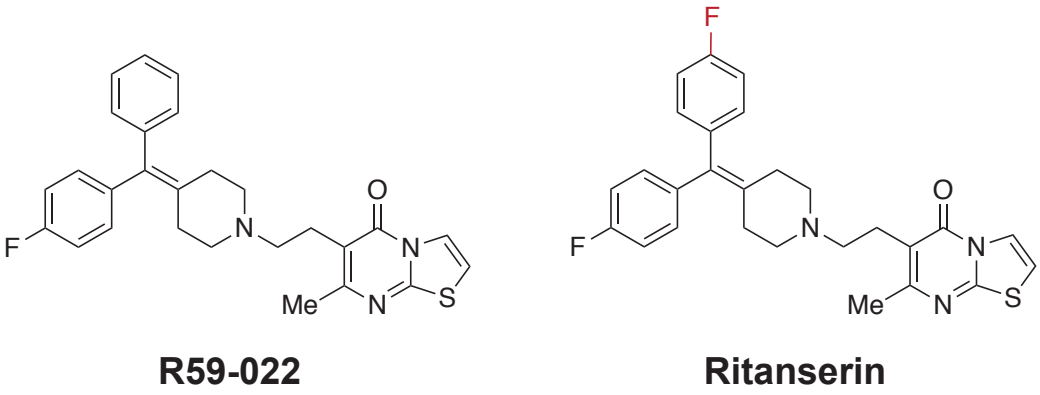

Figure 1.4 Structures of DGKα selective inhibitors R59-022 and ritanserin.

Chapter 2: Discovery of the Diacylglycerol Kinase Ligand Binding Regions

Adapted from: Caroline E. Franks, Sean T. Campbell, Benjamin W. Purow, Thurl E. Harris, and Ku-Lung Hsu. *Cell Chemical Biology* 24, 870-880 (2017).

2.1 Abstract

Diacylglycerol kinases (DGKs) are integral components of signal transduction cascades that regulate cell biology through ATP-dependent phosphorylation of the lipid messenger diacylglycerol. Methods for direct evaluation of DGK activity in native biological systems are lacking and needed to study isoform-specific functions of these multidomain lipid kinases. Here, we utilize ATP acyl phosphate activity-based probes and quantitative mass spectrometry to define, for the first time, ATP and small-molecule binding motifs of representative members from all five DGK subtypes. We use chemical proteomics to discover an unusual binding mode for the DGK-alpha inhibitor, ritanserin, including interactions at the atypical C1 domain distinct from the ATP binding region. Unexpectedly, deconstruction of ritanserin yielded a fragment compound that blocks DGK-alpha activity through a conserved binding mode and enhanced selectivity against the kinome. Collectively, our studies illustrate the power of chemical proteomics to profile protein-small molecule interactions of lipid kinases for fragment-based lead discovery.

2.2 Introduction

Diacylglycerols (DAGs) and phosphatidic acid (PA) play fundamental roles in biology as basic components of membranes, intermediates in lipid metabolism, and secondary messengers in cellular signaling (18, 84). Cells regulate intracellular DAG and PA levels through metabolic networks that utilize distinct enzymes to produce or consume these secondary messengers/metabolites (4, 18, 85, 86). One such enzymatic pathway that is central to signal transduction is ATP-dependent phosphorylation of DAGs to biosynthesize PA (Figure 2.1A) by a set of lipid kinases collectively known as diacylglycerol kinases (DGKs) (4). DAG and PA are important lipid messengers that alter localization (87), activation (88), and protein-protein interactions (84) of distinct sets of receptor proteins. Consequently, disruption of the same DGK protein in different cell types can result in opposing effects that can be leveraged, for example, in cancer to simultaneously block tumor growth and activate antitumor immunity (30, 39). Since DAG and PA serve as key intermediates in lipid metabolism, DGKs are uniquely positioned as key regulators of the structural, bio-energetic, and signaling demands of cells.

Ten mammalian DGKs have been identified and classified into five subtypes based on structural features elucidated from primary sequence analysis (Figure 2.1B). At the N terminus, DGKs contain at least two cysteine-rich zinc-finger-like motifs similar to C1 domains found in protein kinase C (PKC) (18). DGKs contain a C-terminal catalytic domain composed of a conserved catalytic region (SMART domain (89) DAGKc, SM000046), which is present in other eukaryotic lipid kinases and DGKs from Gram-

positive bacteria (90), followed by an accessory subdomain (DAGKa, SM000045) of unknown function (30). While DGKs share the same basic domain organization, individual subtypes differ widely in regulatory domains proposed to mediate metal binding (EF hand motifs), oligomerization (SAM domain), membrane association (PH domain), subcellular localization (MARCKS domain), or protein-protein interactions (ankyrin repeats, PDZ domain) (4). Given the enormous chemical diversity of DAG and PA lipids (91), understanding the crosstalk between regulatory and catalytic domains of DGKs will be critical for assigning metabolic and signaling functions to individual isoforms.

Attempts to define the function of individual DGK domains have resulted in inconclusive results. ATP binding motifs corresponding to the glycine-rich loops found in protein kinases (GxGxxG consensus sequence; (92, 93) were identified in the first C1 and catalytic domains of DGKs (94, 95). Mutation of lysines in these motifs, which abolishes ATP binding and protein kinase activity, did not affect catalytic function of DGKs and led others to hypothesize the existence of a DGK-specific ATP binding motif that remains to be defined (95, 96). The role of C1 domains in DGK function is also enigmatic. With the exception of gamma and beta isoforms (97), the C1 domains of DGKs lack conserved residues identified as being required for DAG binding in other proteins including PKC (98). *In vitro* biochemical studies measuring the activity of C1 truncation mutants have produced conflicting reports with regard to whether C1 motifs are required (99-101) or dispensable (20, 96) for maximal DGK catalytic activity.

Thus, DGK-active sites remain ill-defined and, combined with the lack of crystal

structures for mammalian DGKs, have limited our understanding of substrate and inhibitor binding. As a result, current DGK inhibitors consist of compounds with poor specificity within the DGK superfamily (41, 42) or lack selectivity measurements against other lipid and protein kinases (37, 43, 52). Thus, methods that provide information on small-molecule binding mode and selectivity are needed to guide development of isoform-selective DGK inhibitors. Selective DGK inhibitors are needed to study isoforms where knockout mice viability is an issue (102) and to help realize the translational potential of targeting specific forms, e.g., DGKα, for anticancer (36) and immunotherapy applications (103).

Here, we use ATP acyl phosphate activity-based probes (66, 67) and quantitative mass spectrometry to discover ATP and inhibitor binding sites of representative members of all five principal DGK subtypes. Our findings define, for the first time, the ATP binding motif of DGKs that is distinct from protein kinases and identifies the DAGKa subdomain as a novel region mediating ATP binding. We discovered a fragment of the DGKα inhibitor ritanserin that shows conservation of binding mode and enhanced selectivity against protein kinases, sup- porting the concept that the atypical C1 and accessory region of the catalytic domain (DAGKa) are key ligand binding sites for developing DGKα-selective inhibitors. Our studies demonstrate the utility of chemical proteomics to map ligand binding sites for fragment-based discovery of lipid kinase inhibitors.

2.3 Materials and Methods

Materials. pDONR223-DGKK was a gift from William Hahn & David Root (Addgene plasmid # 23487). pCSF107mT-GATEWAY-3'-FLAG was a gift from Todd Stukenberg (Addgene plasmid # 67619). pCSF107mT-DGKK-FLAG construct was generated by recombination of the Addgene plasmids using the Gateway cloning system (Invitrogen). All other vectors were gifted to Dr. Kevin Lynch (University of Virginia, School of Medicine) by Dr. Kaoru Goto (Yamagata University, School of Medicine) and Dr. Fumio Sakane (Chiba University) and were kindly shared with us: pcDNA3-FLAG-DGKA (rat), pCMV-Tag2B-FLAG-DGKQ (human), pcDNA3-DGKE-3xFlag (human), and pCMV-SPORT6-HA-DGKZ (human). Polyethyleneimine (PEI) was purchased from Polysciences, Inc. 1, 2-dioleoyl-sn-glycerol (DG) and 1,2-dioleoyl-sn-glycero-3-phospho-L-serine (DOPS) were purchased from Avanti Polar Lipids. Primary antibodies were obtained from ThermoFisher Scientific (HA Tag Monoclonal Antibody) or Sigma-Aldrich (anti-FLAG antibody produced in rabbit). Secondary fluorescent conjugated antibodies were obtained from ThermoFisher Scientific. Desthiobiotin ATP acyl phosphate nucleotide probe was obtained from ThermoFisher Scientific (PI88311). Ritanserin and ketanserin tartrate were purchased from Tocris Bioscience. 4-(Bis(4-fluorophenyl)methylene)piperidine (RF001) was purchased from Matrix Scientific. R59022 and R59949 were purchased from Sigma-Aldrich.

Cell Culture. HEK293T cells were cultured in HyClone Dulbecco's Modified Eagles Medium (without L-Glutamine, with L-glucose and sodium pyruvate) supplemented with

10% FBS (Omega Scientific, US Source Fetal Bovine Serum) and 1% L-Glutamine (200 mM, Gibco). SILAC HEK293T cells were cultured in Thermo Scientific Pierce DMEM Media for SILAC (minus L-Lysine and L-Arginine, with L-glutamine) supplemented with 10% dialyzed FBS (Omega Scientific, Dialyzed Fetal Bovine Serum), and either 'Light' L-Lysine and L-Arginine (100 µg/mL, Acros Organics) or 'Heavy' L-Lysine-$^{13}C_6$, $^{15}N_2$ and L-Arginine-$^{13}C_6$, $^{15}N_4$ (100 µg/mL, Sigma-Aldrich) for a minimum of five passages prior to use. Cell lines were grown at 37 °C under 5% CO_2.

Transient transfection. Recombinant DGK proteins were produced by transient transfection of HEK293T cells. HEK293T cells were plated at a concentration of 400,000 cells in complete DMEM and grown to 50-60% confluence. A polyethyleneimine (PEI) stock solution was prepared (1mg/mL, pH 7.4) and filter sterilized. Serum-free DMEM (600 µL) was mixed gently with 2.6 µg DNA and 20 µL of sterile PEI (1 mg/mL, pH 7.4) in a sterile microfuge tube. Mixtures were incubated for 30 min at 25 °C. The mixture was then added drop-wise to each 10 cm plate, rocked back and forth to mix, and placed back in the incubator. Cell pellets were harvested after two full days of growth, snap-frozen in liquid N_2, and stored at -80°C until use. Recombinant proteins were produced by transient transfection in SILAC HEK293T cells using the procedure described above, except that cells were plated at a concentration of 1 x 10^6 cells per 10 cm plate and grown to ~70% confluence prior to introducing transfection mixture.

Western blot analysis of recombinant protein expression. Cell lysates were separated via centrifugation at 100,000 x *g* for 45 min at 4 °C. Proteins separated by SDS-PAGE (7.5% polyacrylamide, TGX Stain-Free Mini Gel) at 150 V for 55 min. Gel transfers were performed using the Bio-Rad Trans-Blot Turbo RTA Midi Nitrocellulose Transfer Kit with a Bio-Rad Trans-Blot Turbo Transfer System (25V, 10 min). The nitrocellulose blot was then incubated in blocking solution (30 mL, 5% Milk in TBS-T (1.5 M NaCl, 0.25 M Tris pH 7.4 in ddH_2O)) for 1 h at 25 °C with gentle shaking. The blot was then transferred immediately to primary antibody solution (1:1,000 anti-FLAG or 1:10,000 anti-HA in TBS-T) and incubated overnight at 4°C with gentle shaking. The blot was then rinsed 5 times for 5 min in TBS-T, transferred immediately into secondary antibody solution (1:10,000 anti-species DyLight 550 or DyLight 650 in TBS-T), and incubated for 1 h at 25 °C with gentle shaking. The blot was then rinsed 5 times for 5 min in TBS-T, transferred into ddH_2O, and imaged by in-blot fluorescence scanning on a ChemiDoc MP Imaging System.

Preparation of cell lysates for gel-based chemical proteomics. Cell pellets were resuspended in kinase buffer (Dulbecco's PBS (DPBS, Hyclone), 20 mM $MgCl_2$, EDTA-free protease inhibitors (Pierce)) and then lysed by sonication (3 x 1 sec pulse, 20% amplitude). The cell lysates were then subjected to centrifugation (100,000 x *g*, 45 min at 4 °C) to isolate the cytosolic fraction in the supernatant and the membrane fraction as a pellet. The membrane pellet was resuspended in kinase buffer by sonication. For all further analyses, only the soluble (cytosolic) fraction was used to prevent the need for

detergents, which have been shown to interfere with DGK activity (104). The only exception was experiments involving DGKE; recombinant DGKE protein was most prominently expressed in the membrane fraction and so this fraction was utilized to study DGKE enzyme (see Figure 2.3). Protein concentrations were measured using the Bio-Rad DC protein assay. Samples were stored at -80 °C until use.

Gel-based chemical proteomic assay. Proteome concentration was adjusted to 2 mg/mL in kinase buffer. Proteomes were first pre-treated with compound (0.6 μL, 50X stock in DMSO) mixed with gentle flicking, and incubated for 30 min at 25 °C in a microfuge tube (30 μL reaction volume). Desthiobiotin ATP acyl phosphate nucleotide probe (0.5 mM in ddH_2O) was then added to each sample (0.6 μL, 10 μM final) and incubated for 30 min at 25 °C. Reactions were then quenched with 10 μL of 4X SDS-PAGE loading buffer. Protein samples (15 μL) were loaded onto 4-20% TGX Stain-Free Protein Midi Gel and resolved by SDS-PAGE at 150V for 55 min. Proteins were then transferred to a nitrocellulose blot by Bio-Rad Trans-Blot Turbo Transfer System (25V, 10 min) to enhance sensitivity. The nitrocellulose blot was then incubated in blocking solution (30 mL, 3% BSA in TBS-T) for 1 h at 25 °C with gentle shaking. The blot was then transferred immediately to antibody solution (30 mL, 5% BSA in ddH_2O with 0.1% Tween20 and 1:3000 Streptavidin DyLight 550) and incubated for 2 h at 25°C with gentle shaking. The blot was then rinsed 5 times for 5 min in TBS-T, and then transferred into ddH_2O. The blot was then imaged by in-blot fluorescence scanning on a ChemiDoc

MP Imaging System. Fluorescence intensity signals were normalized to total lane protein using the Biorad Stain Free imaging (105).

Preparation of cell lysates for ADP-glo assay. The ADP-Glo DAG phosphorylation substrate assay was adapted from Sato et al (45). Transfected HEK cells expressing recombinant FLAG-DGKA were harvested in DPBS and centrifuged at 1400 x *g* for 3 min. Supernatant was removed and 1 mL Lysis Buffer (50 mM HEPES (pH 7.2), 150 mM NaCl, 5 mM $MgCl_2$, 1 mM DTT, 1 mM phenylmethysulfonyl chloride, Phosphatase Inhibitor Cocktail 2 (Sigma-Aldrich), and EDTA-Free Protease Inhibitor Mini Tablets (Pierce)) was added and cells re-suspended. Solutions were sonicated (3 x 1 sec pulse, 20% amplitude) and then centrifuged at 400 x *g* for 5 min. Supernatant was separated and protein concentrations were measured using the Bio-Rad DC protein assay and diluted in Lysis Buffer as appropriate. Samples were stored at -80°C until use.

ADP-glo DAG phosphorylation substrate assay. Micelles were prepared from lipid stocks as follows: Reaction Buffer (50 mM MOPS (pH 7.4), 1 mM DTT, 100 mM NaCl, 20 mM NaF, and 1 μM $CaCl_2$) was prepared in ddH_2O. From this stock, a solution of Reaction Buffer with 50 mM $MgCl_2$ and 1 mM ATP ('Reaction Initiator') and a solution of 0.3% Triton-X100 in Reaction Buffer ('Triton Buffer') were separately prepared. DG and DOPS in chloroform were mixed and then dried under nitrogen. Triton Buffer was added to the dried lipids to a final concentration of 10 mM DG and 8 mM DOPS. This solution was incubated at room temperature for 5 min with gentle shaking, followed by

sonication (3 x 1 sec pulse, 20% amplitude). The micelles were then diluted 4-fold in reaction buffer to yield the final micelle buffer. 1 mg of lysate was aliquoted into each well of a 96 well plate, followed by micelle buffer to a final volume of 20 µL. 19 µL of this mix was added to 1 µL of DMSO or inhibitor solution and incubated at 30 °C for 30 min. After incubation, 5 µL of reaction initiator was added to each well and mixed thoroughly, followed by aliquoting 5 µL of each reaction mixture to a 96-well half area black polystyrene plate and incubated at 30 °C for 30 min. At this point the procedure for the ADP-Glo™ assay (Promega) was performed. 5 µL of 'ADP-Glo Reagent' was added to each well, mixed thoroughly, and allowed to incubate at 25 °C for 40 min. Then 10 µL of the 'Kinase Detection Reagent' was added to each well, mixed thoroughly, and allowed to incubate at 25 °C for 40 min. Luminescence was measured with no filter and an integration time of 1 sec per well on a BMG Labtech CLARIOstar plate reader.

Statistical analysis and determination of IC_{50} values. The percentage of enzyme activity remaining was determined by comparing integrated band intensities or luminescence of inhibitor- with DMSO-treated samples for gel-based chemical proteomic or ADP-glo assays, respectively. For both chemical proteomic and ADP-glo methods, nonlinear regression analysis was used to determine the IC_{50} values from a dose-response curve generated using GraphPad Prism. Data are shown as mean ± s.e.m. Determination of significance was performed by one-way ANOVA. All statistical analyses were performed using GraphPad Prism.

Sample preparation for quantitative LC-MS analysis using ATP acyl phosphates. Proteomes were diluted to 2 mg/mL in kinase buffer. The light and heavy proteomes (0.5 mg, 250 µL total reaction volume) were pre-treated with vehicle or compound, respectively (5 µL, DMSO (light) or 50X stock in DMSO (heavy)), mixed gently, and incubated at 25 °C for 30 min. Desthiobiotin ATP acyl phosphate nucleotide probe (0.5 mM in ddH_2O) was then added to each sample (5 µL, 10 µM final), mixed gently, and allowed to incubate at 25 °C for 30 min. After incubation, matched light and heavy proteomes were transferred and mixed in a 1:1 ratio in a two-dram vial containing 4:1:3 MeOH/$CHCl_3$/H_2O (2 mL MeOH, 500 µL $CHCl_3$, 1.5 mL H_2O) for extraction of proteins to remove excess probe, quickly vortexed, and centrifuged at 1,400 x *g* for 3 min to pellet protein. Organic and aqueous layers were removed using a Pasteur pipette, and the protein pellet was transferred to a screw-top tube in 600 µL MeOH. A second extraction was performed by adding $CHCl_3$ (150 µL) and H_2O (600 µL) to each sample, vortexed, and centrifuged at 1,400 x *g* for 3 min to pellet protein. Organic and aqueous layers were removed by pipetting, MeOH added to pellet (600 µL) and pellets were re-suspended by sonication (3 x 1 sec pulse, 20% amplitude) for a final extraction. Samples were then centrifuged at 17,000 x *g* for 5 min to pellet protein and MeOH was removed by pipetting. The pellets were re-suspended in 10 M urea/25 mM ammonium bicarbonate (500 mL), brought to a final volume of 1 mL with 25 mM ammonium bicarbonate, reduced with 10 mM DTT for 15 min at 65 °C, allowed to cool, and then alkylated with 40 mM iodoacetamide for 30 min at 25°C in the dark. To desalt the samples, each was transferred to a two-dram glass vial, and to the vial 4:1:2 MeOH/$CHCl_3$/H_2O (2 mL

MeOH, 500 µL $CHCl_3$, 1 mL H_2O) was added. The vials were vortexed quickly, spun at 1,400 x *g* for 3 min to pellet protein, and aqueous and organic layers were removed using a Pasteur pipette. The resulting protein pellet was transferred to a screw-top tube in 600 µL MeOH, and then $CHCl_3$ (150 µL) and H_2O (600 µL) were added to extract protein a second time. The samples were vortexed quickly, centrifuged at 1,400 x *g* to pellet protein, and the aqueous and organic layers were removed by pipetting. Resulting protein pellet was suspended in MeOH (600 µL) via sonication (3 x 1sec pulse, 20% amplitude), centrifuged at 17,000 x *g* for 5 min to pellet protein, and MeOH removed by pipetting. Protein pellets were then re-suspended in 25 mM ammonium bicarbonate (500 µL) and digested with 7.5 µg Trypsin/Lys-C (Promega, 15 µL, 0.5 µg/µL) for 3 h at 37 °C. Avidin-agarose beads (Thermo Scientific Pierce, 100 µL aliquot per sample) were washed three times by adding 10 mL DPBS, centrifuged at 1,400 x *g* for 1 min, and decanting. This wash step was repeated for a total of 3 times. Digested protein samples were mixed with washed avidin beads (100 µL) and brought to a volume of 5.5 mL with DPBS in a 15 mL conical and rotated for 1 h to enrich samples for the covalent desthiobiotin modification. The beads were washed with 25 mM ammonium bicarbonate (3X with 10 mL, centrifuge at 1,400 x *g* for 3 min, decant) and then H_2O (3X with 10 mL, centrifuge at 1,400 x *g* for 3 min, decant). Washed beads were then transferred to a low-bind microfuge tube, centrifuged at 1,400 x *g* for 3 min, allowed to rest for 1 min to settle beads, and then excess H_2O was removed *carefully* using a gel-loading pipette tip. To elute peptides, 100 µL of elution buffer (50% acetonitrile, ACN; 0.1% formic acid) was added to each sample and incubated for 3 min. Beads were spun down at 1,400 x *g*

for 3 min, allowed to rest for 1 min to settle beads, and then 75 µL of peptide-containing supernatant was removed carefully using a gel-loading pipette tip and transferred to a new low bind centrifuge tube. This step was repeated two more times with 75 µL of elution buffer and all eluent were collected into the same centrifuge tube (~225 µL total). Peptides were dried on a speed vacuum, resulting peptide samples acidified in 5% (v/v) formic acid, and stored at -80 °C until analysis.

LC-MS/MS analysis of SILAC samples. The peptide samples were analyzed by liquid chromatography-mass spectrometry. An integrated autosampler-LC (Ultimate 3000 RSLC nanoSystem, Dionex) was used to load the peptides onto a trap column (Nano-Trap, Thermo Scientific, 2 cm, 5 µm C18) and washed for 2 minutes with 1% B (80% ACN, 1% formic acid). The peptides were eluted from the trap column and through a homemade nanocapillary analytical column (20 cm, 5 µm C18 packed in 360 µm o.d. x 75 µm i.d. fused silica), with an integrated electrospray tip, using a 180 min 1-95% reverse-phase LC gradient (A: 0.1% formic acid; B: 80% ACN, 0.1% formic acid) with the following parameters: 0-2 min 1% B, 400 nL/min; 2-144 min to 95% B, 300 nL/min; 144.1-180 min 1% B, 400 nL/min. The eluting peptides were electrosprayed into an Orbitrap Q Exactive Plus mass spectrometer (Thermo Scientific), which was operated with a top 10 data-dependent acquisition method that consisted of one full MS1 scan (375 - 1,500 m/z) followed by 10 MS2 scans of the most abundant ions recorded in the MS1 scan. For recombinant DGKE samples, a data-independent parallel reaction monitoring (PRM) method was used to detect DGKE peptides. One full MS1 scan (375 - 1,500 m/z)

was followed by MS2 scans of targeted parent ions from a curated inclusion list (DGKE: EKAPSLFSSR, +2 charge state, 659.3617 m/z (light), 668.3729 m/z (heavy), 103.00-110.00 min). Data analysis was accomplished using the IP2 (Integrated Proteomics Applications) software package, in which RawConverter was used to generate searchable MS1 and MS2 data from the .raw file followed by using the ProLuCID algorithm (publicly available at http://fields.scripps.edu/downloads.php) to search the data against a modified human protein database (UniProt human protein database with rat DGKs, angiotensin I and vasoactive intestinal peptide standards; 40,660 proteins*)* with the following parameters: static carbamidomethyl modification of cysteine (+57.0142 Da), differential modifications of oxidized methionine (+15.9949 Da) and desthiobiotin-labeled lysine residues (+196.1212 Da), added masses of the SILAC "heavy"-labeled amino acids (+10.0083 Da for R, +8.0142 Da for K), and trypsin enzyme specificity with 2 missed cleavages. The resulting MS2 spectra matches were assembled into protein identifications and filtered using DTASelect 2.0 using the --mass, --modstat, and --trypstat options with a 1% peptide FDR. mzIdent files corresponding to searches were generated in IP2-Integrated Proteomics Pipeline, mzXML spectra data was extracted from the raw file using RawConverter, and uploaded into Skyline-daily (106) to determine SILAC ratios (*SR*) of light/heavy (vehicle/compound treated) peptides. Peptides used for analysis were assessed for quality in Skyline by the following criteria: isotope dot-product (iDOTP) $\geq$ 0.8, ratio dot-product (rDOTP) $\geq$ 0.8, and singletons defined by L/H ratios > 20 were set to 20. Dot-product values are measures of similarity between the precursor peak area and expected isotope distribution (iDOTP) and between

the light and heavy peak area (rDOTP) as calculated in Skyline and described by Schilling et al (106). Probe-modified peptides that met these criteria were manually inspected and integrated. Peptide ratios reported were normalized to DMSO/DMSO peptide ratios to account for potential variations in mixing and sample preparations. Additionally, reported DGK and FER peptides were verified by manual inspection of the raw data (MS1 and MS2).

Sequence alignments and generation of sequence logos. Lipid kinase sequences were obtained from Uniprot (http://www.uniprot.org/) and aligned using Clustal Omega (107, 108). Sequence logos shown in **Figure 2.9** were generated with WebLogo (109, 110) (http://weblogo.threeplusone.com).

DgkB monomer molecular model and alignment. PDB model 2QV7 visualized and colored using PyMol software. Partial Structure-Aided Sequence Alignment completed as described previously (111) and added to **Figure 2.8** using GIMP software package.

2.4 Results

2.4.1 *ATP Acyl Phosphate Functions as Activity-Based Probe for DGKα*

To test whether ATP acyl phosphates (Figure 2.2A) can be used to profile DGK activity, our strategy was to transiently express DGKs and test recombinant enzymes directly in cell proteomes without the need for protein purification. We reasoned this approach would mitigate challenges with detection due to differences in endogenous DGK levels while permitting analyses on a proteomic scale. Our initial studies focused on the alpha isoform (DGKα, Figure 2.1B), given the availability of inhibitors and matching negative control compounds (43) for our proof-of-principle experiments (Figure 2.2B). We confirmed overexpression of recombinant FLAG-tagged DGKα by western blot (Figure 2.3), and used published DAG phosphorylation substrate assays (45) to measure recombinant DGKα activity (Figure 2.4A). We observed significantly higher DAG phosphorylation activity (~6-fold on average) in DGKα-compared with mock-transfected or heat-denatured proteomes (Figure 2.4B). Furthermore, recombinant DGKα activity was blocked in a con- centration-dependent manner using the DGKα inhibitor ritanserin (43) compared with DMSO vehicle-treated controls (half maximum inhibitory concentration [IC_{50}] = 25 mM; Figure 2.5A). Since ritanserin exhibits 5-HT2 receptor (5-HT2R) inhibitory activity (53), we included another 5-HT2R antagonist, ketanserin (43) (Figure 2.2B), to control for non-specific effects in our substrate assay. Ketanserin showed negligible activity against DGKα in our substrate assay, confirming the use of ritanserin and ketanserin as paired probes (i.e. DGK-active and -inactive inhibitors, respectively, at 100 mM; Figure 2.4B) suitable for testing in our chemical proteomics

assay.

Next, we set out to determine whether we could use desthiobiotin-tagged, ATP acyl phosphates (66, 67) as a surrogate chemical proteomic assay for measuring recombinant DGKα activity in cell proteomes (Figure 2.2A). ATP acyl phosphate probes enable global profiling of kinase activities by covalent attachment of reporter tags to conserved lysine residues in the ATP binding site of a wide range of kinases as well as other ATP binding proteins (66, 67). Initially, we performed gel-based profiling experiments to allow rapid optimization of probe-labeling parameters (Figure 2.6A). In brief, DGKa-HEK293T-soluble lysates were reacted with the ATP acyl phosphate probe, desthiobiotin- modified proteins separated by SDS-PAGE, transferred to a nitrocellulose membrane, and probe-modified proteins detected using a fluorescently labeled streptavidin. We observed concentration-dependent labeling of an 80 kDa fluorescent band in DGKα- but not mock-transfected HEK293T proteomes (Figure 2.6B). We confirmed by western blot that differences in fluorescence signals in our probe binding assay were not due to expression levels of recombinant DGKα (bottom panel, Figure 2.6B).

From these studies, we identified experimental conditions where ATP acyl phosphate labeling of DGKα was not saturating to allow competitive profiling of reversible inhibitors (112) (10 mM ATP probe, 30 min; Figure 2.6C). Using these kinetically controlled conditions, we showed that pretreatment with ritanserin, but not ketanserin resulted in concentration-dependent blockade of probe labeling (IC_{50} = 57 mM; Figure 2.5B, Figure 2.6D). We included analysis of the non-selective DGK

inhibitors, R59949 (42) and R59022 (41), to show that our gel activity assay can be used to generally profile inhibitor activity against DGKα (Figure 2.6E). Finally, we showed that treatment with free ATP (1 mM) resulted in global reductions in fluorescent protein signals (Figure 2.3C). These results support specific detection of probe-labeling events occurring in the ATP binding site of recombinant DGKα, as well as other native proteins detected in HEK293T cell proteomes. In all of our probe-labeling studies, changes in fluorescent signals in com- pound-treated samples were not due to differences in DGKα protein levels as confirmed by western blot analysis (bottom panels, Figure 2.5C, Figure 2.6D, and Figure 2.6E). Collectively, the comparable potency values determined using substrate (Figure 2.5A) versus chemical proteomic assays (Figure 2.5B) demonstrate that ATP acyl phosphates are capable of measuring authentic DGKα activity with the advantage of enabling rapid assessment of com- pound activity across ATP binding sites detected in native cell proteomes (Figure 2.5C).

2.4.2 *Mapping the ATP Binding Site of DGK-Alpha Using Quantitative Chemical Proteomics*

Results from gel profiling analyses demonstrated the probe binding of DGKα is competed by ATP substrate. While suited for rapid screening, gel-based chemical proteomic assays do not provide information on site of binding of compounds. Thus, we implemented a liquid chromatography-mass spectrometry (LC-MS) assay to discover the ATP binding site(s) of DGKα. For these studies, we overexpressed DGKα in isotopically light and heavy amino acid-labeled HEK293T cells to enable quantitative LC-MS by

stable isotope labeling with amino acids in cell culture (SILAC (113); Figure 2.7A). In brief, light and heavy DGKα-HEK293T lysates were treated differentially with DMSO vehicle or free ATP (1 mM), respectively, prior to addition of ATP acyl phosphate to label active-site lysines. After probe labeling, light and heavy proteomes were combined, digested with trypsin protease, and desthiobiotin-modified peptides were enriched by avidin-affinity chromatography and analyzed by LC-tandem MS to identify and quantify isotopically tagged active-site peptides from DGKα (Figure 2.7A).

Using our quantitative chemical proteomics assay, we identified two probe-labeled peptides that were highly competed with ATP treatment as determined by SILAC ratios (*SR*) of MS1 chromatographic peak areas >5 in DMSO/ATP comparisons (Figure 2.7B and Table 2.1). All peptides reported met quality control criteria and were observed in two biological replicates. The sites of labeling for probe-modified peptides of DGKα were confirmed by identifying ions corresponding to peptide fragments that contain the modified lysine residue in MS2 spectra (red asterisk, Figure 2.7B). Both ATP-sensitive peptides are located within the predicted catalytic domain, albeit at different subdomain regions (K377-DAGKc, *SR* = 16.3; K539-DAGKa, *SR* = 16.4; Figure 2.7B). Comparison of these peptide sequences with ATP binding motifs found in protein kinases (92, 94) revealed no apparent homology, supporting previous speculation that DGKs mediate ATP binding through a non-canonical binding motif (95). Closer inspection of the DAGKc peptide did reveal homology with ATP binding sites of DgkB from *S. aureus*, and placement of K377 at the homologous residue in the bacterial DGK crystal structure (threonine 12) positions this lysine in the vicinity of phosphate groups of ADP (111)

(Figure 2.8).

The second ATP-sensitive peptide (K539, Figure 2.7B) is located in the poorly annotated DAGKa subdomain that, to the best of our knowledge, has not been implicated in ATP binding in DGKα or any other DGK isoform. Our results help explain previous findings from other groups showing that C-terminal truncations (which remove the DAGKa subdomain) result in impaired DGK catalytic activity (114). Finally, we identified a probe-modified peptide located in the first C1 domain of DGKα (K237, Figure 2.7A). The C1 site was competed with ATP treatments (K237, *SR* = 2.4, ~58% inhibition; Figure 2.7B; Table 2.1), but with lower potency compared with probe-modified peptides from DAGKc and DAGKa subdomains (~94% competition with ATP). The difference in sensitivity to ATP competition at C1 versus DAGKc/DAGKa suggests that the latter sites largely mediate ATP binding of DGKα. The partial sensitivity of C1 to ATP competition suggests the existence of a distinct binding site in the C1 domain that can bind ATP probe separate from interactions at the DAGKc/DAGKa sites (Figure 2.7C). In summary, our LC-MS findings provide evidence that ATP acyl phosphate probes can map important binding regions of DGKα domains to reveal ATP (DAGKc/DAGKa) and other ligand binding sites (C1) important for mediating catalytic functions.

2.4.3 *Chemical Proteomic Profiling of the DGK Superfamily Using ATP Acyl Phosphates*

Next, we sought to expand our chemical proteomics analysis to other DGK subtypes to

identify conserved and distinguishing features of active sites in comparison with type 1 DGKα. For these studies, we chose to test a representative member from each of the DGK subtypes: kappa (DGKκ (115), type 2; epsilon (DGKε (116)), type 3; zeta (DGKζ (117)), type 4; and theta (DGKθ [(100)]), type 5 (Figure 2.1B). Recombinant DGKs were transiently transfected in light and heavy HEK293T cells, protein overexpression confirmed by western blot (Figure 2.3), and recombinant lysates subjected to quantitative chemical proteomics (Figure 2.7A). The identified probe-modified peptides for each DGK isoform and their corresponding sensitivities to ATP competition are listed in Table 2.1. Akin to DGKα, we identified probe-modified peptides in C1, DAGKc, and DAGKa binding sites of DGKζ and DGKθ (Figure 2.9A). Treatment with free ATP resulted in potent competition at DAGKc (K596, *SR* = 7.6) and DAGKa (K768, *SR* = 14.4) sites within the catalytic domain of DGKθ (Figure 2.9A; Table 2.1). Similar inhibition profiles were observed for DGKζ, with the exception of a lower sensitivity to ATP competition at the DAGKc (K500, *SR* = 2.9) compared with DAGKa site (K662, *SR* = 16.7; Figure 2.9A; Table 2.1). Probe-modified peptides corresponding to C1 domains of both DGKζ (K323) and DGKθ (K202) showed moderate competition with ATP (*SR* ~3 for both isoforms; Figure 2.9A; Table 2.1). Of the remaining subtypes, we identified a single probe-modified peptide in the DAGKa subdomain of DGKκ and DGKε, which were competed with ATP with high (K892, *SR* = 15.0) or moderate inhibition (K392, *SR* = 2.6; Figure 2.9A; Table 2.1), respectively. Based on ATP sensitivity, our findings position the primary ATP binding site within the DAGKa subdomain of type 2 (DGKκ), type 3 (DGKε), and type 4 (DGKζ) enzymes. Similar to DGKα, type 5 DGKθ likely requires

both DAGKa and DAGKc regions for ATP substrate binding.

We performed multiple sequence alignments and sequence logo analysis (109, 110) to identify a potential DGK-specific ATP binding motif. We used ATP-competed peptide sequences identified in our LC- MS analyses to discover potential regions of sequence conservation across all five DGK subtypes tested. Our analyses identified clusters of amino acid conservation in regions that contained probe-modified lysines within both DAGKc (positions 7–17; Figure 2.9B) and DAGKa subdomains (positions 7–19; Figure 2.9C). We used our results to determine whether DGKs are probe- labeled at conserved lysines in the active site, which would pro- vide preliminary evidence of a common ATP binding orientation. Closer inspection of the data revealed that the lysine showing highest conservation in the DAGKc motif was also probe modified with the highest frequency (position 9; Figure 2.9B). In contrast, the correlation between conserved lysines and frequency of probe modifications at these sites was less clear in the DAGKa motif. For example, probe modification of the lysine with highest conservation (position 19) was only observed in the DGKκ active-site peptide (Figure 2.9C). The identification of probe modifications at both conserved (DAGKc) and non-conserved lysines (DAGKa) in the DGK ATP binding site is different from protein kinases, which are probe modified largely at conserved lysines in the ATP binding site (66). Future studies are needed to determine how these differences in DGK-active sites impart substrate specificity *in vivo* and whether these features can be exploited for inhibitor development.

2.4.4 *Inhibitor Profiling to Determine Ritanserin Binding Mode and Selectivity*

We next asked whether we could use quantitative chemical proteomics to determine the binding mode and selectivity of inhibitors against DGK isoforms. Ritanserin was originally tested in the clinic as a serotonin receptor antagonist for treatment of psychiatric disorders (53) and has recently generated interest as a lead DGKα inhibitor for drug repurposing to treat cancer (37, 43). DGKα-HEK293T soluble proteomes were treated with ritanserin or ketanserin (100 mM compounds; Figure 2.2B) followed by labeling with ATP acyl phosphate and quantitative chemical proteomics analysis (Figure 2.7A). Ritanserin concentrations were chosen to provide ~70% blockade of DGKα activity as determined from substrate (Figure 2.3A) and chemical proteomic assays (Figure 2.3B). Probe- modified peptides showing high competition, as judged by *SR* values, were identified as ritanserin binding sites in DMSO/ritanserin comparisons (*SR* > 5, Figure 2.10A; Table 2.1).

We used these criteria to discover whether ritanserin inhibits DGKα predominantly through binding interactions at the C1 (K237, *SR* = 7.0) and DAGKa sites (K539, *SR* = 7.0; Figure 2.10B; Table 2.1). Surprisingly, we observed minimal competition at the DAGKc domain (K377, *SR* = 2.0; Table 2.1). Ritanserin competed at common (DAGKa) as well as distinct binding sites (C1) compared with the ATP substrate (Table 2.1). The unusual binding mode of ritanserin identified from our LC-MS studies may help explain previous kinetic assays describing a mixed competitive mechanism of inhibition for this inhibitor; ritanserin is hypothesized to bind a DGKα-ATP complex through an unidentified binding site (43). We propose that C1 could be a potential site mediating ritanserin binding to DGKα distinct from the ATP pocket.

Inhibitor profiling of other DGKs revealed that ritanserin showed minimal activity against other isoforms (*SR* < 2 at all binding sites detected; Figure 2.10A; Table 2.1). Ritanserin competition was specific because treatment with the negative control probe ketanserin resulted in negligible competition at all probe binding sites, with the exception of a lower *SR* for DGKκ peptide, which indicates a potential activating effect for this isoform (Figure 2.10A; Table 2.1). Future studies will be required to determine whether ritanserin shows similar selectivity profiles against native DGKs.

One of the advantages of using chemical proteomics is the ability to simultaneously evaluate on- and off-target activity of inhibitors directly in cell proteomes (118, 119). Here, we measured the selectivity of ritanserin against >50 native kinases quantified in HEK293T soluble proteomes (Figure 2.11A). On average, we detected >200 probe-modified peptides from ~85 protein and lipid kinases per individual SILAC sample. Our kinome coverage is comparable with previous reports using ATP acyl phosphates and data-dependent MS scan modes (66). Native kinases reported in Figure 2.11A and Table 2.1 were quantified in at least two biological replicates across all treatment conditions and competed by treatment with free ATP (*SR* > 5; Table 2.1). The latter criterion (i.e., ATP competition) was important for identifying non-specific probe-labeling events in our studies. Kinase targets of ritanserin were defined as those active-site peptides that showed *SR* R 5. Based on this criterion, the most potent targets of ritanserin were DGKα and the non-receptor tyrosine protein kinase FER (120) (*SR* = 7.9; Figure 2.11A and 2.11B). We confirmed that ritanserin was competing at ATP binding sites of FER by demonstrating potent competition at the same site (K591) with free ATP

(*SR* = 19.3; Table 2.1). Collectively, our studies demonstrate the use of chemical proteomics to elucidate the binding mode and selectivity of ritanserin, resulting in discovery of the C1 domain as a novel ligand binding site and FER as an unanticipated off-target.

2.4.5 *Discovery of a Lead Fragment Inhibitor of DGKα by Ritanserin Deconstruction*

In an effort to improve the selectivity of ritanserin for DGKα, we explored ligand deconstruction (121-123) strategies to evaluate the contributions of representative fragments for binding affinity and selectivity. We hypothesized that the 4-substituted piperidine moiety of ritanserin (highlighted in red, Figure 2.11C) is a likely pharmacophore required for DGKα inhibition because of conservation of this motif across several DGKα inhibitors (43) (Figure 2.6E). Here, we tested the capacity of quantitative chemical proteomics to evaluate binding mode and selectivity of a ritanserin fragment (designated RF001, Figure 2.11C) against recombinant DGKs and endogenous kinases directly in native cell proteomes.

We confirmed that RF001 blocked DGKα activity in a concentration-dependent manner using the DAG phosphorylation substrate assay (IC_{50} = 223 mM; Figure 2.11C). Our data show substantially lower potency of RF001 compared with ritanserin (~10-fold difference in IC_{50} values when comparing Figure 2.5A and 2.11C), which is expected of low-molecular-weight fragments (<300 Da) that typically exhibit binding affinities in the high micromolar to millimolar range (124). To account for differences in potency, we tested RF001 at 10-fold higher concentrations (1 mM) in our subsequent LC-MS assays. This concentration of RF001 was chosen to provide >80% inhibition of DGKα activity in

our probe binding assay (Figure 2.12A and 2.12B).

Akin to ritanserin, RF001 treatment resulted in potent competition at C1 (*SR* = 12.6) and DAGKa sites (*SR* = 9.1), while showing weak activity at the DAGKc site (*SR* = 1.7; Figure 2.11D; Table 2.1). We also confirmed that RF001 was largely inactive against other DGK subtypes as determined by low *SR* values at all detected DGK probe-modified sites (average *SR* ~1; Figure 2.11A; Table 2.1). The similar inhibition profiles of RF001 and ritanserin observed in our LC-MS analyses support that the ritanserin binding mode is conserved with the ritanserin fragment and that the 4-substituted piperidine group represents a core binding motif of DGKα inhibitors.

While ritanserin and RF001 share similar inhibition profiles within the DGK family, they differed substantially in cross-reactivity against the kinome. A striking finding from our studies is the dramatic improvement in selectivity against the kinome observed with RF001 compared with ritanserin (Figure 2.11A). Specifically, the potent FER off-target activity observed with ritanserin was largely eliminated using RF001 (*SR* = 1.2; Figure 2.11B). In fact, RF001 showed potent activity ($SR \geq 5$) against a single kinase target, DGKα, across all detectable kinases (native and recombinant DGKs) quantified in our chemical proteomics studies (Figure 2.11A; Table 2.1). Closer inspection of the data revealed that, unlike ritanserin, RF001 maintained good selectivity, even for kinase targets that show moderate to weak inhibitory activity (25 versus 3 kinase targets that show $SR \geq 2$ for ritanserin versus RF001, respectively; Figure 2.11E). Future studies are needed to explore whether synthetic elaboration of RF001, potentially using fragment-based approaches (124), can improve affinity for αα while maintaining

selectivity against the kinome.

2.5 Discussion

We used ATP acyl phosphates and quantitative LC-MS to map ligand binding regions corresponding to the active site of mammalian DGKs. We defined, for the first time, the location of the ATP binding site of representative isoforms from all five principal DGK sub- types (Figure 2.9). Inspection of the DGK ATP binding sites reveals several important features that are unique to this lipid kinase family. First, we identified ATP-sensitive, probe-modified pep- tides from both DAGKc and DAGKa subdomains, supporting interactions between these regions within the catalytic domain to constitute a potential ATP binding cleft. Crystal structures of soluble bacterial lipid kinases with homology to mammalian DGKs have also been found with active sites located in an interdomain cleft (125). Our finding that the DAGKa region is involved in substrate binding was important for assigning a catalytic role to this domain, and helps explain previous reports that C-terminal truncations impair DGK enzymatic activity (114). Second, conserved sequences corresponding to ATP binding sites of DGKs (Figure 2.9B and 2.9C) are not homologous with glycine-rich loops mediating ATP binding of protein kinases (92, 93). Our data provide the first experimental evidence in support of a unique DGK ATP binding motif that was postulated over 20 years ago (95). Finally, it is tempting to speculate that detection of a single ATP binding site (as opposed to two sites in other DGKs) for DGKκ and DGKε is a reflection of functional differences in substrate binding of DGK subtypes (Figure 2.9A). In support of this hypothesis, DGKκ, along with other type 2 members, contain an unusual peptide motif that physically separates the DAGKc and DAGKa subdomains (115). DGKε, the sole type 3 member, is the only

subtype that lacks regulatory do- mains and shows acyl chain preference in DAG substrate assays *in vitro* (116). We should note that DGKκ and DGKε showed lower recombinant protein expression compared with other isoforms (Figure 2.3), and so we cannot rule out the possibility of detection limits using our LC-MS approach. Future studies will be required to evaluate how these distinctions in active sites influence substrate (DAG) specificity and function across DGK subtypes.

We also discovered important clues to domain binding sites of DGKs and how to exploit these regions for development of DGKα-selective inhibitors. The identification of a probe-modified site at the C1 domain provided the first evidence of a ligand binding site remote from the ATP binding region of DGKs. Although we cannot rule out the possibility of alternative mechanisms, e.g., probe binding due to domain (126) or protein interactions (127), we do provide evidence that the C1 domain serves as a ligand binding site for ritanserin distinct from the ATP binding region of DGKα (Figure 2.9A and 2.10A). The overlapping (DAGKa) and distinct (C1) binding sites of ritanserin compared with ATP helps explain previous kinetic findings of a mixed competitive mechanism of inhibition whereby ritanserin prefers to bind a DGKα-ATP complex (43). We investigated how the binding mode of ritanserin affects selectivity against other DGK isoforms as well as >50 native kinases detected in cell proteomes. While ritanserin showed good selectivity within the DGK superfamily, we discovered substantial cross-reactivity against protein kinases, including the non-receptor tyrosine kinase FER that was inactivated to a similar magnitude as DGKα (*SR* = 7.9; Figure 2.11A and 2.11B). An un- expected finding was the discovery that a ritanserin fragment (RF001) functioned as a

DGKα inhibitor that retained binding at C1 and DAGKa sites (Figure 2.11D), and largely removed FER and other kinase off-target activity (Figure 2.11A and 2.11E). Conservation of fragment binding mode is characteristic of ligand binding hotspots (122, 128) of proteins suitable for fragment-based lead and drug discovery (124). In this regard, future studies are needed to investigate whether RF001 can serve as a core fragment for synthetic elaboration of high-affinity ligands with selectivity for DGKα.

				Ratios			
Kinase name	Peptide	Labeling site	Uniprot Accession	ATP	Ketanserin	Ritanserin	RF001
Recombinant DGKs							
DGKA	QGLSCNLCKYIVHDHCAMK	C1	P51556	2.4	1.4	7.0	12.6
DGKA	IEPVSNTHPLLVFINPKSGGK	DAGKc	P51556	16.3	1.2	2.0	1.7
DGKA	YPEKFNSR	DAGKa	P51556	16.4	1.3	7.0	9.1
DGKK	NKMWYGLLGTK	DAGKa	Q5KSL6	15.0	0.2	0.7	1.6
DGKE	EKAPSLFSSR	DAGKa	P52429	2.6	1.3	1.0	0.7
DGKZ	CAACKIVVHTPCIEQLEK	C1	Q13574	3.1	1.3	1.4	1.1
DGKZ	SGGNQGAKIIQSFLWYLNPR	DAGKc	Q13574	2.9	1.5	1.2	0.9
DGKZ	EANPEKFNSR	DAGKa	Q13574	16.7	1.4	1.8	1.1
DGKQ	KTCGSSDVLAGVR	C1	P52824	3.6	0.9	1.3	0.7
DGKQ	LPPDSCPLLVFVNPKSGGLK	DAGKc	P52824	7.6	1.2	1.1	0.9
DGKQ	EEEPGKFTSR	DAGKa	P52824	14.4	1.1	1.4	1.2
Native kinases in HEK293T							
AAPK1/AAPK2	DLKPENVLLDAHMNAK	Lys2	Q13131	9.1	1.4	2.4	1.1
BRAF	DLKSNNIFLHEDLTVK	Lys2	P15056	>20	1.6	1.8	1.1
CDK1	DLKPQNLLIDDKGTIK	Lys2	P06493	8.4	1.4	2.4	1.1
CDK2	DLKPQNLLINTEGAIK	Lys2	P24941	>20	1.6	2.9	0.7
CDK5	DLKPQNLLINR	Lys2	Q00535	10.7	1.3	1.9	1.1
CHK2	VAIKIISK	Lys1	O96017	>20	1.6	2.2	0.2
CSK	VSDFGLTKEASSTQDTGKLPVK	ACT	P41240	15.8	1.2	1.8	1.1
E2AK2	DLKPSNIFLVDTK	Lys2	P19525	>20	1.3	2.8	1.2
FER	TSVAVKTCKEDLPQELK	Lys1	P16591	19.3	1.4	7.9	1.2
IRAK1	AIQFLHQDSPSLIHGDIKSSNVLLDER	Lys2	P51617	14.7	1.4	2.6	2.2
KCC1D	LFAVKCIPK	Lys1	Q8IU85	>20	1.5	2.3	1.1
KCC2D	IPTGQEYAAKIINTK	Lys1	Q13557	10.3	1.5	2.3	1.2
KCC2G	TSTQEYAAKIINTK	Lys1	Q13555	14.7	1.5	2.7	1.6
KS6A1	LTDFGLSKEAIDHEK	ACT	Q15418	19.5	1.4	2.1	1.3
KS6A1/KS6A2/KS6A3	DLKPENILLDEEGHIK	Lys2	Q15418	19.4	1.4	2.0	1.2
KS6A4/KS6A5	VLGTGAYGKVFLVR	ATP Loop	O75676	>20	1.3	2.2	1.1
KS6B1	DLKPENIMLNHQGHVK	Lys2	P23443	>20	1.2	1.3	1.0
KS6B2	DLKPENIMLSSQGHIK	Lys2	Q9UBS0	19.2	1.1	1.4	1.7
LATS1	ALYATKTLR	Lys1	O95835	>20	1.2	1.8	1.4
M3K2/M3K3	DIKGANILR	Lys2	Q9Y2U5	19.2	1.1	1.2	1.0
M3K4	DIKGANIFLTSSGLIK	Lys2	Q9Y6R4	6.8	1.2	1.9	0.8
M4K3	DIKGANILLTDNGHVK	Lys2	Q8IVH8	14.2	1.4	1.8	1.1
M4K4/MINK1/TNIK	DIKGQNVLLTENAEVK	Lys2	O95819	>20	1.3	1.8	1.1
M4K5	NVHTGELAAVKIIK	Lys1	Q9Y4K4	>20	1.3	2.4	0.9
M4K5	DIKGANILLTDHGDVK	Lys2	Q9Y4K4	>20	1.3	1.9	1.3
MARK3/MARK4	EVAVKIIDK	Lys1	P27448	>20	1.4	2.0	1.1
MP2K1/MP2K2	DVKPSNILVNSR	Lys2	Q02750	>20	1.3	1.9	0.9
MP2K3	DVKPSNVLINK	Lys2	P46734	19.1	1.4	1.7	1.2
MP2K4	DIKPSNILLDR	Lys2	P45985	>20	1.3	1.6	0.9
MP2K6	HVPSGQIMAVKR	Lys1	P52564	>20	1.4	2.2	1.1
NEK3	SKNIFLTQNGK	ACT	P51956	>20	1.0	2.2	1.0
PAN3	VMDPTKILITGK	ATP	Q58A45	>20	1.3	1.8	1.3
PI42C	FKEYCPQVFR	C2	Q8TBX8	6.9	1.2	1.7	0.8
PLK1	CFEISDADTKEVFAGKIVPK	Lys1	P53350	12.2	1.0	1.5	0.9
RAF1	DMKSNNIFLHEGLTVK	Lys2	P04049	>20	1.4	3.9	2.1
SLK	DLKAGNILFTLDGDIK	Lys2	Q9H2G2	>20	1.3	3.0	1.5
SMG1	DTVTIHSVGGTITILPTKTKPK	ATP	Q96Q15	15.9	1.3	1.7	1.0
STK10	DLKAGNVLMTLEGDIR	Lys2	O94804	7.4	1.3	1.7	1.1
STK3/STK4	DIKAGNILLNTEGHAK	Lys2	Q13188	>20	1.2	1.6	0.9
STK38	DTGHVYAMKILR	Lys1	Q15208	5.2	1.3	2.0	1.4
ULK3	EVVAIKCVAK	Lys1	Q6PHR2	>20	2.3	1.8	1.4

Table 2.1 SILAC Ratios for ATP, Ritanserin, Ketanserin, and RF001 Treatment of Recombinant DGK-HEK293T Soluble Lysates.

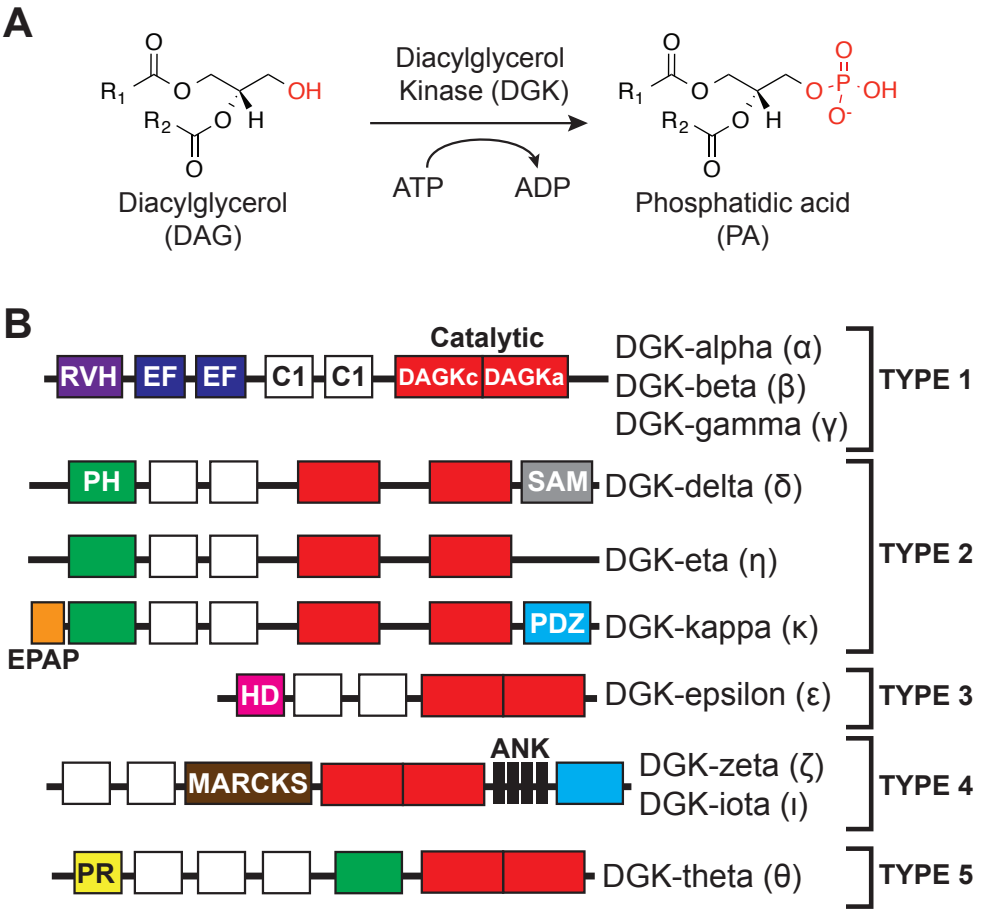

Figure 2.1 The Mammalian Diacylglycerol Kinase Superfamily (A) Diacylglycerol kinase (DGK) enzymes catalyze transfer of phosphate from ATP to diacylglycerol (DAG) to biosynthesize phosphatidic acid (PA). The molecular structure of fatty acyl chains regulates functional properties of DAG and PA lipids. **(B)** The ten DGK isoforms identified to date are divided into five principal subtypes based on the organization of structural motifs. Alternative splicing of certain DGK subtypes can generate additional structural diversity. RVH, recoverin homology domain; EF, EF Hands motif; C1, atypical/typical C1 domain; PH, pleckstrin homology domain; SAM, sterile alpha motif; EPAP, Glu-Pro-Ala-Pro repeats; PDZ, protein-protein interactions; HD, hydrophobic

domain; MARCKS, myristolated alanine-rich C kinase substrate domain; ANK, Ankyrin repeats; PR, proline-rich region.

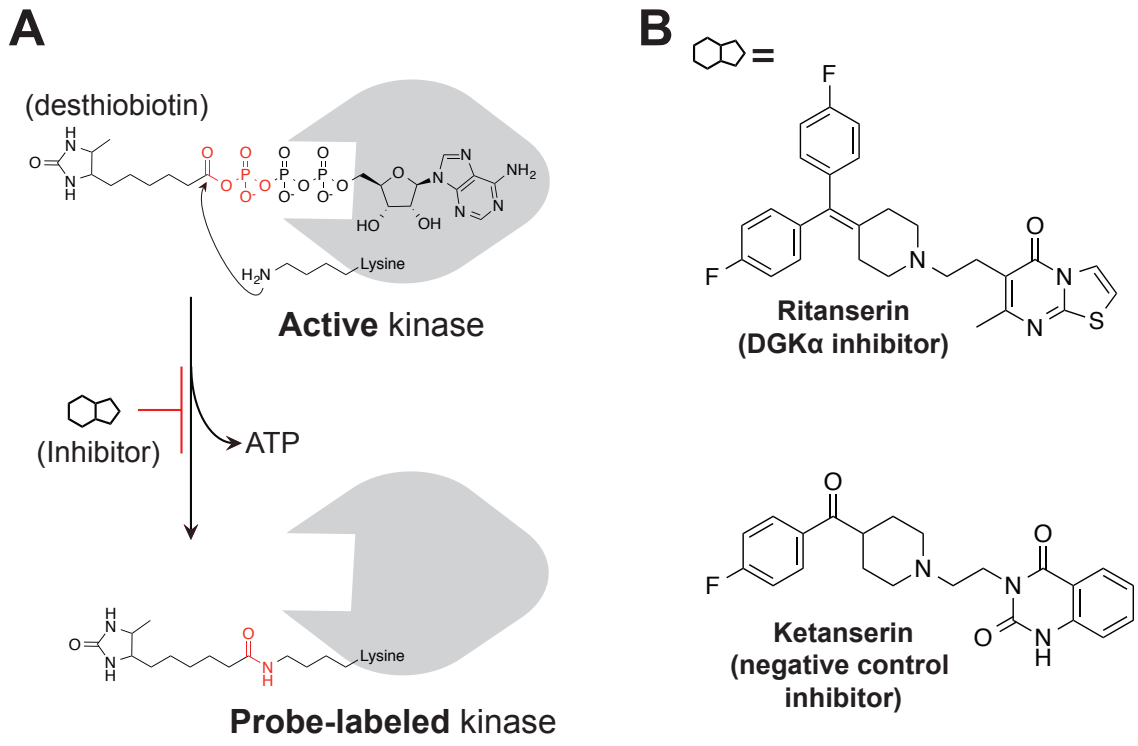

Figure 2.2 Activity-Based Probes and Inhibitors for Functional Analysis of DGKs **(A)** Chemical structure and mechanism of ATP acyl phosphate probe labeling. The ATP binding group mediates interactions with lipid and protein kinases to place the reactive acyl phosphate group in proximity of lysines in the active site. The side chain amino group of lysine covalently reacts with the probe, releasing ATP, and covalently attaches desthiobiotin to kinase through an amide bond. **(B)** The DGKα inhibitor ritanserin and matching negative control inhibitor ketanserin.

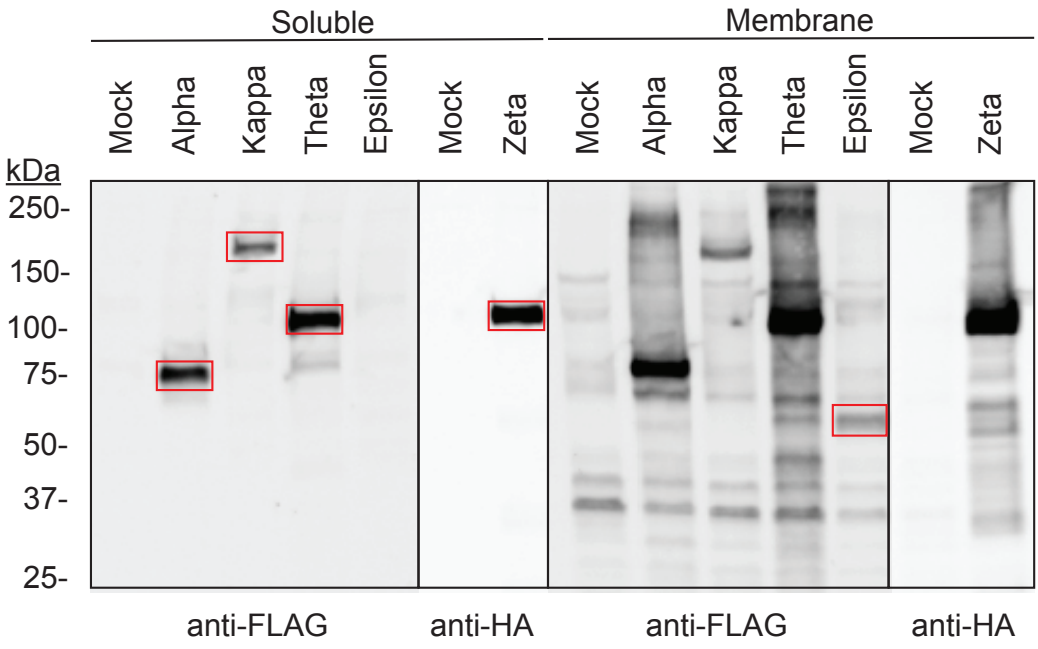

Figure 2.3 Western blot analysis of recombinantly overexpressed DGK isoforms. DGK isoforms were recombinantly expressed in HEK293T cells and proteomes subjected to western blot analysis (anti- FLAG, 0.8 µg/mL; anti-HA, 0.1 µg/mL). Soluble fractions were used for analysis with the exception of epsilon, which is expressed predominantly in the membrane fraction (highlighted by red boxes).

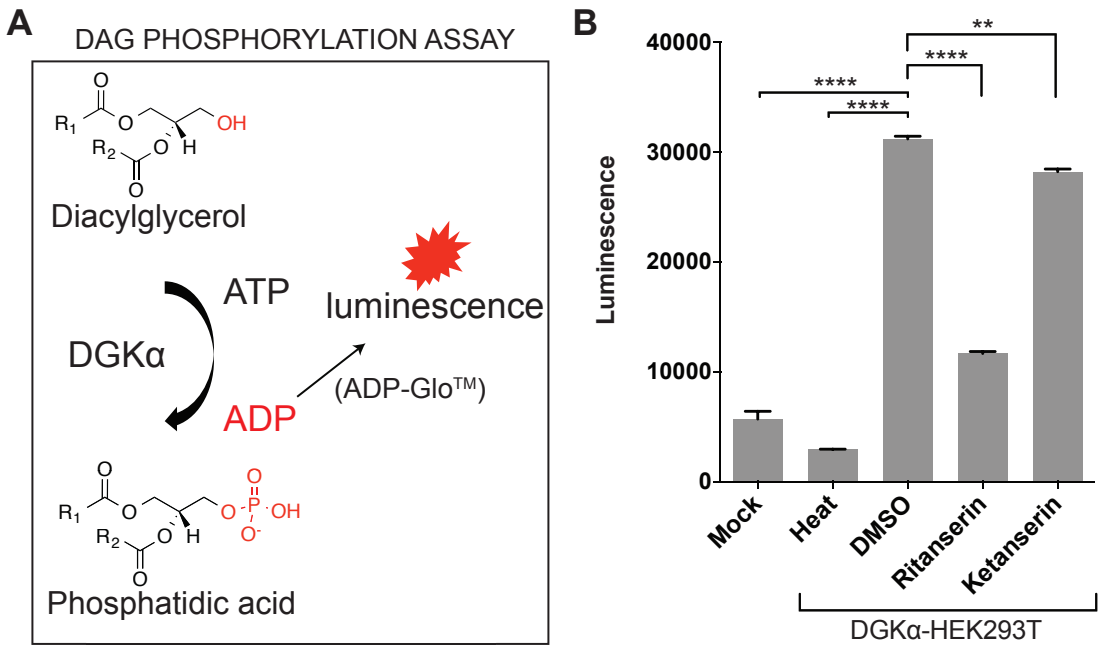

Figure 2.4 Measuring activity and inhibition of recombinant DGKα in HEK293T cells by substrate assay. **(A)** The ADP-glo assay measures ATP that has been converted to ADP by the action of kinases in the cell lysate though production of luminescent signal in proportion to ADP produced. **(B)** Production of active recombinant DGKα was determined by enhanced activity in DGKα-HEK293T versus mock-transfected soluble proteomes as measured using ADP-glo assay. The lack of activity with heat-denatured (95° C for 5 min) DGKα-HEK293T proteomes supports that activity was specific for recombinant DGKα. Pretreatment with ritanserin but not ketanserin (100 μM compounds) resulted in ~80% blockade of recombinant DGKα activity. Data shown are mean +/- SEM. for two independent biological replicates; n = 2 per group. ****$P \leq$ 0.0001 for mock versus DGKα overexpressed group (DMSO); **$P \leq$ 0.01, ****$P \leq$

0.0001 for vehicle-treated versus heat-denatured or inhibitor-treated DGKα overexpressed groups (DMSO).

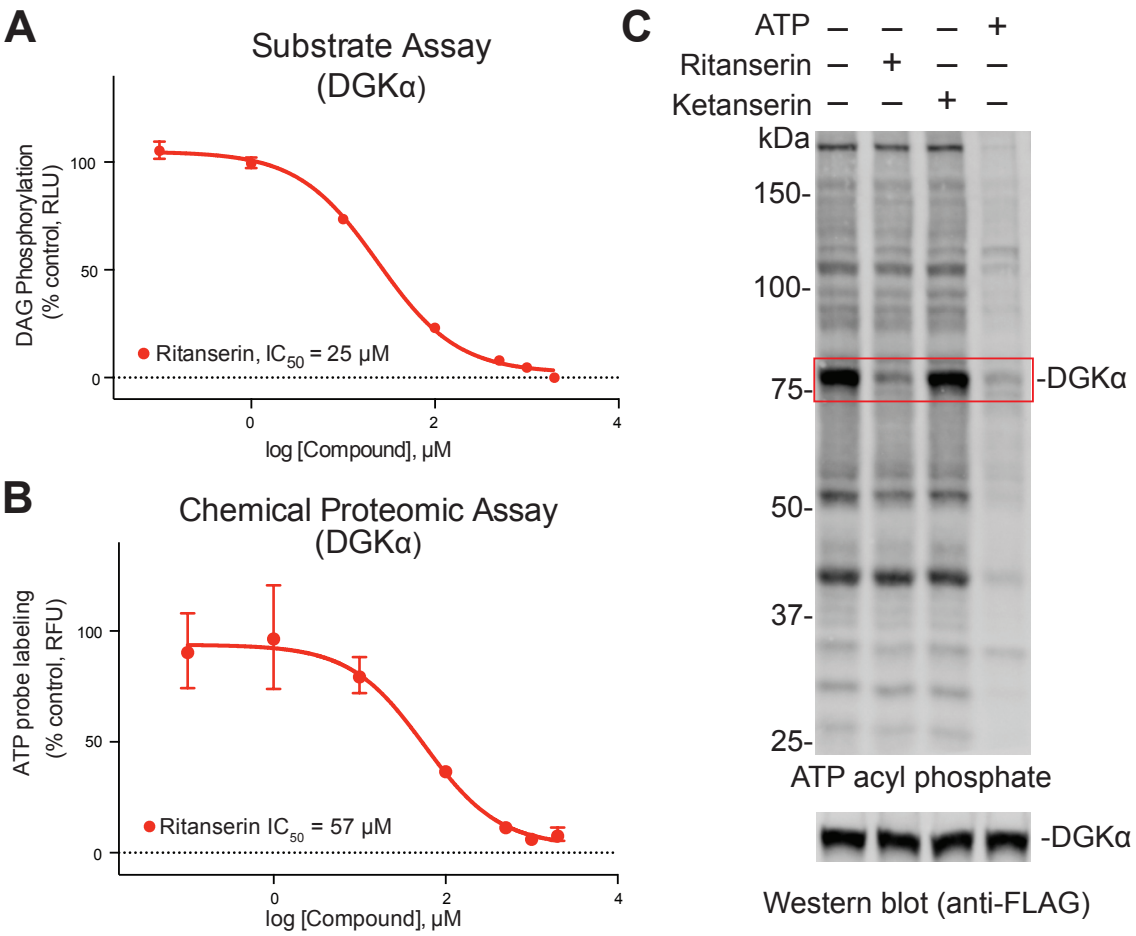

Figure 2.5 ATP Acyl Phosphates Enable Gel- Based Activity-Based Profiling of DGKα (A) *In vitro* IC_{50} values for DGKα inhibition by ritanserin as measured by the DAG phosphorylation substrate assay described in Figure 2.4. Data shown are mean ± SEM for triplicate measurements. Results are representative of two independent biological replicates. 95% confidence intervals for IC_{50} values: 20–30 mM. **(B)** A gel-based ATP acyl phosphate assay was used to determine *in vitro* IC_{50} values for DGKα inhibition by ritanserin (95% confidence intervals for IC_{50} values: 17–192 mM). Details of the assay and representative gels used to calculate potency values can be found in Figure 2.6. **(C)** DGKα-HEK293T soluble proteomes were pre- treated with ritanserin

(100 mM), ketanserin (100 mM), or ATP (1 mM) for 30 min prior to addition of ATP acyl phosphate probe (10 mM, 30 min) and gel-based analysis, as described in Figure 2.6. Pretreatment with ritanserin, but not ketanserin, blocked probe labeling of ~80 kDa recombinant DGKα. Western blot analysis (anti-FLAG, 0.8 mg/mL) confirmed equivalent recombinant protein expression across treatment conditions.

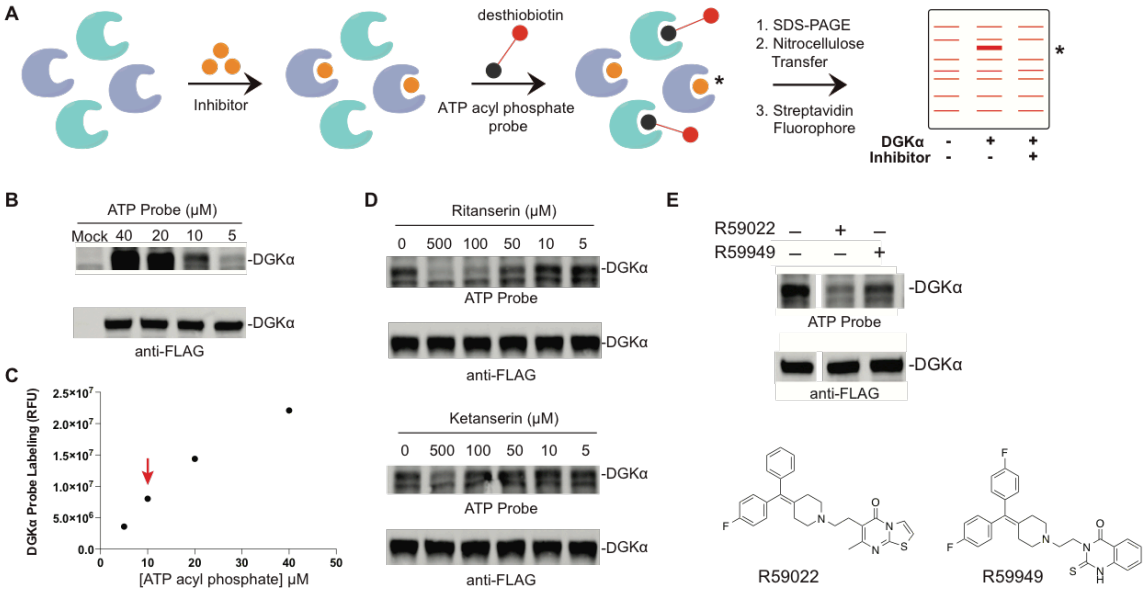

Figure 2.6 Optimization of gel-based ATP acyl phosphate assay for profiling DGK inhibitors. **(A)** Schematic of gel-based chemical proteomic analysis of recombinant DGKα activity. DGKα- HEK293T soluble proteomes were labeled with ATP acyl phosphate, proteins separated by SDS-PAGE, transferred to nitrocellulose, and desthiobiotin-modified proteins detected by streptavidin fluorophore and in-blot fluorescence. Pretreatment of proteomes with inhibitors blocks labeling at ATP probe binding sites, resulting in reductions in fluorescence signals to profile on- and off-targets of recombinant DGKα. **(B)** DGKα-HEK293T soluble proteomes were treated with ATP probe at the indicated concentrations for 30 min, quenched with gel loading buffer, and subjected to gel-based analysis as described above. **(C)** Integrated band intensities from these studies were plotted as a function of ATP probe concentrations to identify a suitable treatment condition for profiling of reversible inhibitors (10 μM ATP probe, 30 min; labeling reaction was ~40% complete). **(D)** DGKα-HEK293T soluble proteomes were

pretreated with ritanserin or ketanserin for 30 min at the indicated concentrations followed by ATP probe labeling (10 μM, 30 min) and gel-based chemical proteomics analysis as described above. Ritanserin but not ketanserin showed concentration dependent blockade of ATP probe labeling. **(E)** Pretreatment with the widely used DGK inhibitors R59022 and R59949 (100 μM compounds) also blocked DGKα probe labeling as measured by gel- based chemical proteomics. For all chemical proteomics studies, western blots (anti-FLAG, 0.8 μg/mL) were included to confirm that changes in fluorescence were not due to variations in recombinant protein expression (bottom panels).

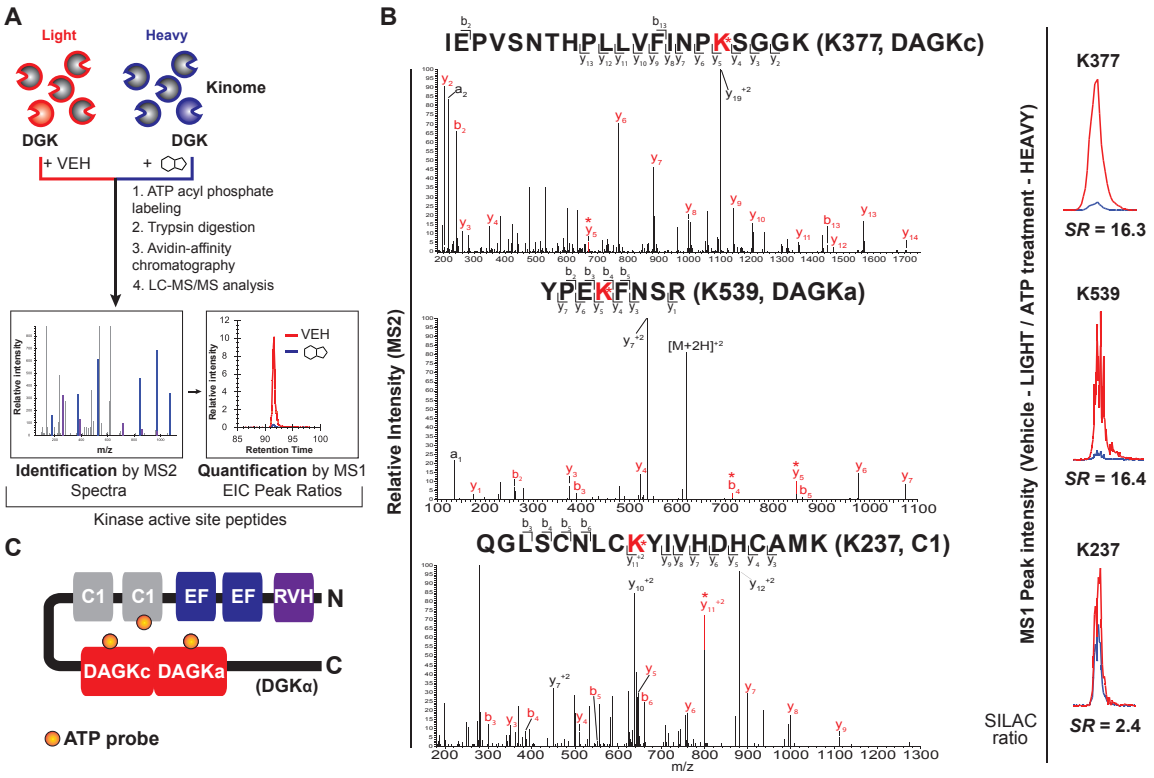

Figure 2.7 Elucidation of ATP and Ligand Binding Sites of DGKα by Quantitative Chemical Proteomics (A) Schematic of quantitative LC-MS proteomics workflow to identify ligand binding sites of recombinant DGKs using ATP acyl phosphate probe. **(B)** Left: MS2 spectra of probe-modified peptides corresponding to the active site of DGKα. Major *b*- and *y*-ion fragments derived from neutral losses of the precursor (M) are indicated on spectrum in red. An asterisk denotes fragments containing probe-modified lysine residues corresponding to the red-labeled lysine shown in the peptide sequence. Right: MS1-extracted ion chromatograms of probe-modified peptides with corresponding SILAC ratios quantifying vehicle- treated (light) or compound-treated (heavy). **(C)** Schematic of DGKα showing domains where ATP probe binding is detected by quantitative chemical proteomics. Orange circles represent ATP probe binding at K237 of the C1 domain, K377 of the DAGKc domain, and K539 of the DAGKa domain.

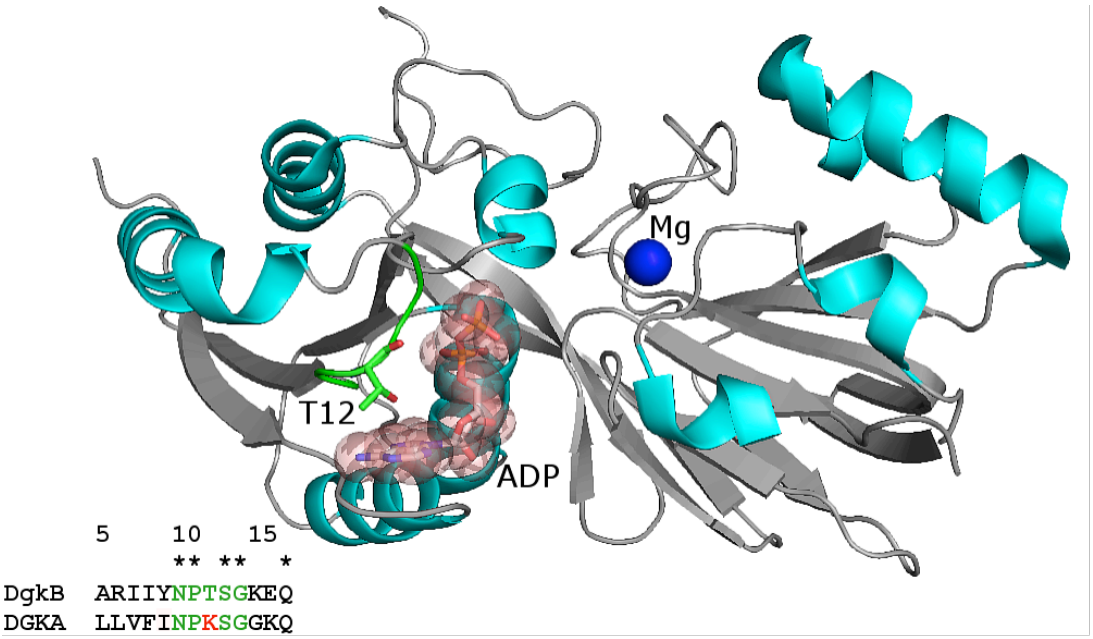

Figure 2.8 Proximity of *S. aureus* DgkB residue, with homology to DGKα K377, to phosphate groups of ADP. Cartoon Diagram of DgkB monomer (PDB code: 2QV7): α helices are cyan, β sheets and loops are grey, ADP is transparent spheres with a stick model, Mg is blue, the aligned region is green and the homologous residue (threonine 12) is depicted as a green stick model. Partial Structure-Aided Sequence Alignment of *S. aureus* DgkB and rat DGKα: aligned region is green and ATP acyl phosphate probe-modified DGKα residue is red (K377). Note the threonine residue homologous to the probe-modified lysine of DGKα is in proximity to phosphate groups of ADP.

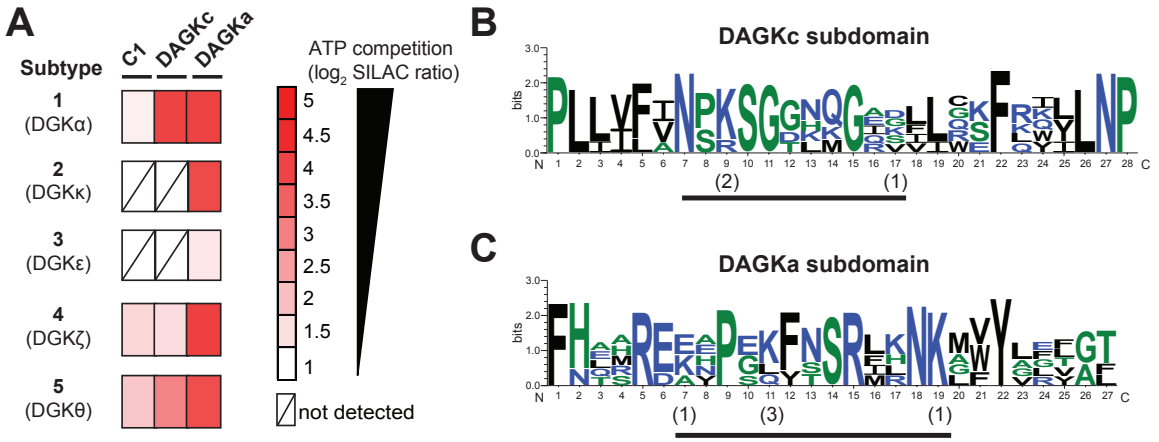

Figure 2.9 Chemical Proteomic Profiling of the DGK Superfamily **(A)** Heatmap showing SILAC ratios for probe binding sites of respective DGK isoforms in ATP (1 mM, 30 min) versus DMSO vehicle-treated recombinant HEK293T proteomes. DGK ATP binding sites are defined by *SR* > 5. **(B and C)** Sequence similarity of ATP binding sites of DGK isoforms measured by quantitative proteomics. Multiple sequence alignments of probe-modified peptides were performed using Clustal Omega, and results analyzed by sequence logos, to search for common motifs within the DAGKc **(B)** and DAGKa **(C)** ATP binding sites of DGKs. The height of each stack denotes sequence conservation at the respective position (measured in bits). The height of individual residues within the stack indicates the relative frequency of corresponding amino acids at that position. The numbers in parentheses indicate the number of DGKs that show modification at the respective probe-modified lysine. The color scheme for the amino acids in sequence logos is as follows: hydrophilic, blue; neutral, green; hydrophobic, black.

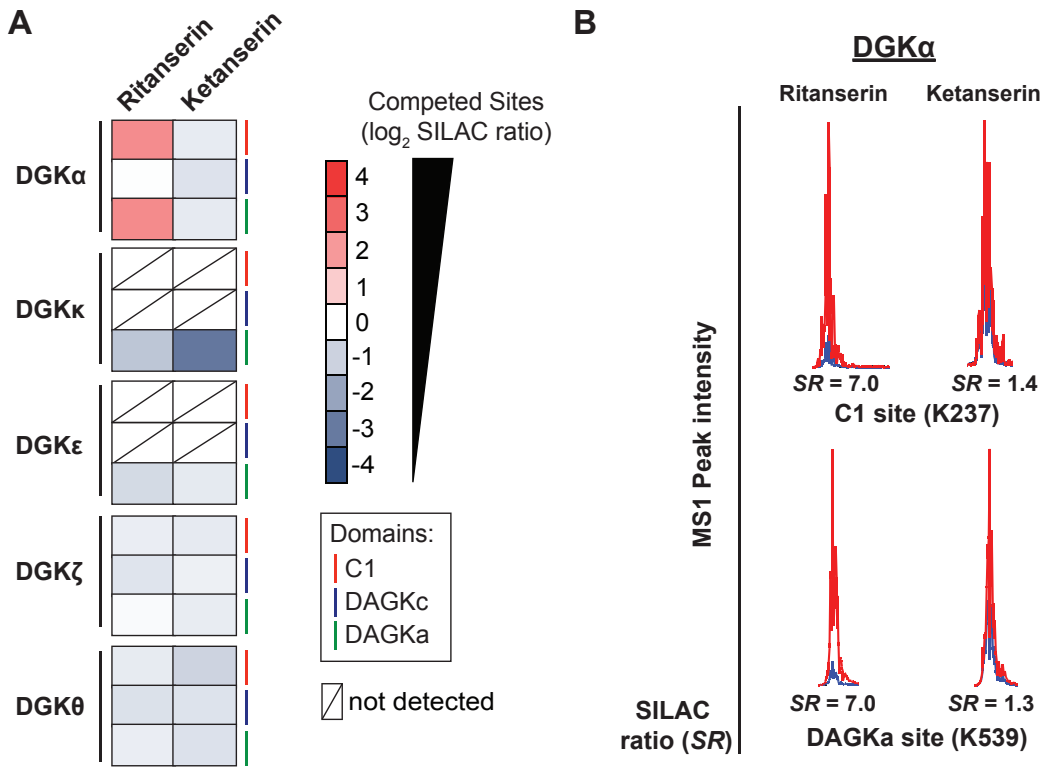

Figure 2.10 Inhibitor Profiling of the DGK Superfamily (A) Heatmap showing SILAC ratios of DGK probe binding sites that are competed (*SR* > 5) with ritanserin versus DMSO vehicle control-treated samples. Lack of competition at respective sites in ketanserin-treated samples indicates ritanserin competition was specific. **(B)** Representative extracted ion chromatograms (MS1) of probe-modified peptides from DGKα C1 and DAGKa domains, which represent the primary sites of binding for ritanserin. Ketanserin is inactive at these same sites. For all studies, proteomes were pretreated with compounds (100 mM) for 30 min prior to labeling with ATP acyl phosphate probe (10 mM, 30 min).

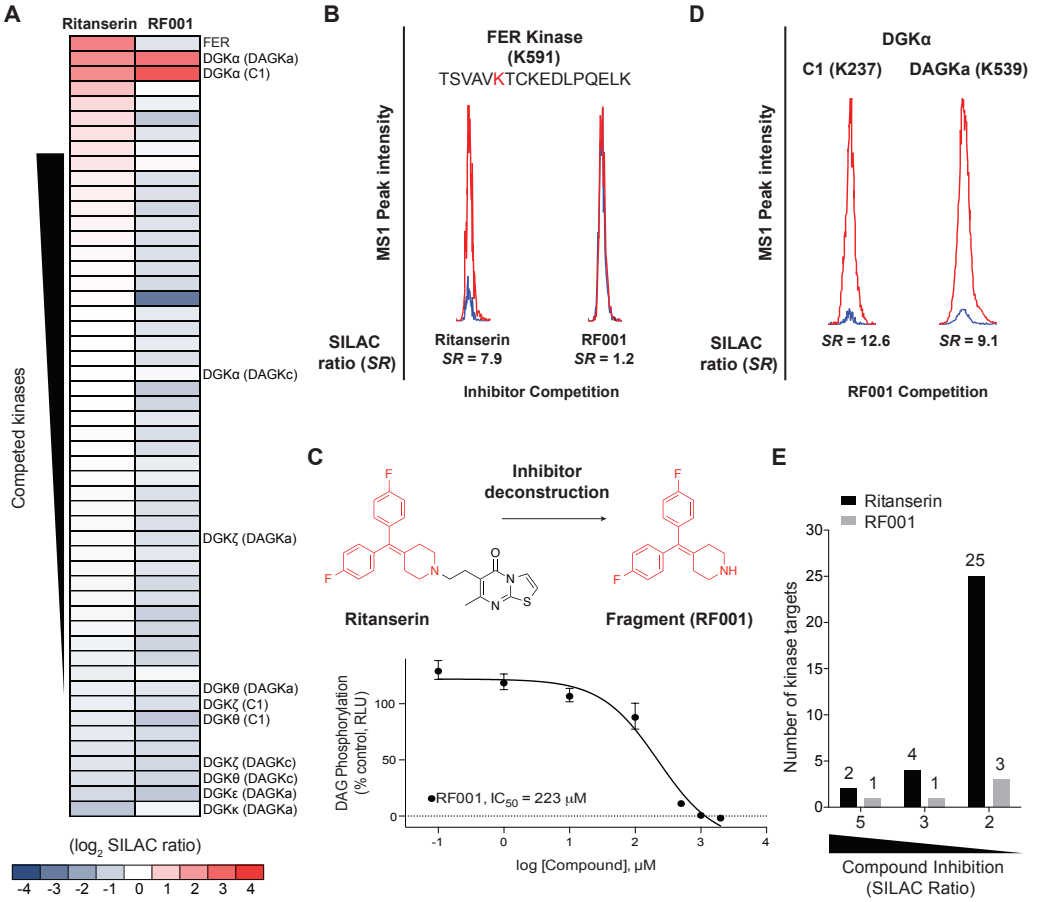

Figure 2.11 Discovery of a Lead Fragment Inhibitor of DGKα by Chemical Proteomics (A) Heatmap showing potency and selectivity of ritanserin and RF001 against recombinant DGKs and native kinases detected in HEK293T proteomes. **(B)** Representative extracted ion chromatograms (MS1) of probe-modified peptides from FER showing potent competition with ritanserin, but not RF001. **(C)** Ritanserin deconstruction to identify the fragment RF001, which shows concentration-dependent blockade of recombinant DGKα as measured by substrate assay (Figure 2.4). Data shown are mean ± SEM for triplicate measurements. Results are representative of two independent biological replicates; 95% confidence intervals for IC_{50} values: 120–414 mM. The dotted line represents background activity detected in non-transfected

HEK293T proteomes. **(D)** Representative extracted ion chromatograms (MS1) showing the primary sites of binding for RF001 against DGKα. Quantified SILAC ratios shown are averages of two biological replicates. **(E)** Bar graph comparing the total number of kinase targets (recombinant DGKs and native kinases in HEK293T proteomes) observed with potent ($SR \geq 5$), moderate ($SR \geq 3$), and weak competition ($SR \geq 2$) at respective probe binding sites in ritanserin- versus RF001-treated samples. For quantitative LC-MS experiments, proteomes were pretreated with compounds (100 mM) for 30 min prior to labeling with ATP acyl phosphate probe (10 mM, 30 min).

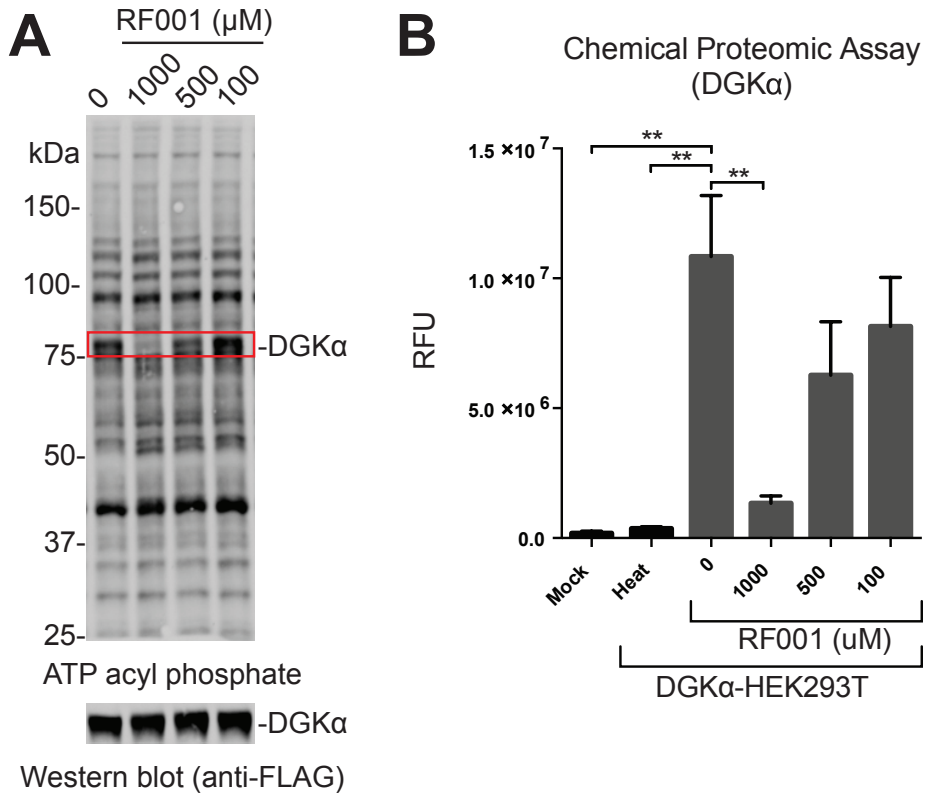

Figure 2.12 Chemical proteomic analysis of RF001 activity against recombinant DGKα in HEK293T proteomes. **(A)** DGKα-HEK293T soluble proteomes were pretreated with RF001 at the indicated concentrations for 30 min prior to labeling with ATP acyl phosphate probe (10 μM, 30 min). After probe labeling, proteomes were subjected to gel-based analyses as described in **Figure 2.6.** RF001 blocked probe labeling in a concentration-dependent manner and the decrease in fluorescence signals was not due to differences in recombinant protein expression as confirmed by western blot (bottom panel, anti-FLAG, 0.8 μg/mL). Integrated band intensities from these gel-based ATP acyl phosphate assays **(B)** were used to quantify DGKα inhibition by RF001. Mock-transfected and heat-denatured (95° C for 2 min) recombinant DGKα lysates were

included as additional controls. Data shown are mean +/- SEM. for three biological replicates. $^{**}P \leq 0.01$ for mock versus DGKα overexpressed group; $^{**}P \leq 0.01$ for vehicle-treated versus heat-denatured or inhibitor-treated DGKα overexpressed groups.

2.6 Acknowledgements

We thank Mark M. Ross and Adam Borne for assistance with experiments and manuscript preparation. We thank all members of the Hsu Lab and colleagues for review of the manuscript. This work was supported by the LaunchPad for Diabetes Program funded by the Manning Family Foundation at the University of Virginia (Dr. Ku-Lung Hsu), University of Virginia Start-up Funds (Dr. Ku-Lung Hsu), and the NIH (DA035864 to Dr. Ku-Lung Hsu; T32 GM007055 to Caroline Franks; T32 CA009109 to Dr. Sean Campbell; DK101946 to Dr. Thurl Harris; CA180699 and CA189524 to Dr. Benjamin Purow).

Author Contributions

Caroline Franks, Dr. Benjamin Purow, Dr. Thurl Harris and Dr. Ku-Lung Hsu conceived this study. Caroline Franks, Dr. Sean Campbell, and Dr. Ku-Lung Hsu coordinated and designed this study. Caroline Franks designed, conducted, and analyzed the experiments shown in Figures 2.3, 2.5, 2.6, 2.7, 2.9, 2.10, 2.11A, B, D, and E, 2.12A and Table 2.1. Dr. Sean Campbell designed, conducted, and analyzed the experiments shown in Figures 2.4, 2.11C, and 2.12B. The manuscript was drafted and edited by Caroline Franks, Dr. Sean Campbell, and Dr. Ku-Lung Hsu.

Chapter 3: Identification of the Structural Region of Ritanserin Mediating Off-Target Activity

Adapted with permission from Rebecca L. McCloud, Caroline E. Franks, Sean T. Campbell, Benjamin W. Purow, Thurl E. Harris, and Ku-Lung Hsu. *Biochemistry* 57, 231-236 (2018).

3.1 Abstract

Diacylglycerol kinases (DGKs) regulate lipid metabolism and cell signaling through ATP-dependent phosphorylation of diacylglycerol to biosynthesize phosphatidic acid. Selective chemical probes for studying DGKs are currently lacking and are needed to annotate isoform-specific functions of these elusive lipid kinases. Previously, we explored fragment-based approaches to discover a core fragment of DGK-α (DGKα) inhibitors responsible for selective binding to the DGKα active site. Here, we utilize quantitative chemical proteomics to deconstruct widely used DGKα inhibitors to identify structural regions mediating off-target activity. We tested the activity of a fragment (RLM001) derived from a nucleotide-like region found in the DGKα inhibitors R59022 and ritanserin and discovered that RLM001 mimics ATP in its ability to broadly compete at ATP- binding sites of DGKα as well as >60 native ATP-binding proteins (kinases and ATPases) detected in cell proteomes. Equipotent inhibition of activity-based probe labeling by RLM001 supports a contiguous ligand-binding site composed of C1, DAGKc, and DAGKa domains in the DGKα active site. Given the lack of available crystal structures of DGKs, our studies highlight the utility of chemical proteomics in revealing active-site features of lipid kinases to enable development of inhibitors with enhanced selectivity against the human proteome.

3.2 Introduction

Diacylglycerol kinases (DGKs) are members of the lipid kinase superfamily that catalyze phosphorylation of diacylglycerol (DAG) to generate phosphatidic acid (2-4) [PA (Figure 3.1A)]. Both DAG and PA serve as potent lipid messengers to shape cellular responses by altering the subcellular localization, activation, and function of essential receptor proteins (ranging from enzymes to transcription factors) (18, 84). DAG and PA also serve as building blocks for phospholipid and triglyceride biosynthesis and are integral to membrane architecture and bioenergetics(4). To date, 10 mammalian DGKs have been identified, and comparative analysis of primary sequences has classified individual isoforms into five principal subtypes (4) [types 1−5 (Figure 3.1B)]. Mammalian DGKs are composed of at least two cysteine-rich zinc finger-like motifs analogous to C1 domains found in protein kinase C (18) (PKC) and a C-terminal catalytic domain containing both a lipid kinase (DAGKc) and an accessory (DAGKa) subdomain (30). Individual isoforms are differentiated on the basis of protein regions with homology to domains known to mediate lipid, protein, and other small molecule interactions that are thought to control when and where DGKs are active (4). Thus, DGKs hold enormous potential as therapeutic targets because of their fundamental role in sculpting the lipidome to support metabolic, structural, and signaling demands of cells but currently lack selective chemical probes for exploiting their isoform-specific biology (39).

Recent studies have identified diacylglycerol kinase-α (DGKα) as a promising target for cancer immunotherapy because of its critical role in regulating lipid signaling necessary for proper T cell activation (30, 33, 34). T cell receptor signaling is mediated

by secondary messengers, including diacylglycerols (DAGs) that act as ligands to alter the subcellular localization and activation of key kinase proteins (e.g., Ras/Erk) that are essential for T cell activation (31). DGKα negatively regulates TCR signaling by phosphorylating DAG to terminate its signaling activity (129) (Figure 3.1A). Excessive DGKα activity (and thus attenuated DAG signaling) has been linked to defective T cell function. In the clinic, tumor-infiltrating lymphocytes (TILs) isolated from renal carcinoma patients showed an increased level of expression of DGKα, which correlated with impaired cytotoxic responses that could be reversed with nonselective DGKα inhibitors (103). Finally, DGKα inactivation in chimeric antigen receptor (CAR)-modified T cells (T cells genetically modified for tumor antigen specificity (130) enhances immune responses against tumors (131). Thus, development of highly selective DGKα inhibitors is a promising therapeutic strategy for reversing immunosuppressive metabolic pathways operating in the tumor microenvironment. The challenge with developing DGKα-selective inhibitors is this lipid kinase along with >500 other mammalian kinases (132) utilize ATP as a common substrate and targeting the canonical ATP-binding pocket will likely result in substantial off-target activity.

Previously, we initiated efforts to address the challenge of developing DGKα-selective inhibitors using chemical proteomics (76) and quantitative mass spectrometry (118, 119, 133). Specifically, we utilized ATP acyl phosphate activity-based probes (66, 67) (Figure 3.2A) to discover ligand-binding sites mediating substrate and inhibitor recognition of DGKα along with representative members from all five DGK subtypes (134). From these studies, we identified DAGKc/DAGKa as the primary ATP-binding

site of DGKα and the atypical C1 domain as a novel inhibitor-binding site of the dual DGKα/FER inhibitor ritanserin. We also discovered the DGKα lipid kinase inhibitory activity of ritanserin could be recapitulated by a fragment [RF001 (Figure 3.2B)] derived from a hydrophobic region of ritanserin with enhanced selectivity against protein kinases compared with that of the parent molecule (134). Our approach was necessary because crystal structures of mammalian DGKs are currently not available. Compared with conventional substrate assays using purified protein, our chemical proteomics strategy enabled rapid evaluation of compound potency against DGKs and selectivity against other kinase activities detected in the cell proteome. Notably, we used chemical proteomics to identify the site of binding and quantify inhibition at respective binding sites for DGK inhibitors, which is a challenging task using traditional profiling methods. Finally, chemical proteomic profiling of DGKs in cell proteomes permits analysis in more native environments to preserve functional conformations of lipid kinases. However, the structural region contributing to FER protein kinase off-target activity of ritanserin is unknown and critical for enabling fragment-based design of DGKα-selective inhibitors.

3.3 Materials and Methods

Cell Culture. HEK293T cells were cultured in HyClone Dulbecco's Modified Eagles Medium (without L-Glutamine, with L-glucose and sodium pyruvate) supplemented with 10% FBS (Omega Scientific, US Source Fetal Bovine Serum) and 1% L-Glutamine (200 mM, Gibco). SILAC HEK293T cells were cultured in Thermo Scientific Pierce DMEM Media for SILAC (minus L-Lysine and L-Arginine, with L-glutamine) supplemented with 10% dialyzed FBS (Omega Scientific, Dialyzed Fetal Bovine Serum), and either 'Light' L-Lysine and L-Arginine (100 µg/mL, Acros Organics) or 'Heavy' L-Lysine-$^{13}C_6$, $^{15}N_2$ and L-Arginine-$^{13}C_6$, $^{15}N_4$ (100 µg/mL, Sigma-Aldrich) for a minimum of five passages prior to use. Cell lines were grown at 37 °C under 5% CO_2.

Transient Transfection. Recombinant DGK proteins were produced in HEK293T cells by transient transfection of HEK293T cells with recombinant DNA. pcDNA3-FLAG-DGKA (rattus norvegicus) was kindly provided as a gift from Dr. Kevin Lynch (University of Virginia, School of Medicine). HEK293T cells were plated in 10 cm plates at a concentration of 400,000 cells in complete DMEM and grown to 50-60% confluency. A polyethyleneimine (PEI) stock solution was prepared (1 mg/mL, pH 7.4) and filter sterilized. Serum-free DMEM (600 µL) was mixed gently with 2.6 µg DNA and 20 µL of sterile PEI (1 mg/mL, pH 7.4) in a sterile microfuge tube. Mixtures were incubated for 30 min at 25°C. The mixture was added drop-wise to each 10 cm plate, rocked back and forth to mix, and placed back in the incubator. Cell pellets were harvested after two full days of growth, snap-frozen in liquid N_2, and stored at -80°C until use. Recombinant

proteins were produced by transient transfection in SILAC HEK293T cells using the procedure described above, except that cells were plated at a concentration of 1 x 10^6 cells per 10 cm plate and grown to ~70% confluency prior to introducing transfection mixture.

Western Blot Analysis of Recombinant Protein Expression. After harvesting cells, pellets were re-suspended and lysed (sonication; 3 x 1 sec pulse, 20% amplitude) in kinase buffer (Dulbecco's PBS (DPBS, Hyclone), 20mM $MgCl_2$, EDTA-free protease inhibitors (Pierce)). To separate membrane and soluble fractions, lysates were centrifuged at 100,000 x g for 45 minutes at 4°C. Recombinant protein expression was analyzed in both soluble and membrane fractions. Lysates (10 μg) were resolved by SDS-PAGE (4-20% polyacrylamide, TGX Stain-Free Mini Gel) at 150 V for 60 min. Gel transfers were performed using the Bio-Rad Trans-Blot Turbo RTA Midi Nitrocellulose Transfer Kit with a Bio-Rad Trans-Blot Turbo Transfer System (25V, 10 min). The nitrocellulose blot was incubated in blocking solution (30 mL, 3% BSA in TBS-T (150 mM NaCl, 25 mM Tris, .1% Tween-20 pH 7.4 in ddH_2O)) for 1 h at 25°C with gentle shaking. The blot was transferred immediately to primary antibody solution (1:1,000 anti-FLAG in TBS-T) and incubated overnight at 4°C with gentle shaking. The blot was subsequently rinsed 5 times for 5 min in TBS-T, transferred immediately into secondary antibody solution (1:10,000 anti-rabbit DyLight 550 in TBS-T), and incubated for 1 h at 25°C with gentle shaking. The blot was rinsed 5 times for 5 min in TBS-T, transferred into ddH_2O, and imaged by in-blot fluorescence scanning on a ChemiDoc MP Imaging System.

Preparation of Cell Lysates for Gel-Based Chemical Proteomics. Lysates were prepared as described previously (Chapter 2.3).

Gel-Based Chemical Proteomic Assay. Proteome concentration was adjusted to 2 mg/mL in kinase buffer. Proteomes were first pre-treated with compound (0.6 μL, 50X stock in DMSO) mixed with gentle flicking, and incubated for 30 min at 25°C in a microfuge tube (30 μL reaction volume). Desthiobiotin ATP acyl phosphate nucleotide probe (0.5 mM in ddH_2O) was added to each sample (0.6 μL, 10 μM final) and incubated for 30 min at 25°C. Reactions were quenched with 10 μL of 4X SDS-PAGE loading buffer. Protein samples (15 μL) were loaded onto 4-20% TGX Stain-Free Protein Midi Gel and resolved by SDS-PAGE at 150V for 55 min. Proteins were transferred to a nitrocellulose blot by Bio-Rad Trans-Blot Turbo Transfer System (25V, 10 min) to enhance sensitivity. The nitrocellulose blot was incubated in blocking solution (30 mL, 3% BSA in TBS-T) for 1 h at 25°C with gentle shaking. The blot was transferred immediately to antibody solution (30 mL, 5% BSA in ddH_2O with 0.1% Tween20 and 1:3000 Streptavidin DyLight 550) and incubated for 2 h at 25°C with gentle shaking. The blot was rinsed 5 times for 5 min in TBS-T, and transferred into ddH_2O. The blot was imaged by in-blot fluorescence scanning on a ChemiDoc MP Imaging System. Fluorescence intensity signals were normalized to total lane protein using the Bio-rad Stain Free imaging.

Preparation of cell lysates for ADP-glo assay. Cell lysates were prepared for substrate assay analysis as described previously (Chapter 2.3).

ADP-glo DAG phosphorylation substrate assay. The ADP-glo substrate assay was performed as described previously (Chapter 2.3) except 2 μL of DMSO/inhibitors was added to 18 μL of micelle/lysate mix for testing of RLM001 to account for poor solubility of this compound.

SILAC Sample Preparation for Quantitative LC-MS Analysis Using ATP Acyl Phosphates. Samples for LC-MS analysis were prepared and analyzed as described previously (Chapter 2.3). Data shown in Figure 3.7 and Table 3.1 represent median values from two biological replicates and two technical replicates of each biological replicate. Median peptide ratios from experimental data (compound treated) were normalized to the median DMSO peptide ratio to account for potential variations in mixing and sample preparations.

Statistical Analysis and Determination of IC_{50} Values. The percentage of enzyme activity remaining was determined by comparing integrated band intensities or luminescence of inhibitor- with DMSO-treated samples for gel-based chemical proteomic or ADP-glo assays, respectively. For chemical proteomic methods, nonlinear regression analysis was used to determine the IC_{50} values from a dose-response curve generated using GraphPad Prism. Values are shown as mean ± SEM. For ADP-glo assay data,

determination of significance for treatment with ritanserin, ketanserin, and R59022 was performed by one-way ANOVA with comparison to signal from vehicle treated lysates (DMSO). IC_{50} values for RLM001 competition at individual active site peptides were determined using RLM001/DMSO (heavy/light) SILAC ratios to calculate percent of control. Nonlinear regression was used to determine the IC_{50} values from a dose-response curve generated using GraphPad Prism. Values were normalized to 0% and 100% for the smallest and largest mean values, respectively. Values are shown as mean ± SEM. All statistical analyses were performed using GraphPad Prism.

3.4 Results

3.4.1 *Fragment Based Deconstruction of Ritanserin Yields RLM001*

In this report, our studies began with examination of chemical structures of commonly used DGKα inhibitors to identify a thiazolopyrimidinone region (Figure 3.3) common in ritanserin and R59022 (37, 41, 43). The resemblance of this heterocycle to the adenine portion of ATP led us to hypothesize its role in mediating protein kinase off-target activity observed with ritanserin (134). We tested a fragment [designated as RLM001 (Figure 3.2B)] derived from this region for both DGKα and general kinase inhibitory activity using competitive gel-based chemical proteomics (Figure 3.4). First, we overexpressed recombinant DGKα in HEK293T cells, validated protein expression by Western blot (Figure 3.5A), and confirmed recombinant DGKα activity in soluble proteomes using our previously described DAG phosphorylation substrate assay (134). We observed significantly higher DAG phosphorylation activity in DGKα-overexpressed versus mock-transfected soluble proteomes (Figure 3.5B). The specificity of recombinant DGKα activity was confirmed by demonstrating blockade of catalytic activity with both ritanserin and R59022 but not the negative control compound ketanserin (43, 134) (Figure 3.5B).

3.4.2 *Chemical Proteomics Reveals RLM001 Site of Binding*

Next, we used ATP acyl phosphates as activity-based probes to evaluate the activity of RLM001 against recombinant DGKα. ATP acyl phosphate probes enable global profiling of kinase activities by covalent attachment of reporter tags [desthiobiotin (Figure 3.2A)] to conserved lysine residues in the ATP-binding site, (66, 67) and we

recently adapted this probe for chemical proteomic profiling of DGKs (134). Using conditions optimized previously for fragment screening (134), we tested the potency and selectivity of RLM001 directly in recombinant DGKα-HEK293T soluble proteomes by chemical proteomics (Figure 3.4A). In brief, DGKα-HEK293T soluble proteomes were pretreated with varying concentrations of RLM001 (0.15−10 mM) followed by reaction with the ATP acyl phosphate probe, desthiobiotin-modified proteins separated by sodium dodecyl sulfate−polyacrylamide gel electrophoresis and transferred to a nitrocellulose membrane, and probe-modified proteins detected using a fluorescently labeled streptavidin (Figure 3.4B). Pretreatment with RLM001 resulted in concentration-dependent blockade of DGKα probe labeling as measured by the decreasing magnitudes of the fluorescent protein signals (IC_{50} = 4 mM, 95% confidence interval of 2−11 mM; Figure 3.4C). We also confirmed that potency values determined by chemical proteomics matched those measured using conventional DAG phosphorylation substrate assays (IC_{50} = 3 mM, 95% confidence interval of 1−19 mM; Figure 3.4D). These results support a role for the thiazolopyrimidinone group in mediating inhibitory activity of ritanserin and R59022 against DGKα (Figure 3.5B). Surprisingly, we also observed global decreases in the magnitudes of fluorescent protein signals in HEK293T soluble proteomes with RLM001 treatments, especially at the higher concentrations (Figure 3.4B). Our results suggest RLM001 is broadly competing at ATP-binding sites of kinases as well as other ATP-binding proteins detected in cell proteomes. To test this concept, we directly compared the selectivity of RLM001 with free ATP to evaluate whether the former fragment mimics the latter kinase substrate in binding activity. The inhibition

profiles of RLM001 (5 mM) and free ATP (1 mM) were indistinguishable with the exception of a handful of fluorescent protein bands that showed mild differences in competition (Figure 3.4B). We tested the selectivity of RLM001 at concentrations substantially higher than those of free ATP because low-molecular weight fragments such as RLM001 (196.18 Da) typically exhibit binding affinities in the millimolar range (124). Next, we implemented a liquid chromatography−mass spectrometry (LC−MS) quantitative chemical proteomic assay to discover RLM001-binding site(s) of DGKα (134) (Figure 3.6). For these LC−MS studies, quantitation was enabled by stable isotope labeling with amino acids in cell culture (SILAC (113); Figure 3.6). In brief, recombinant DGKα was overexpressed in isotopically light and heavy amino acid-labeled HEK293T cells. Light and heavy DGKα-HEK293T lysates were treated differentially with dimethyl sulfoxide (DMSO) vehicle and RLM001 (10 mM), respectively, prior to addition of ATP acyl phosphate to label active-site lysines. After probe labeling, light and heavy proteomes were combined and digested with trypsin, and desthiobiotin-modified peptides were enriched by avidin affinity chromatography and analyzed by LC−MS/MS to identify and quantify isotopically labeled active-site peptides from DGKα as previously described (134) and depicted in Figure 3.6. Probe-modified peptides showing a high level of competition, as judged by SILAC ratios (SR), were identified as RLM001-binding sites in DMSO/RLM001 comparisons (SR > 5; Figure 3.7A and Table 3.1). We used these criteria to discover that all three probe-binding sites previously identified in DGKα active sites (134) were highly sensitive to RLM001 competition at the highest concentration tested (10 mM): C1 (K237; SR > 20), DAGKc (K377; SR>20), and

DAGKa (K539, SR>20; Figure 3.8 and Table 3.1). We compared inhibition profiles of RLM001 directly with those of free ATP to determine whether these compounds bind at the same sites. Both RLM001 and ATP showed near-complete blockade of probe labeling at the primary ATP-binding sites (DAGKc/DAGKa) of DGKα (Figure 3.8). In contrast, RLM001 (SR > 20) strongly competed with the C1-binding site but ATP did not (SR ~ 2; Figure 3.8). We also performed a RLM001 dose−response study to determine whether RLM001 inhibits all three DGKα active-site peptides with equal affinity. These studies would allow us to determine whether C1, DAGKc, and DAGKa domains form a contiguous binding site for RLM001 or whether distinct binding sites exist. As shown in Figure 3.7B, pretreatment with RLM001 resulted in the equipotent blockade of all three DGKα active-site peptides (IC_{50} ~ 1−3 mM across C1, DAGKc, and DAGKa sites; Figure 3.7B). Collectively, our results provide the first evidence that C1, DAGKc, and DAGKa form a connected ligand-binding site that mediates interactions with the thiazolopyrimidinone region of ritanserin. Our gel-based findings provided initial evidence that RLM001 is broadly competing at ATP-binding sites across the kinome, but target identification and site of binding information are needed to validate this hypothesis. We used quantitative chemical proteomics (Figure 3.6) to demonstrate that RLM001 competes at ATP-binding sites of ~60 native kinases quantified in HEK293T soluble proteomes (Figure 3.7A). All probe-modified peptides from native kinases reported in Figure 3.7 and Table 3.1 were manually inspected for quality control as previously described (134). Native kinase targets of RLM001 were identified by active-site peptides showing SILAC ratios of ≥5. We discovered that inhibition profiles of

kinase active-site peptides from RLM001- versus ATP-treated samples were largely indistinguishable (Figure 3.7A), matching the results from our gel-based chemical proteomics (Figure 3.4B). Closer inspection of individual active-site peptides from several example protein kinases, including BRAF and MAP2K1/2 (also known as MEK1/2), which are critical kinase regulators of oncogenic signaling (135), clearly demonstrates the ability of RLM001 to compete efficiently at respective ATP-binding sites (for BRAF and K578, SR > 20, Figure 3.7C; for MAP2K1, K192/MAP2K2, and K196, SR > 20, Figure 3.9). Globally, this trend is recapitulated across ~90% of kinases detected in HEK293T soluble proteomes in our LC−MS analyses (Figure 3.7A and Table 3.1).

3.4.3 *RLM001 Functions as a General Ligand for ATP-Binding Pockets*

We also performed dose−response studies to determine whether specific classes of protein kinases show differences in sensitivity to RLM001 competition at respective active sites. For these studies, we chose to evaluate a representative member from the TKL (BRAF), CMGC (CDK5), CAMK (CHK2), TK (CSK), AGC (KS6A1), and STE (M3K2) protein kinase classes (132). We found that all protein kinases tested showed comparable sensitivity to RLM001 competition at respective ATP-binding sites with potency (IC_{50}) values ranging from 1 to 3 mM (Figure 3.7D). We also tested whether RLM001 can compete at active sites of ATPases (126) (heat shock proteins (HSPs); Figure 3.7C). We found that both ATP and RLM001 can compete at ATP- binding pockets of HSP90 (HSP90α, K112/HSP90β, K107; for ATP, SR > 20; for RLM001, SR > 20) and HSP70 proteins (HSP70-1A, K56/HSP70-1B, K56; for ATP, SR = 5.2; for

RLM001, SR = 19.1; Figure 3.7C and Table 3.1). We performed dose−response studies to determine whether HSPs show differences in sensitivity to RLM001 treatments and found that potency values were comparable between HSP90 (IC_{50} = 2.8 271 mM, 95% confidence interval of 1.9−4.1 mM) and HSP70 (IC_{50} = 1.0 mM, 95% confidence interval of 0.4−2.5 mM; Figure 3.7E). Collectively, the comparable potency of RLM001 against kinases and ATPases supports this compound as a general ligand for ATP-binding pockets. Interestingly, not all protein kinase active sites show equivalent sensitivity to RLM001 and ATP competition. For example, we discovered that RLM001 treatments do not completely block probe labeling of MARK1/2 ATP-binding sites (MARK1, K89/MARK2, K82, SR = 4.1; Figure 3.9). The functional implications of this differential sensitivity are not clear but could provide interesting insights into MARK1/2 function, which are implicated in phosphorylating microtubule- associated proteins, including Tau (136). In summary, our results demonstrate that the RLM001 fragment broadly competes at ATP-binding sites, supporting our hypothesis that the RLM001 region of ritanserin contributes to off-target activity.

3.5 Discussion

DGKs are responsible for balancing intracellular levels of DAG and PA lipids at the interface of membrane architecture, bioenergetics, and cellular signaling (2-4). How these complex tasks are accomplished through the metabolic activity of 10 mammalian DGK isoforms is currently unknown and being explored. Development of isoform-selective inhibitors would greatly advance our ability to probe the function of these lipid kinases in vivo. Here, we have taken important steps to address this challenge by deconstructing known DGK inhibitors to identify structural regions contributing to on- versus off-target activity. We hypothesized that the thiazolopyrimidinone region of widely used DGKα inhibitors contributes to protein kinase off-target activity based on the structural resemblance to the nucleotide portion of ATP. We tested our hypothesis by using quantitative chemical proteomics to demonstrate that a fragment (RLM001) derived from both ritanserin and R59022 mimics ATP in its ability to bind active sites of DGKα as well as >60 ATP-binding proteins, including protein kinases and ATPases detected in cell proteomes. Our studies also provide the first evidence that the C1, DAGKc, and DAGKa domains of DGKα form a contiguous binding site for ligands such as RLM001. Given the emerging role of DGKα for immuno-oncology (30, 33, 34, 103, 131), we believe our findings will guide future development of DGKα inhibitors with enhanced selectivity against the human proteome to mitigate potential toxicity associated with off-target activity. While RLM001 is likely a poor candidate for developing selective lipid kinase inhibitors, this fragment has attractive features as a starting point for developing an activity-based probe, including broad reactivity at ATP-binding sites of kinases and

other ATP-binding proteins (e.g., ATPases). We envision the incorporation of electrophilic groups into the RLM001 scaffold to mediate covalent reaction with nucleophilic residues (e.g., cysteine and/or lysines) in ATP-binding pockets for live cell activity-based profiling studies. Inclusion of an alkyne handle will facilitate downstream detection of direct protein targets of RLM001 activity-based probes. Furthermore, conversion of RLM001 from a reversible fragment to a covalent activity-based probe should help mitigate the poor potency observed with the parent molecule by taking advantage of the non-equilibrium binding mechanism of covalent compounds to lower the required concentration needed for activity (137).

Kinase name	Peptide	Labeling site	Uniprot Accession	ATP	RLM001
Recombinant DGKs					
DGKA	QGLSCNLCKYIVHDHCAMK	C1	P51556	1.6	>20
DGKA	IEPVSNTHPLLVFINPKSGGK	DAGKc	P51556	>20	>20
DGKA	YPEKFNSR	DAGKa	P51556	16.4	>20
Native kinases in HEK293T					
LATS1	ALYATKTLR	Lys1	O95835	>20	>20
AAPK1	DLKPENVLLDAHMNAK	Lys2	Q13131	>20	>20
AAPK1	VAVKILNR	Lys1	Q13131	>20	>20
AAPK2	DLKPENVLLDAHMNAK	Lys2	P54646	>20	>20
AAPK2	VAVKILNR	Lys1	P54646	>20	>20
BRAF	DLKSNNIFLHEDLTVK	Lys2	P15056	14.4	>20
CDK1	DLKPQNLLIDDKGTIK	Lys2	P06493	12.1	10
CDK5	DLKPQNLLINR	Lys2	Q00535	15	>20
CDK5	NRETHEIVALKR	Lys1	Q00535	12.4	>20
CHK2	VAIKIISK	Lys1	O96017	12.4	>20
CSK	VSDFGLTKEASSTQDTGKLPVK	Activation Loop	P41240	>20	>20
E2AK2	DLKPSNIFLVDTK	Lys2	P19525	18.6	>20
FER	TSVAVKTCKEDLPQELK	Lys1	P16591	>20	>20

GWL	LYAVKVVK	Lys1	Q96GX5	>20	>20
ILK	ISMADVKFSFQCPGR	Protein Kinase Domain	Q13418	>20	>20
KCC1A	LVAIKCIAK	Lys1	Q14012	>20	>20
KCC1D	LFAVKCIPK	Lys1	Q8IU85	>20	15.6
KS6A1	DLKPENILLDEEGHIK	Lys2	Q15418	13.8	>20
KS6A2	DLKPENILLDEEGHIK	Lys2	Q15349	13.8	>20
KS6A3	DLKPENILLDEEGHIK	Lys2	P51812	13.8	>20
KS6B1	DLKPENIMLNHQGHVK	Lys2	P23443	>20	>20
KS6B2	DLKPENIMLSSQGHIK	Lys2	Q9UBS0	17.5	16.8
M3K2	DIKGANILR	Lys2	Q9Y2U5	>20	>20
M3K3	DIKGANILR	Lys2	Q99759	>20	>20
M4K3	DIKGANILLTDNGHVK	Lys2	Q8IVH8	>20	>20
M4K4	DIKGQNVLLTENAEVK	Lys2	O95819	16.3	19.6
M4K5	DIKGANILLTDHGDVK	Lys2	Q9Y4K4	>20	>20
M4K5	NVHTGELAAVKIIK	Lys1	Q9Y4K4	>20	>20
MARK1	EVAVKIIDK	Lys1	Q9P0L2	>20	4.1
MARK2	EVAVKIIDK	Lys1	Q7KZI7	>20	4.1
MINK1	DIKGQNVLLTENAEVK	Lys2	Q8N4C8	16.3	19.6

MP2K1	DVKPSNILVNSR	Lys2	Q02750	>20	>20
MP2K1	KLIHLEIKPAIR	Lys1	Q02750	>20	>20
MP2K2	DVKPSNILVNSR	Lys2	P36507	>20	>20
MP2K2	KLIHLEIKPAIR	Lys1	P36507	>20	>20
MP2K3	DVKPSNVLINK	Lys2	P46734	>20	>20
MP2K4	DIKPSNILLDR	Lys2	P45985	>20	>20
MP2K4	MVHKPSGQIMAVKR	Lys1	P45985	>20	>20
MP2K6	DVKPSNVLINALGQVK	Lys2	P52564	8.1	>20
MP2K6	HVPSGQIMAVKR	Lys1	P52564	>20	>20
NEK9	LGDYGLAKK	Activation Loop	Q8TD19	6.3	14.6
PAN3	VMDPTKILITGK	ATP	Q58A45	>20	>20
PI42A	AYSKIK	PIPK Domain	P48426	8.3	>20
PI42B	AYSKIK	PIPK Domain	P78356	8.3	>20
PI4KB	VPHTQAVVLNSKDK	ATP	Q9UBF8	11.4	>20
PLK1	CFEISDADTKEVFAGKIVPK	Lys1	P53350	13.8	12.6
PRKDC	GHDEREHPFLVKGGEDLR	PI3K/PI4K Domain	P78527	>20	>20
SGK3	FYAVKVLQK	Lys1	Q96BR1	9.1	>20
SMG1	DTVTIHSVGGTITILPTKTKPK	ATP	Q96Q15	>20	>20

ST38L	KDTGHIYAMKILR	ATP	Q9Y2H1	7	>20
STK24	DIKAANVLLSEHGEVK	Lys2	Q9Y6E0	>20	>20
STK3	DIKAGNILLNTEGHAK	Lys2	Q13188	>20	>20
STK4	DIKAGNILLNTEGHAK	Lys2	Q13043	>20	>20
TLK2	YVAVKIHQLNK	Lys1	Q86UE8	>20	>20
TNIK	DIKGQNVLLTENAEVK	Lys2	Q9UKE5	16.3	19.6
ULK3	EVVAIKCVAK	Lys1	Q6PHR2	>20	>20
ULK3	NISHLDLKPQNILLSSLEKPHLK	Lys2	Q6PHR2	>20	13.3

Table 3.1 SILAC Ratios of Peptides Detected by ATP Acyl Phosphate Probe. Peptides shared by multiple kinases are shown to match data in Figure 3.7. All data were manually integrated to verify accuracy. Complete inhibition of heavy peptides (singletons) with compound treatments are shown as SILAC ratios >20.

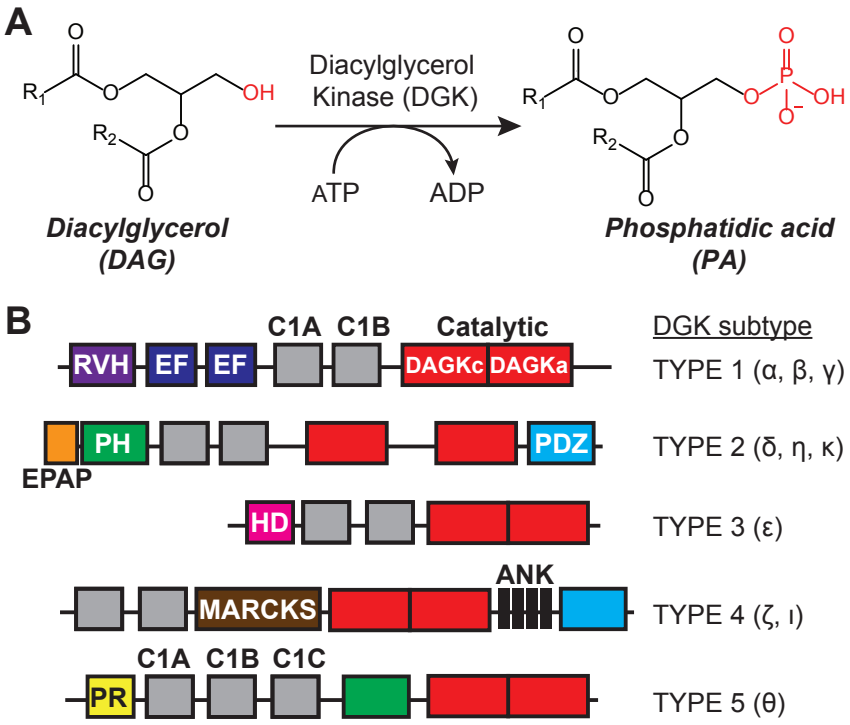

Figure 3.1 Diacylglycerol kinase superfamily. (A) Diacylglycerol kinase enzymes (DGKs) catalyze the conversion of diacylglycerol to produce phosphatidic acid. **(B)** Ten mammalian isoforms of DGKs classified into five subtypes based on structural motifs. RVH: recoverin homology domain, EF: EF hands motif, C1: atypical/typical C1 domain, EPAP: Glu-Pro-Ala-Pro repeats, PDZ: protein-protein interactions, HD: hydrophobic domain, MARCKS: myristoylated alanine-rich C-kinase substrate domain, ANK: Ankyrin repeats, PR:proline-rich region.

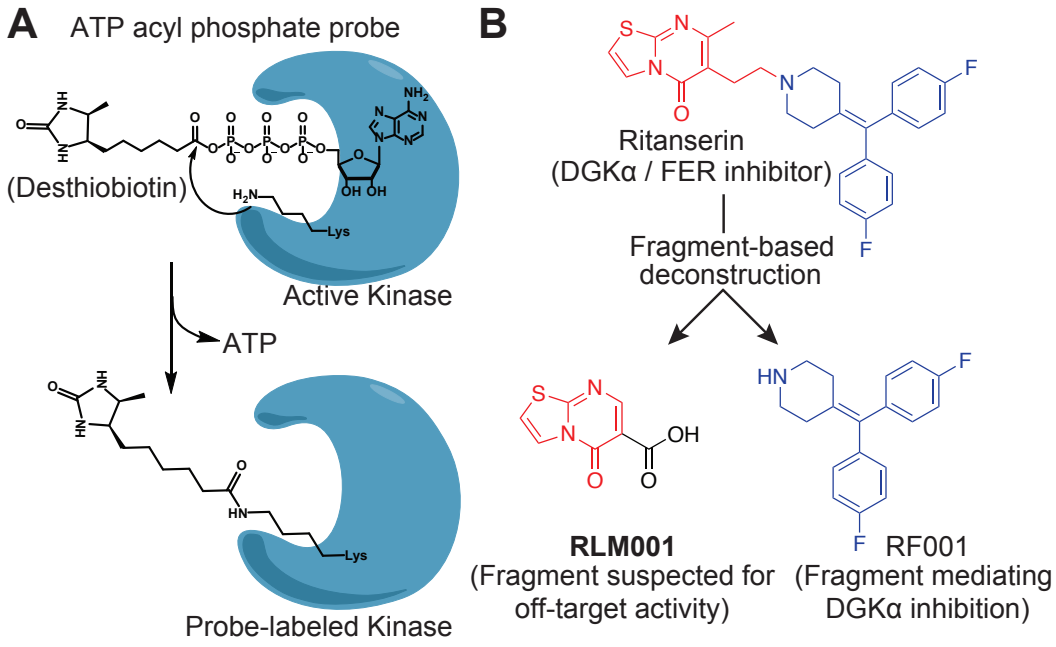

Figure 3.2 Evaluating the activity of DGKα inhibitor fragments using kinase activity-based probes. (A) Mechanism for ATP acyl phosphate probe reaction. The nucleophilic ε-amine group of lysine side chains attacks the acyl phosphate, resulting in covalent modification of kinase active sites with a desthiobiotin tag for downstream detection via gel- or mass spectrometry-based readouts. **(B)** Ritanserin is a dual DGKα/FER kinase inhibitor that is deconstructed to evaluate the resulting fragments for lipid vs protein kinase activity. RF001 was previously shown to mediate selective inactivation of the lipid kinase DGKα (134). This study will test whether RLM001 mediates general off-target activity of ritanserin against ATP-binding sites.

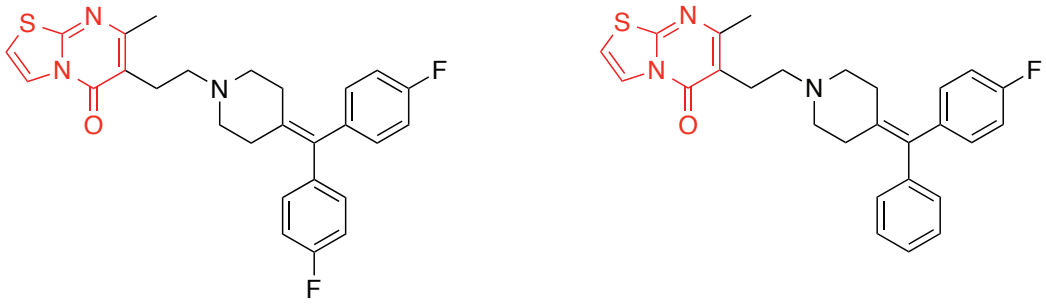

Ritanserin **R59022**

Figure 3.3. Structures of ritanserin and R59022. Both compounds have been widely used as DGKα inhibitors and contain the thiazolopyrimidinone fragment region (highlighted in red) tested in this study.

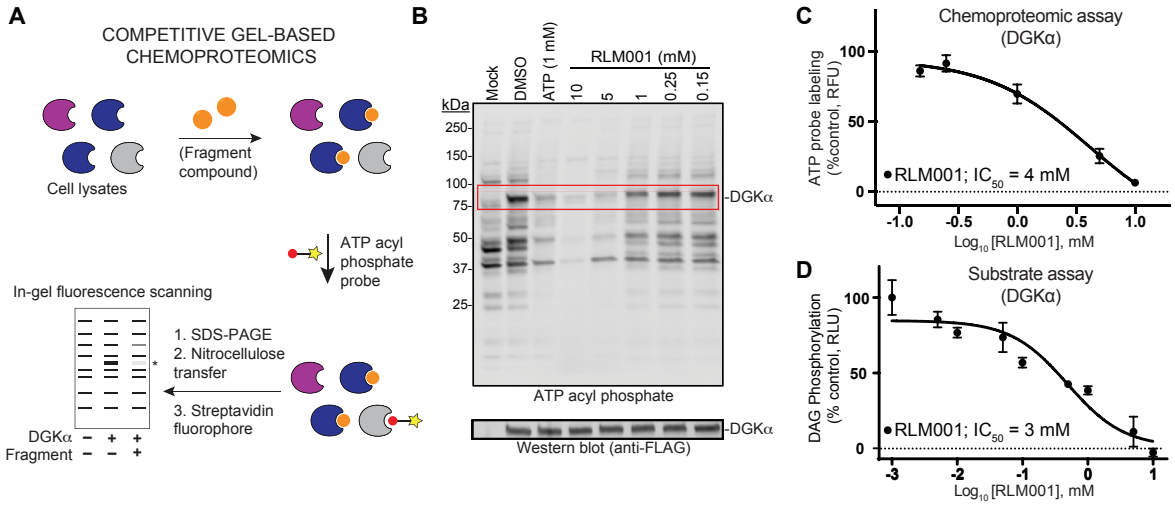

Figure 3.4. Gel-based chemical proteomics for evaluating the potency and selectivity of RLM001. (A) Schematic of competitive gel-based chemical proteomics using ATP acyl phosphates to screen fragments for kinase binding activity. **(B)** Gel-based ATP acyl phosphate assay used to determine in vitro IC_{50} values for DGKα inhibition by RLM001 (10, 5, 1, 0.25, and 0.15 mM). Western blot analysis (anti-FLAG, 0.8 mg/mL) confirmed equivalent recombinant DGKα expression across treatment conditions. **(C)** Dose-response curve of the gel-based ATP acyl phosphate assay to determine RLM001 potency (IC_{50}). Data are means ± the standard error of the mean for five biological replicates; 95% confidence intervals for IC50 values of 2–11 mM**. (D)** Dose–response curve of the DAG phosphorylation substrate assay to determine RLM001 potency (IC_{50}). Data are means ± the standard error of the mean for two biological replicates; 95% confidence intervals for IC_{50} values of 1–19 mM.

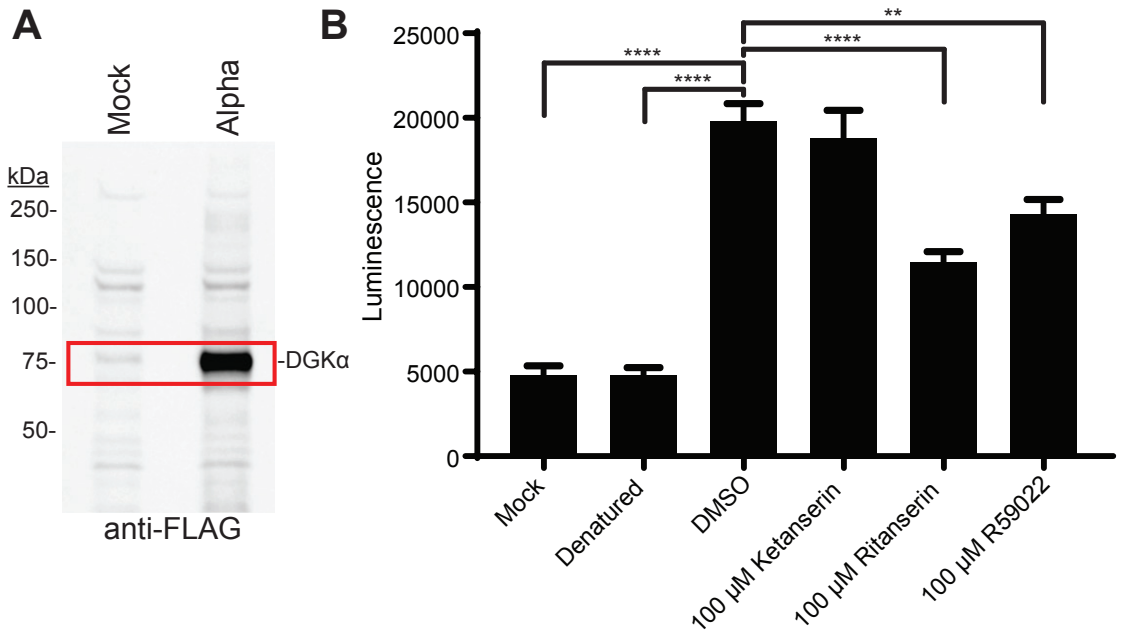

Figure 3.5 Analysis of DGKα. (A) Western blot showing overexpression of FLAG-tagged DGKα enzyme. **(B)** Activity of DGKα overexpressed lysates against vehicle (DMSO), known DGK inhibitors (ritanserin, R59022), or negative control compounds (ketanserin). Data are from three independent biological replicates. Significance is determined in comparison with DMSO control. * $P \leq 0.05$, ** $P \leq 0.01$, *** $P \leq .001$, and **** $P \leq 0.0001$.

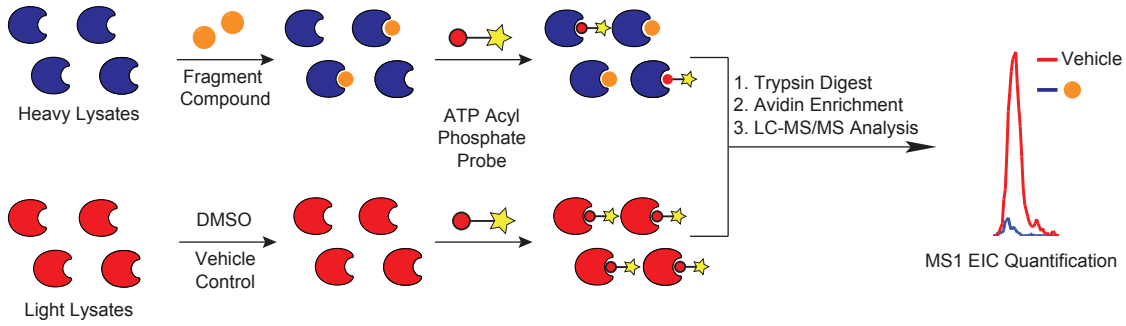

Figure 3.6 Schematic of quantitative chemoproteomic LC-MS/MS analysis. Isotopically heavy lysates are pre-treated with fragment compound while light counterparts receive DMSO vehicle. After incubation with ATP acyl phosphate probe, heavy and light lysates are subsequently mixed, and undergo trypsin digestion. Avidin affinity chromatography enriches probe-labeled peptides for LC-MS/MS experiments. Extracted ion chromatographs (EICs) obtained from MS1 spectra are integrated to quantify differential enrichment and thus kinase activity between heavy and light samples.

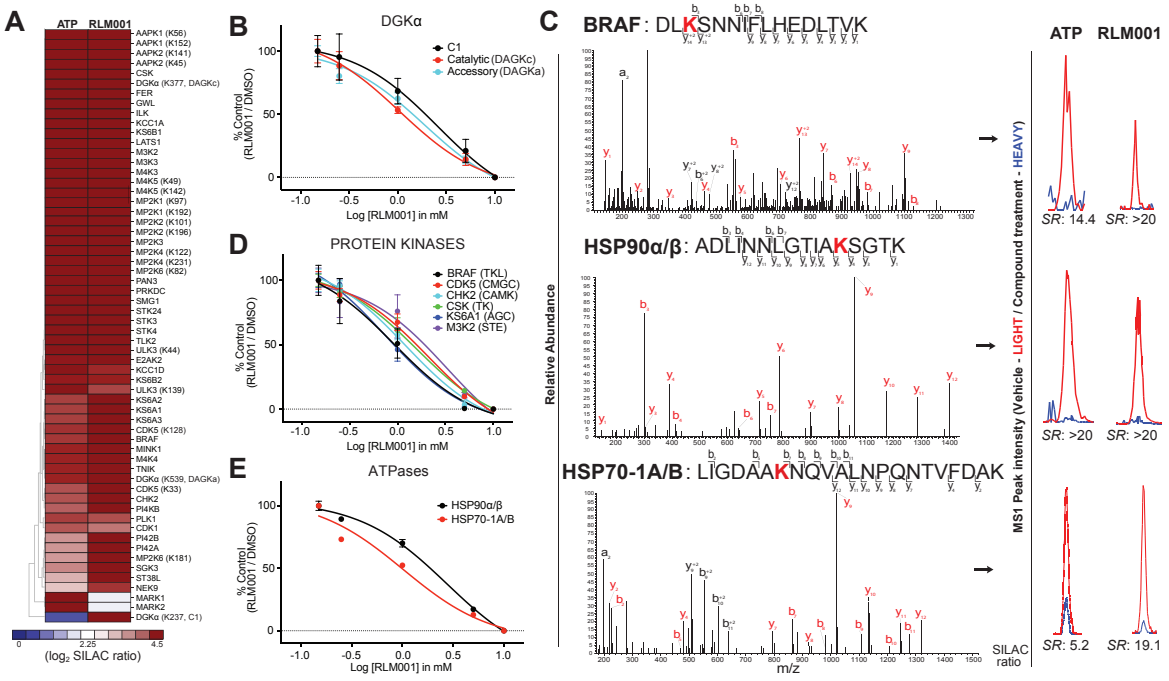

Figure 3.7 Identification of RLM001-binding sites by quantitative chemical proteomics. (A) Heat map showing the potency and selectivity of ATP (1 mM) and RLM001 (10 mM) against recombinant DGKα and native kinases detected in HEK293T proteomes. Kinases containing mutiple probe-binding sites are differentiated by unique lysine-modified positions shown in parentheses. Peptide ratios for the heat map shown are listed in Table S1. **(B)** Dose–response curves to determine the potency (IC50) of RLM001 at DGKα active-site peptides: C1, IC50 = 2.6 mM, 95% confidence interval (CI) of 0.5–13.7 mM; DAGKc, IC50 = 1.1 mM, 95% CI of 0.4–2.6 mM; DAGKa, IC50 = 1.9 mM, 95% CI of 0.9–3.8 mM. **(C)** MS2 spectra (left) of probe-modified peptides corresponding to BRAF, HSP90α/β, and HSP70-1A/B. Major b- and y-ions produced by fragmentation of the precursor peptide ion (MS1) are indicated on the spectrum in red. Probe-modified lysines are indicated in red on the peptide sequence. MS1-extracted ion

chromatograms (right) of probe-modified peptides with corresponding SILAC ratios quantifying vehicle (light) or compound treatment (heavy). MS1 peptides for BRAF, HSP90α/β, and HSP70-1A/B are all potently inhibited by both ATP (1 mM) and RLM001 (10 mM) as defined by SR > 5. **(D)** Dose–response curves to determine the potency of RLM001 against members of different protein classes: BRAF, IC50 = 0.9 mM, 95% CI of 0.2–3.8 mM; CDK5, IC50 = 2.1 mM, 95% CI of 1.1–4.2 mM; CHK2, IC50 = 1.2 mM, 95% CI of 0.7–2.2 mM; CSK, IC50 = 1.6 mM, 95% CI of 0.8–3.3 mM; KS6A1, IC50= 0.8 mM, 95% CI of 0.4–1.4 mM; M3K2, IC50 = 3.3 mM, 95% CI of 0.8–14 mM. **(E)** Dose–response curves to determine the potency of RLM001 against ATPases: HSP90α/β, IC50 = 2.8 mM, 95% CI of 1.9–4.1 mM; HSP70-1A/B, IC50 = 1.0 mM, 95% CI of 0.4–2.5 mM.

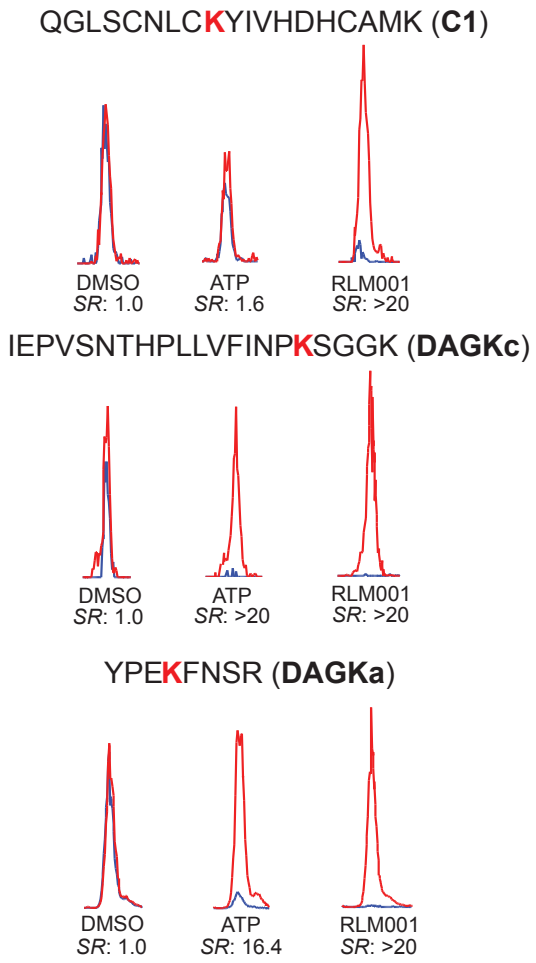

Figure 3.8. MS1-extracted ion chromatograms of probe-modified peptides corresponding to the active site of DGKα with corresponding SILAC ratios quantifying vehicle-treated (light, in red) or compound-treated (heavy, in blue). **Top:** Peptide corresponding to the C1 domain sensitive mildly inhibited by ATP (1 mM) and inhibited by RLM001 (10 mM). **Middle:** Peptide corresponding to the DAGKc domain inhibited by ATP (1 mM) and RLM001 (10 mM). **Bottom:** Peptide corresponding to the DAGKa domain inhibited by ATP (1 mM) and RLM001 (10 mM).

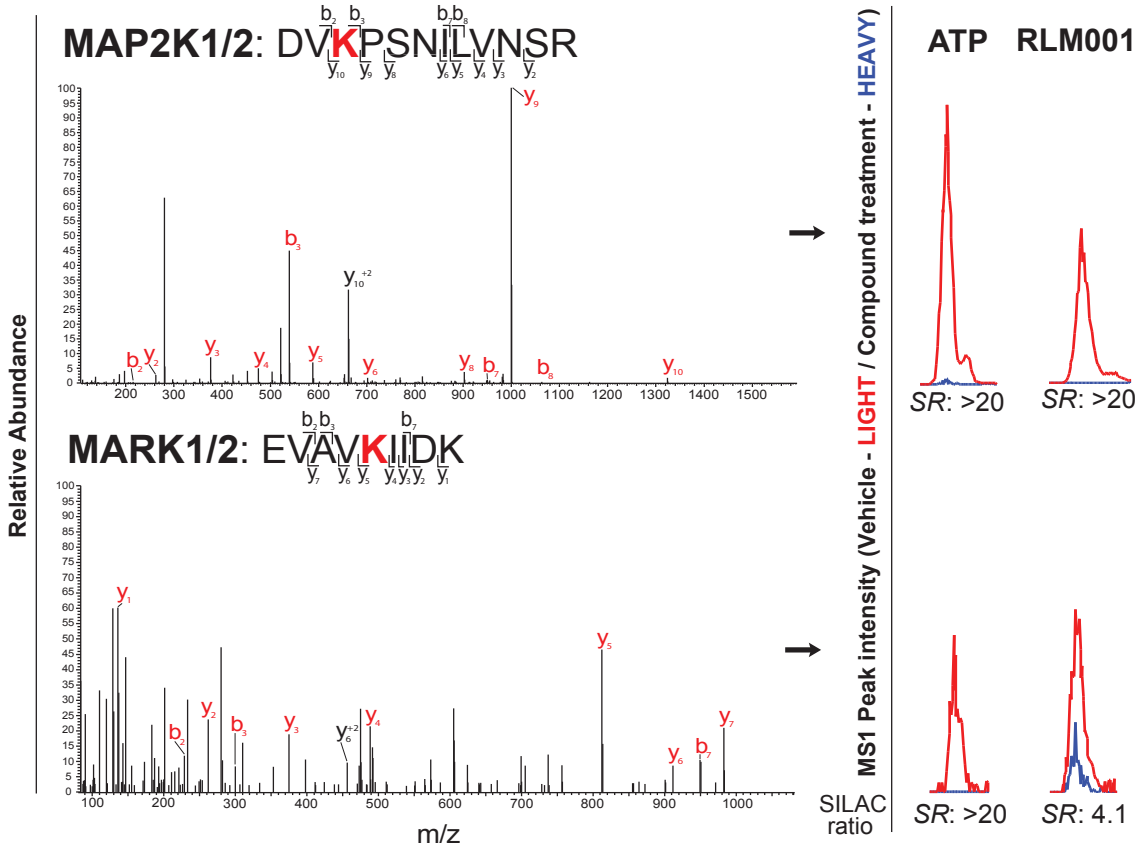

Figure 3.9. MS2 spectra of probe-modified peptides corresponding to MAP2K1/2, and MARK1/2. Major b- and y-ion fragments derived from neutral losses of the precursor (M) are indicated on spectrum in red. Probe modified lysines are indicated in red on peptide sequence. Right: MS1-extracted ion chromatograms of probe-modified peptides with corresponding SILAC ratios quantifying vehicle-(light) or compound-treatments (heavy). MAP2K1/2 shows potent inhibition by both ATP (1 mM) and RLM001 (10 mM) while MARK1/2 is inhibited by ATP (1 mM) but only mildly inhibited by RLM001 (10 mM).

3.6 Acknowledgements

We thank all members of the Hsu laboratory and colleagues at the University of Virginia for review of the manuscript. This work was supported by the University of Virginia (start-up funds to Dr. Ku-Lung Hsu.), the LaunchPad for Diabetes Program funded by the Manning Family Foundation at the University of Virginia (Dr. Ku-Lung Hsu), National Institutes of Health Grants DA035864 and DA043571 to Dr. Ku-Lung Hsu, T32 GM007055 to Caroline E. Franks, T32 CA009109 to Dr. Sean T. Campbell, DK101946 to Dr. Thurl E. Harris, and CA180699 and CA189524 to Dr. Benjamin W. Purow, the Schiff Foundation (Dr. Ku-Lung Hsu, Dr. Thurl E. Harris, and Dr. Benjamin W. Purow), and U.S. Department of Defense (W81XWH-17-1-0487 to Dr. Ku-Lung Hsu).

Author Contributions

Rebecca McCloud, Caroline Franks, Dr. Sean Campbell, Dr. Benjamin Purow, Dr. Thurl Harris and Dr. Ku-Lung Hsu conceived this study. Rebecca McCloud, Caroline Franks, Dr. Sean Campbell, and Dr. Ku-Lung Hsu coordinated and designed this study. Rebecca McCloud designed, conducted, and analyzed the experiments shown in 3.4B and 3.4C. Caroline Franks and Rebecca McCloud designed, conducted, and analyzed the experiments shown in Figures 3.7, 3.8, 3.9 and Table 3.1. Dr. Sean Campbell designed, conducted, and analyzed the experiments shown in Figures 3.4D and 3.5. The manuscript was drafted and edited by Rebecca McCloud, Caroline Franks, Dr. Sean Campbell, and Dr. Ku-Lung Hsu.

Chapter 4: Chemoproteomic Discovery of a Ritanserin-Targeted Kinase Network Mediating Apoptotic Cell Death of Lung Tumor Cells

Adapted from: Sean T. Campbell, Caroline E. Franks, Adam L. Borne, Myungsun Shin, Liuzhi Zhang, and Ku-Lung Hsu. *Molecular Pharmacology* 94, 1246-1255 (2018).[1]

4.1 Abstract

Ritanserin was tested in the clinic as a serotonin receptor inverse agonist but recently emerged as a novel kinase inhibitor with potential applications in cancer. Here, we discovered that ritanserin induced apoptotic cell death of non-small cell and small cell lung cancer (NSCLC, SCLC) cells via a serotonin-independent mechanism. We used quantitative chemical proteomics to reveal a ritanserin-dependent kinase network that includes key mediators of lipid (DGKα, PI4KB) and protein signaling (FER, RAF), metabolism (EF2K, E2AK4), and DNA damage response (TLK2) to broadly kill lung tumor cell types. While ritanserin exhibits polypharmacology in NSCLC proteomes, this compound shows unexpected specificity for c-RAF in the SCLC subtype with negligible activity against other kinases mediating MAPK signaling. We show ritanserin blocks c-RAF but not B-RAF activation of established oncogenic signaling pathways in live cells, providing evidence in support of c-RAF as a key target mediating its anticancer activity. Given the role of c-RAF activation in RAS-mutated cancers resistant to clinical B-RAF inhibitors, our findings may have implications in overcoming resistance mechanisms associated with c-RAF biology. The unique target landscape, combined with acceptable safety profiles in humans, provides new opportunities for repositioning ritanserin in cancer.

4.2 Introduction

Ritanserin is a serotonin (5-hydroxytryptamine, 5-HT) receptor inverse agonist with specificity for the 5-HT_2 subtype (138). As a drug candidate, ritanserin was tested for treatment of several neuropsychiatric disorders but never received approval for clinical use (53). The oral bioavailability and lack of adverse side effects in humans have since prompted studies to explore ritanserin for clinical applications beyond serotonin signaling (37). Comparison of ritanserin with existing lipid kinase inhibitors revealed structural similarities that led to its discovery as an inhibitor of diacylglycerol kinase-alpha (DGKa) (37, 43) (Figure 4.1A). We recently used quantitative chemical proteomics to discover ritanserin as an active-site inhibitor of DGKa and the non- receptor tyrosine protein kinase FER (134, 139). While distinct in substrate preference, DGKa (3) and FER (120) are kinases related by their role in coupling receptor activation with intracellular signaling important for cell survival and proliferation. Thus, ritanserin is capable of perturbing cellular signaling through serotonin-independent mechanisms. We and others have proposed that ritanserin may have potential applications in oncology by disrupting regulatory pathways through its largely unexplored action against the kinase superfamily.

In this study, we set out to define the target spectrum of ritanserin in order to better understand its mode of action in tumor cells. Previous reports demonstrated that ritanserin is cytotoxic against glioblastoma and melanoma through putative downstream targets of DGKa including mTOR (36), HIF-1a (36), and GGTase I (140). We hypothesize that ritanserin's cellular activity is mediated through blockade of kinase networks to explain its broad action against diverse tumor cell types. An advantage of

multi-targeted strategies is to minimize the potential for development of resistance mechanisms (141). We conducted cell viability assays to determine the impact of ritanserin treatments on survival of different lung cancer subtypes. We used quantitative chemoproteomics to determine the kinase targets of ritanserin in both non-small cell lung cancer (NSCLC) and small cell lung cancer (SCLC) proteomes. Our findings reveal that ritanserin shows novel activity against c-RAF in SCLC proteomes. The lack of activity against other kinases involved in MAPK signaling suggests that ritanserin mediates its cellular activity in SCLC cells at least in part through blockade of c-RAF.

4.3 Materials and Methods

Materials. Desthiobiotin ATP acyl phosphate nucleotide probe was obtained from ThermoFisher Scientific (PI88311). Ritanserin and ketanserin tartrate were purchased from Tocris Bioscience. WST-1 reagent kits were purchased from Cayman Chemical. Trypan Blue was purchased from ThermoFisher Scientific. CaspaseGlo Assay kits were purchased from Promega. PMA was purchased from Cayman Chemicals.

WST-1 Cell Proliferation Assays. Tumor cells were plated in transparent tissue-culture treated 96-well plates at a density of 100,000 cells/mL (A549, H1650) or 200,000 cells/mL (H82) in a volume of 100 μL per well. Cells were treated with dimethyl sulfoxide (DMSO) vehicle or inhibitors dissolved in DMSO at the indicated concentrations (final DMSO concentration of 0.5%). Cells were allowed to grow for indicated times at 37 °C under 5% CO_2, equal parts of WST-1 developer reagent and electron mediator solution were mixed, and 10 μL of the resulting solution ('WST-1 reagent') were added to each well. Plates were shaken in an orbital shaker for 60 s and then returned to the incubator for two hrs. Plates were again shaken followed measurement of absorbance at 450 nm. Data were normalized to DMSO- treated wells and significance values determined with one-way ANOVA.

Cell Counts. Tumor cells were plated in 60 mm plates at a density of 100,000 cells/mL (A549, H1650) or 200,000 cells/mL (H82) at a volume of 3.5 mL/plate. Cells were treated with inhibitors at the indicated concentrations (final DMSO concentration of

0.5%) for 48 hrs at 37 °C, adherent cells were washed and detached with trypsin, and all cells were collected and concentrated by spinning at 400 x *g* for 3 min followed by aspiration of media. Cells were resuspended in 10 nM Trypan Blue and 10 μL of this solution was counted via a hemocytometer. Dead cells were excluded from all counts. Data were normalized to DMSO-treated wells and significance values determined with one-way ANOVA.

Caspase Glo Assays. Assays were performed as directed by the manufacturer (Promega). Briefly, tumor cells were plated in black tissue culture treated transparent-bottom 96 well plates at a density of 200,000 cells/mL (A549, H1650) or 400,000 cells/mL (H82) in a volume of 50 μL/well. Cells were treated with inhibitors at the indicated concentrations (final DMSO oncentration of 0.5%) for 24 hrs. Afterwards, 50 μL of the prepared CaspaseGlo reagent was added to each well. The reaction was allowed to proceed for 1 hr, at which point the cells were shaken in an orbital shaker at 500 rpm for 60 s and then luminescence was read for each well. Data were normalized to DMSO-treated wells and significance values determined with one-way ANOVA.

LC-MS analysis of SILAC samples using ATP acyl phosphates. Quantitative chemoproteomics was performed as previously described (Chapter 2.3)

Phospho-MEK assay of RAF activity. HEK293T cells were grown and transiently transfected with c-RAF plasmid as previously described (Chapter 2.3) and allowed to

grow for 48 hours after transfection. c-RAF plasmid (pCSF107mT-cRAF-FLAG) was generated by recombination of the Addgene plasmids using the Gateway cloning system (Invitrogen) as previously described (Chapter 2.3). Recombinant RAF- HEK293T cells were pretreated with DMSO vehicle or inhibitors at the indicated concentrations for 1 hr, followed by addition of PMA (20 ng/mL) for an additional 20 min at 37 °C. Cells were harvested for western blots and phospho-MEK detected using rabbit anti-phospho-MEK antibody (S217/S221; Cell Signaling Technology) followed by goat anti-rabbit Dylight 550 secondary antibody (Thermo Scientific) for fluorescence detection. Western blot measurement of MEK (rabbit anti-MEK1/2, Cell Signaling Technology) was included to evaluate protein loading between samples.

Computational Methods. Data for A549 and H82 cell lines were searched with IP2 and manually validated using the methods previously described (Chapter 2.3). Data for desthiobiotin-tagged ATP acyl-phosphate probes and ATP competitive peptides were compared and clustered. Ritanserin and ketanserin inhibition profiles were compared using SILAC ratios and normalized to DMSO. The kinase profiles were displayed as a heatmap and clustered with hierarchical clustering using R package d3heatmaps (https://blog.rstudio.org/2015/06/24/d3heatmap/) as previously described (Chapter 2.3).

Lipid kinase phylogenetic tree. Phylogenetic tree of human lipid kinases was generated using MUSCLE multiple sequence alignment (142) of annotated lipid kinases and a least

squared distance method for determining evolutionary distance. Calculations were conducted using the EMBOSS software suite (143).

Statistical analysis and determination of IC_{50} values. For all cell viability measurements, results were normalized to values obtained from DMSO treated cells. For CaspaseGlo assays, raw luminescence values are reported. All significance values for Cell Viability and CaspaseGlo assays were calculated with one-way ANOVA and Dunnett's multiple comparison test (post-hoc analysis). IC_{50} values were calculated using a four-parameter logistic model of the response curve. All data are shown as mean + S.E.M. All statistical analyses were performed using GraphPad Prism.

4.4 Results

4.4.1 *Ritanserin Shows Serotonin-Independent Cytotoxic Activity in Lung Tumor Cells*

We chose H1650 and A549 as our non-small cell lung cancer (NSCLC) cell models to evaluate sensitivity of cells with different genetic backgrounds to ritanserin exposure. H1650 cells express EGFR receptors containing activating mutations in the kinase domain (exon 19 deletion E746-A750) of this receptor tyrosine kinase. A549 cells express wild-type EGFR but harbor mutant KRAS (G12S). We also included H82 cells in our studies to evaluate ritanserin activity in small cell lung cancer (SCLC). The mutational backgrounds of cell lines used in this study are listed in Table 4.1. Ketanserin (Boroda et al., 2017; Franks et al., 2017) was used alongside ritanserin to control for potential 5-H2 receptor (5-HTR) inverse agonist activity and other nonspecific pharmacological effects in our cell biology (Figure 4.1A).

Cells were treated with varying ritanserin concentrations (5 – 50 μM) and cell viability measured using established WST-1 metabolic assays (144). We observed concentration-dependent decreases in viability in cells exposed to ritanserin but not ketanserin treatments (Figure 4.1B and 4.2A). At a moderate concentration of ritanserin (25 μM), we observed >70% blockade of cell proliferation across all NSCLC and SCLC lines tested (Figure 4.1B). At lower concentrations (5 μM), ritanserin showed enhanced cytotoxicity against the SCLC H82 (~50% cell death) cells compared with NSCLC cells (~5-15% cell death for A549 and H1650 cells, Figure 4.1B). Cell killing with ritanserin was rapid with >50% of cell death occurring after 1 day and near-maximal cytotoxicity after 2 days of treatment in all cell lines tested (25 μM dose, Figure 4.1C). The lack of

activity using ketanserin under the same treatment conditions supports a serotonin-independent mechanism of cytotoxicity for ritanserin (Figure 4.1B and C, Figure 4.2A). In contrast to the pan-kinase inhibitor staurosporine, which showed general cytotoxicity across all cells tested (Figure 4.1C and 4.2B), ritanserin demonstrated negligible cell killing against noncancerous primary cells at high concentrations (25 μM, Figure 4.2B).

We performed a separate cell biology assay comparing the effects of serotonin, ritanserin and ketanserin treatments on global protein kinase-C (PKC) and -A (PKA) activity in A549 and H82 cells (Figure 4.3A). PKC and PKA are downstream mediators of serotonin receptors (5-HTR) and global changes in substrate phosphorylation profiles of either enzyme would allow evaluation of compound activity on 5-HTR signaling. We observed negligible changes in PKC and PKA substrate phosphorylation between cell treatment conditions (serotonin, 10 μM; ritanserin and ketanserin, 25 μM; Figure 4.2B). In contrast, treatment with PMA, a known PKC activator, resulted in moderate increases in PKC substrate phosphorylation, which matches previous reports using this same assay (43). The consistent lack of 5-HTR activity with equivalent doses of ritanserin and ketanserin further supports that ritanserin effects observed in cellular assays are serotonin independent. Collectively, our results show that ritanserin is not generally cytotoxic but displays potent cell killing of NSCLC and SCLC cells tested.

4.4.2 *Ritanserin Activates Apoptotic Cell Death of Broad Lung Tumor Cell Types*

Since changes in cell metabolism can occur from non-lethal perturbations (144), we also used live cell counts to further support cytotoxicity of lung cancer cells using

ritanserin. Akin to results from cell viability assays, we observed substantial cell killing across all lung cancer cell lines exposed to ritanserin but not ketanserin (Figure 4.4A). We observed potent cell killing (~70%) even at the lower dose tested (10 μM, Figure 4.4A). Next, we measured caspase activity in treated cells to determine whether ritanserin mediates cell killing through activation of apoptosis. Cells treated with ritanserin showed statistically significant ($P < 0.05$) enhanced caspase 3/7 activity after 24 hours compared with vehicle controls (Figure 4.4B). Caspase activation by ritanserin was specific because ketanserin treatments under the same experimental conditions did not induce these effects (Figure 4.4B). We compared ritanserin effects directly with staurosporine, which served as a positive control based on previous reports of activating apoptosis in treated lung cancer cells (145, 146). In both H1650 and H82 cells, we observed comparable activation of caspase 3/7 activity compared with staurosporine (Figure 4.4B). While ritanserin treatment of A549 cells resulted in a lower degree of activation, the increase in caspase 3/7 activity was statistically significant compared with vehicle treated cells ($P = 0.01$, Figure 4.4B). In summary, our cell viability and caspase activation data support ritanserin-mediated activation of apoptotic cell death in lung cancer cells that differ in mutation status (EGFR, KRAS) and subtype (NSCLC vs SCLC).

4.4.3 *Chemoproteomic Kinome Profiling of Ritanserin Action in Lung Tumor Cell Proteomes*

Based on previous chemical proteomic analyses (134, 139), we hypothesized that ritanserin is functioning as a kinase inhibitor to mediate cytotoxicity in our lung cancer

cell studies. Since A549 and H1650 displayed similar sensitivities to ritanserin in our cell viability assays, we selected A549 and H82 for chemical proteomic evaluation of ritanserin targets in NSCLC and SCLC proteomes, respectively. We used desthiobiotin-tagged, ATP acyl-phosphates (66, 67, 147) to measure selectivity of compounds against native kinases detected in lung cancer proteomes. ATP acyl-phosphate probes permit global profiling of kinase activities by covalent attachment of reporter tags to conserved lysines in the ATP binding site of protein/lipid kinases as well as other ATP-binding proteins (66, 67, 134, 139, 147). For these studies, NSCLC and SCLC cells were cultured in media containing isotopically light and heavy amino acids to enable quantitative chemical proteomics (118, 119, 133) by stable isotope labeling with amino acids in cell culture (SILAC, Figure 4.5). Light and heavy cell proteomes were treated with DMSO vehicle or compound, respectively, prior to addition of ATP acyl phosphate to label active site lysines. After probe labeling, light and heavy proteomes were combined, digested with trypsin protease, and desthiobiotin-modified peptides enriched by avidin affinity chromatography and analyzed by LC-MS/MS to identify and quantify isotopically tagged active-site peptides from native kinases as previously described (134, 139) and depicted in Figure 4.5.

Using our quantitative chemical proteomics assay, we compared kinase activity profiles between A549 and H82 cell proteomes. Kinases included in our comparisons showed potent competition with free ATP (SILAC ratios (*SR*) > 5, Fig. 5.6A). The latter criterion was important to distinguish specific probe binding at ATP-binding sites versus non-specific labeling of surface lysines. We detected ~120 unique probe-modified

peptides from ~110 distinct kinases. Using ATP competition profiles, we separated kinases into groups detected in both proteomes (shared) or detected in either A549 (NSCLC) or H82 samples (SCLC, Fig. 5.6A and Table 4.2). Specifically, we observed probe-dependent detection of several kinases (AKT1/2/3 and IKKA) in A549 proteomes that are associated with PI3K/AKT signaling (148) (Figure 4.6A and Table 4.2). These findings are consistent with enhanced PI3K/AKT signaling in NSCLC subtypes containing KRAS mutations (149). Finally, we detected native DGKa activity in A549 proteomes (Figure 4.7 shows MS1 data for DGKa peptide), which may indicate a potential role for DAG and PA metabolism/signaling in these NSCLC cells. A similar analysis of SCLC kinase profiles revealed enrichment of kinases involved in RAF signaling (A-RAF, B-RAF, and c-RAF (150) as well as DNA damage response (ATR, CHK2, PRKDC, and TLK2 (151); Fig. 5.6A and Table 4.2). These findings support previous reports that c-RAF is one of several proto-oncogenes that are highly expressed in SCLC cells and tumor tissues (152). Collectively, our kinase profiling studies establish a global map of kinase activities detected in A549 and H82 proteomes, including discovery of kinases that appear enriched in NSCLC compared with SCLC subtypes.

4.4.4 *Chemoproteomic Profiling Reveals c-RAF as a Principal Target of Ritanserin in SCLC Proteomes*

Next, we used our competitive ATP probe assay to determine the kinase targets of ritanserin in A549 and H82 proteomes (Figure 4.6B). Ketanserin was included in our LC-MS studies to discern ritanserin-specific from general non-specific activity of 5-HTR inverse agonists against the kinome. We chose to test inhibitor concentrations (100 μM)

10-fold higher than required for potent cell killing (10 μM, Figure 4.4A) to account for potential shifts in potency of reversible inhibitors due to irreversible labeling kinetics of the ATP acyl phosphate probe (67). Kinase targets of ritanserin were defined as those active-site peptides that showed SILAC ratios > 4. As expected based on previous findings (134), we detected potent inhibition of FER and DGKa in A549 proteomes with ritanserin treatments (FER, *SR* = 9; DGKa, *SR* = 6; Figure 4.7 and Table 4.2). We identified an additional lipid kinase target, PI4KB in A549 proteomes, which is involved in modulating lipid-mediated PI3K/AKT signaling in tumor cells (153). In addition to signaling, ritanserin treatment perturbed kinases implicated in glycolysis (EF2K(154)), amino acid metabolism (E2AK4 (155)), and DNA damage response (TLK2 (156)).

In contrast to polypharmacology observed in A549 proteomes, we identified c-RAF as the primary target of ritanserin in H82 proteomes (Figure 4.6B and C; Figure 4.8 shows MS1 and MS2 data for c-RAF peptide). Ketanserin treatments did not perturb activity of key kinases involved in metabolism and signaling (Figure 4.6C). Since c-RAF is a key regulator of the mitogen-activated protein kinase (MAPK) pathway, we also measured activity of ritanserin against other MAPK targets in H82 SCLC proteomes including B-RAF, MAPK (ERK1 and ERK2), and MAP2K (MEK1 and MEK2) kinases. We show that ritanserin shows selective perturbation of c-RAF compared with other MAPK mediators in H82 proteomes (Figure 4.9A). Collectively, our findings reveal, for the first time, a ritanserin-targeted lipid/protein kinase network involved in signaling, metabolism, and stress responses that help explain its broad anti- proliferative activity in

lung tumor cells. In addition, we demonstrate that ritanserin shows selective blockade of c-RAF when compared with other MAPK kinases in H82 SCLC proteomes.

4.4.5 *Ritanserin Block c-RAF But Not B-RAF Activation of MEK Signaling in Live Cells*

Our chemoproteomic studies identified c-RAF as a potential target mediating ritanserin anti-tumor activity. Here, we sought to test whether ritanserin blocked c-RAF signaling pathways relevant for its anti-tumor activity. RAFs are part of the mitogen-activated protein kinase (MAPK) pathway involved in regulation of cellular responses to external signals (157-159). Growth factors and mitogens trigger activation of receptor tyrosine kinases (RTKs) that mediate guanosine triphosphate (GTP) loading of the RAS GTPase (160). GTP-loaded RAS activate RAFs (A-RAF, B-RAF, and c-RAF) via recruitment to the cell membrane. Activated RAFs phosphorylate and activate MEK (MEK1 and MEK2), which phosphorylates and activates ERK (ERK1 and ERK2) as part of a signaling cascade to modulate cell proliferation, differentiation, apoptosis, and migration in cancer (161).

To directly measure c-RAF-mediated MEK phosphorylation in live cells, we overexpressed recombinant c-RAF in HEK293T cells, activated cells with PMA (162), and measured the resulting levels of phosphorylated MEK1/2 (phospho-MEK) by western blots (Figure 4.9B). We also overexpressed recombinant B-RAF to directly compare specificity of ritanserin activity against the various RAF isoforms. Both c-RAF and B-RAF overexpression resulted in substantially enhanced phospho-MEK levels compared with non-overexpressed (mock) counterparts (Figure 4.9B). Pretreatment of

cells with ritanserin (50 μM) resulted in substantial blockade of recombinant c-RAF but not B-RAF signaling activity as judged by reductions in phospho-MEK levels (Figure 4.9B). Ketanserin did not produce the same effects as ritanserin, which supports ritanserin-specific effects in our assay. The RAF inhibitor sorafenib (163) was used as a positive control to demonstrate blockade of both recombinant c- RAF- and B-RAF-mediated increases in phospho-MEK levels. Taken together, our results demonstrate ritanserin specifically blocks c-RAF activity in MAPK signaling pathways known to be important for tumor cell biology (161).

4.5 Discussion

In summary, we provide evidence that ritanserin functions as a lipid and protein kinase inhibitor with broad action against diverse lung cancer types that is serotonin-independent. Using quantitative chemical proteomics, we discovered that ritanserin targets a kinase network in A549 proteomes (Figure 4.6B), which suggests polypharmacology as a likely mode of action in A549 and potentially other NSCLC cells (including H1650). Despite promiscuous activity in the kinome, ritanserin was not cytotoxic in noncancerous primary cells (Figure 4.2B), which is likely due to differences in cell metabolism and signaling between tumor and noncancerous cells as previously reported for ritanserin in glioblastoma (36); further investigations are needed to determine whether ritanserin can specifically kill lung tumor cells *in vivo*.

A surprising finding from our studies was the identification of c-RAF as the primary target for ritanserin in H82 SCLC proteomes (Figure 4.6 and 4.9). Recent studies demonstrated that loss of c-RAF activity resulted in tumor regression of aggressive K-RAS driven cancers with reduced systemic toxicity because canonical MAPK signaling is unaffected (150). Our chemoproteomic (Figure 4.6) and cell biology (Figure 4.9) studies show ritanserin specificity for blockade of c-RAF versus B-RAF activity. Thus, our findings position ritanserin as a novel scaffold for future medicinal chemistry efforts to develop potent and selective c-RAF inhibitors. The utility of targeting c-RAF in the clinic extends beyond studies of lung cancers. For example, clinical efficacy of B-RAF inhibitors in RAS-mutated cancers is limited by resistance through paradoxical activation (164-166). Drugs that selectively block B-RAF drive B-RAF binding to c-RAF in a RAS-

dependent manner, c-RAF activation, and consequent elevations in MEK and ERK signaling. Future studies are needed to determine whether ritanserin can be used to overcome resistance mechanisms associated with c- RAF activation.

We recognize our selectivity profiling studies have been performed in lysates and development of new activity-based probes for live cell profiling will be critical to fully understand the mechanism of action of ritanserin in future studies. Nonetheless, we identify a novel anticancer activity for ritanserin along with clinically relevant kinase targets like c-RAF that, coupled with its safety profiles in humans, should prove valuable for potential drug repurposing in cancer.

Cell line	Subtype	Mutation
A549	NSCLC	KRAS (G12S)
H1650	NSCLC	EGFR (E746_A750del)
H82	SCLC	RB1

Table 4.1 Tumor cell line mutations.

Uniprot_ID	Peptide	Detected group	Treatment	Normalized SILAC ratio (DMSO/inhibitor; light/heavy)
Q13131	DLKPENVLLDAHMNAK	shared	A549-ATP	4.7
Q13131	DLKPENVLLDAHMNAK	shared	A549-Ket	0.8
Q13131	DLKPENVLLDAHMNAK	shared	A549-Rit	1.4
Q13131	DLKPENVLLDAHMNAK	shared	H82-ATP	13
Q13131	DLKPENVLLDAHMNAK	shared	H82-Ket	0.4
Q13131	DLKPENVLLDAHMNAK	shared	H82-Rit	0.3
Q13131	VAVKILNR	shared	A549-ATP	20
Q13131	VAVKILNR	shared	A549-Ket	0.8
Q13131	VAVKILNR	shared	A549-Rit	1.5
Q13131	VAVKILNR	shared	H82-ATP	20
Q13131	VAVKILNR	shared	H82-Ket	0.6
Q13131	VAVKILNR	shared	H82-Rit	0.3
P54646	DLKPENVLLDAHMNAK	shared	A549-ATP	4.7
P54646	DLKPENVLLDAHMNAK	shared	A549-Ket	0.8
P54646	DLKPENVLLDAHMNAK	shared	A549-Rit	1.4
P54646	DLKPENVLLDAHMNAK	shared	H82-ATP	13
P54646	DLKPENVLLDAHMNAK	shared	H82-Ket	0.4
P54646	DLKPENVLLDAHMNAK	shared	H82-Rit	0.3
P54646	VAVKILNR	shared	A549-ATP	20
P54646	VAVKILNR	shared	A549-Ket	0.8
P54646	VAVKILNR	shared	A549-Rit	1.5
P54646	VAVKILNR	shared	H82-ATP	20
P54646	VAVKILNR	shared	H82-Ket	0.6
P54646	VAVKILNR	shared	H82-Rit	0.3
P00519	LMTGDTYTAHAGAKFPIK	shared	A549-ATP	11.5
P00519	LMTGDTYTAHAGAKFPIK	shared	A549-Ket	2
P00519	LMTGDTYTAHAGAKFPIK	shared	A549-Rit	2.6
P00519	LMTGDTYTAHAGAKFPIK	shared	H82-ATP	20
P00519	LMTGDTYTAHAGAKFPIK	shared	H82-Ket	0.7
P00519	LMTGDTYTAHAGAKFPIK	shared	H82-Rit	1.2
P00519	YSLTVAVKTLKEDTMEVEEFLK	NA	A549-ATP	2.7
P00519	YSLTVAVKTLKEDTMEVEEFLK	NA	A549-Ket	1.8

P00519	YSLTVAVKTLKEDTMEVEEFLK	NA	A549-Rit	3.1
P00519	YSLTVAVKTLKEDTMEVEEFLK	NA	H82-ATP	2.3
P00519	YSLTVAVKTLKEDTMEVEEFLK	NA	H82-Ket	0.9
P00519	YSLTVAVKTLKEDTMEVEEFLK	NA	H82-Rit	1.5
P42684	LMTGDTYTAHAGAKFPIK	shared	A549-ATP	11.5
P42684	LMTGDTYTAHAGAKFPIK	shared	A549-Ket	2
P42684	LMTGDTYTAHAGAKFPIK	shared	A549-Rit	2.6
P42684	LMTGDTYTAHAGAKFPIK	shared	H82-ATP	20
P42684	LMTGDTYTAHAGAKFPIK	shared	H82-Ket	0.7
P42684	LMTGDTYTAHAGAKFPIK	shared	H82-Rit	1.2
P42684	YSLTVAVKTLKEDTMEVEEFLK	NA	A549-ATP	2.7
P42684	YSLTVAVKTLKEDTMEVEEFLK	NA	A549-Ket	1.8
P42684	YSLTVAVKTLKEDTMEVEEFLK	NA	A549-Rit	3.1
P42684	YSLTVAVKTLKEDTMEVEEFLK	NA	H82-ATP	4.3
P42684	YSLTVAVKTLKEDTMEVEEFLK	NA	H82-Ket	0.9
P42684	YSLTVAVKTLKEDTMEVEEFLK	NA	H82-Rit	1.5
P31749	GTFGKVILVK	NSCLC	A549-ATP	12.1
P31749	GTFGKVILVK	NSCLC	A549-Ket	0.7
P31749	GTFGKVILVK	NSCLC	A549-Rit	1.5
P31749	GTFGKVILVK	NSCLC	H82-ATP	0.8
P31749	GTFGKVILVK	NSCLC	H82-Ket	0.4
P31749	GTFGKVILVK	NSCLC	H82-Rit	0.2
P31751	GTFGKVILVR	NSCLC	A549-ATP	7.9
P31751	GTFGKVILVR	NSCLC	A549-Rit	2
P31751	GTFGKVILVR	NSCLC	H82-ATP	0.5
P31751	GTFGKVILVR	NSCLC	H82-Ket	0.4
P31751	GTFGKVILVR	NSCLC	H82-Rit	0.2
Q9Y243	GTFGKVILVR	NSCLC	A549-ATP	7.9
Q9Y243	GTFGKVILVR	NSCLC	A549-Rit	2
Q9Y243	GTFGKVILVR	NSCLC	H82-ATP	0.5

Q9Y243	GTFGKVILVR	NSCLC	H82-Ket	0.4
Q9Y243	GTFGKVILVR	NSCLC	H82-Rit	0.2
P10398	DLKSNNIFLHEGLTVK	SCLC	H82-ATP	17.8
P10398	DLKSNNIFLHEGLTVK	SCLC	H82-Ket	0.4
P10398	DLKSNNIFLHEGLTVK	SCLC	H82-Rit	0.3
Q13535	FYIMMCKPK	SCLC	A549-ATP	1.1
Q13535	FYIMMCKPK	SCLC	A549-Ket	0.6
Q13535	FYIMMCKPK	SCLC	A549-Rit	0.3
Q13535	FYIMMCKPK	SCLC	H82-ATP	11.8
Q13535	FYIMMCKPK	SCLC	H82-Ket	0.5
Q13535	FYIMMCKPK	SCLC	H82-Rit	0.6
O14965	DIKPENLLLGSAGELK	SCLC	H82-ATP	4.3
O14965	DIKPENLLLGSAGELK	SCLC	H82-Ket	0.9
O14965	DIKPENLLLGSAGELK	SCLC	H82-Rit	0.6
O14965	FILALKVLFK	SCLC	H82-ATP	5.7
O14965	FILALKVLFK	SCLC	H82-Ket	0.7
O14965	FILALKVLFK	SCLC	H82-Rit	1
O14965	GKFGNVYLAR	SCLC	H82-ATP	5.8
O14965	GKFGNVYLAR	SCLC	H82-Ket	0.6
O14965	GKFGNVYLAR	SCLC	H82-Rit	0.5
Q96GD4	GKFGNVYLAR	SCLC	H82-ATP	5.8
Q96GD4	GKFGNVYLAR	SCLC	H82-Ket	0.6
Q96GD4	GKFGNVYLAR	SCLC	H82-Rit	0.5
Q9UQB9	GKFGNVYLAR	SCLC	H82-ATP	5.8
Q9UQB9	GKFGNVYLAR	SCLC	H82-Ket	0.6
Q9UQB9	GKFGNVYLAR	SCLC	H82-Rit	0.5
P15056	DLKSNNIFLHEDLTVK	SCLC	A549-ATP	1
P15056	DLKSNNIFLHEDLTVK	SCLC	A549-Ket	0.1
P15056	DLKSNNIFLHEDLTVK	SCLC	A549-Rit	1
P15056	DLKSNNIFLHEDLTVK	SCLC	H82-ATP	20
P15056	DLKSNNIFLHEDLTVK	SCLC	H82-Ket	0.6
P15056	DLKSNNIFLHEDLTVK	SCLC	H82-Rit	0.7
P21127	DLKTSNLLLSHAGILK	NA	H82-ATP	1.2
P06493	DLKPQNLLIDDK	NA	H82-ATP	2.8
P06493	DLKPQNLLIDDK	NA	H82-Ket	0.2
P06493	DLKPQNLLIDDK	NA	H82-Rit	0.1
P06493	DLKPQNLLIDDKGTIK	NA	H82-ATP	1.6
P06493	DLKPQNLLIDDKGTIK	NA	H82-Ket	0.4
P06493	DLKPQNLLIDDKGTIK	NA	H82-Rit	0.3

Q9BWU1	DLKPANILVMGEGPER	NA	H82-ATP	3.4
Q9BWU1	DLKPANILVMGEGPER	NA	H82-Ket	0.6
Q9BWU1	DLKPANILVMGEGPER	NA	H82-Rit	0.4
P24941	DLKPQNLLINTEGAIK	SCLC	H82-ATP	4.8
P24941	DLKPQNLLINTEGAIK	SCLC	H82-Ket	0.5
P24941	DLKPQNLLINTEGAIK	SCLC	H82-Rit	0.3
Q00535	DLKPQNLLINR	NSCLC	A549-ATP	18.1
Q00535	DLKPQNLLINR	NSCLC	A549-Ket	0.9
Q00535	DLKPQNLLINR	NSCLC	A549-Rit	1.3
Q00535	DLKPQNLLINR	NSCLC	H82-ATP	3.8
Q00535	DLKPQNLLINR	NSCLC	H82-Ket	0.8
Q00535	DLKPQNLLINR	NSCLC	H82-Rit	0.6
Q00535	NRETHEIVALKR	shared	A549-ATP	18.9
Q00535	NRETHEIVALKR	shared	A549-Ket	1
Q00535	NRETHEIVALKR	shared	A549-Rit	1.2
Q00535	NRETHEIVALKR	shared	H82-ATP	20
Q00535	NRETHEIVALKR	shared	H82-Ket	0.8
Q00535	NRETHEIVALKR	shared	H82-Rit	1.2
P50613	DLKPNNLLLDENGVLK	NA	H82-ATP	0.8
P50613	DLKPNNLLLDENGVLK	NA	H82-Ket	0.2
P50613	DLKPNNLLLDENGVLK	NA	H82-Rit	0.2
P49336	DLKPANILVMGEGPER	NA	H82-ATP	3.4
P49336	DLKPANILVMGEGPER	NA	H82-Ket	0.6
P49336	DLKPANILVMGEGPER	NA	H82-Rit	0.4
O96017	VAIKIISK	SCLC	H82-ATP	20
O96017	VAIKIISK	SCLC	H82-Ket	0.4
O96017	VAIKIISK	SCLC	H82-Rit	0.3
P41240	VSDFGLTKEASSTQDTGKLPVK	shared	A549-ATP	20
P41240	VSDFGLTKEASSTQDTGKLPVK	shared	A549-Ket	0.9
P41240	VSDFGLTKEASSTQDTGKLPVK	shared	A549-Rit	1.2
P41240	VSDFGLTKEASSTQDTGKLPVK	shared	H82-ATP	9.1
P41240	VSDFGLTKEASSTQDTGKLPVK	shared	H82-Ket	0.6
P41240	VSDFGLTKEASSTQDTGKLPVK	shared	H82-Rit	0.5

P68400	GGPNIITLADIVKDPVSR	NA	H82-Rit	0.3
Q8NEV1	GGPNIITLADIVKDPVSR	NA	H82-Rit	0.3
P23743	YPEKFNSR	NSCLC	A549-ATP	20
P23743	YPEKFNSR	NSCLC	A549-Rit	6.1
P19525	DLKPSNIFLVDTK	NSCLC	A549-ATP	8.5
P19525	DLKPSNIFLVDTK	NSCLC	A549-Ket	0.7
P19525	DLKPSNIFLVDTK	NSCLC	A549-Rit	1.4
P19525	DLKPSNIFLVDTK	NSCLC	H82-ATP	3.8
P19525	DLKPSNIFLVDTK	NSCLC	H82-Ket	0.5
P19525	DLKPSNIFLVDTK	NSCLC	H82-Rit	0.3
P19525	IGDFGLVTSLKNDGKR	NA	H82-ATP	1.5
P19525	IGDFGLVTSLKNDGKR	NA	H82-Ket	0.9
P19525	IGDFGLVTSLKNDGKR	NA	H82-Rit	1.3
Q9P2K8	DLKPVNIFLDSDDHVK	NA	A549-ATP	0.6
Q9P2K8	DLKPVNIFLDSDDHVK	NA	A549-Rit	0.6
Q9P2K8	DLKPVNIFLDSDDHVK	NA	H82-ATP	0.1
Q9P2K8	DLKPVNIFLDSDDHVK	NA	H82-Ket	0.6
Q9P2K8	DLKPVNIFLDSDDHVK	NA	H82-Rit	0.5
Q9P2K8	LDGCCYAVKR	shared	A549-ATP	20
Q9P2K8	LDGCCYAVKR	shared	A549-Rit	4.4
Q9P2K8	LDGCCYAVKR	shared	H82-ATP	12.2
Q9P2K8	LDGCCYAVKR	shared	H82-Ket	0.6
Q9P2K8	LDGCCYAVKR	shared	H82-Rit	0.7
O00418	YIKYNSNSGFVR	shared	A549-ATP	20
O00418	YIKYNSNSGFVR	shared	A549-Ket	0.3
O00418	YIKYNSNSGFVR	shared	A549-Rit	4.2
O00418	YIKYNSNSGFVR	shared	H82-ATP	20
O00418	YIKYNSNSGFVR	shared	H82-Ket	0.4
O00418	YIKYNSNSGFVR	shared	H82-Rit	0.5
P16591	QEDGGVYSSSGLKQIPIK	NA	A549-ATP	2.6
P16591	QEDGGVYSSSGLKQIPIK	NA	A549-Ket	0.6
P16591	TSVAVKTCKEDLPQELK	NSCLC	A549-ATP	20
P16591	TSVAVKTCKEDLPQELK	NSCLC	A549-Ket	1.2
P16591	TSVAVKTCKEDLPQELK	NSCLC	A549-Rit	9
Q9Y2I7	GGKSGAAFYATEDDRFILK	NA	H82-ATP	1.3
Q9Y2I7	GGKSGAAFYATEDDRFILK	NA	H82-Ket	1.1
Q9Y2I7	GGKSGAAFYATEDDRFILK	NA	H82-Rit	0.8
P49840	DIKPQNLLVDPDTAVLK	NA	A549-ATP	1.5
P49840	DIKPQNLLVDPDTAVLK	NA	A549-Ket	0.8

P49840	DIKPQNLLVDPDTAVLK	NA	A549-Rit	1.2
P49840	DIKPQNLLVDPDTAVLK	NA	H82-ATP	2.9
P49840	DIKPQNLLVDPDTAVLK	NA	H82-Ket	2.1
P49841	DIKPQNLLLDPDTAVLK	NA	A549-ATP	0.8
P49841	DIKPQNLLLDPDTAVLK	NA	A549-Rit	1.1
O15111	DLKPENIVLQDVGGK	NSCLC	A549-ATP	20
O14920	WHNQETGEQIAIKQCR	NSCLC	A549-ATP	20
O14920	WHNQETGEQIAIKQCR	NSCLC	A549-Ket	2.5
O14920	WHNQETGEQIAIKQCR	NSCLC	A549-Rit	2.6
Q13418	GRWQGNDIVVKVLK	NSCLC	A549-Rit	2.9
Q13418	ISMADVKFSFQCPGR	NSCLC	A549-ATP	4.5
Q13418	ISMADVKFSFQCPGR	NSCLC	A549-Ket	0.9
Q13418	ISMADVKFSFQCPGR	NSCLC	A549-Rit	1.3
Q13418	ISMADVKFSFQCPGR	NSCLC	H82-ATP	3.1
Q13418	ISMADVKFSFQCPGR	NSCLC	H82-Ket	0.2
Q13418	ISMADVKFSFQCPGR	NSCLC	H82-Rit	0.1
Q13418	WQGNDIVVKVLK	NSCLC	A549-ATP	17
Q13418	WQGNDIVVKVLK	NSCLC	A549-Rit	2.5
P51617	AIQFLHQDSPSLIHGDIKSSN VLLDER	NA	A549-ATP	2.3
P51617	AIQFLHQDSPSLIHGDIKSSN VLLDER	NA	A549-Ket	0.3
P51617	AIQFLHQDSPSLIHGDIKSSN VLLDER	NA	A549-Rit	1.6
Q9NWZ3	DIKSANILLDEAFTAK	NA	A549-ATP	1.1
Q9NWZ3	DIKSANILLDEAFTAK	NA	A549-Ket	1
Q13572	ESIFFNSHNVSKPESSSVLTEL DK	shared	A549-ATP	13.6
Q13572	ESIFFNSHNVSKPESSSVLTEL DK	shared	A549-Rit	2.8
Q13572	ESIFFNSHNVSKPESSSVLTEL DK	shared	H82-ATP	8.6
Q13572	ESIFFNSHNVSKPESSSVLTEL DK	shared	H82-Ket	0.5
Q13572	ESIFFNSHNVSKPESSSVLTEL DK	shared	H82-Rit	1.5
Q8IU85	LFAVKCIPK	NSCLC	A549-ATP	20
Q8IU85	LFAVKCIPK	NSCLC	A549-Ket	0.5
Q8IU85	LFAVKCIPK	NSCLC	A549-Rit	1.5
Q13557	IPTGQEYAAKIINTK	NSCLC	A549-ATP	7.3

Q13557	IPTGQEYAAKIINTK	NSCLC	A549-Ket	1
Q13557	IPTGQEYAAKIINTK	NSCLC	A549-Rit	1.2
Q13557	IPTGQEYAAKIINTK	NSCLC	H82-ATP	1.4
Q13557	IPTGQEYAAKIINTK	NSCLC	H82-Ket	0.5
Q13557	IPTGQEYAAKIINTK	NSCLC	H82-Rit	0.3
Q13557	IPTGQEYAAKIINTKK	SCLC	A549-ATP	1.4
Q13557	IPTGQEYAAKIINTKK	SCLC	A549-Ket	0.2
Q13557	IPTGQEYAAKIINTKK	SCLC	A549-Rit	1.7
Q13557	IPTGQEYAAKIINTKK	SCLC	H82-ATP	20
Q13557	IPTGQEYAAKIINTKK	SCLC	H82-Ket	0.2
Q13557	IPTGQEYAAKIINTKK	SCLC	H82-Rit	0.7
Q13555	TSTQEYAAKIINTK	NA	A549-ATP	3.2
Q13555	TSTQEYAAKIINTK	NA	A549-Ket	0.1
Q13555	TSTQEYAAKIINTK	NA	A549-Rit	2.5
Q13555	TSTQEYAAKIINTK	NA	H82-ATP	2.9
Q13555	TSTQEYAAKIINTK	NA	H82-Ket	0.6
Q13555	TSTQEYAAKIINTK	NA	H82-Rit	0.5
Q16566	DLKPENLLYATPAPDAPLK	NA	H82-ATP	2.7
Q16566	DLKPENLLYATPAPDAPLK	NA	H82-Ket	0.7
Q16566	DLKPENLLYATPAPDAPLK	NA	H82-Rit	0.5
Q15418	LTDFGLSKEAIDHEK	SCLC	A549-Ket	1.2
Q15418	LTDFGLSKEAIDHEK	SCLC	A549-Rit	2
Q15418	LTDFGLSKEAIDHEK	SCLC	H82-ATP	12.9
Q15418	LTDFGLSKEAIDHEK	SCLC	H82-Ket	0.6
Q15418	LTDFGLSKEAIDHEK	SCLC	H82-Rit	0.4
Q15418	LTDFGLSKEAIDHEKK	NA	A549-ATP	0.6
Q15418	LTDFGLSKEAIDHEKK	NA	A549-Ket	0.2
Q15418	LTDFGLSKEAIDHEKK	NA	A549-Rit	1.1
Q15418	LTDFGLSKEAIDHEKK	NA	H82-ATP	0.6
Q15418	LTDFGLSKEAIDHEKK	NA	H82-Ket	0.7
Q15418	LTDFGLSKEAIDHEKK	NA	H82-Rit	1.3
Q15349	DLKPENILLDEEGHIK	shared	A549-ATP	19.6
Q15349	DLKPENILLDEEGHIK	shared	A549-Ket	0.9
Q15349	DLKPENILLDEEGHIK	shared	A549-Rit	1.5
Q15349	DLKPENILLDEEGHIK	shared	H82-ATP	11.4
Q15349	DLKPENILLDEEGHIK	shared	H82-Ket	0.6
Q15349	DLKPENILLDEEGHIK	shared	H82-Rit	0.4
P51812	DLKPENILLDEEGHIK	shared	A549-ATP	19.6
P51812	DLKPENILLDEEGHIK	shared	A549-Ket	0.9

P51812	DLKPENILLDEEGHIK	shared	A549-Rit	1.5
P51812	DLKPENILLDEEGHIK	shared	H82-ATP	11.4
P51812	DLKPENILLDEEGHIK	shared	H82-Ket	0.6
P51812	DLKPENILLDEEGHIK	shared	H82-Rit	0.4
P51812	LTDFGLSKESIDHEKK	shared	A549-ATP	20
P51812	LTDFGLSKESIDHEKK	shared	A549-Ket	0.7
P51812	LTDFGLSKESIDHEKK	shared	A549-Rit	1.7
P51812	LTDFGLSKESIDHEKK	shared	H82-ATP	12
P51812	LTDFGLSKESIDHEKK	shared	H82-Ket	0.4
P51812	LTDFGLSKESIDHEKK	shared	H82-Rit	1.1
O75676	VLGTGAYGKVFLVR	shared	A549-ATP	20
O75676	VLGTGAYGKVFLVR	shared	A549-Ket	0.8
O75676	VLGTGAYGKVFLVR	shared	A549-Rit	1.4
O75676	VLGTGAYGKVFLVR	shared	H82-ATP	20
O75676	VLGTGAYGKVFLVR	shared	H82-Ket	0.7
O75676	VLGTGAYGKVFLVR	shared	H82-Rit	0.6
O75582	DIKLENILLDSNGHVVLTDFGLSK	SCLC	A549-ATP	3.7
O75582	DIKLENILLDSNGHVVLTDFGLSK	SCLC	A549-Ket	1.2
O75582	DIKLENILLDSNGHVVLTDFGLSK	SCLC	A549-Rit	2.1
O75582	DIKLENILLDSNGHVVLTDFGLSK	SCLC	H82-ATP	11.1
O75582	DIKLENILLDSNGHVVLTDFGLSK	SCLC	H82-Ket	0.6
O75582	DIKLENILLDSNGHVVLTDFGLSK	SCLC	H82-Rit	0.4
O75582	VLGTGAYGKVFLVR	shared	A549-ATP	20
O75582	VLGTGAYGKVFLVR	shared	A549-Ket	0.8
O75582	VLGTGAYGKVFLVR	shared	A549-Rit	1.4
O75582	VLGTGAYGKVFLVR	shared	H82-ATP	20
O75582	VLGTGAYGKVFLVR	shared	H82-Ket	0.7
O75582	VLGTGAYGKVFLVR	shared	H82-Rit	0.6
P23443	DLKPENIMLNHQGHVK	shared	A549-ATP	20
P23443	DLKPENIMLNHQGHVK	shared	A549-Ket	1.1
P23443	DLKPENIMLNHQGHVK	shared	A549-Rit	1
P23443	DLKPENIMLNHQGHVK	shared	H82-ATP	17.3
P23443	DLKPENIMLNHQGHVK	shared	H82-Ket	0.8

P23443	DLKPENIMLNHQGHVK	shared	H82-Rit	0.9
P23443	GGYGKVFQVR	NA	H82-ATP	0.4
P23443	GGYGKVFQVR	NA	H82-Rit	0.3
Q9UBS0	DLKPENIMLSSQGHIK	shared	A549-ATP	18.1
Q9UBS0	DLKPENIMLSSQGHIK	shared	A549-Ket	1
Q9UBS0	DLKPENIMLSSQGHIK	shared	A549-Rit	1.1
Q9UBS0	DLKPENIMLSSQGHIK	shared	H82-ATP	7.6
Q9UBS0	DLKPENIMLSSQGHIK	shared	H82-Ket	0.7
Q9UBS0	DLKPENIMLSSQGHIK	shared	H82-Rit	1.2
Q9UBS0	GGYGKVFQVR	NA	H82-ATP	0.4
Q9UBS0	GGYGKVFQVR	NA	H82-Rit	0.3
O95835	ALYATKTLR	shared	A549-ATP	13.8
O95835	ALYATKTLR	shared	A549-Ket	0.7
O95835	ALYATKTLR	shared	A549-Rit	1.9
O95835	ALYATKTLR	shared	H82-ATP	17.6
O95835	ALYATKTLR	shared	H82-Ket	0.7
O95835	ALYATKTLR	shared	H82-Rit	0.6
Q9Y2U5	DIKGANILR	shared	A549-ATP	20
Q9Y2U5	DIKGANILR	shared	A549-Ket	1.1
Q9Y2U5	DIKGANILR	shared	A549-Rit	1
Q9Y2U5	DIKGANILR	shared	H82-ATP	6.2
Q9Y2U5	DIKGANILR	shared	H82-Ket	0.8
Q9Y2U5	DIKGANILR	shared	H82-Rit	0.7
Q99759	DIKGANILR	shared	A549-ATP	20
Q99759	DIKGANILR	shared	A549-Ket	1.1
Q99759	DIKGANILR	shared	A549-Rit	1
Q99759	DIKGANILR	shared	H82-ATP	6.2
Q99759	DIKGANILR	shared	H82-Ket	0.8
Q99759	DIKGANILR	shared	H82-Rit	0.7
Q9Y6R4	DIKGANIFLTSSGLIK	NSCLC	A549-ATP	20
Q9Y6R4	DIKGANIFLTSSGLIK	NSCLC	A549-Rit	1.5
Q9Y6R4	DIKGANIFLTSSGLIK	NSCLC	H82-ATP	3.9
Q9Y6R4	DIKGANIFLTSSGLIK	NSCLC	H82-Ket	0.9
Q9Y6R4	DIKGANIFLTSSGLIK	NSCLC	H82-Rit	1
Q92918	DIKGANILINDAGEVR	NA	H82-ATP	4.2
Q92918	DIKGANILINDAGEVR	NA	H82-Ket	0.5
Q92918	DIKGANILINDAGEVR	NA	H82-Rit	0.4
Q92918	VSGDLVALKMVK	SCLC	H82-ATP	20
Q92918	VSGDLVALKMVK	SCLC	H82-Ket	0.3

Q92918	VSGDLVALKMVK	SCLC	H82-Rit	1
Q8IVH8	DIKGANILLTDNGHVK	shared	A549-ATP	20
Q8IVH8	DIKGANILLTDNGHVK	shared	A549-Ket	1
Q8IVH8	DIKGANILLTDNGHVK	shared	A549-Rit	1.9
Q8IVH8	DIKGANILLTDNGHVK	shared	H82-ATP	20
Q8IVH8	DIKGANILLTDNGHVK	shared	H82-Ket	0.9
Q8IVH8	DIKGANILLTDNGHVK	shared	H82-Rit	0.7
Q8IVH8	NVNTGELAAIKVIK	NA	H82-Ket	1.5
O95819	DIKGQNVLLTENAEVK	shared	A549-ATP	15.7
O95819	DIKGQNVLLTENAEVK	shared	A549-Ket	0.7
O95819	DIKGQNVLLTENAEVK	shared	A549-Rit	2.3
O95819	DIKGQNVLLTENAEVK	shared	H82-ATP	19.9
O95819	DIKGQNVLLTENAEVK	shared	H82-Ket	0.6
O95819	DIKGQNVLLTENAEVK	shared	H82-Rit	0.4
Q9Y4K4	DIKGANILLTDHGDVK	shared	A549-ATP	17
Q9Y4K4	DIKGANILLTDHGDVK	shared	A549-Ket	0.8
Q9Y4K4	DIKGANILLTDHGDVK	shared	A549-Rit	1.8
Q9Y4K4	DIKGANILLTDHGDVK	shared	H82-ATP	13.6
Q9Y4K4	DIKGANILLTDHGDVK	shared	H82-Ket	0.5
Q9Y4K4	DIKGANILLTDHGDVK	shared	H82-Rit	0.5
Q9Y4K4	NVHTGELAAVKIIK	shared	A549-ATP	20
Q9Y4K4	NVHTGELAAVKIIK	shared	A549-Ket	0.8
Q9Y4K4	NVHTGELAAVKIIK	shared	A549-Rit	2.6
Q9Y4K4	NVHTGELAAVKIIK	shared	H82-ATP	17
Q9Y4K4	NVHTGELAAVKIIK	shared	H82-Ket	0.5
Q9Y4K4	NVHTGELAAVKIIK	shared	H82-Rit	0.7
Q9P0L2	EVAVKIIDK	shared	A549-ATP	20
Q9P0L2	EVAVKIIDK	shared	A549-Ket	0.5
Q9P0L2	EVAVKIIDK	shared	A549-Rit	1.1
Q9P0L2	EVAVKIIDK	shared	H82-ATP	6.6
Q9P0L2	EVAVKIIDK	shared	H82-Ket	0.3
Q9P0L2	EVAVKIIDK	shared	H82-Rit	0.2
Q7KZI7	EVAVKIIDK	shared	A549-ATP	20
Q7KZI7	EVAVKIIDK	shared	A549-Ket	0.5
Q7KZI7	EVAVKIIDK	shared	A549-Rit	1.1
Q7KZI7	EVAVKIIDK	shared	H82-ATP	6.6
Q7KZI7	EVAVKIIDK	shared	H82-Ket	0.3
Q7KZI7	EVAVKIIDK	shared	H82-Rit	0.2
Q9Y2H9	DLKPDNLLITSMGHIK	SCLC	A549-ATP	0.6

Q9Y2H9	DLKPDNLLITSMGHIK	SCLC	A549-Ket	0.2
Q9Y2H9	DLKPDNLLITSMGHIK	SCLC	A549-Rit	0.9
Q9Y2H9	DLKPDNLLITSMGHIK	SCLC	H82-ATP	10.1
Q9Y2H9	DLKPDNLLITSMGHIK	SCLC	H82-Ket	0.6
Q9Y2H9	DLKPDNLLITSMGHIK	SCLC	H82-Rit	0.5
Q6P0Q8	DLKPDNLLITSMGHIK	SCLC	A549-ATP	0.6
Q6P0Q8	DLKPDNLLITSMGHIK	SCLC	A549-Ket	0.2
Q6P0Q8	DLKPDNLLITSMGHIK	SCLC	A549-Rit	0.9
Q6P0Q8	DLKPDNLLITSMGHIK	SCLC	H82-ATP	10.1
Q6P0Q8	DLKPDNLLITSMGHIK	SCLC	H82-Ket	0.6
Q6P0Q8	DLKPDNLLITSMGHIK	SCLC	H82-Rit	0.5
O60307	DLKPDNLLITSLGHIK	SCLC	H82-ATP	14.3
O60307	DLKPDNLLITSLGHIK	SCLC	H82-Ket	0.5
O60307	DLKPDNLLITSLGHIK	SCLC	H82-Rit	0.2
O15021	DLKPDNLLVTSMGHIK	NSCLC	A549-ATP	5.2
O15021	DLKPDNLLVTSMGHIK	NSCLC	A549-Ket	0.6
O15021	DLKPDNLLVTSMGHIK	NSCLC	A549-Rit	1.7
Q8N4C8	DIKGQNVLLTENAEVK	shared	A549-ATP	15.7
Q8N4C8	DIKGQNVLLTENAEVK	shared	A549-Ket	0.7
Q8N4C8	DIKGQNVLLTENAEVK	shared	A549-Rit	2.3
Q8N4C8	DIKGQNVLLTENAEVK	shared	H82-ATP	13.4
Q8N4C8	DIKGQNVLLTENAEVK	shared	H82-Ket	0.6
Q8N4C8	DIKGQNVLLTENAEVK	shared	H82-Rit	0.4
P28482	DLKPSNLLLNTTCDLK	NSCLC	A549-ATP	4.9
P28482	DLKPSNLLLNTTCDLK	NSCLC	A549-Ket	0.9
P28482	DLKPSNLLLNTTCDLK	NSCLC	A549-Rit	1.3
P28482	DLKPSNLLLNTTCDLK	NSCLC	H82-ATP	3.9
P28482	DLKPSNLLLNTTCDLK	NSCLC	H82-Ket	0.7
P28482	DLKPSNLLLNTTCDLK	NSCLC	H82-Rit	0.5
P27361	DLKPSNLLINTTCDLK	NSCLC	A549-ATP	4.8
P27361	DLKPSNLLINTTCDLK	NSCLC	A549-Ket	1
P27361	DLKPSNLLINTTCDLK	NSCLC	A549-Rit	1.3
P27361	DLKPSNLLINTTCDLK	NSCLC	H82-ATP	3.4
P27361	DLKPSNLLINTTCDLK	NSCLC	H82-Ket	0.6
P27361	DLKPSNLLINTTCDLK	NSCLC	H82-Rit	0.5
P45983	DLKPSNIVVK	shared	A549-ATP	11.4
P45983	DLKPSNIVVK	shared	A549-Ket	0.8
P45983	DLKPSNIVVK	shared	A549-Rit	2.7
P45983	DLKPSNIVVK	shared	H82-ATP	20

P45983	DLKPSNIVVK	shared	H82-Ket	0.5
P45983	DLKPSNIVVK	shared	H82-Rit	0.9
Q8NB16	APVAIKVFK	NSCLC	A549-ATP	20
Q8NB16	APVAIKVFK	NSCLC	A549-Ket	0.8
Q8NB16	APVAIKVFK	NSCLC	A549-Rit	1.6
Q9NYL2	WISQDKEVAVKK	SCLC	H82-ATP	5.4
Q9NYL2	WISQDKEVAVKK	SCLC	H82-Ket	0.7
Q9NYL2	WISQDKEVAVKK	SCLC	H82-Rit	0.8
Q02750	DVKPSNILVNSR	shared	A549-ATP	20
Q02750	DVKPSNILVNSR	shared	A549-Ket	0.8
Q02750	DVKPSNILVNSR	shared	A549-Rit	1.3
Q02750	DVKPSNILVNSR	shared	H82-ATP	14.9
Q02750	DVKPSNILVNSR	shared	H82-Ket	0.5
Q02750	DVKPSNILVNSR	shared	H82-Rit	0.4
Q02750	KLIHLEIKPAIR	NSCLC	A549-ATP	20
Q02750	KLIHLEIKPAIR	NSCLC	A549-Ket	1.1
Q02750	KLIHLEIKPAIR	NSCLC	A549-Rit	1.3
Q02750	KLIHLEIKPAIR	NSCLC	H82-ATP	3.9
Q02750	KLIHLEIKPAIR	NSCLC	H82-Ket	0.5
Q02750	KLIHLEIKPAIR	NSCLC	H82-Rit	0.3
P36507	DVKPSNILVNSR	shared	A549-ATP	20
P36507	DVKPSNILVNSR	shared	A549-Ket	0.8
P36507	DVKPSNILVNSR	shared	A549-Rit	1.3
P36507	DVKPSNILVNSR	shared	H82-ATP	14.9
P36507	DVKPSNILVNSR	shared	H82-Ket	0.5
P36507	DVKPSNILVNSR	shared	H82-Rit	0.4
P36507	KLIHLEIKPAIR	NSCLC	A549-ATP	20
P36507	KLIHLEIKPAIR	NSCLC	A549-Ket	1.1
P36507	KLIHLEIKPAIR	NSCLC	A549-Rit	1.3
P36507	KLIHLEIKPAIR	NSCLC	H82-ATP	3.9
P36507	KLIHLEIKPAIR	NSCLC	H82-Ket	0.5
P36507	KLIHLEIKPAIR	NSCLC	H82-Rit	0.3
P46734	DVKPSNVLINK	NSCLC	A549-ATP	17.6
P46734	DVKPSNVLINK	NSCLC	A549-Ket	1.2
P46734	DVKPSNVLINK	NSCLC	A549-Rit	1
P46734	DVKPSNVLINK	NSCLC	H82-ATP	1.8
P46734	DVKPSNVLINK	NSCLC	H82-Ket	0.5
P46734	DVKPSNVLINK	NSCLC	H82-Rit	0.3
P45985	DIKPSNILLDR	shared	A549-ATP	20

P45985	DIKPSNILLDR	shared	A549-Ket	1
P45985	DIKPSNILLDR	shared	A549-Rit	1.2
P45985	DIKPSNILLDR	shared	H82-ATP	20
P45985	DIKPSNILLDR	shared	H82-Ket	0.5
P45985	DIKPSNILLDR	shared	H82-Rit	0.3
P45985	MVHKPSGQIMAVKR	NSCLC	A549-ATP	20
P45985	MVHKPSGQIMAVKR	NSCLC	A549-Ket	1
P45985	MVHKPSGQIMAVKR	NSCLC	A549-Rit	1.9
Q13163	DVKPSNMLVNTR	NSCLC	A549-ATP	18.5
Q13163	DVKPSNMLVNTR	NSCLC	A549-Ket	2.5
Q13163	DVKPSNMLVNTR	NSCLC	A549-Rit	2.7
P52564	DVKPSNVLINALGQVK	shared	A549-ATP	8
P52564	DVKPSNVLINALGQVK	shared	A549-Ket	1
P52564	DVKPSNVLINALGQVK	shared	A549-Rit	1.3
P52564	DVKPSNVLINALGQVK	shared	H82-ATP	5
P52564	DVKPSNVLINALGQVK	shared	H82-Ket	0.6
P52564	DVKPSNVLINALGQVK	shared	H82-Rit	0.4
P52564	HVPSGQIMAVKR	shared	A549-ATP	20
P52564	HVPSGQIMAVKR	shared	A549-Ket	0.9
P52564	HVPSGQIMAVKR	shared	A549-Rit	1.2
P52564	HVPSGQIMAVKR	shared	H82-ATP	10.3
P52564	HVPSGQIMAVKR	shared	H82-Ket	0.6
P52564	HVPSGQIMAVKR	shared	H82-Rit	1.4
P42345	IQSIAPSLQVITSKQRPR	NSCLC	A549-ATP	14.6
P42345	IQSIAPSLQVITSKQRPR	NSCLC	A549-Ket	1.3
P42345	IQSIAPSLQVITSKQRPR	NSCLC	A549-Rit	2.2
P42345	IQSIAPSLQVITSKQRPR	NSCLC	H82-ATP	3.3
P42345	IQSIAPSLQVITSKQRPR	NSCLC	H82-Ket	0.5
P42345	IQSIAPSLQVITSKQRPR	NSCLC	H82-Rit	0.3
P51956	SKNIFLTQNGK	shared	H82-ATP	20
P51956	SKNIFLTQNGK	shared	H82-Rit	0.7
P51957	DLKTQNVFLTR	shared	A549-Rit	13.1
P51957	DLKTQNVFLTR	shared	H82-ATP	20
P51957	DLKTQNVFLTR	shared	H82-Ket	0.4
P51957	DLKTQNVFLTR	shared	H82-Rit	0.3
Q9HC98	DIKPANVFITATGVVK	shared	A549-ATP	20
Q9HC98	DIKPANVFITATGVVK	shared	A549-Ket	0.7
Q9HC98	DIKPANVFITATGVVK	shared	A549-Rit	2.2
Q9HC98	DIKPANVFITATGVVK	shared	H82-ATP	20

Q9HC98	DIKPANVFITATGVVK	shared	H82-Ket	0.4
Q9HC98	DIKPANVFITATGVVK	shared	H82-Rit	0.2
Q8TDX7	DIKPANVFITATGVVK	shared	A549-ATP	20
Q8TDX7	DIKPANVFITATGVVK	shared	A549-Ket	0.7
Q8TDX7	DIKPANVFITATGVVK	shared	A549-Rit	2.2
Q8TDX7	DIKPANVFITATGVVK	shared	H82-ATP	20
Q8TDX7	DIKPANVFITATGVVK	shared	H82-Ket	0.4
Q8TDX7	DIKPANVFITATGVVK	shared	H82-Rit	0.2
Q8TD19	DIKTLNIFLTK	SCLC	A549-ATP	2.2
Q8TD19	DIKTLNIFLTK	SCLC	A549-Rit	3.7
Q8TD19	DIKTLNIFLTK	SCLC	H82-ATP	11.8
Q8TD19	DIKTLNIFLTK	SCLC	H82-Ket	0.4
Q8TD19	DIKTLNIFLTK	SCLC	H82-Rit	0.3
Q8TD19	LGDYGLAKK	shared	A549-ATP	20
Q8TD19	LGDYGLAKK	shared	A549-Ket	0.7
Q8TD19	LGDYGLAKK	shared	A549-Rit	1.5
Q8TD19	LGDYGLAKK	shared	H82-ATP	6.5
Q8TD19	LGDYGLAKK	shared	H82-Ket	0.5
Q8TD19	LGDYGLAKK	shared	H82-Rit	0.4
Q58A45	VMDPTKILITGK	shared	A549-ATP	7.5
Q58A45	VMDPTKILITGK	shared	A549-Ket	0.9
Q58A45	VMDPTKILITGK	shared	A549-Rit	1.5
Q58A45	VMDPTKILITGK	shared	H82-ATP	20
Q58A45	VMDPTKILITGK	shared	H82-Ket	0.4
Q58A45	VMDPTKILITGK	shared	H82-Rit	0.2
P15735	ATGHEFAVKIMEVTAER	SCLC	A549-ATP	1.7
P15735	ATGHEFAVKIMEVTAER	SCLC	A549-Ket	0.9
P15735	ATGHEFAVKIMEVTAER	SCLC	A549-Rit	1.1
P15735	ATGHEFAVKIMEVTAER	SCLC	H82-ATP	10.2
P15735	ATGHEFAVKIMEVTAER	SCLC	H82-Ket	0.7
P15735	ATGHEFAVKIMEVTAER	SCLC	H82-Rit	0.5
P48426	AYSKIK	NA	A549-ATP	2.7
P48426	AYSKIK	NA	A549-Ket	0.8
P48426	AYSKIK	NA	A549-Rit	0.8
P48426	AYSKIK	NA	H82-ATP	3.7
P48426	AYSKIK	NA	H82-Ket	0.5
P48426	AYSKIK	NA	H82-Rit	0.4
P78356	AYSKIK	NA	A549-ATP	2.7
P78356	AYSKIK	NA	A549-Ket	0.8

P78356	AYSKIK	NA	A549-Rit	0.8
P78356	AYSKIK	NA	H82-ATP	3.7
P78356	AYSKIK	NA	H82-Ket	0.5
P78356	AYSKIK	NA	H82-Rit	0.4
Q8TBX8	FKEYCPQVFR	NSCLC	A549-ATP	7.7
Q8TBX8	FKEYCPQVFR	NSCLC	A549-Ket	0.7
Q8TBX8	FKEYCPQVFR	NSCLC	A549-Rit	1.8
Q8TBX8	FKEYCPQVFR	NSCLC	H82-ATP	1.9
Q8TBX8	FKEYCPQVFR	NSCLC	H82-Ket	0.4
Q8TBX8	FKEYCPQVFR	NSCLC	H82-Rit	0.3
Q9UBF8	VPHTQAVVLNSKDK	NSCLC	A549-ATP	10.5
Q9UBF8	VPHTQAVVLNSKDK	NSCLC	A549-Rit	6
Q9UBF8	VPHTQAVVLNSKDK	NSCLC	H82-ATP	4.4
Q9UBF8	VPHTQAVVLNSKDK	NSCLC	H82-Ket	0.6
Q9UBF8	VPHTQAVVLNSKDK	NSCLC	H82-Rit	1.1
P53350	CFEISDADTKEVFAGKIVPK	SCLC	H82-ATP	8.7
P53350	CFEISDADTKEVFAGKIVPK	SCLC	H82-Ket	0.8
P53350	CFEISDADTKEVFAGKIVPK	SCLC	H82-Rit	0.7
P78527	EHPFLVKGGEDLR	SCLC	A549-ATP	0.8
P78527	EHPFLVKGGEDLR	SCLC	A549-Ket	0.4
P78527	EHPFLVKGGEDLR	SCLC	A549-Rit	2.1
P78527	EHPFLVKGGEDLR	SCLC	H82-ATP	20
P78527	EHPFLVKGGEDLR	SCLC	H82-Ket	0.5
P78527	EHPFLVKGGEDLR	SCLC	H82-Rit	0.5
P78527	GHDEREHPFLVKGGEDLR	NA	A549-Ket	0.6
P78527	GHDEREHPFLVKGGEDLR	NA	A549-Rit	1.5
P78527	KGGSWIQEINVAEK	SCLC	A549-ATP	3
P78527	KGGSWIQEINVAEK	SCLC	A549-Ket	0.6
P78527	KGGSWIQEINVAEK	SCLC	A549-Rit	0.7
P78527	KGGSWIQEINVAEK	SCLC	H82-ATP	20
Q96S44	FLSGLELVKQGAEAR	SCLC	A549-ATP	0.9
Q96S44	FLSGLELVKQGAEAR	SCLC	A549-Ket	0.6
Q96S44	FLSGLELVKQGAEAR	SCLC	A549-Rit	1.6
Q96S44	FLSGLELVKQGAEAR	SCLC	H82-ATP	17.3
Q96S44	FLSGLELVKQGAEAR	SCLC	H82-Ket	0.4
Q96S44	FLSGLELVKQGAEAR	SCLC	H82-Rit	0.2
P04049	DMKSNNIFLHEGLTVK	SCLC	H82-ATP	6.2
P04049	DMKSNNIFLHEGLTVK	SCLC	H82-Ket	0.7
P04049	DMKSNNIFLHEGLTVK	SCLC	H82-Rit	5.7

Q96BR1	FYAVKVLQK	shared	A549-ATP	20
Q96BR1	FYAVKVLQK	shared	A549-Ket	1.3
Q96BR1	FYAVKVLQK	shared	A549-Rit	1.6
Q96BR1	FYAVKVLQK	shared	H82-ATP	14
Q96BR1	FYAVKVLQK	shared	H82-Ket	0.8
Q96BR1	FYAVKVLQK	shared	H82-Rit	0.7
Q9H2G2	DLKAGNILFTLDGDIK	shared	A549-ATP	7.4
Q9H2G2	DLKAGNILFTLDGDIK	shared	A549-Ket	1
Q9H2G2	DLKAGNILFTLDGDIK	shared	A549-Rit	1
Q9H2G2	DLKAGNILFTLDGDIK	shared	H82-ATP	6.5
Q9H2G2	DLKAGNILFTLDGDIK	shared	H82-Ket	0.7
Q9H2G2	DLKAGNILFTLDGDIK	shared	H82-Rit	0.5
Q96Q15	DTVTIHSVGGTITILPTKTKPK	shared	A549-ATP	19.8
Q96Q15	DTVTIHSVGGTITILPTKTKPK	shared	A549-Ket	1.6
Q96Q15	DTVTIHSVGGTITILPTKTKPK	shared	A549-Rit	2.2
Q96Q15	DTVTIHSVGGTITILPTKTKPK	shared	H82-ATP	5
Q96Q15	DTVTIHSVGGTITILPTKTKPK	shared	H82-Ket	0.4
Q96Q15	DTVTIHSVGGTITILPTKTKPK	shared	H82-Rit	0.3
Q96SB4	FVAMKVVK	shared	A549-ATP	18
Q96SB4	FVAMKVVK	shared	A549-Ket	0.6
Q96SB4	FVAMKVVK	shared	A549-Rit	2.5
Q96SB4	FVAMKVVK	shared	H82-ATP	20
Q96SB4	FVAMKVVK	shared	H82-Ket	0.3
Q96SB4	FVAMKVVK	shared	H82-Rit	0.2
P78362	FVAMKVVK	shared	A549-ATP	18
P78362	FVAMKVVK	shared	A549-Ket	0.6
P78362	FVAMKVVK	shared	A549-Rit	2.5
P78362	FVAMKVVK	shared	H82-ATP	20
P78362	FVAMKVVK	shared	H82-Ket	0.3
P78362	FVAMKVVK	shared	H82-Rit	0.2
Q9Y2H1	DTGHIYAMKILR	NA	A549-ATP	0.2
Q9Y2H1	DTGHIYAMKILR	NA	A549-Rit	0.8
O94804	DLKAGNVLMTLEGDIR	shared	A549-ATP	5.1
O94804	DLKAGNVLMTLEGDIR	shared	A549-Ket	0.4
O94804	DLKAGNVLMTLEGDIR	shared	A549-Rit	0.9
O94804	DLKAGNVLMTLEGDIR	shared	H82-ATP	5.1
O94804	DLKAGNVLMTLEGDIR	shared	H82-Ket	0.6
O94804	DLKAGNVLMTLEGDIR	shared	H82-Rit	1.3
Q9Y6E0	DIKAANVLLSEHGEVK	shared	A549-ATP	13.5

Q9Y6E0	DIKAANVLLSEHGEVK	shared	A549-Ket	0.8
Q9Y6E0	DIKAANVLLSEHGEVK	shared	A549-Rit	1.2
Q9Y6E0	DIKAANVLLSEHGEVK	shared	H82-ATP	13.1
Q9Y6E0	DIKAANVLLSEHGEVK	shared	H82-Ket	0.5
Q9Y6E0	DIKAANVLLSEHGEVK	shared	H82-Rit	0.2
O00506	DIKAANVLLSEQGDVK	SCLC	A549-ATP	2.3
O00506	DIKAANVLLSEQGDVK	SCLC	A549-Ket	0.6
O00506	DIKAANVLLSEQGDVK	SCLC	A549-Rit	1.2
O00506	DIKAANVLLSEQGDVK	SCLC	H82-ATP	20
O00506	DIKAANVLLSEQGDVK	SCLC	H82-Ket	0.7
O00506	DIKAANVLLSEQGDVK	SCLC	H82-Rit	0.2
Q9P289	DIKAANVLLSEQGDVK	SCLC	A549-ATP	2.3
Q9P289	DIKAANVLLSEQGDVK	SCLC	A549-Ket	0.6
Q9P289	DIKAANVLLSEQGDVK	SCLC	A549-Rit	1.2
Q9P289	DIKAANVLLSEQGDVK	SCLC	H82-ATP	11.2
Q9P289	DIKAANVLLSEQGDVK	SCLC	H82-Ket	0.7
Q9P289	DIKAANVLLSEQGDVK	SCLC	H82-Rit	0.2
Q13188	DIKAGNILLNTEGHAK	shared	A549-ATP	20
Q13188	DIKAGNILLNTEGHAK	shared	A549-Ket	0.8
Q13188	DIKAGNILLNTEGHAK	shared	A549-Rit	1.3
Q13188	DIKAGNILLNTEGHAK	shared	H82-ATP	15.7
Q13188	DIKAGNILLNTEGHAK	shared	H82-Ket	0.6
Q13188	DIKAGNILLNTEGHAK	shared	H82-Rit	0.5
Q13188	ESGQVVAIKQVPVESDLQEIIK	SCLC	A549-ATP	0.3
Q13188	ESGQVVAIKQVPVESDLQEIIK	SCLC	A549-Rit	2.1
Q13188	ESGQVVAIKQVPVESDLQEIIK	SCLC	H82-ATP	20
Q13188	ESGQVVAIKQVPVESDLQEIIK	SCLC	H82-Ket	0.6
Q13188	ESGQVVAIKQVPVESDLQEIIK	SCLC	H82-Rit	0.4
Q15208	DTGHVYAMKILR	NSCLC	A549-ATP	7.5
Q15208	DTGHVYAMKILR	NSCLC	A549-Ket	0.7
Q15208	DTGHVYAMKILR	NSCLC	A549-Rit	1.4
Q15208	KDTGHVYAMKILR	NA	A549-ATP	1.3
Q15208	KDTGHVYAMKILR	NA	A549-Ket	0.3
Q15208	KDTGHVYAMKILR	NA	A549-Rit	1.5

Q13043	DIKAGNILLNTEGHAK	shared	A549-ATP	20
Q13043	DIKAGNILLNTEGHAK	shared	A549-Ket	0.8
Q13043	DIKAGNILLNTEGHAK	shared	A549-Rit	1.3
Q13043	DIKAGNILLNTEGHAK	shared	H82-ATP	15.3
Q13043	DIKAGNILLNTEGHAK	shared	H82-Ket	0.6
Q13043	DIKAGNILLNTEGHAK	shared	H82-Rit	0.4
Q13043	ETGQIVAIKQVPVESDLQEIIK	SCLC	H82-ATP	20
Q13043	ETGQIVAIKQVPVESDLQEIIK	SCLC	H82-Ket	0.5
Q13043	ETGQIVAIKQVPVESDLQEIIK	SCLC	H82-Rit	0.4
Q7L7X3	DIKAGNILLTEPGQVK	NSCLC	A549-ATP	6.6
Q7L7X3	DIKAGNILLTEPGQVK	NSCLC	A549-Ket	0.3
Q7L7X3	DIKAGNILLTEPGQVK	NSCLC	A549-Rit	2
Q9H2K8	DIKAGNILLTEPGQVK	NSCLC	A549-ATP	6.6
Q9H2K8	DIKAGNILLTEPGQVK	NSCLC	A549-Ket	0.3
Q9H2K8	DIKAGNILLTEPGQVK	NSCLC	A549-Rit	2
Q9UKI8	YLNEIKPPIIHYDLKPGNILLVDGTACGEIK	NA	H82-Ket	0.5
Q9UKI8	YLNEIKPPIIHYDLKPGNILLVDGTACGEIK	NA	H82-Rit	0.8
Q86UE8	YLNEIKPPIIHYDLKPGNILLVNGTACGEIK	SCLC	H82-ATP	13.3
Q86UE8	YLNEIKPPIIHYDLKPGNILLVNGTACGEIK	SCLC	H82-Ket	0.7
Q86UE8	YLNEIKPPIIHYDLKPGNILLVNGTACGEIK	SCLC	H82-Rit	1.7
Q86UE8	YVAVKIHQLNK	shared	A549-ATP	20
Q86UE8	YVAVKIHQLNK	shared	A549-Ket	0.7
Q86UE8	YVAVKIHQLNK	shared	A549-Rit	5.9
Q86UE8	YVAVKIHQLNK	shared	H82-ATP	8.9
Q86UE8	YVAVKIHQLNK	shared	H82-Ket	0.7
Q86UE8	YVAVKIHQLNK	shared	H82-Rit	1.1
Q9UKE5	DIKGQNVLLTENAEVK	shared	A549-ATP	15.7
Q9UKE5	DIKGQNVLLTENAEVK	shared	A549-Ket	0.7
Q9UKE5	DIKGQNVLLTENAEVK	shared	A549-Rit	2.3
Q9UKE5	DIKGQNVLLTENAEVK	shared	H82-ATP	13.4
Q9UKE5	DIKGQNVLLTENAEVK	shared	H82-Ket	0.6
Q9UKE5	DIKGQNVLLTENAEVK	shared	H82-Rit	0.4

Q6PHR2	EVVAIKCVAK	shared	A549-ATP	17.8
Q6PHR2	EVVAIKCVAK	shared	A549-Ket	1.2
Q6PHR2	EVVAIKCVAK	shared	A549-Rit	1.1
Q6PHR2	EVVAIKCVAK	shared	H82-ATP	20
Q6PHR2	EVVAIKCVAK	shared	H82-Ket	1.4
Q6PHR2	EVVAIKCVAK	shared	H82-Rit	0.5
Q6PHR2	NISHLDLKPQNILLSSLEKPHLK	NSCLC	A549-ATP	7
Q6PHR2	NISHLDLKPQNILLSSLEKPHLK	NSCLC	A549-Ket	1.5
Q6PHR2	NISHLDLKPQNILLSSLEKPHLK	NSCLC	A549-Rit	1.1
Q6PHR2	NISHLDLKPQNILLSSLEKPHLK	NSCLC	H82-ATP	0.5
Q6PHR2	NISHLDLKPQNILLSSLEKPHLK	NSCLC	H82-Ket	2.9
Q6PHR2	NISHLDLKPQNILLSSLEKPHLK	NSCLC	H82-Rit	1.7

Table 4.2 SILAC ratios of peptides detected by LC-MS/MS analysis. Table denoted whether peptides are shared between SCLC/NSCLC or unique to a particular tumor cell type.

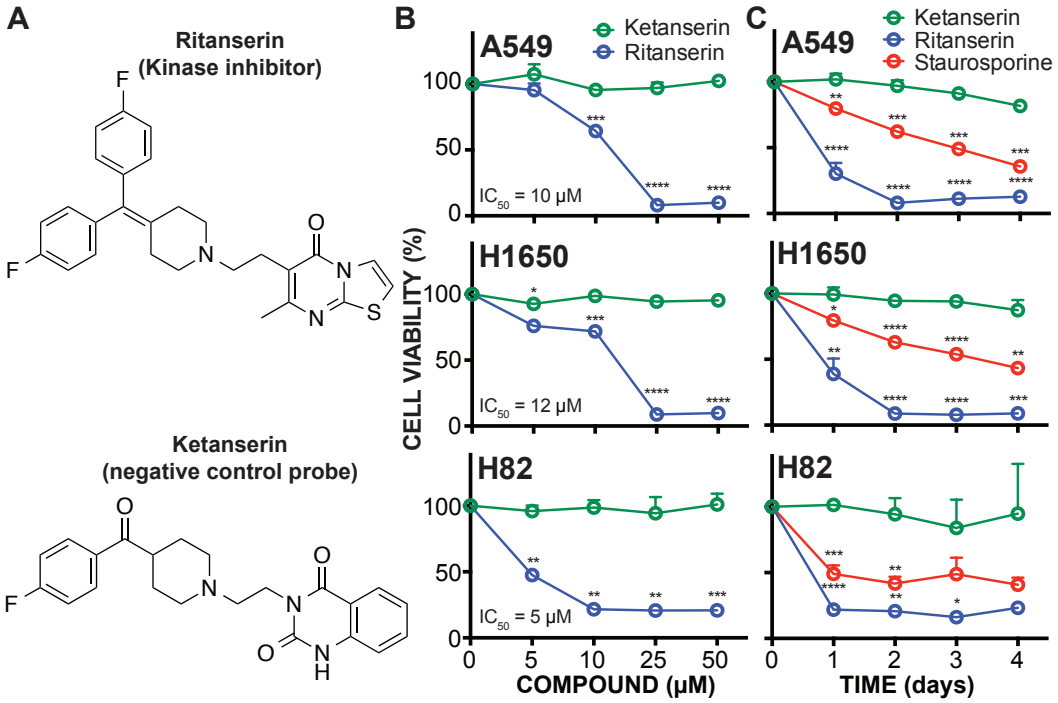

Figure 4.1. Ritanserin shows cytotoxic activity in lung tumor cells. **(A)** Ritanserin is a 5-HT_2 receptor (5-HT_2R) inverse agonist with known activity against lipid (DGKα) and protein (FER) kinases. Ketanserin is a 5-HT_2 R inverse agonist that lacks DGKα/FER inhibitory activity and serves as a negative control. **(B)** Cell viability dose-response curves for NSCLC (A549, H1650) and SCLC (H82) tumor cells treated with ritanserin or ketanserin at the indicated concentrations for 2 days. **(C)** Time course of cell viability in tumor cells treated with 25 μM ritanserin, 25 μM ketanserin, or 1 μM staurosporine for 4 days. Staurosporine is a pan-kinase inhibitor and included as a positive control of tumor cell death. All experiments were performed in triplicate and data are from two independent biological replicates performed on separate days (n = 6). Statistical significance was calculated with respect to ketanserin treatment. Data are shown as mean + S.E.M. *P ≤ 0.05, **P ≤ 0.01, *** P ≤ .001, and ****P ≤ 0.0001.

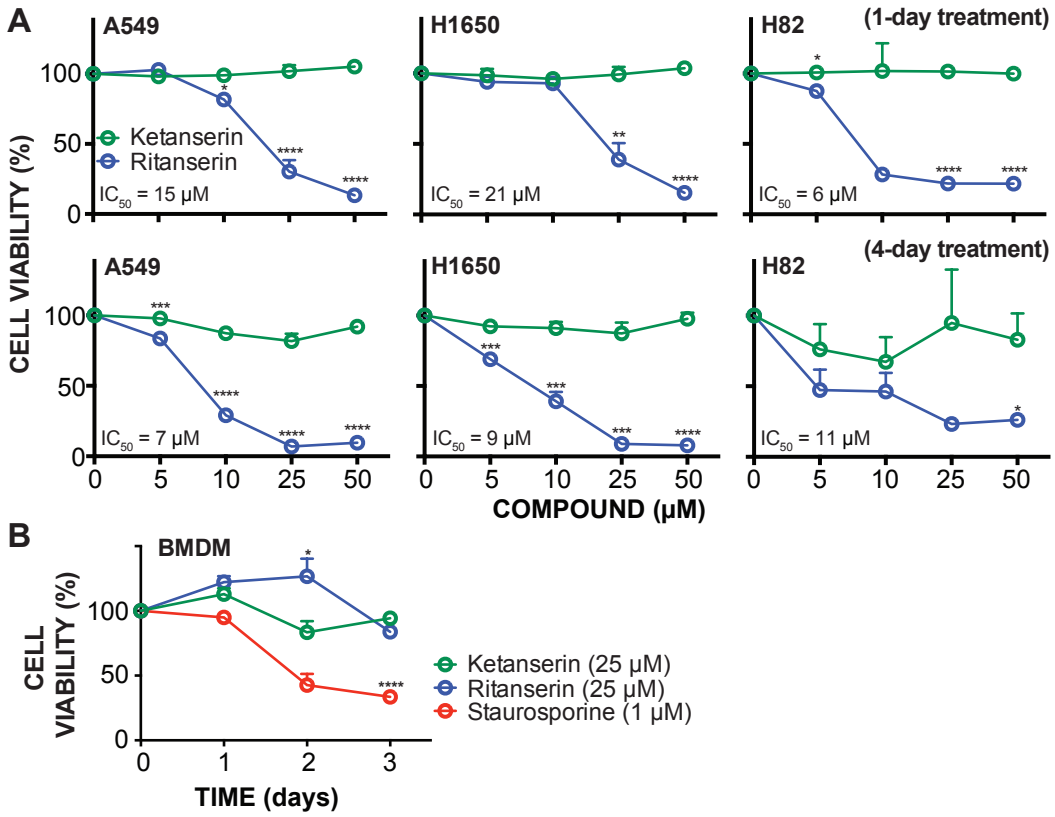

Figure 4.2. **Ritanserin activity in lung tumor cells**. **(A)** Lung cancer cell viability (%) at 1 and 4 days after treatment with compounds at the indicated concentrations as determined by the WST-1 metabolic assay. **(B)** Time course of cell metabolic activity (WST-1 assay) of primary bone marrow derived macrophages (BMDMs) treated with 1 µM staurosporine, 25 µM ritanserin, or 25 µM ketanserin. All experiments were performed in triplicate and data are from two independent biological replicates performed on separate days (n = 6). Statistical significance was determined by comparison with ketanserin treatment (negative control) at the same concentration and treatment time. Cell viability shown is normalized to vehicle treated samples. Data are shown as mean + S.E.M. * $P \leq 0.05$, ** $P \leq 0.01$, *** $P \leq .001$, and **** $P \leq 0.0001$.

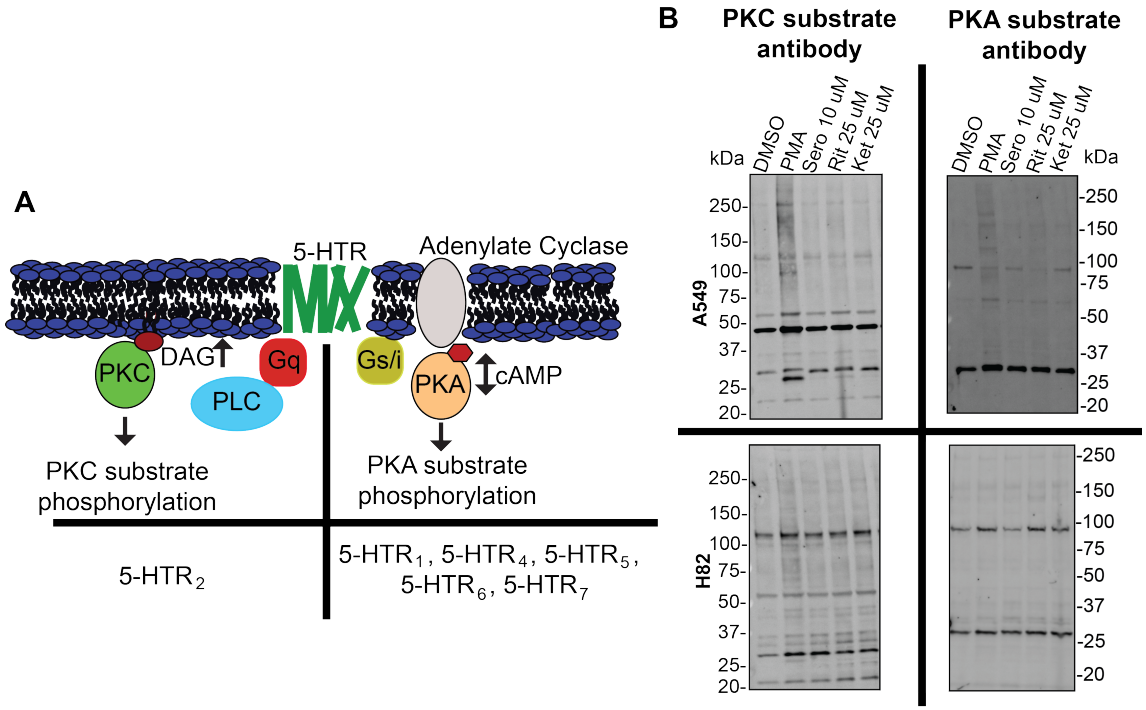

Figure 4.3. Ritanserin and ketanserin show negligible effects on 5-HTR signaling. **(A)** Schematic showing G-protein coupled receptor (GPCR) 5-HTR signaling. Activation of different members of the 5- HTR family leads to activation of Gq or Gs/i G-proteins, resulting in enhanced phospholipase C (PLC)- mediated diacylglycerol (DAG) activity or changes in adenylate cyclase-mediated cyclic adenosine monophosphate (cAMP) signaling, respectively. DAG and cAMP activate protein kinase-C (PKC) or -A (PKA), respectively, and their activity (as measured by substrate phosphorylation) can be used to monitor potential 5-HTR signaling activity. **(B)** A549 or H82 cells were treated with DMSO vehicle, PMA (100 ng/µL), serotonin (Sero, 10 µM), ritanserin (Rit, 25 µM), or ketanserin (Ket, 25 µM) to determine effects of each compound on global PKC and PKA activity. We observed negligible changes in 5-HTR signaling activity across all conditions tested, except for a mild increase in PKC substrate phosphorylation using

PMA as expected (PKC activator; positive control). Protein kinase substrate phosphorylation assays were performed as previously described (43).

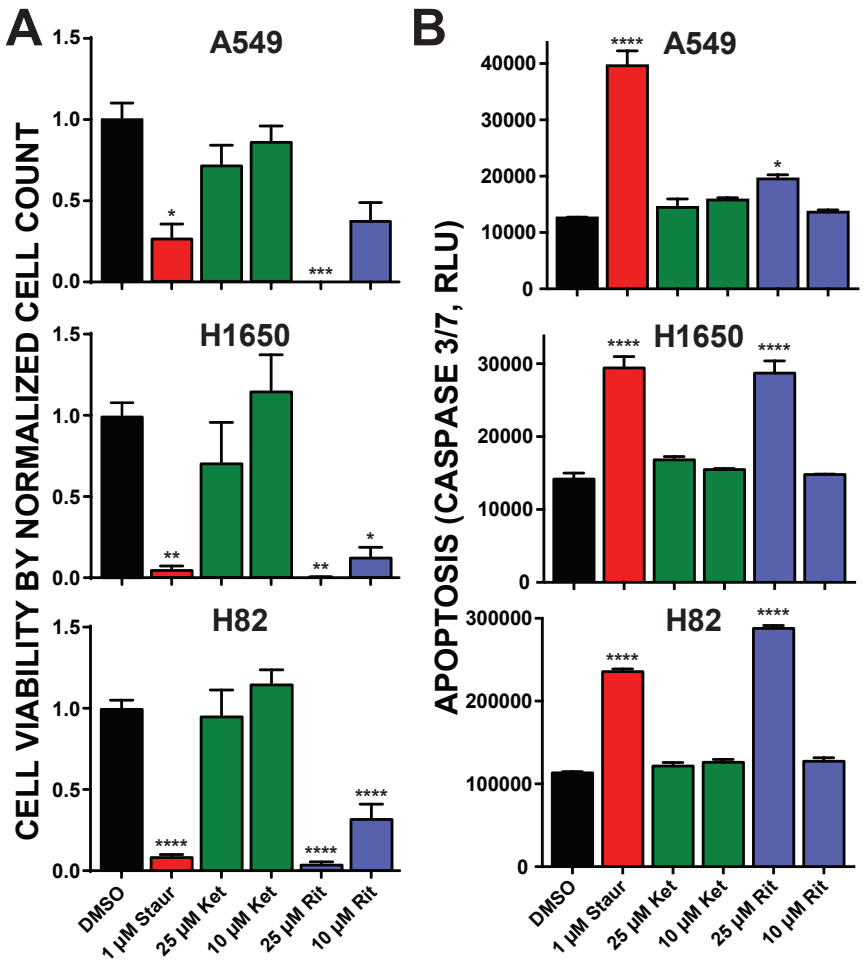

Figure 4.4. **Ritanserin treatments activate apoptosis in NSCLC and SCLC tumor cells**. A) Cell viability as measured by Trypan blue cell counts after treatment with staurosporine (Staur), ketanserin (Ket), or ritanserin (Rit) at the indicated concentrations for 2 days. Cell counts were normalized to vehicle control (DMSO). Statistical significance was calculated by comparison with 10 μM ketanserin treatment. B) Activation of apoptosis was determined by commercial CaspaseGlo 3/7 assay (see ESI for additional details). Cells were incubated with compounds at the concentrations given and allowed to grow for 1 day, at which point caspase activity was measured. Statistical

significance was calculated by comparison with vehicle control. All experiments were performed in triplicate and data are from two independent biological replicates performed on separate days (n = 6). Data are shown as mean + S.E.M. *P ≤ 0.05, **P ≤ 0.01, *** P ≤ .001, and ****P ≤ 0.0001.

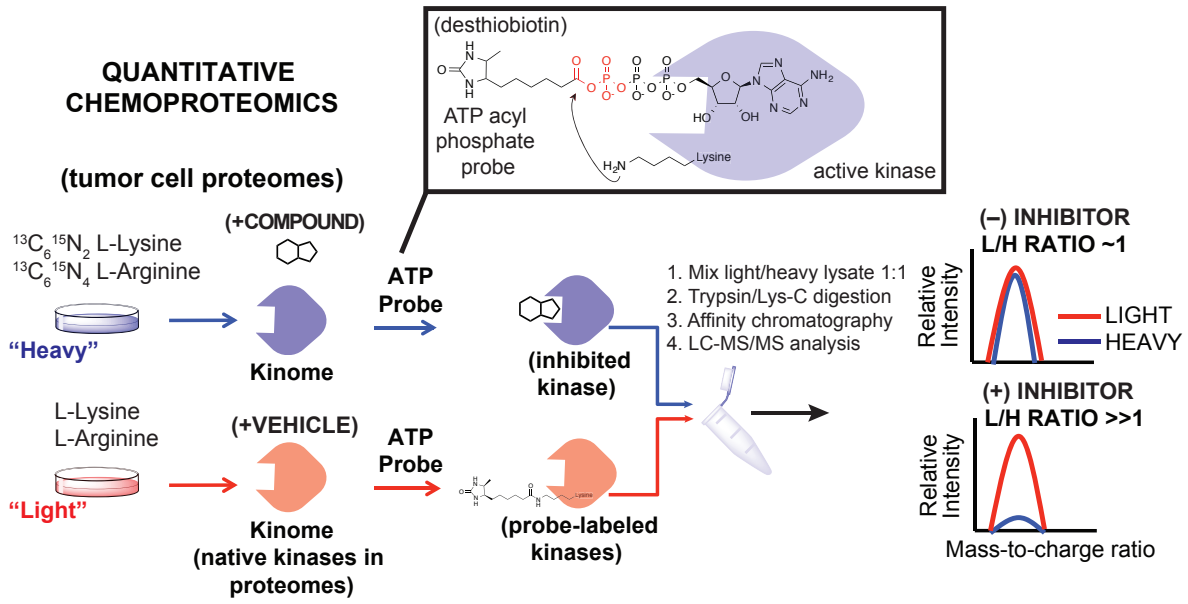

Figure 4.5. **Quantitative chemoproteomics to define the target spectrum of ritanserin in tumor cell proteomes**. Proteomes from lung tumor cells cultured in SILAC media are treated differentially with DMSO vehicle (light) or compound (heavy). Next, ATP acyl phosphate probe is added to both light and heavy proteomes to label active kinase via covalent modification of conserved lysines in kinase active sites. Proteomes are digested to tryptic peptides using proteases. Active-site probe-labeled peptides are enriched by avidin affinity chromatography and quantified by LC-MS/MS. SILAC (light/heavy) ratios are used to evaluate compound activity at individual kinase active sites. No inhibition results in a SILAC ratio of ~1 while competition at respective kinase active sites blocks probe labeling and enrichment resulting in SILAC ratios >>1 to identify targets of small molecule inhibitors.

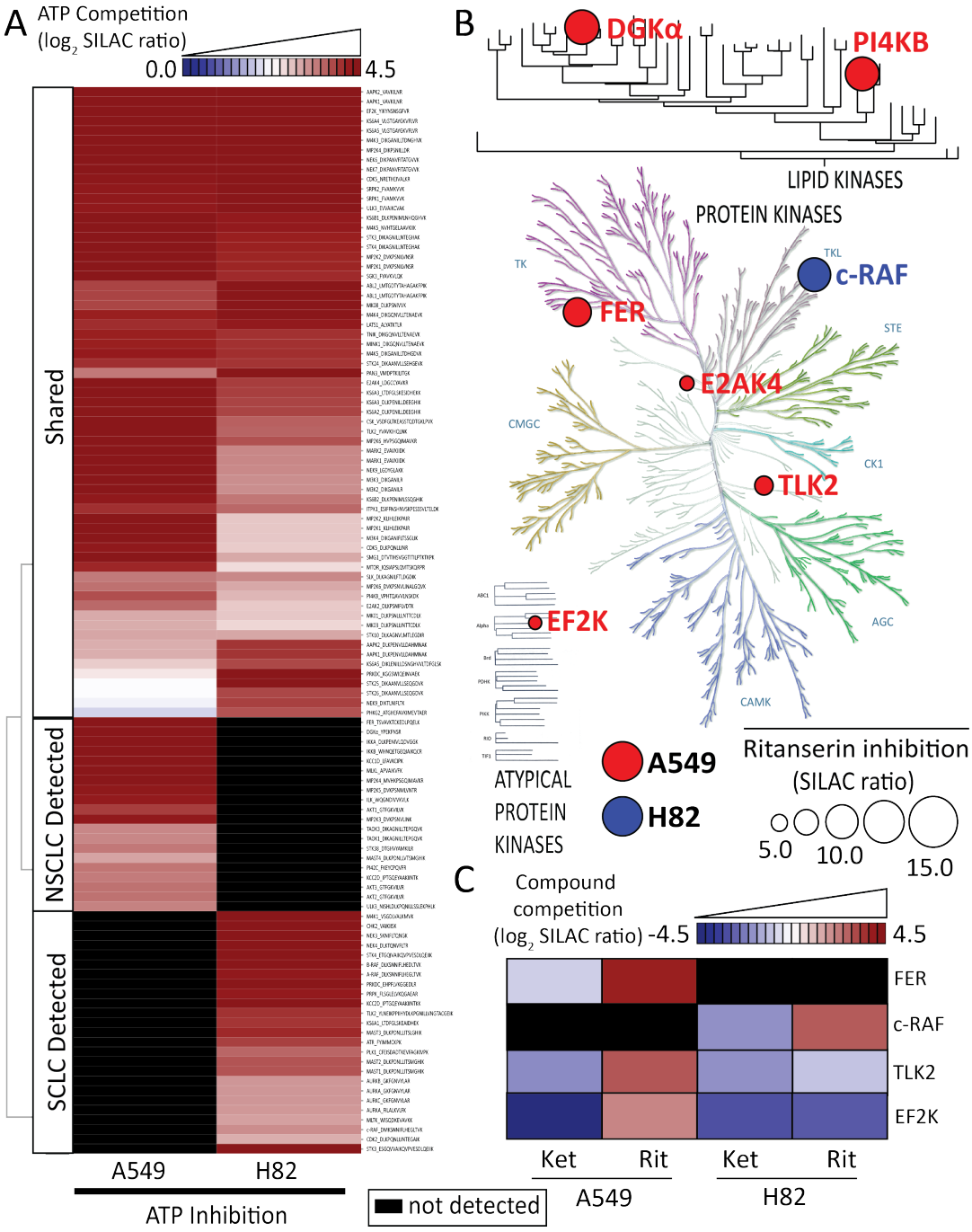

Figure 4.6. **Target landscape of ritanserin in lung cancer kinomes**. **(A)** Heatmap showing average $\log_2$ SILAC ratios of ATP competition at kinase active-sites detected in A549 and H82 cell proteomes. **(B)** Kinome tree showing proteins with SILAC ratios > 4

when treated with ritanserin. The size of the circle is proportional to SILAC ratio measured. Background image for protein kinase tree used by permission of Cell Signaling Technology (http://www.cellsignal.com). The lipid kinase tree was generated in-house using least-squared distances of MUSCLE aligned sequences. **(C)** Heatmap showing $\log_2$ SILAC ratios for kinases inactivated by ritanserin but not ketanserin that have a minimum DMSO:ritanserin SILAC ratio > 4. All experiments were measured 2-3 times (technical replicates in LC- MS) using data from 2-3 independent biological replicates performed on separate days (n = 6-9). All values shown are normalized to DMSO control and can be found in Table 4.1.

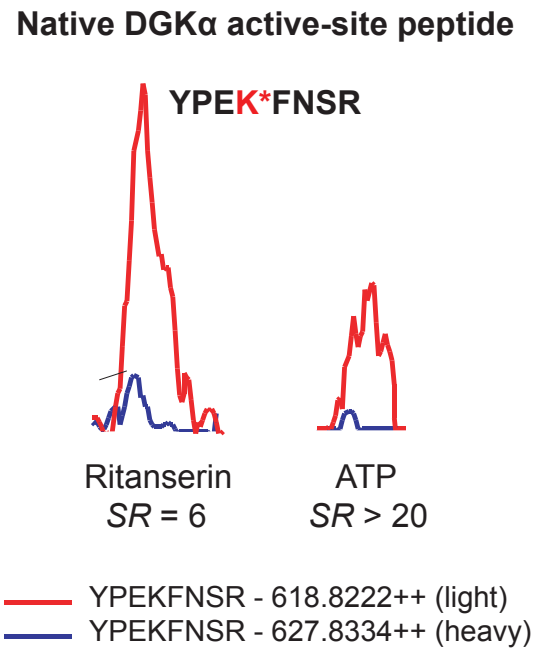

Figure 4.7. **Detection and inhibition of native DGKa in A549 proteomes**. MS1-extracted ion chromatograms of the probe labeled active-site peptide of DGKa. Pre-treatment of heavy A549 proteomes with ritanserin (100 μM) or ATP (1 mM) resulted in inhibition of DGKa active-site peptide probe labeling (ritanserin *SR* = 6; ATP *SR* > 20). All experiments were measured 3 times (technical replicates in LC-MS) using data from 3 independent biological replicates performed on separate days (n = 9). Peak images are a representative image from an individual injection.

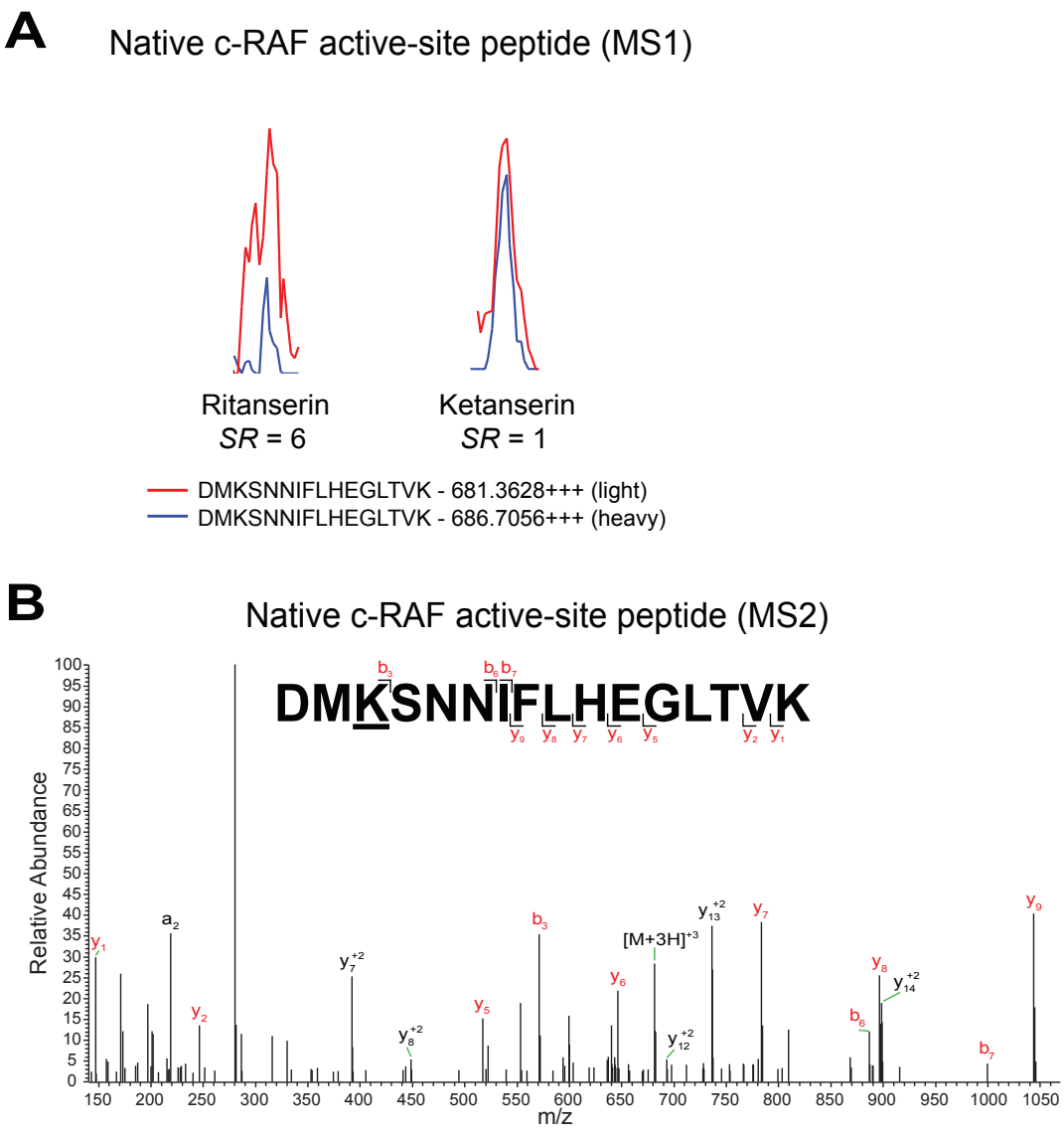

Figure 4.8. **Native c-RAF active-site peptide detected in H82 proteomes**. **(A)** MS1-extracted ion chromatograms of the probe labeled active-site peptide for c-RAF identified in H82 proteomes. Pre- treatment of heavy H82 proteomes with ritanserin (100 μM) results in blockade of c-RAF active-site probe labeling (*SR* > 6). Pre-treatment with ketanserin (100 μM) results in no inhibition (*SR* = 1). **(B)** MS2 spectra of probe-modified peptide corresponding to the active-site of c-RAF. Major b- and y-ion fragments derived

from neutral losses of the precursor (M) are shown in red in the spectrum. All experiments were measured 2-3 times (technical replicates in LC-MS) using data from 2 independent biological replicates performed on separate days (n = 6). A and B are representative images from a single measurement.

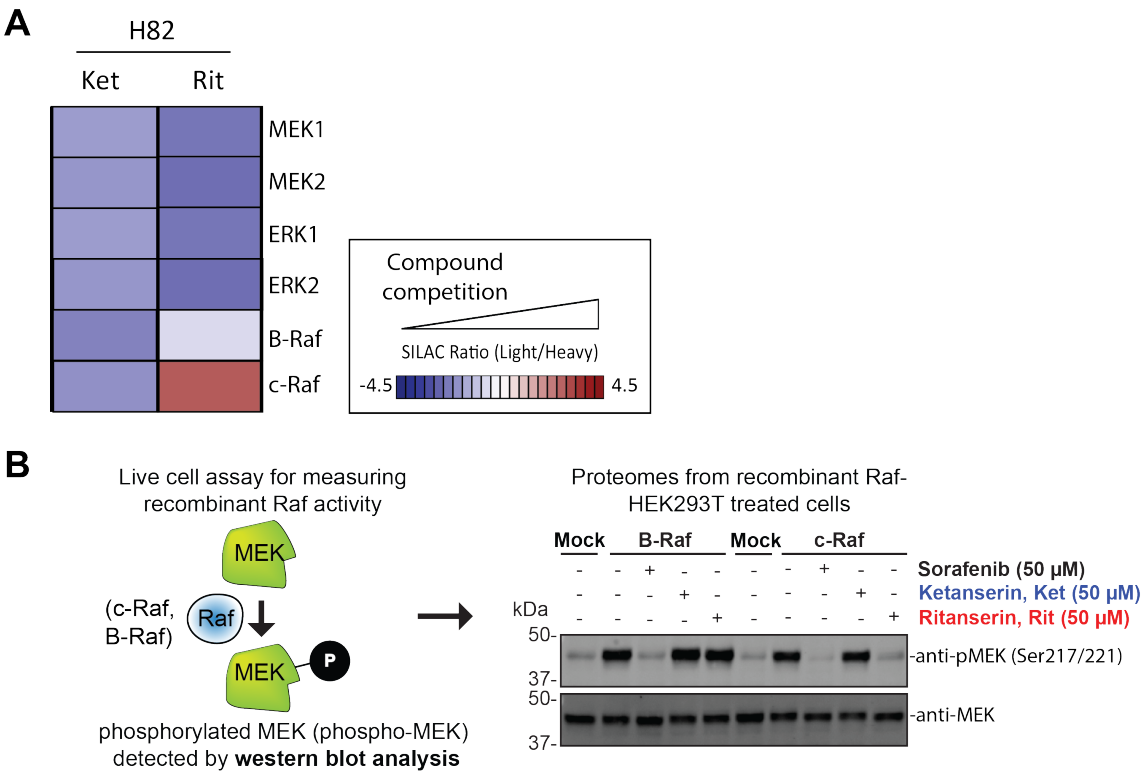

Figure 4.9. **Activity of ritanserin against kinases involved in MAPK signaling. (A)** Activity of ritanserin against native kinases involved in MAPK signaling as evaluated by quantitative chemoproteomics described in Fig. 4 and 5. The results show that in H82 SCLC proteomes, ritanserin shows selective blockade of c-RAF when compared with other MAPK kinases detected. Ketanserin show negligible activity, which supports serotonin-independent and ritanserin-specific effects. **(B)** Live cell activity assay to validate c-RAF as a target of ritanserin. RAF kinases (c-RAF and B-RAF) phosphorylate MEK and phosphorylated MEK (phospho-MEK (S217/S221), ~40 kDa) can be used to measure RAF activity in live cells by western blot (anti-phospho-MEK antibody). Recombinant c-RAF and B-RAF were overexpressed in HEK293T cells, recombinant RAF-HEK293T cells pretreated with DMSO vehicle or inhibitors (50 µM), followed by

activation of cells with PMA (20 ng/mL, 20 min). Cells were lysed and proteomes subjected to western blots to measure endogenous phospho-MEK. Overexpression of c-RAF and B-RAF resulted in enhanced phospho-MEK levels. Pretreatment with the pan-RAF inhibitor sorafenib blocked c-RAF- and B- RAF-mediated enhancement of phospho-MEK. In contrast, ritanserin showed inhibition of c-RAF but not B-RAF in overexpressing cells. Ketanserin was largely inactive in this assay. Blots shown are representative of 2 independent biological replicates (n = 2). Protein loading was comparable between sample conditions as evidenced by equivalent MEK levels measured (anti-MEK blot).

4.6 Acknowledgements

The authors thank all members of the Hsu laboratory and colleagues at the University of Virginia for review of the manuscript. We thank Mark M. Ross for his assistance with mass spectrometry experiments and data analysis. We thank Prof. Kwon-Sik Park for kindly providing lung tumor cell lines.

Author Contributions

Dr. Sean Campbell, Caroline Franks, Adam Borne and Dr. Ku-Lung Hsu conceived this study. Dr. Sean Campbell, Caroline Franks, Adam Borne, Myungsun Shin, and Liuzhi Zhang coordinated and designed this study. Dr. Sean Campbell designed, conducted, and analyzed the experiments shown in Figures 1, 2A, and 3A. Caroline Franks designed and conducted the experiments shown in Figures 5, 6, and 7. Adam Borne designed and conducted the experiments shown in Figure 8. Myungsun Shin designed and conducted the experiment shown in Figure 2B. Liuzhi Zhang conducted the experiment shown in Figure 3B. Dr. Sean Campbell, Caroline Franks, Adam Borne, and Dr. Ku-Lung Hsu performed the data analysis. The manuscript was drafted and edited by Dr. Sean Campbell, Caroline Franks, Adam Borne, and Dr. Ku-Lung Hsu.

Chapter 5: Identification of a Key Serine Hydrolase Enzyme Mediating the Induction of T cell Anergy

In progress: Caroline E. Franks and Ku-Lung Hsu.

5.1 Abstract

Tumor antigen-specific $CD4^+$ T cells mediate immune cell response to recognize and eradicate malignancies. In tumor microenvironments (TMEs), activation of antigen-specific $CD4^+$ T cells is limited due to dysfunctional antigen-presenting cells (APCs), which leads to rapid exhaustion of effector T cells characterized by impaired cytotoxicity and cytokine production. The enhancement of $CD4^+$ T cell response has been explored as a cancer immunotherapy strategy by direct activation of $CD4^+$ T cell help or indirect activation of downstream effectors; methods include therapeutic vaccination, CAR T cell therapies, and adoptive cell therapy. We hypothesized that small molecule serine hydrolase inhibitors could function to enhance $CD4^+$ T cell function in tumors and serve as novel immunomodulators for cancer therapy. We identified a 1,2,3-triazole urea, AA741, capable of enhancing $CD4^+$ T cell function. In Jurkats and primary murine $CD4^+$ T cells, AA741 increased IL-2 production in anti-CD3 stimulated, anergic populations while simultaneously diminishing NDRG1 expression. Future analyses will reveal the full capability of AA741 to revive $CD4^+$ T cell effector function.

5.2 Introduction

Cancer immunotherapy has become standard practice for treatment of cancer, akin to surgery, radiotherapy, and chemotherapy (167). The goal of immunotherapy is to enhance tumor-specific T cell response, as the tumor microenvironment (TME) suppresses tumor antigen-specific T cell activity (167). The biggest obstacles to consider in developing immunotherapies are overcoming central tolerance (elimination of developing tumor-reactive T cells in the thymus) and peripheral tolerance (tumor-reactive cells become functionally unresponsive or anergic), which are consequences of autoimmune preventive response, and tumor-associated immune suppression (167, 168). Historically, $CD8^+$ cytotoxic T lymphocytes (CTLs) have been the preferred target for tumor eradication, as they detect antigens expressed by all tumor types (167, 169). Recently, $CD4^+$ T cells have been revealed as important mediators of the tumor immune response and explored as targets for novel, effective, long-term therapy.

Antigen-specific $CD4^+$ T cells perform various functions to regulate tumor immune response. They provide help to $CD8^+$ T cells, aid in the activation and maturation of APCs, produce cytokines that are vital to cell differentiation and long-term T cell response, and activate B cells to produce tumor antigen-specific antibodies (169). Thus, it is postulated that cancer immunotherapies would benefit from both the inclusion and targeting of $CD4^+$ T cells. In the clinic, it has been shown that adoptive transfer of tumor-infiltrating $CD4^+$ T cells (where T cells specific for unique tumor mutations are isolated, expanded, and infused into patients to produce an antitumor immune response) in a patient with epithelial cancer resulted in tumor regression and

stabilization of condition (170). Of particular interest to us was the investigation of peripheral tolerance mechanisms in the TME that render $CD4^+$ T cells hyporesponsive (or anergic) and unable to efficiently "help" $CD8^+$ T cell antitumor responses (171). Anergy is a crucial tumor survival mechanism that has been described as a process of self-inactivation in the absence of appropriate co-stimulation (i.e. via CD28), resulting in evasion of immune tumor recognition and response (171). Targeting the anergic state may represent a powerful tool to improve immune response and enhance immunotherapy efficacy (171).

The majority of current first-generation, approved cancer immunotherapy agents are either engineered T cells or antibody-based biologics targeting tumors and immune checkpoint cascade, respectively. However, these strategies are not always specific and can result in immune attack on normal tissue resulting in immune-related adverse effects with severe and fatal consequences (172). Novel, second- and third-generation immunotherapies have focused on the design of small molecules that act on intracellular targets and receptors to abrogate immune suppression or promote effective cytotoxic lymphocyte response (172). Small molecules have distinct advantages over biologics: access to a broader range of molecular targets, control over dosing, and greater patient access due to lower production and development costs (172). We postulated that serine hydrolase small molecule inhibitors could potentially be exploited as novel immunomodulators to enhance the $CD4^+$ T cell tumor response by inhibiting or reversing induction of $CD4^+$ T cell anergy.

5.3 Materials and Methods

Mice and cell lines. C57BL6 (B6) mice were obtained from Jackson Laboratories. Human Jurkat T lymphocytes were obtained from ATCC. Jurkats were maintained in complete RPMI-1640 (Thermo Fisher Scientific) containing 10% FBS (Omega Scientific) and 1% L-glutamine (Thermo Fisher Scientific).

Materials and reagents. Anti-human CD3 antibody was purchased from BD Biosciences (#555336). Anti-human CD28 antibody was purchased from BD Biosciences (#555725). Anti-mouse CD3e antibody (Clone 145-2C11) was purchased from BD Biosciences (#553057). Anti-mouse CD28 antibody (Clone 37.51) was purchased from BD Biosciences (#553294). Rabbit anti-NDRG1 antibody was purchased from Cell Signaling Technology (# 5196S). Goat Anti-rabbit DyLight 550 was purchased from Thermo Fisher Scientific (#84541). Recombinant human IL-2 was purchased from PeproTech (#200-02-50ug). Recombinant murine IL-2 was purchased from PeproTech (#212-12-50ug).

Murine T cell preparation. Mouse splenocytes were harvested from 6-8 week old mice, subjected to red blood cell lysis, and washed. Naïve $CD4^+$ or $CD8^+$ T cells were purified using EasySep Mouse CD4 or CD8 T-Cell Isolation Kits (Stemcell Technologies). Cells were maintained for experiments in murine CTL media (RPMI-1640 containing 10% FBS, 1.5 mM HEPES, 1X MEM Nonessential AAs, 1X Essential AAs, 8 mM NaOH, 0.05 mg/mL gentamicin, 1 mM sodium pyruvate, 1% L-glutmatine, 50μM 2-ME).

T cell-based inhibitor screening platform. Primary mouse $CD4^+$ T cells were purified and resuspended in media (1 $x10^6$/mL). Cells were plated on a 96-well plate (200 µL/well) and pre-treated with compound (1 µM; 0.01% DMSO) for two hours at 37°C. Dynabead CD3/CD28 T cell activator beads (Gibco) were then added to each well to stimulate T cells. Cells were treated with compound daily for 3 full days. Supernatant was collected at 24, 48, and 72 hours for analysis of cytokine production using a human IL-2 DuoSet ELISA (R&D Systems)

***In vitro* clonal anergy model**. Human Jurkat or primary mouse $CD4^+$ T cells (5 x 10^5 mL^{-1}) were anergized by stimulation with 1 µg mL^{-1} of plate-bound anti-CD3 for 48h at 37°C on a round bottom, non-treated 96-well plate (200 µL/well) in the presence of IL-2 (10U mL^{-1}). Cells were centrifuged (400 x G for 5 minutes), supernatant removed and cells resuspended in fresh media. Supernatant was collected and analyzed for cytokine levels using human or murine IL-2 DuoSet ELISA (R&D Systems) or IFN-g DuoSet ELISA (R&D Systems). Cells were then 'rested' in the absence of IL-2 for 3 days. On day 3 of the rest, cells were treated acutely with compound for 4h at 37°C. Human Jurkat or primary mouse CD4+ T cells (5 x 10^5 mL^{-1}) were activated by stimulation with anti-CD3 (1 µg mL^{-1}) and anti-CD28 (1 µg mL^{-1}) for 48h at 37°C on a round bottom, non-treated 96-well plate (200 µL/well) in the presence of IL-2 (10U mL^{-1}). Cells were then 'rested' in the presence of IL-2 for 3 days. Cytokine production was measured by acute restimulation with anti-CD3 (1 µg mL^{-1}) and anti-CD28 (1 µg mL^{-1}) in the presence of IL-2 (10U mL^{-1}) and Brefeldin A (5 µg mL^{-1}) for 4h at 37°C followed by FACS analysis.

Proliferation was measured by restimulation with anti-CD3 (1 μg mL^{-1}) and anti-CD28 (1 μg mL^{-1}) in the presence of IL-2 (10U mL^{-1}) for 3 days at 37°C with CellTrace Violet.

Cell staining. Samples were stained with Live/Dead Green (Invitrogen) and a fluorescent conjugate antibody specific to surface proteins (CD8 or CD4, CD25, CD69 and CD44). After surface staining, samples were fixed/permeabilized with FOXP3 buffer and nuclear staining protocol (Thermo Fisher Scientific) and then stained with antibodies specific to intracellular proteins: TNFα (eBioscience #17-7321-81), IL-2 (eBioscience #12-7021-81), IFN-γ (eBioscience #25-7311-82), and Ki67 (BD Biosciences #563757).

FACS analysis. Flow cytometric analysis of the stained cells was conducted by using a Cytoflex (Beckman Coulter) cytometer. Data were analyzed using FlowJo software (Version 10, TreeStar). To identify the T cell population of interest, we gated on singlets, lymphocytes, $CD4^+$ or $CD8^+$ cells, and live cells, followed by $CD25^+$ $CD69^+$ or $CD44^+$ surface markers of activation, then $TNF\alpha^+$, IL-2^+, IFN-γ^+ or $Ki67^+$ intracellular proteins.

Western blot of NDRG1. Cell lysates were separated by ultracentrifugation (100,000 x G for 45 minutes) into soluble and membrane fractions, subjected to SDS-PAGE, transferred to a nitrocellulose membrane and membrane blocked (5% nonfat dry milk in 1X TBST) for 1h at room temperature. Membrane was then incubated in primary antibody (1:1000 NDRG1 antibody in 1X TBST) overnight at 4C. After rinsing (5X for 5 minutes in 1X TBST), DyLight 550 conjugated secondary antibody (1:10000 goat anti-

rabbit for 1h at room temperature) was used to detect primary antibody. Blots were rinsed (5X for 5 minutes in 1X TBST) and then visualized by fluorescence using a gel imager.

Gel-based ABPP with FP-Rhodamine. Jurkats were harvested, resuspended in phosphate-buffered saline (PBS; 100 μL), and separated into soluble and membrane fractions via ultracentrifugation (100,000 x G for 45 mins at 4°C). Proteomes were then diluted to 1 mg/mL in PBS and aliquoted into microtubes (50 μL total reaction volumes). FP-rhodamine probe was added to each sample (1 μM final concentration) and samples incubated for 30 mins at 37°C. Reactions were then immediately quenched with 4X SDS-PAGE loading buffer. After separation by SDS-PAGE (10% acrylamide), proteomes were visualized by in-gel fluorescence imaging.

5.4 Results

5.4.1 *APEH Inhibition Enhances IL-2 Production in CD4$^+$ T cells*

To identify new serine hydrolase targets in the regulation of CD4$^+$ effector T cell function, we designed a T cell-based assay capable of screening a large library of 1,2,3-triazole urea inhibitors. We isolated CD4$^+$ T cell splenocytes from C57BL/6J mice and treated cells with vehicle control (0.01% final DMSO concentration) or serine hydrolase inhibitor (200 structurally-diverse compound library; 1 μM final concentration) for 2 hours. After compound pretreatment, isolated CD4$^+$ T cells were stimulated with anti-CD3 and -CD28 antibody coated beads to provide TCR and co-stimulatory signals. Cells were treated once daily with vehicle or serine hydrolase inhibitor (1 μM final concentration). Supernatants were collected at 24 and 48 hours after anti-CD3/CD28 stimulation and commercial ELISA kits were used to measure IL-2 production. We observed substantial production of IL-2 in CD4$^+$ T cells after stimulation with anti-CD3/CD28 beads for 48 hours (Fig 5.1A). In contrast, activation with beads for 24 hours resulted in a slight increase in IL-2 production that was not significantly different from unstimulated vehicle-treated CD4$^+$ T cell controls. Interestingly, we identified several compounds that enhanced IL-2 production >10-fold compared with vehicle-treated counterparts under this suboptimal (24 hour) activation paradigm (AA323, AA741, KLH-PC1, and KLH41, Fig 5.1B). Notably, the molecular target for AA323 and AA741 (Figure 5.2) is acyl-peptide hydrolase (APEH), a serine hydrolase involved in hydrolysis of N-terminally acetylated proteins (78). We demonstrated in previous studies that APEH is expressed in T cells and inactivation of APEH results in accumulation of N-acetylated

proteins and promotes proliferation of a T-cell hybridoma cell line (78). Here, we provide the first evidence that this serine hydrolase dramatically enhances IL-2 production.

5.4.2 *Inhibition of APEH by AA741 Enhances Cytokine Production and Diminishes NDRG1 Expression in Anergic T cells*

We hypothesized that AA741 could function as a potential immunotherapy drug candidate. Previous studies revealed that the most potent substrate of APEH (targeted by AA741) is NDRG1, a novel factor in T cell clonal anergy (78, 173). In A.E7 cells (a $CD4^+$ T cell clone) NDRG1 was shown to be upregulated in anergic signaling and resting anergic cells (173). NDRG1 was negatively regulated by CD28 signaling in a proteasome-dependent manner, and IL-2 treatment of anergic cells lead to reversal of anergy, NDRG1 phosphorylation and subsequent degradation (173). Combined, we postulated that NDRG1-associated clonal anergy in $CD4^+$ T cells could be repressed by AA741-induced APEH inactivation.

To translate our findings towards clinically relevant applications, we implemented an *in vitro* model of T cell clonal anergy to test the capability of AA741 to reverse the induction of anergy in $CD4^+$ T cells. Anergic T cells are alive, but exhibit poor proliferation and IL-2 production in response to antigenic stimulation (173, 174). Often, T cells specific for tumor-associated antigens in cancer patients are detected but exhibit unresponsiveness (174). Reversal of the anergic state could potentially restore immune response in tumor environments, and is essential for immunotherapy applications such as tumor vaccinations and adoptive immunotherapy (174). We used immortalized human

Jurkat T cell lymphocytes initially as a representative model for assay development. Jurkats were plated on a 96-well plate coated with either plate bound human anti-CD3 (to induce anergy) or anti-CD3/CD28 (to activate) and stimulated for 48 hours in the presence of recombinant human IL-2. The cells were then centrifuged, supernatant collected for cytokine analysis, cells resuspended in fresh media, and then rested for three days. In order to assess the ability of AA741 to reverse the anergic state, the cells were treated with vehicle (DMSO) or compound for four hours, and then transferred to a 96-well plate coated with plate bound human anti-CD3/CD28 for restimulation. Supernatant was then collected after 48 hours of restimulation to assess cell function. Supernatant collected 48 hours after initial anti-CD3 or anti-CD3/CD28 activation revealed that Jurkats exposed to only anti-CD3 produced ~4-fold less IL-2 than anti-CD3/CD28 stimulated counterparts, indicating a distinct functional difference between anti-CD3 and anti-CD3/28 exposed cells (Figure 5.3A). We also observed significant increases in IL-2 production of anergic cells pre-treated with AA741 prior to restimulation with anti-CD3/CD28 (Figure 5.3B). Notably, at concentrations of 1 nM and 10 nM we observed no significant difference between IL-2 production in restimulated cells initially exposed to anti-CD3 versus anti-CD3/28, suggesting that low doses of AA741 may be capable of restoring effector function in anergic T cell populations.

We also investigated the mechanism by which AA741 was inducing changes in IL-2 production. We hypothesized that inhibition of APEH by AA741 results in inactivation of T cell clonal anergy factor NDRG1. In order to test this hypothesis we used a western blot to detect NDRG1 expression in anti-CD3 or anti-CD3/28 stimulated

Jurkats treated with AA741 (Figure 5.4). As predicted, anti-CD3 stimulated cells express increased levels of NDRG1 as compared to anti-CD3/28 stimulated cells. Interestingly, at the lowest treatment doses of AA741 (1 nM and 10 nM) we saw a reduction in the expression of NDRG1. This suggests that increased IL-2 cytokine production in AA741 treated cells may be due to differences in expression of NDRG1.

We next assessed whether or not these results could be emulated in primary murine $CD4^+$ T cells. In order to obtain as much information as possible from these analyses, we used fluorescence-activated cell sorting (FACS) to evaluate surface marker expression, cytokine secretion, and proliferation of restimulated cells. We used a gating strategy (Figure 5.5) to filter for $CD4^+$ T cells expressing either CD25 or CD69/CD44 surface markers of activation. We found no significant differences in the percentage of total cell population expressing CD25 or CD69/CD44 in anti-CD3 or anti-CD3/28 stimulated cells (Figure 5.6A and B). Treatment with 10 nM AA741 did not affect expression of surface markers of activation (Figure 5.6A and B). We then assessed the expression of intracellular cytokines IL-2, IFNγ, and TNFα, and Ki67 (associated with cell proliferation) in $CD25^+$ or $CD69^+/CD44^+$ $CD4^+$ T cells (Figure 5.6A and B). The expression of all intracellular proteins except IFNγ was not significantly different between anti-CD3 or anti-CD3/28 stimulated cells. Interestingly, though, anergic anti-CD3 exposed $CD4^+$ T cells had a significantly lower percentage of cells that produced IFNγ.

We also assessed the ability of $CD4^+$ T cells to proliferate upon restimulation with anti-CD3/28 using Cell Trace Violet (Figure 5.6C). We would expect functionally

activated T cells to proliferate and expand upon TCR stimulation (CD3) with co-stimulatory signal (CD28). While we do see extremely low levels of cell proliferation in unstimulated cells, no differences in proliferation were identified between anti-CD3 versus anti-CD3/28 stimulated $CD4^+$ T cells and treatment with AA741 (10 nM) did not alter proliferation (Figure 5.6C).

5.4.3 *Chemical Proteomic Profiling of AA741*

In order to validate that we were engaging and inactivating the expected target of AA741, APEH, we implemented activity-based protein profiling using fluorophosphonate probe FP-rhodamine (FP-Rh) to assess serine hydrolase activities in Jurkats under each stimulation model. Fluorophosphonates are the most broadly reactive identified warhead that selectively targets serine hydrolases (75). Jurkats were stimulated with either plate bound anti-CD3 or anti-CD3/28 in petri dishes for 48 hours, transferred to uncoated petri dishes, and then treated with AA741 for 4 hours. Cells were immediately harvested, lysed, and treated with FP-Rh. Proteins were then separated by SDS-PAGE and visualized by in-gel fluorescence (Figure 5.7). We found that in anti-CD3 and anti-CD3/28 stimulated Jurkats, AA741 selectively inactivates APEH even at the lowest dosage (1 nM) compared to vehicle (DMSO) control. This data reveals that we are, in fact, engaging and inhibiting APEH.

5.5 Discussion

The TME drives immunosuppression through a variety of processes that prevent the development of an effective antitumor immune response. T cells are one of the main targets for immunosuppression. In the TME, lack of dendritic cell maturation results in inefficient presentation of tumor antigens, which leads to the induction of T cell anergy. In this state, T cells become hyporesponsive and unable to further aid in the T cell antitumor response due to the absence of appropriate co-stimulation (i.e. via CD28). Targeting and reversing the anergic state would improve immune response and enhance immunotherapy efficacy (171).

Here, we demonstrate a novel application for the serine hydrolase inhibitor AA741 as an enhancer of $CD4^+$ T cell function. In human Jurkats and primary murine $CD4^+$ T cells pre-treatment of anergic, anti-CD3 exposed cells with AA741 resulted in significant increase in IL-2 cytokine production, and NDRG1 expression was decreased at doses corresponding to increased IL-2 production. This may suggest that AA741 has the capability to restore T cell effector function through inactivation of NDRG1-induced T cell clonal anergy. Unfortunately, we were unable to identify significant changes in functionality of primary murine $CD4^+$ T cells by FACS analysis. Additional studies to will be necessary to validate this study in a clinically relevant biological system (i.e. in primary cells or animal models).

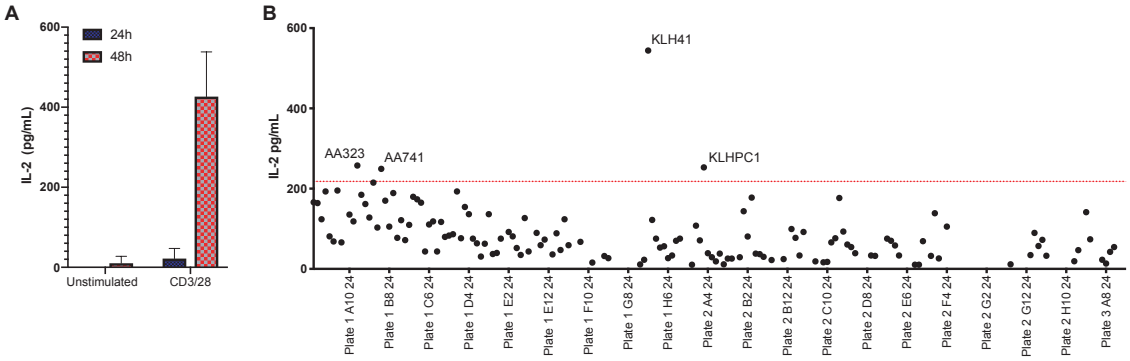

Figure 5.1 (A) Primary $CD4^+$ splenocytes were stimulated with CD3/28-coated beads for 48 hours. Supernatant was collected at 24 and 48 hours and IL-2 production quantified by human IL-2 ELISA. Production of IL-2 by $CD4^+$ T cells is significantly increased after 48 hours of stimulation compared to unstimulated control. **(B)** Primary $CD4^+$ splenocytes were isolated and pre-treated with a library of serine hydrolase inhibitor compounds (1 μM) for 2 hours prior to stimulation with CD3/28-coated beads. After 24 hours of stimulation, supernatant from AA323, AA741, KLH41, and KLHPC1 treated cells had >10-fold (denoted by dotted red line) increases in levels of IL-2 compared to DMSO control.

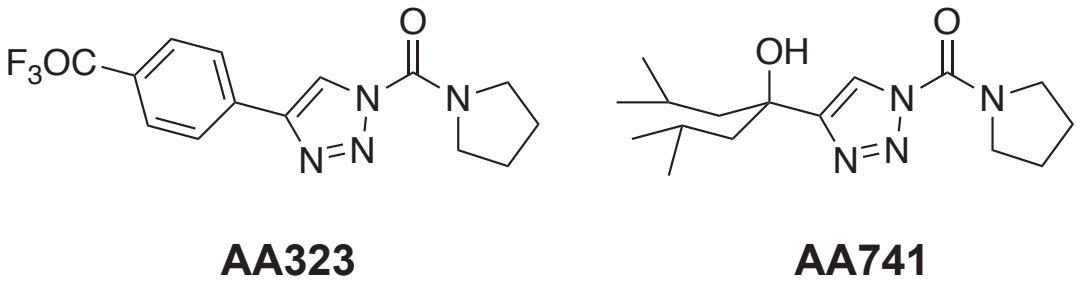

Figure 5.2 Structures of AA323 and AA741. Compounds identified as inhibitors of acyl-peptide hydrolase (APEH).

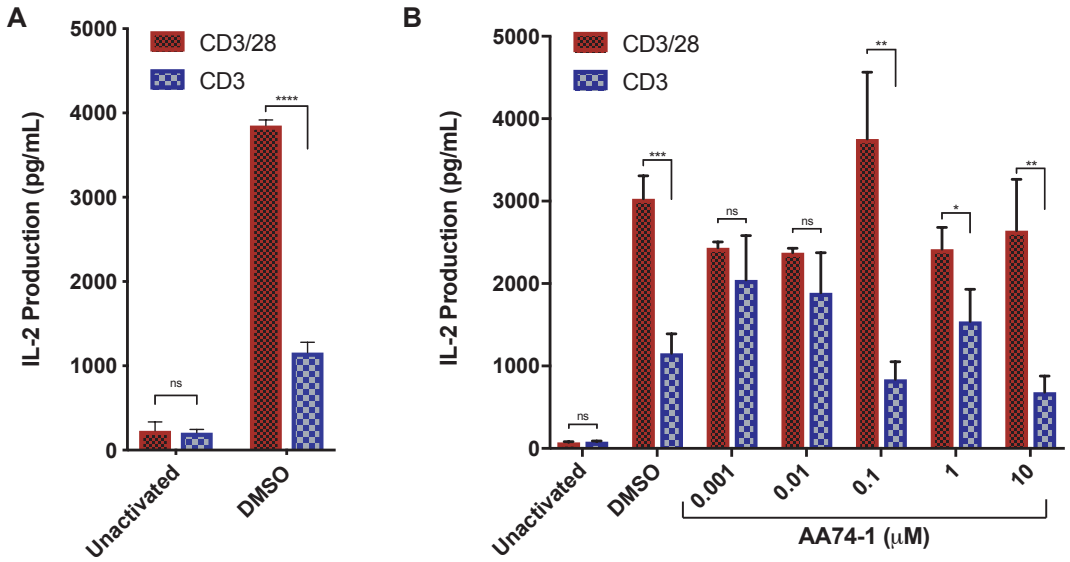

Figure 5.3 Analysis of AA741 in Jurkats stimulated with anti-CD3 or anti-CD3/28. **(A)** Jurkats were stimulated with plate bound anti-CD3 or anti-CD3/28 for 48 hours. Supernatant was collected and analyzed for IL-2 production by ELISA. Cells stimulated with anti-CD3/28 display significantly increased IL-2 production compared to anti-CD3 stimulated cells. **(B)** Jurkats were stimulated with plate bound anti-CD3 or anti-CD3/28 for 48 hours, rested for one day, and then treated for four hours with indicated concentrations of AA741 or vehicle. Cells were then restimulated with anti-CD3/CD28 for 48 hours, and supernatant was collected to assess IL-2 production. Cells pre-treated with 1 nM or 10 nM of AA741 produced levels of IL-2 that were not significantly different compared to anti-CD3/28 stimulated paired sample replicates. Data shown are mean +/- SD for at least three replicates. *$P \leq 0.05$, **$P \leq 0.01$, ***$P \leq 0.001$, ****$P \leq 0.0001$, and ns is not significant for anti-CD3 versus anti-CD3/28 paired samples.

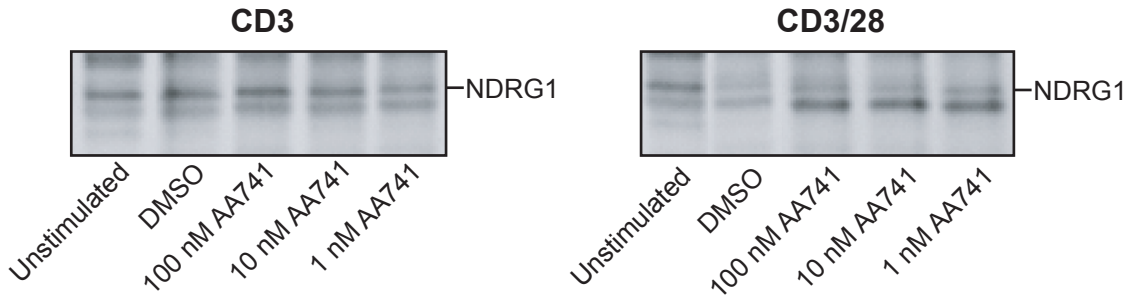

Figure 5.4 Western blot of NDRG1 expression. Jurkats were stimulated with plate bound anti-CD3 or anti-CD3/28 for 48 hours. Cells were transferred to an untreated dish to rest for 24 hours and treated with indicated concentrations of compound or vehicle (DMSO) for four hours. Cells were restimulated with plate bound anti-CD3/CD28 for 48 hours, then cells collected for analysis by western (Primary - 1:1000 anti-NDRG1 produced in rabbit; Secondary - 1:10000 goat anti-rabbit DyLight 550).

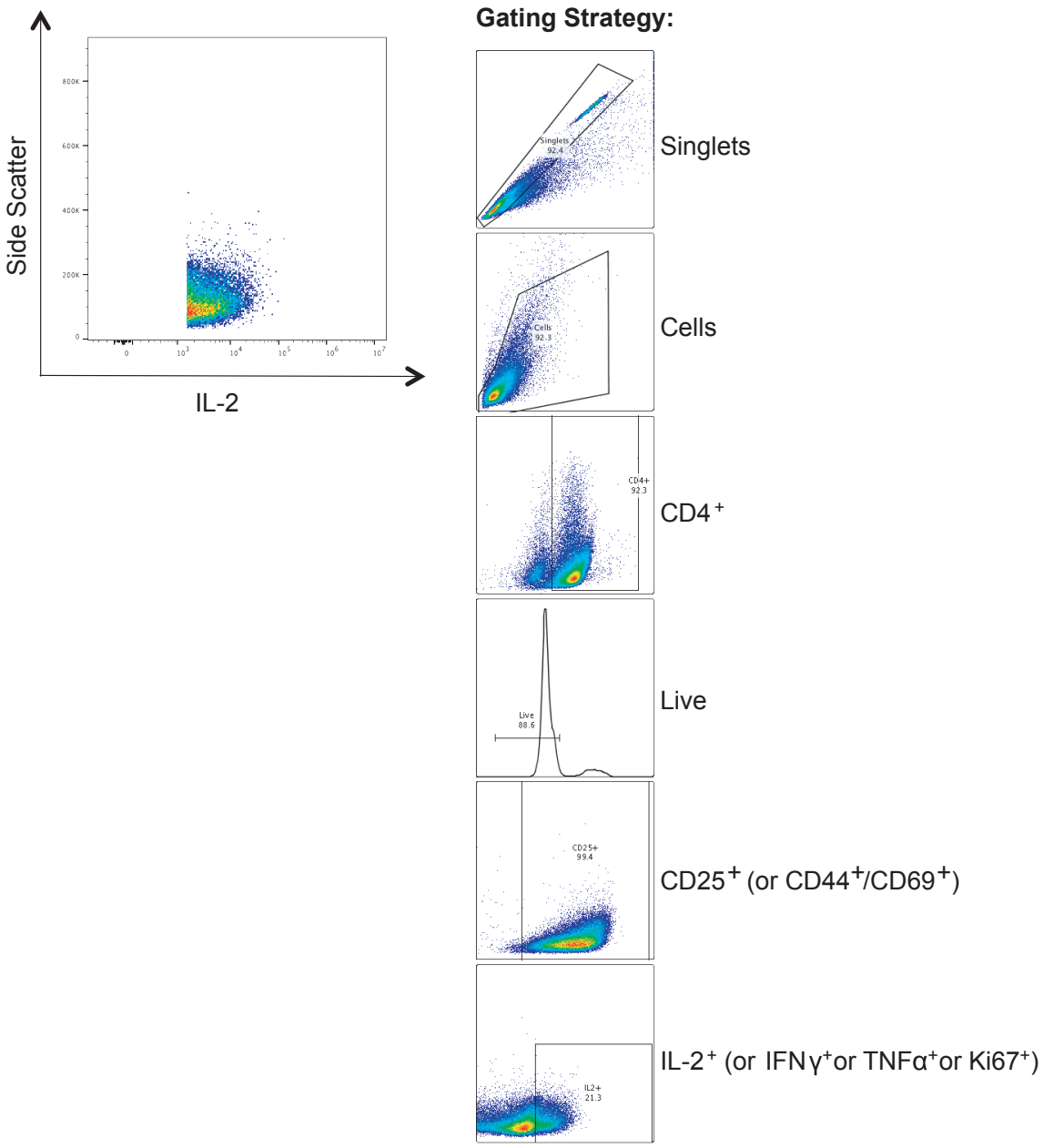

Figure 5.5 Gating strategy for FACS experiments. Primary $CD4^+$ splenocytes were stained and analyzed by flow cytometry. Cells were gated for single events, cells, expression of CD4, live cells and then expression of either CD25 or CD44/CD69. Cells expressing CD25 or CD44/CD69 were gated for production of IL-2, IFNγ, TNFα, and Ki67.

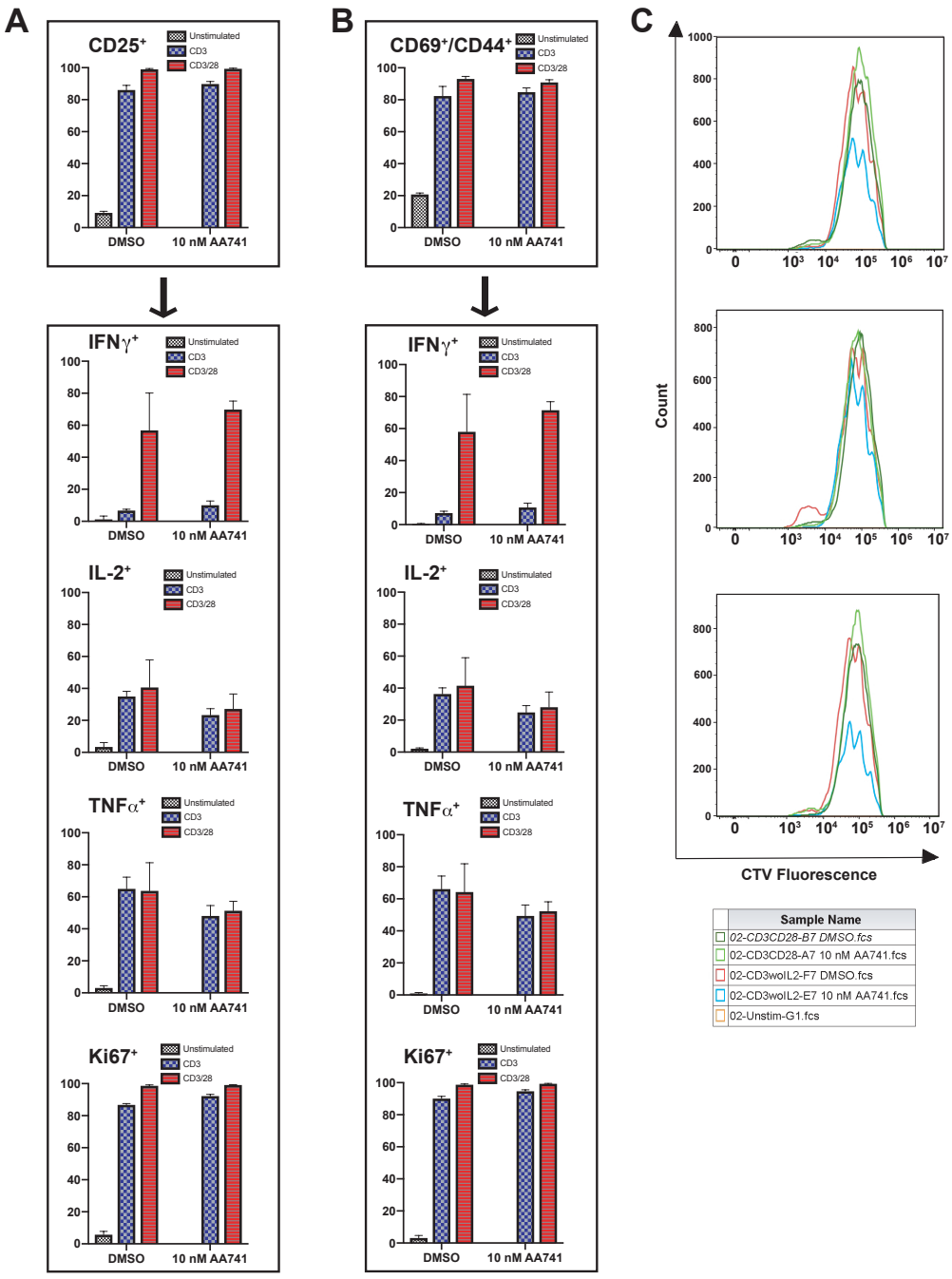

Figure 5.6 FACS Analysis of primary murine CD4+ T cells. (A) Analysis of cytokine production in T cells expressing CD25. Expression of CD25 and cytokine production is quantified as a percentage of total cells. **(B)** Analysis of cytokine production in T cells expressing CD69/CD44. Expression of CD69/CD44 and cytokine production is

quantified as a percentage of total cells. **(C)** Analysis of proliferation of T cells by CellTrace Violet fluorescence. Each plot is representative of one biological replicate, three total. Data shown in **A** and **B** are for at least three replicates.

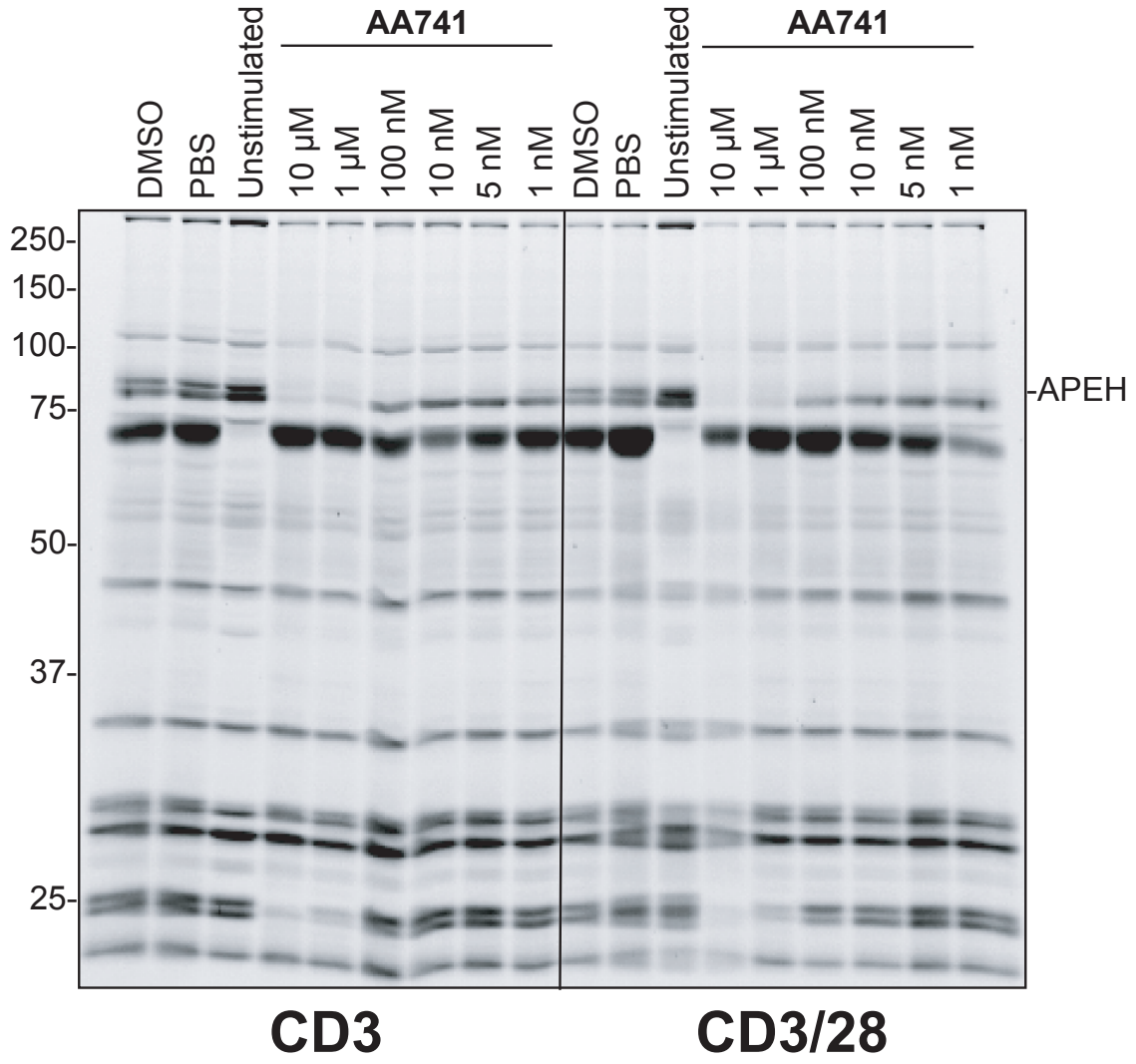

Figure 5.7. Gel ABPP Analysis of AA741 Treated Jurkats. Cells were stimulated for 48 hours with plate bound anti-CD3 or anti-CD3/CD28 and transferred to untreated petri dishes. Cells were treated with compound at the indicated concentrations or vehicle (DMSO) for 4 hours and then harvested for analysis by FP-Rh. APEH is inhibited in anti-CD3 and anti-CD3/28 stimulated cells at each tested concentration.

5.6 Acknowledgements

The authors thank all members of the Hsu laboratory and colleagues at the University of Virginia for providing continual feedback and suggestions throughout the development of this project. Thank you especially to Marissa Gonzales and Dr. Timothy N. J. Bullock for assistance with design of the *in vitro* T cell clonal anergy model, in depth training in cell staining and FACS experimental setup, and the analysis of FACS data.

Chapter 6: Conclusions and Future Directions

6.1 *Conclusions and Significance*

This dissertation highlights the extensive capability of chemical proteomic profiling as a tool to evaluate potential drug candidates in a variety of biological contexts. We have used chemical proteomic profiling to provide insight as to regions of a lipid kinase important for enzyme function, evaluate the selectivity of inhibitor compounds against larger kinase and serine hydrolase families, reveal novel clinical applications for a kinase inhibitor and a serine hydrolase inhibitor, and even identify a new lipid kinase inhibitor compound with greater selectivity and potency for DGKα. Over the past five years we have made significant contributions to the field of chemical biology that will be used to drive efforts to target and treat human disease, and contribute to our greater understanding of human biology.

In our early work, we showed that ATP acyl phosphate probes, combined with quantitative LC-MS could be used to profile lipid kinases. Using this technology, we were the first to define the location of the ATP binding site for all five classes of DGKs, providing the first experimental evidence in support of a unique DGK ATP binding motif. We also identified important domain binding sites of DGKs that may aid in the future development of DGK isoform-selective inhibitors.

We then used ATP acyl phosphate probes to assess the ability of ritanserin to function as a selective DGKα inhibitor. We identified the C1 and DAGKa domain as the major ritanserin ligand binding sites, distinct from the ATP binding region. This information helps to support and explain previous kinetic findings of a mixed competitive

mechanism of inhibition for ritanserin. Within the DGK superfamily, we showed that ritanserin was selective for DGKα, but we discovered substantial cross-reactivity against protein kinases, including the non-receptor tyrosine kinase FER that was inactivated to a similar magnitude as DGKα. This study emphasizes the need for new small molecules to target this lipid kinase family in the clinic.

Using fragment-based screening, we evaluated the structural regions of ritanserin responsible for inactivation of DGKα. We discovered that the 'lipophilic' region (RF001) is the major contributor to DGKα selectivity that retains binding at the C1 and DAGKa sites while removing FER and other kinase off-target activity. We found that the nucleotide-like region (RLM001) mimics ATP in its ability to broadly compete at ATP-binding sites of DGKα, as well as >60 native ATP-binding proteins (kinases and ATPases) detected in cell proteomes. Our studies highlight the utility of chemical proteomics in revealing active-site features of lipid kinases to enable development of inhibitors with enhanced selectivity against the human proteome.

In an effort to diversify the clinical potential of ritanserin, we investigated its ability function as a lipid and protein kinase inhibitor in diverse lung cancer types. We revealed a ritanserin-dependent kinase network that includes key mediators of lipid (DGKα, PI4KB) and protein signaling (FER, RAF), metabolism (EF2K, E2AK4), and DNA damage response (TLK2) to broadly kill lung tumor cell types. Ritanserin selectivity targets c-RAF in the SCLC subtype with negligible activity against other kinases mediating MAPK signaling, providing evidence in support of c-RAF as a key target mediating its anticancer activity. Our findings may have implications in

overcoming resistance mechanisms associated with c-RAF biology and provides new opportunities for repurposing ritanserin in cancer.

Finally, we demonstrated a novel application for the serine hydrolase inhibitor AA741 as an enhancer of $CD4^+$ T cell function. In the TME, T cells often become anergic, or hyporesponsive, due to inefficient presentation of tumor antigens. Targeting and reversing the anergic state would improve immune response and enhance immunotherapy efficacy (171). We show that in human Jurkats and primary murine $CD4^+$ T cells, pre-treatment of anergic, anti-CD3 exposed cells with AA741 resulted in significant increase in IL-2 cytokine production and decreased NDRG1 expression. This may suggest that AA741 has the capability to restore T cell effector function through inactivation of NDRG1-induced T cell clonal anergy. However, additional studies will be necessary to validate this study in a clinically relevant biological system.

6.2 *Future Directions*

The work presented in this dissertation was the first to identify the ATP and ligand binding regions of diacylglycerol kinases. We hypothesized that ATP occupies a contiguous binding site comprising the first C1 domain, DAGKc and DAGKa subdomains based on the unique sites where probe labeling was outcompeted with ATP, distinct from ligand binding regions. Future studies are necessary to validate this hypothesis to ensure that the binding site is in fact contiguous, as opposed to simply three separate and distinct ATP binding events.

Förster resonance energy transfer (or FRET) is a powerful technique that permits visualization of molecular interactions inside living cells (175). It involves the use of donor and acceptor fluorophores (coming from a class of autofluorescent proteins called GFPs) that fluoresce at unique wavelengths depending on their physical proximity to one another (175). FRET techniques may be capable of generating readout of the DGK contiguous ATP binding site. Expression of distinct GFP donors and acceptors on the catalytic domain and first C1 domain followed by addition of ATP to cell lysates would result in change in fluorescent wavelength if the sites interact with one another. The major disadvantage to this type of analysis is the effect of GFP tags on protein function. Purified GFP-tagged kinase would need to be analyzed using a traditional kinase activity assay to ensure that GFP has no impact on kinase function. The interaction may also be difficult to capture by FRET as domain interactions are dynamic and occur only briefly.

An alternative technique that may provide insight as to whether a contiguous ATP binding site exists for DGKs is chemical crosslinking. Chemical crosslinking has the

advantage of 'freezing' non-covalent molecular interactions (or even just proximity) by covalent modification, which can then be evaluated by mass spectrometry (176). Data generated from chemical crosslinking experiments provides structural details of protein complexes, which can be determined by identifying amino acid groups that are in close proximity to one another (176). Addition of chemical crosslinking reagents to cell lysates containing recombinant DGKS that have been pre-treated with ATP can be compared to control, un-treated samples to determine the sites of differential domain interactions. We would expect to see modified (cross-linked) peptides corresponding to the first C1 domain, DAGKc and DAGKa subdomains in samples pre-treated with a high concentration of ATP if a contiguous binding site exists.

Selectivity data for ritanserin, RF001, and RLM001 generated from the ATP acyl phosphate probe chemical proteomic assay revealed a number of different kinase targets for each compound. In order to validate that the activity of these targets is, in fact, modulated by compound treatment, complementary future studies should be performed to evaluate the activity of each identified kinase target.

Kinase activity assays are an efficient way to readout whether kinase activity is inhibited by compound treatment. As previously described in Chapter 1.2.1.a, radiolabeled or fluorescent techniques can be used to determine whether the kinase is turning over substrate to form product. Although this method is less efficient than the chemical proteomic assay, it is important to validate that the chemical probe has generated a readout of true activity modification, as opposed to just displaying decreased binding due to artifacts such as blockade of an unactivated active site.

Chapter 7: Publications Resulting From This Work

(*Co-authors and contributed equally to this work)

Franks CE, Campbell ST, Purow BW, Harris TE, Hsu KL. The Ligand Binding Landscape of Diacylglycerol Kinases. *Cell Chemical Biology* 24, 870-880 (2017).

McCloud RL*, **Franks CE***, Campbell ST*, Purow BW, Harris TE, Hsu KL. Deconstructing Lipid Kinase Inhibitors by Chemical Proteomics. *Biochemistry* 57, 231-236 (2018).

Campbell ST*, **Franks CE***, Borne AL*, Shin M, Zhang L, Hsu KL. Chemoproteomic discovery of a ritanserin-targeted kinase network mediating apoptotic cell death of lung tumor cells. *Molecular Pharmacology.* 94, 1246-1255 (2018).

Franks CE and Hsu KL. Activity-Based Kinome Profiling by ATP Acyl Phosphate Probes. *Manuscript in preparation.*

Additional Publications

Shin M, **Franks CE**, Hsu KL. Isoform-selective activity-based profiling of ERK signaling. *Chemical Science* 9, 2419-2431 (2018).

References

1. Shirai Y, Saito N. Diacylglycerol kinase as a possible therapeutic target for neuronal diseases. J Biomed Sci. 2014;21:28. doi: 10.1186/1423-0127-21-28. PubMed PMID: 24708409; PMCID: PMC4005014.
2. Merida I, Avila-Flores A, Merino E. Diacylglycerol kinases: at the hub of cell signalling. Biochem J. 2008;409(1):1-18. doi: 10.1042/BJ20071040. PubMed PMID: 18062770.
3. Sakane F, Imai S, Kai M, Yasuda S, Kanoh H. Diacylglycerol kinases: why so many of them? Biochim Biophys Acta. 2007;1771(7):793-806. doi: 10.1016/j.bbalip.2007.04.006. PubMed PMID: 17512245.
4. Shulga YV, Topham MK, Epand RM. Regulation and functions of diacylglycerol kinases. Chem Rev. 2011;111(10):6186-208. doi: 10.1021/cr1004106. PubMed PMID: 21800853.
5. Hokin LE, Hokin MR. Diglyceride phosphokinase: an enzyme which catalyzes the synthesis of phosphatidic acid. Biochim Biophys Acta. 1959;31(1):285-7. Epub 1959/01/01. PubMed PMID: 13628646.
6. Holub BJ, Piekarski. Suitability of different molecular species of 1,2-diacylglycerols as substrates for diacylglycerol kinase in rat brain microsomes. J Neurochem. 1978;31(4):903-8. Epub 1978/10/01. PubMed PMID: 212534.
7. Holub BJ, Piekarski J. Substrate selectivity of diacylglycerol kinase in guinea pig brain. Lipids. 1979;14(3):309-11. Epub 1979/03/01. PubMed PMID: 221772.
8. Bohnenberger E, Sandermann H, Jr. Diglyceride kinase from Escherichia coli. Purification in organic solvent and some properties of the enzyme. Eur J Biochem. 1979;94(2):401-7. Epub 1979/03/01. PubMed PMID: 218816.
9. Schneider EG, Kennedy EP. Phosphorylation of ceramide by diglyceride kinase preparations from Escherichia coli. J Biol Chem. 1973;248(10):3739-41. Epub 1973/05/25. PubMed PMID: 4573983.
10. Schneider EG, Kennedy EP. Partial purification and properties of diglyceride kinase from Escherichia coli. Biochim Biophys Acta. 1976;441(2):201-12. Epub 1976/08/23. PubMed PMID: 182252.
11. Walsh JP, Fahrner L, Bell RM. sn-1,2-diacylglycerol kinase of Escherichia coli. Diacylglycerol analogues define specificity and mechanism. J Biol Chem. 1990;265(8):4374-81. Epub 1990/03/15. PubMed PMID: 2155227.
12. Bohnenberger E, Sandermann H, Jr. Lipid dependence of diacylglycerol kinase from Escherichia coli. Eur J Biochem. 1983;132(3):645-50. Epub 1983/05/16. PubMed PMID: 6303781.
13. Kanoh H, Akesson B. Properties of microsomal and soluble diacylglycerol kinase in rat liver. Eur J Biochem. 1978;85(1):225-32. Epub 1978/04/01. PubMed PMID: 205418.
14. Kanoh H, Kondoh H, Ono T. Diacylglycerol kinase from pig brain. Purification and phospholipid dependencies. J Biol Chem. 1983;258(3):1767-74. Epub 1983/02/10. PubMed PMID: 6296111.

15. Yamada K, Kanoh H. Occurrence of immunoreactive 80 kDa and non-immunoreactive diacylglycerol kinases in different pig tissues. Biochem J. 1988;255(2):601-8. Epub 1988/10/15. PubMed PMID: 2849422; PMCID: PMC1135269.
16. Yamada K, Sakane F, Kanoh H. Immunoquantitation of 80 kDa diacylglycerol kinase in pig and human lymphocytes and several other cells. FEBS Lett. 1989;244(2):402-6. Epub 1989/02/27. PubMed PMID: 2537763.
17. Han GS, O'Hara L, Siniossoglou S, Carman GM. Characterization of the yeast DGK1-encoded CTP-dependent diacylglycerol kinase. J Biol Chem. 2008;283(29):20443-53. Epub 2008/05/07. doi: 10.1074/jbc.M802866200. PubMed PMID: 18458076; PMCID: PMC2459283.
18. Carrasco S, Merida I. Diacylglycerol, when simplicity becomes complex. Trends Biochem Sci. 2007;32(1):27-36. doi: 10.1016/j.tibs.2006.11.004. PubMed PMID: 17157506.
19. Rahman GM, Das J. Modeling studies on the structural determinants for the DAG/phorbol ester binding to C1 domain. J Biomol Struct Dyn. 2015;33(1):219-32. Epub 2014/03/29. doi: 10.1080/07391102.2014.895679. PubMed PMID: 24666138.
20. Merino E, Sanjuan MA, Moraga I, Cipres A, Merida I. Role of the diacylglycerol kinase alpha-conserved domains in membrane targeting in intact T cells. J Biol Chem. 2007;282(48):35396-404. Epub 2007/10/04. doi: 10.1074/jbc.M702085200. PubMed PMID: 17911109.
21. Topham MK, Epand RM. Mammalian diacylglycerol kinases: molecular interactions and biological functions of selected isoforms. Biochim Biophys Acta. 2009;1790(6):416-24. Epub 2009/04/15. doi: 10.1016/j.bbagen.2009.01.010. PubMed PMID: 19364481; PMCID: PMC2744455.
22. Topham MK, Bunting M, Zimmerman GA, McIntyre TM, Blackshear PJ, Prescott SM. Protein kinase C regulates the nuclear localization of diacylglycerol kinase-zeta. Nature. 1998;394(6694):697-700. Epub 1998/08/26. doi: 10.1038/29337. PubMed PMID: 9716136.
23. Sanjuan MA, Jones DR, Izquierdo M, Merida I. Role of diacylglycerol kinase alpha in the attenuation of receptor signaling. J Cell Biol. 2001;153(1):207-20. Epub 2001/04/04. PubMed PMID: 11285286; PMCID: PMC2185527.
24. Nagaya H, Wada I, Jia YJ, Kanoh H. Diacylglycerol kinase delta suppresses ER-to-Golgi traffic via its SAM and PH domains. Mol Biol Cell. 2002;13(1):302-16. Epub 2002/01/26. doi: 10.1091/mbc.01-05-0255. PubMed PMID: 11809841; PMCID: PMC65090.
25. Jiang Y, Qian W, Hawes JW, Walsh JP. A domain with homology to neuronal calcium sensors is required for calcium-dependent activation of diacylglycerol kinase alpha. J Biol Chem. 2000;275(44):34092-9. Epub 2000/08/05. doi: 10.1074/jbc.M004914200. PubMed PMID: 10918059.

26. Lemmon MA. Pleckstrin homology (PH) domains and phosphoinositides. Biochem Soc Symp. 2007(74):81-93. Epub 2007/01/20. doi: 10.1042/BSS0740081. PubMed PMID: 17233582; PMCID: PMC3777418.
27. Epand RM, So V, Jennings W, Khadka B, Gupta RS, Lemaire M. Diacylglycerol Kinase-epsilon: Properties and Biological Roles. Front Cell Dev Biol. 2016;4:112. Epub 2016/11/03. doi: 10.3389/fcell.2016.00112. PubMed PMID: 27803897; PMCID: PMC5067486.
28. Li J, Mahajan A, Tsai MD. Ankyrin repeat: a unique motif mediating protein-protein interactions. Biochemistry. 2006;45(51):15168-78. Epub 2006/12/21. doi: 10.1021/bi062188q. PubMed PMID: 17176038.
29. Tu-Sekine B, Goldschmidt HL, Raben DM. DGK-theta: Structure, Enzymology, and Physiological Roles. Front Cell Dev Biol. 2016;4:101. Epub 2016/09/30. doi: 10.3389/fcell.2016.00101. PubMed PMID: 27683659; PMCID: PMC5021689.
30. Merida I, Torres-Ayuso P, Avila-Flores A, Arranz-Nicolas J, Andrada E, Tello-Lafoz M, Liebana R, Arcos R. Diacylglycerol kinases in cancer. Adv Biol Regul. 2017;63:22-31. doi: 10.1016/j.jbior.2016.09.005. PubMed PMID: 27697466.
31. Krishna S, Zhong XP. Regulation of Lipid Signaling by Diacylglycerol Kinases during T Cell Development and Function. Front Immunol. 2013;4:178. doi: 10.3389/fimmu.2013.00178. PubMed PMID: 23847619; PMCID: PMC3701226.
32. Chen SS, Hu Z, Zhong XP. Diacylglycerol Kinases in T Cell Tolerance and Effector Function. Front Cell Dev Biol. 2016;4:130. Epub 2016/11/29. doi: 10.3389/fcell.2016.00130. PubMed PMID: 27891502; PMCID: PMC5103287.
33. Zha Y, Marks R, Ho AW, Peterson AC, Janardhan S, Brown I, Praveen K, Stang S, Stone JC, Gajewski TF. T cell anergy is reversed by active Ras and is regulated by diacylglycerol kinase-alpha. Nat Immunol. 2006;7(11):1166-73. doi: 10.1038/ni1394. PubMed PMID: 17028589.
34. Olenchock BA, Guo R, Carpenter JH, Jordan M, Topham MK, Koretzky GA, Zhong XP. Disruption of diacylglycerol metabolism impairs the induction of T cell anergy. Nat Immunol. 2006;7(11):1174-81. doi: 10.1038/ni1400. PubMed PMID: 17028587.
35. Su AI, Wiltshire T, Batalov S, Lapp H, Ching KA, Block D, Zhang J, Soden R, Hayakawa M, Kreiman G, Cooke MP, Walker JR, Hogenesch JB. A gene atlas of the mouse and human protein-encoding transcriptomes. Proc Natl Acad Sci U S A. 2004;101(16):6062-7. Epub 2004/04/13. doi: 10.1073/pnas.0400782101. PubMed PMID: 15075390; PMCID: PMC395923.
36. Dominguez CL, Floyd DH, Xiao A, Mullins GR, Kefas BA, Xin W, Yacur MN, Abounader R, Lee JK, Wilson GM, Harris TE, Purow BW. Diacylglycerol kinase alpha is a critical signaling node and novel therapeutic target in glioblastoma and other cancers. Cancer Discov. 2013;3(7):782-97. doi: 10.1158/2159-8290.CD-12-0215. PubMed PMID: 23558954; PMCID: PMC3710531.
37. Purow B. Molecular Pathways: Targeting Diacylglycerol Kinase Alpha in Cancer. Clin Cancer Res. 2015;21(22):5008-12. doi: 10.1158/1078-0432.CCR-15-0413. PubMed PMID: 26420856; PMCID: PMC4644682.

38. Hilty DM, Leamon MH, Lim RF, Kelly RH, Hales RE. A review of bipolar disorder in adults. Psychiatry (Edgmont). 2006;3(9):43-55. Epub 2006/09/01. PubMed PMID: 20975827; PMCID: PMC2963467.
39. Sakane F, Mizuno S, Komenoi S. Diacylglycerol Kinases as Emerging Potential Drug Targets for a Variety of Diseases: An Update. Front Cell Dev Biol. 2016;4:82. Epub 2016/09/02. doi: 10.3389/fcell.2016.00082. PubMed PMID: 27583247; PMCID: PMC4987324.
40. Velnati S, Ruffo E, Massarotti A, Talmon M, Varma KSS, Gesu A, Fresu LG, Snow AL, Bertoni A, Capello D, Tron GC, Graziani A, Baldanzi G. Identification of a novel DGKalpha inhibitor for XLP-1 therapy by virtual screening. Eur J Med Chem. 2019;164:378-90. Epub 2019/01/06. doi: 10.1016/j.ejmech.2018.12.061. PubMed PMID: 30611057.
41. de Chaffoy de Courcelles DC, Roevens P, Van Belle H. R 59 022, a diacylglycerol kinase inhibitor. Its effect on diacylglycerol and thrombin-induced C kinase activation in the intact platelet. J Biol Chem. 1985;260(29):15762-70. PubMed PMID: 2999135.
42. de Chaffoy de Courcelles D, Roevens P, Van Belle H, Kennis L, Somers Y, De Clerck F. The role of endogenously formed diacylglycerol in the propagation and termination of platelet activation. A biochemical and functional analysis using the novel diacylglycerol kinase inhibitor, R 59 949. J Biol Chem. 1989;264(6):3274-85. PubMed PMID: 2536741.
43. Boroda S, Niccum M, Raje V, Purow BW, Harris TE. Dual activities of ritanserin and R59022 as DGKalpha inhibitors and serotonin receptor antagonists. Biochem Pharmacol. 2017;123:29-39. doi: 10.1016/j.bcp.2016.10.011. PubMed PMID: 27974147; PMCID: PMC5164959.
44. Jiang Y, Sakane F, Kanoh H, Walsh JP. Selectivity of the diacylglycerol kinase inhibitor 3-[2-(4-[bis-(4-fluorophenyl)methylene]-1-piperidinyl)ethyl]-2, 3-dihydro-2-thioxo-4(1H)quinazolinone (R59949) among diacylglycerol kinase subtypes. Biochem Pharmacol. 2000;59(7):763-72. Epub 2000/03/16. PubMed PMID: 10718334.
45. Sato M, Liu K, Sasaki S, Kunii N, Sakai H, Mizuno H, Saga H, Sakane F. Evaluations of the selectivities of the diacylglycerol kinase inhibitors R59022 and R59949 among diacylglycerol kinase isozymes using a new non-radioactive assay method. Pharmacology. 2013;92(1-2):99-107. doi: 10.1159/000351849. PubMed PMID: 23949095.
46. Redman C, Lefevre J, MacDonald ML. Inhibition of diacylglycerol kinase by the antitumor agent calphostin C. Evidence for similarity between the active site of diacylglycerol kinase and the regulatory site of protein kinase C. Biochem Pharmacol. 1995;50(2):235-41. Epub 1995/07/17. PubMed PMID: 7632168.
47. Machida T, Higashi K, Ogawara H. Cochlioquinone A, an inhibitor of diacylglycerol kinase. J Antibiot (Tokyo). 1995;48(10):1076-80. Epub 1995/10/01. PubMed PMID: 7490210.

48. Choi H, Allahdadi KJ, Tostes RC, Webb RC. Diacylglycerol Kinase Inhibition and Vascular Function. Curr Enzym Inhib. 2009;5(3):148-52. Epub 2009/01/01. doi: 10.2174/157340809789071137. PubMed PMID: 21547002; PMCID: PMC3086769.
49. Nobe K, Miyatake M, Nobe H, Sakai Y, Takashima J, Momose K. Novel diacylglycerol kinase inhibitor selectively suppressed an U46619-induced enhancement of mouse portal vein contraction under high glucose conditions. Br J Pharmacol. 2004;143(1):166-78. Epub 2004/08/04. doi: 10.1038/sj.bjp.0705910. PubMed PMID: 15289283; PMCID: PMC1575271.
50. Bishop WR, Ganong BR, Bell RM. Attenuation of sn-1,2-diacylglycerol second messengers by diacylglycerol kinase. Inhibition by diacylglycerol analogs in vitro and in human platelets. J Biol Chem. 1986;261(15):6993-7000. Epub 1986/05/25. PubMed PMID: 3009483.
51. Roskoski R. Properties of FDA-approved small molecule protein kinase inhibitors. Pharmacol Res. 2019. Epub 2019/03/17. doi: 10.1016/j.phrs.2019.03.006. PubMed PMID: 30877063.
52. Liu K, Kunii N, Sakuma M, Yamaki A, Mizuno S, Sato M, Sakai H, Kado S, Kumagai K, Kojima H, Okabe T, Nagano T, Shirai Y, Sakane F. A novel diacylglycerol kinase alpha-selective inhibitor, CU-3, induces cancer cell apoptosis and enhances immune response. J Lipid Res. 2016;57(3):368-79. Epub 2016/01/16. doi: 10.1194/jlr.M062794. PubMed PMID: 26768655; PMCID: PMC4766986.
53. Barone JA, Bierman RH, Cornish JW, Hsuan A, Drake ND, Colaizzi JL. Safety evaluation of ritanserin--an investigational serotonin antagonist. Drug Intell Clin Pharm. 1986;20(10):770-5. PubMed PMID: 3095082.
54. Berg JM, Tymoczko JL, Stryer L. Section 8.5: Enzymes Can Be Inhibited by Specific Molecules. 5th edition ed. New York: W H Freeman; 2002.
55. Fabbro D. 25 years of small molecular weight kinase inhibitors: potentials and limitations. Mol Pharmacol. 2015;87(5):766-75. Epub 2015/01/01. doi: 10.1124/mol.114.095489. PubMed PMID: 25549667.
56. Cheng HC, Qi RZ, Paudel H, Zhu HJ. Regulation and function of protein kinases and phosphatases. Enzyme Res. 2011;2011:794089. Epub 2011/12/24. doi: 10.4061/2011/794089. PubMed PMID: 22195276; PMCID: PMC3238372.
57. Adams JA. Kinetic and catalytic mechanisms of protein kinases. Chem Rev. 2001;101(8):2271-90. Epub 2001/12/26. PubMed PMID: 11749373.
58. Glickman JF. Assay Development for Protein Kinase Enzymes. In: Sittampalam GS, Coussens NP, Brimacombe K, Grossman A, Arkin M, Auld D, Austin C, Baell J, Bejcek B, Caaveiro JMM, Chung TDY, Dahlin JL, Devanaryan V, Foley TL, Glicksman M, Hall MD, Haas JV, Inglese J, Iversen PW, Kahl SD, Kales SC, Lal-Nag M, Li Z, McGee J, McManus O, Riss T, Trask OJ, Jr., Weidner JR, Wildey MJ, Xia M, Xu X, editors. Assay Guidance Manual. Bethesda (MD)2004.

59. Hastie CJ, McLauchlan HJ, Cohen P. Assay of protein kinases using radiolabeled ATP: a protocol. Nat Protoc. 2006;1(2):968-71. Epub 2007/04/05. doi: 10.1038/nprot.2006.149. PubMed PMID: 17406331.
60. Newman M, Josiah S. Utilization of fluorescence polarization and time resolved fluorescence resonance energy transfer assay formats for SAR studies: Src kinase as a model system. J Biomol Screen. 2004;9(6):525-32. Epub 2004/09/29. doi: 10.1177/1087057104264597. PubMed PMID: 15452339.
61. Turek-Etienne TC, Kober TP, Stafford JM, Bryant RW. Development of a fluorescence polarization AKT serine/threonine kinase assay using an immobilized metal ion affinity-based technology. Assay Drug Dev Technol. 2003;1(4):545-53. Epub 2004/04/20. doi: 10.1089/154065803322302808. PubMed PMID: 15090251.
62. Moshinsky DJ, Ruslim L, Blake RA, Tang F. A widely applicable, high-throughput TR-FRET assay for the measurement of kinase autophosphorylation: VEGFR-2 as a prototype. J Biomol Screen. 2003;8(4):447-52. Epub 2003/10/22. doi: 10.1177/1087057103255282. PubMed PMID: 14567797.
63. Waddleton D, Ramachandran C, Wang Q. Development of a time-resolved fluorescent assay for measuring tyrosine-phosphorylated proteins in cells. Anal Biochem. 2002;309(1):150-7. Epub 2002/10/17. PubMed PMID: 12381374.
64. Koresawa M, Okabe T. High-throughput screening with quantitation of ATP consumption: a universal non-radioisotope, homogeneous assay for protein kinase. Assay Drug Dev Technol. 2004;2(2):153-60. Epub 2004/05/29. doi: 10.1089/154065804323056495. PubMed PMID: 15165511.
65. Ferguson FM, Gray NS. Kinase inhibitors: the road ahead. Nat Rev Drug Discov. 2018;17(5):353-77. Epub 2018/03/17. doi: 10.1038/nrd.2018.21. PubMed PMID: 29545548.
66. Patricelli MP, Szardenings AK, Liyanage M, Nomanbhoy TK, Wu M, Weissig H, Aban A, Chun D, Tanner S, Kozarich JW. Functional interrogation of the kinome using nucleotide acyl phosphates. Biochemistry. 2007;46(2):350-8. doi: 10.1021/bi062142x. PubMed PMID: 17209545.
67. Patricelli MP, Nomanbhoy TK, Wu J, Brown H, Zhou D, Zhang J, Jagannathan S, Aban A, Okerberg E, Herring C, Nordin B, Weissig H, Yang Q, Lee JD, Gray NS, Kozarich JW. In situ kinase profiling reveals functionally relevant properties of native kinases. Chem Biol. 2011;18(6):699-710. doi: 10.1016/j.chembiol.2011.04.011. PubMed PMID: 21700206; PMCID: PMC3142620.
68. Bantscheff M, Eberhard D, Abraham Y, Bastuck S, Boesche M, Hobson S, Mathieson T, Perrin J, Raida M, Rau C, Reader V, Sweetman G, Bauer A, Bouwmeester T, Hopf C, Kruse U, Neubauer G, Ramsden N, Rick J, Kuster B, Drewes G. Quantitative chemical proteomics reveals mechanisms of action of clinical ABL kinase inhibitors. Nat Biotechnol. 2007;25(9):1035-44. Epub 2007/08/28. doi: 10.1038/nbt1328. PubMed PMID: 17721511.

69. Medard G, Pachl F, Ruprecht B, Klaeger S, Heinzlmeir S, Helm D, Qiao H, Ku X, Wilhelm M, Kuehne T, Wu Z, Dittmann A, Hopf C, Kramer K, Kuster B. Optimized chemical proteomics assay for kinase inhibitor profiling. J Proteome Res. 2015;14(3):1574-86. Epub 2015/02/11. doi: 10.1021/pr5012608. PubMed PMID: 25660469.
70. Zhao Q, Ouyang X, Wan X, Gajiwala KS, Kath JC, Jones LH, Burlingame AL, Taunton J. Broad-Spectrum Kinase Profiling in Live Cells with Lysine-Targeted Sulfonyl Fluoride Probes. J Am Chem Soc. 2017;139(2):680-5. Epub 2017/01/05. doi: 10.1021/jacs.6b08536. PubMed PMID: 28051857; PMCID: PMC5858558.
71. Rostovtsev VV, Green LG, Fokin VV, Sharpless KB. A stepwise huisgen cycloaddition process: copper(I)-catalyzed regioselective "ligation" of azides and terminal alkynes. Angew Chem Int Ed Engl. 2002;41(14):2596-9. Epub 2002/08/31. doi: 10.1002/1521-3773(20020715)41:14<2596::AID-ANIE2596>3.0.CO;2-4. PubMed PMID: 12203546.
72. Vasta JD, Corona CR, Wilkinson J, Zimprich CA, Hartnett JR, Ingold MR, Zimmerman K, Machleidt T, Kirkland TA, Huwiler KG, Ohana RF, Slater M, Otto P, Cong M, Wells CI, Berger BT, Hanke T, Glas C, Ding K, Drewry DH, Huber KVM, Willson TM, Knapp S, Muller S, Meisenheimer PL, Fan F, Wood KV, Robers MB. Quantitative, Wide-Spectrum Kinase Profiling in Live Cells for Assessing the Effect of Cellular ATP on Target Engagement. Cell Chem Biol. 2018;25(2):206-14 e11. Epub 2017/11/28. doi: 10.1016/j.chembiol.2017.10.010. PubMed PMID: 29174542; PMCID: PMC5814754.
73. Long JZ, Cravatt BF. The metabolic serine hydrolases and their functions in mammalian physiology and disease. Chem Rev. 2011;111(10):6022-63. Epub 2011/06/24. doi: 10.1021/cr200075y. PubMed PMID: 21696217; PMCID: PMC3192302.
74. Bachovchin DA, Cravatt BF. The pharmacological landscape and therapeutic potential of serine hydrolases. Nat Rev Drug Discov. 2012;11(1):52-68. Epub 2012/01/04. doi: 10.1038/nrd3620. PubMed PMID: 22212679; PMCID: PMC3665514.
75. Cravatt BF, Wright AT, Kozarich JW. Activity-based protein profiling: from enzyme chemistry to proteomic chemistry. Annu Rev Biochem. 2008;77:383-414. Epub 2008/03/28. doi: 10.1146/annurev.biochem.75.101304.124125. PubMed PMID: 18366325.
76. Niphakis MJ, Cravatt BF. Enzyme inhibitor discovery by activity-based protein profiling. Annu Rev Biochem. 2014;83:341-77. Epub 2014/06/07. doi: 10.1146/annurev-biochem-060713-035708. PubMed PMID: 24905785.
77. Cai YD, Zhou GP, Jen CH, Lin SL, Chou KC. Identify catalytic triads of serine hydrolases by support vector machines. J Theor Biol. 2004;228(4):551-7. Epub 2004/06/05. doi: 10.1016/j.jtbi.2004.02.019. PubMed PMID: 15178202.
78. Adibekian A, Martin BR, Wang C, Hsu KL, Bachovchin DA, Niessen S, Hoover H, Cravatt BF. Click-generated triazole ureas as ultrapotent in vivo-active serine

hydrolase inhibitors. Nat Chem Biol. 2011;7(7):469-78. Epub 2011/05/17. doi: 10.1038/nchembio.579. PubMed PMID: 21572424; PMCID: PMC3118922.

79. Ebdrup S, Sorensen LG, Olsen OH, Jacobsen P. Synthesis and structure-activity relationship for a novel class of potent and selective carbamoyl-triazole based inhibitors of hormone sensitive lipase. J Med Chem. 2004;47(2):400-10. Epub 2004/01/09. doi: 10.1021/jm031004s. PubMed PMID: 14711311.
80. Lowe DB, Magnuson S, Qi N, Campbell AM, Cook J, Hong Z, Wang M, Rodriguez M, Achebe F, Kluender H, Wong WC, Bullock WH, Salhanick AI, Witman-Jones T, Bowling ME, Keiper C, Clairmont KB. In vitro SAR of (5-(2H)-isoxazolonyl) ureas, potent inhibitors of hormone-sensitive lipase. Bioorg Med Chem Lett. 2004;14(12):3155-9. Epub 2004/05/20. doi: 10.1016/j.bmcl.2004.04.015. PubMed PMID: 15149665.
81. Adibekian A, Hsu KL, Speers AE, Brown SJ, Spicer T, Fernandez-Vega V, Ferguson J, Cravatt BF, Hodder P, Rosen H. Optimization and characterization of a triazole urea inhibitor for alpha/beta hydrolase domain-containing protein 11 (ABHD11): anti-probe for LYPLA1/LYPLA2 dual inhibitor ML211. Probe Reports from the NIH Molecular Libraries Program. Bethesda (MD)2010.
82. Hsu KL, Tsuboi K, Speers AE, Brown SJ, Spicer T, Fernandez-Vega V, Ferguson J, Cravatt BF, Hodder P, Rosen H. Optimization and characterization of a triazole urea inhibitor for diacylglycerol lipase beta (DAGL-beta). Probe Reports from the NIH Molecular Libraries Program. Bethesda (MD)2010.
83. Adams JA. Activation loop phosphorylation and catalysis in protein kinases: is there functional evidence for the autoinhibitor model? Biochemistry. 2003;42(3):601-7. Epub 2003/01/22. doi: 10.1021/bi020617o. PubMed PMID: 12534271.
84. Fang Y, Vilella-Bach M, Bachmann R, Flanigan A, Chen J. Phosphatidic acid-mediated mitogenic activation of mTOR signaling. Science. 2001;294(5548):1942-5. Epub 2001/12/01. doi: 10.1126/science.1066015. PubMed PMID: 11729323.
85. Brown HA, Thomas PG, Lindsley CW. Targeting phospholipase D in cancer, infection and neurodegenerative disorders. Nat Rev Drug Discov. 2017;16(5):351-67. Epub 2017/02/18. doi: 10.1038/nrd.2016.252. PubMed PMID: 28209987; PMCID: PMC6040825.
86. Hsu KL, Tsuboi K, Adibekian A, Pugh H, Masuda K, Cravatt BF. DAGLbeta inhibition perturbs a lipid network involved in macrophage inflammatory responses. Nat Chem Biol. 2012;8(12):999-1007. doi: 10.1038/nchembio.1105. PubMed PMID: 23103940; PMCID: PMC3513945.
87. Takai Y, Kishimoto A, Kikkawa U, Mori T, Nishizuka Y. Unsaturated diacylglycerol as a possible messenger for the activation of calcium-activated, phospholipid-dependent protein kinase system. Biochem Biophys Res Commun. 1979;91(4):1218-24. Epub 1979/12/28. PubMed PMID: 526298.
88. Newton AC, Koshland DE, Jr. High cooperativity, specificity, and multiplicity in the protein kinase C-lipid interaction. J Biol Chem. 1989;264(25):14909-15. Epub 1989/09/05. PubMed PMID: 2768246.

89. Schultz J, Milpetz F, Bork P, Ponting CP. SMART, a simple modular architecture research tool: identification of signaling domains. Proc Natl Acad Sci U S A. 1998;95(11):5857-64. Epub 1998/05/30. PubMed PMID: 9600884; PMCID: PMC34487.
90. Adams DR, Pyne S, Pyne NJ. Sphingosine Kinases: Emerging Structure-Function Insights. Trends Biochem Sci. 2016;41(5):395-409. Epub 2016/03/30. doi: 10.1016/j.tibs.2016.02.007. PubMed PMID: 27021309.
91. Yetukuri L, Ekroos K, Vidal-Puig A, Oresic M. Informatics and computational strategies for the study of lipids. Mol Biosyst. 2008;4(2):121-7. Epub 2008/01/24. doi: 10.1039/b715468b. PubMed PMID: 18213405.
92. Hanks SK, Quinn AM, Hunter T. The protein kinase family: conserved features and deduced phylogeny of the catalytic domains. Science. 1988;241(4861):42-52. Epub 1988/07/01. PubMed PMID: 3291115.
93. Hemmer W, McGlone M, Tsigelny I, Taylor SS. Role of the glycine triad in the ATP-binding site of cAMP-dependent protein kinase. J Biol Chem. 1997;272(27):16946-54. Epub 1997/07/04. PubMed PMID: 9202006.
94. Sakane F, Yamada K, Kanoh H, Yokoyama C, Tanabe T. Porcine diacylglycerol kinase sequence has zinc finger and E-F hand motifs. Nature. 1990;344(6264):345-8. Epub 1990/03/22. doi: 10.1038/344345a0. PubMed PMID: 2156169.
95. Schaap D, van der Wal J, van Blitterswijk WJ. Consensus sequences for ATP-binding sites in protein kinases do not apply to diacylglycerol kinases. Biochem J. 1994;304 (Pt 2):661-2. Epub 1994/12/01. PubMed PMID: 7999005; PMCID: PMC1137542.
96. Sakane F, Kai M, Wada I, Imai S, Kanoh H. The C-terminal part of diacylglycerol kinase alpha lacking zinc fingers serves as a catalytic domain. Biochem J. 1996;318 (Pt 2):583-90. Epub 1996/09/01. PubMed PMID: 8809050; PMCID: PMC1217660.
97. Shindo M, Irie K, Masuda A, Ohigashi H, Shirai Y, Miyasaka K, Saito N. Synthesis and phorbol ester binding of the cysteine-rich domains of diacylglycerol kinase (DGK) isozymes. DGKgamma and DGKbeta are new targets of tumor-promoting phorbol esters. J Biol Chem. 2003;278(20):18448-54. Epub 2003/03/07. doi: 10.1074/jbc.M300400200. PubMed PMID: 12621060.
98. Hurley JH, Misra S. Signaling and subcellular targeting by membrane-binding domains. Annu Rev Biophys Biomol Struct. 2000;29:49-79. Epub 2000/08/15. doi: 10.1146/annurev.biophys.29.1.49. PubMed PMID: 10940243; PMCID: PMC4781318.
99. Abe T, Lu X, Jiang Y, Boccone CE, Qian S, Vattem KM, Wek RC, Walsh JP. Site-directed mutagenesis of the active site of diacylglycerol kinase alpha: calcium and phosphatidylserine stimulate enzyme activity via distinct mechanisms. Biochem J. 2003;375(Pt 3):673-80. Epub 2003/08/12. doi: 10.1042/BJ20031052. PubMed PMID: 12908872; PMCID: PMC1223725.
100. Houssa B, Schaap D, van der Wal J, Goto K, Kondo H, Yamakawa A, Shibata M, Takenawa T, van Blitterswijk WJ. Cloning of a novel human diacylglycerol

kinase (DGKtheta) containing three cysteine-rich domains, a proline-rich region, and a pleckstrin homology domain with an overlapping Ras-associating domain. J Biol Chem. 1997;272(16):10422-8. Epub 1997/04/18. PubMed PMID: 9099683.

101. Santos T, Carrasco S, Jones DR, Merida I, Eguinoa A. Dynamics of diacylglycerol kinase zeta translocation in living T-cells. Study of the structural domain requirements for translocation and activity. J Biol Chem. 2002;277(33):30300-9. Epub 2002/05/17. doi: 10.1074/jbc.M200999200. PubMed PMID: 12015310.
102. Crotty T, Cai J, Sakane F, Taketomi A, Prescott SM, Topham MK. Diacylglycerol kinase delta regulates protein kinase C and epidermal growth factor receptor signaling. Proc Natl Acad Sci U S A. 2006;103(42):15485-90. Epub 2006/10/06. doi: 10.1073/pnas.0604104103. PubMed PMID: 17021016; PMCID: PMC1622849.
103. Prinz PU, Mendler AN, Masouris I, Durner L, Oberneder R, Noessner E. High DGK-alpha and disabled MAPK pathways cause dysfunction of human tumor-infiltrating CD8+ T cells that is reversible by pharmacologic intervention. J Immunol. 2012;188(12):5990-6000. Epub 2012/05/11. doi: 10.4049/jimmunol.1103028. PubMed PMID: 22573804.
104. Yada Y, Ozeki T, Kanoh H, Nozawa Y. Purification and characterization of cytosolic diacylglycerol kinases of human platelets. J Biol Chem. 1990;265(31):19237-43. Epub 1990/11/05. PubMed PMID: 2172248.
105. Posch A, Kohn J, Oh K, Hammond M, Liu N. V3 stain-free workflow for a practical, convenient, and reliable total protein loading control in western blotting. J Vis Exp. 2013(82):50948. Epub 2014/01/17. doi: 10.3791/50948. PubMed PMID: 24429481; PMCID: PMC4094170.
106. Schilling B, Rardin MJ, MacLean BX, Zawadzka AM, Frewen BE, Cusack MP, Sorensen DJ, Bereman MS, Jing E, Wu CC, Verdin E, Kahn CR, Maccoss MJ, Gibson BW. Platform-independent and label-free quantitation of proteomic data using MS1 extracted ion chromatograms in skyline: application to protein acetylation and phosphorylation. Mol Cell Proteomics. 2012;11(5):202-14. Epub 2012/03/29. doi: 10.1074/mcp.M112.017707. PubMed PMID: 22454539; PMCID: PMC3418851.
107. Goujon M, McWilliam H, Li W, Valentin F, Squizzato S, Paern J, Lopez R. A new bioinformatics analysis tools framework at EMBL-EBI. Nucleic Acids Res. 2010;38(Web Server issue):W695-9. Epub 2010/05/05. doi: 10.1093/nar/gkq313. PubMed PMID: 20439314; PMCID: PMC2896090.
108. Sievers F, Wilm A, Dineen D, Gibson TJ, Karplus K, Li W, Lopez R, McWilliam H, Remmert M, Soding J, Thompson JD, Higgins DG. Fast, scalable generation of high-quality protein multiple sequence alignments using Clustal Omega. Mol Syst Biol. 2011;7:539. Epub 2011/10/13. doi: 10.1038/msb.2011.75. PubMed PMID: 21988835; PMCID: PMC3261699.
109. Crooks GE, Hon G, Chandonia JM, Brenner SE. WebLogo: a sequence logo generator. Genome Res. 2004;14(6):1188-90. Epub 2004/06/03. doi: 10.1101/gr.849004. PubMed PMID: 15173120; PMCID: PMC419797.

110. Schneider TD, Stephens RM. Sequence logos: a new way to display consensus sequences. Nucleic Acids Res. 1990;18(20):6097-100. Epub 1990/10/25. PubMed PMID: 2172928; PMCID: PMC332411.
111. Miller DJ, Jerga A, Rock CO, White SW. Analysis of the Staphylococcus aureus DgkB structure reveals a common catalytic mechanism for the soluble diacylglycerol kinases. Structure. 2008;16(7):1036-46. Epub 2008/07/10. doi: 10.1016/j.str.2008.03.019. PubMed PMID: 18611377; PMCID: PMC2847398.
112. Adibekian A, Martin BR, Chang JW, Hsu KL, Tsuboi K, Bachovchin DA, Speers AE, Brown SJ, Spicer T, Fernandez-Vega V, Ferguson J, Hodder PS, Rosen H, Cravatt BF. Confirming target engagement for reversible inhibitors in vivo by kinetically tuned activity-based probes. J Am Chem Soc. 2012;134(25):10345-8. Epub 2012/06/14. doi: 10.1021/ja303400u. PubMed PMID: 22690931; PMCID: PMC3392194.
113. Mann M. Functional and quantitative proteomics using SILAC. Nat Rev Mol Cell Biol. 2006;7(12):952-8. Epub 2006/12/02. doi: 10.1038/nrm2067. PubMed PMID: 17139335.
114. Los AP, van Baal J, de Widt J, Divecha N, van Blitterswijk WJ. Structure- activity relationship of diacylglycerol kinase theta. Biochim Biophys Acta. 2004;1636(2-3):169-74. Epub 2004/05/29. doi: 10.1016/j.bbalip.2003.11.008. PubMed PMID: 15164764.
115. Imai S, Kai M, Yasuda S, Kanoh H, Sakane F. Identification and characterization of a novel human type II diacylglycerol kinase, DGK kappa. J Biol Chem. 2005;280(48):39870-81. Epub 2005/10/08. doi: 10.1074/jbc.M500669200. PubMed PMID: 16210324.
116. Tang W, Bunting M, Zimmerman GA, McIntyre TM, Prescott SM. Molecular cloning of a novel human diacylglycerol kinase highly selective for arachidonate-containing substrates. J Biol Chem. 1996;271(17):10237-41. Epub 1996/04/26. PubMed PMID: 8626589.
117. Goto K, Kondo H. A 104-kDa diacylglycerol kinase containing ankyrin-like repeats localizes in the cell nucleus. Proc Natl Acad Sci U S A. 1996;93(20):11196-201. Epub 1996/10/01. PubMed PMID: 8855332; PMCID: PMC38307.
118. Chang JW, Zuhl AM, Speers AE, Niessen S, Brown SJ, Mulvihill MM, Fan YC, Spicer TP, Southern M, Scampavia L, Fernandez-Vega V, Dix MM, Cameron MD, Hodder PS, Rosen H, Nomura DK, Kwon O, Hsu KL, Cravatt BF. Selective inhibitor of platelet-activating factor acetylhydrolases 1b2 and 1b3 that impairs cancer cell survival. ACS Chem Biol. 2015;10(4):925-32. Epub 2015/01/21. doi: 10.1021/cb500893q. PubMed PMID: 25602368; PMCID: PMC4402257.
119. Nagano JM, Hsu KL, Whitby LR, Niphakis MJ, Speers AE, Brown SJ, Spicer T, Fernandez-Vega V, Ferguson J, Hodder P, Srinivasan P, Gonzalez TD, Rosen H, Bahnson BJ, Cravatt BF. Selective inhibitors and tailored activity probes for lipoprotein-associated phospholipase A(2). Bioorg Med Chem Lett. 2013;23(3):839-43. Epub 2012/12/25. doi: 10.1016/j.bmcl.2012.11.061. PubMed PMID: 23260346; PMCID: PMC3549684.

120. Greer P. Closing in on the biological functions of Fps/Fes and Fer. Nat Rev Mol Cell Biol. 2002;3(4):278-89. Epub 2002/05/08. doi: 10.1038/nrm783. PubMed PMID: 11994747.
121. Hajduk PJ, Gomtsyan A, Didomenico S, Cowart M, Bayburt EK, Solomon L, Severin J, Smith R, Walter K, Holzman TF, Stewart A, McGaraughty S, Jarvis MF, Kowaluk EA, Fesik SW. Design of adenosine kinase inhibitors from the NMR-based screening of fragments. J Med Chem. 2000;43(25):4781-6. Epub 2000/12/22. PubMed PMID: 11123986.
122. Kozakov D, Hall DR, Jehle S, Luo L, Ochiana SO, Jones EV, Pollastri M, Allen KN, Whitty A, Vajda S. Ligand deconstruction: Why some fragment binding positions are conserved and others are not. Proc Natl Acad Sci U S A. 2015;112(20):E2585-94. doi: 10.1073/pnas.1501567112. PubMed PMID: 25918377; PMCID: PMC4443342.
123. Lingel A, Sendzik M, Huang Y, Shultz MD, Cantwell J, Dillon MP, Fu X, Fuller J, Gabriel T, Gu J, Jiang X, Li L, Liang F, McKenna M, Qi W, Rao W, Sheng X, Shu W, Sutton J, Taft B, Wang L, Zeng J, Zhang H, Zhang M, Zhao K, Lindvall M, Bussiere DE. Structure-Guided Design of EED Binders Allosterically Inhibiting the Epigenetic Polycomb Repressive Complex 2 (PRC2) Methyltransferase. J Med Chem. 2017;60(1):415-27. doi: 10.1021/acs.jmedchem.6b01473. PubMed PMID: 27992714.
124. Erlanson DA, Fesik SW, Hubbard RE, Jahnke W, Jhoti H. Twenty years on: the impact of fragments on drug discovery. Nat Rev Drug Discov. 2016;15(9):605-19. Epub 2016/07/16. doi: 10.1038/nrd.2016.109. PubMed PMID: 27417849.
125. Bakali HM, Herman MD, Johnson KA, Kelly AA, Wieslander A, Hallberg BM, Nordlund P. Crystal structure of YegS, a homologue to the mammalian diacylglycerol kinases, reveals a novel regulatory metal binding site. J Biol Chem. 2007;282(27):19644-52. Epub 2007/03/14. doi: 10.1074/jbc.M604852200. PubMed PMID: 17351295.
126. Nordin BE, Liu Y, Aban A, Brown HE, Wu J, Hainley AK, Rosenblum JS, Nomanbhoy TK, Kozarich JW. ATP Acyl Phosphate Reactivity Reveals Native Conformations of Hsp90 Paralogs and Inhibitor Target Engagement. Biochemistry. 2015;54(19):3024-36. Epub 2015/04/24. doi: 10.1021/acs.biochem.5b00148. PubMed PMID: 25905789.
127. Okerberg ES, Brown HE, Minimo L, Alemayehu S, Rosenblum J, Patricelli M, Nomanbhoy T, Kozarich JW. Monitoring native p38alpha:MK2/3 complexes via trans delivery of an ATP acyl phosphate probe. J Am Chem Soc. 2014;136(12):4664-9. Epub 2014/03/08. doi: 10.1021/ja4129907. PubMed PMID: 24601623.
128. Hall DR, Kozakov D, Whitty A, Vajda S. Lessons from Hot Spot Analysis for Fragment-Based Drug Discovery. Trends Pharmacol Sci. 2015;36(11):724-36. Epub 2015/11/06. doi: 10.1016/j.tips.2015.08.003. PubMed PMID: 26538314; PMCID: PMC4640985.

129. Merida I, Andrada E, Gharbi SI, Avila-Flores A. Redundant and specialized roles for diacylglycerol kinases alpha and zeta in the control of T cell functions. Sci Signal. 2015;8(374):re6. doi: 10.1126/scisignal.aaa0974. PubMed PMID: 25921290.
130. June CH, Riddell SR, Schumacher TN. Adoptive cellular therapy: a race to the finish line. Sci Transl Med. 2015;7(280):280ps7. Epub 2015/03/27. doi: 10.1126/scitranslmed.aaa3643. PubMed PMID: 25810311.
131. Riese MJ, Wang LC, Moon EK, Joshi RP, Ranganathan A, June CH, Koretzky GA, Albelda SM. Enhanced effector responses in activated CD8+ T cells deficient in diacylglycerol kinases. Cancer Res. 2013;73(12):3566-77. Epub 2013/04/12. doi: 10.1158/0008-5472.CAN-12-3874. PubMed PMID: 23576561; PMCID: PMC3686869.
132. Manning G, Whyte DB, Martinez R, Hunter T, Sudarsanam S. The protein kinase complement of the human genome. Science. 2002;298(5600):1912-34. Epub 2002/12/10. doi: 10.1126/science.1075762. PubMed PMID: 12471243.
133. Hsu KL, Tsuboi K, Whitby LR, Speers AE, Pugh H, Inloes J, Cravatt BF. Development and optimization of piperidyl-1,2,3-triazole ureas as selective chemical probes of endocannabinoid biosynthesis. J Med Chem. 2013;56(21):8257-69. Epub 2013/10/25. doi: 10.1021/jm400898x. PubMed PMID: 24152245; PMCID: PMC3984011.
134. Franks CE, Campbell ST, Purow BW, Harris TE, Hsu KL. The Ligand Binding Landscape of Diacylglycerol Kinases. Cell Chem Biol. 2017;24(7):870-80 e5. Epub 2017/07/18. doi: 10.1016/j.chembiol.2017.06.007. PubMed PMID: 28712745; PMCID: PMC5551460.
135. Holderfield M, Deuker MM, McCormick F, McMahon M. Targeting RAF kinases for cancer therapy: BRAF-mutated melanoma and beyond. Nat Rev Cancer. 2014;14(7):455-67. Epub 2014/06/25. doi: 10.1038/nrc3760. PubMed PMID: 24957944; PMCID: PMC4250230.
136. Marx A, Nugoor C, Panneerselvam S, Mandelkow E. Structure and function of polarity-inducing kinase family MARK/Par-1 within the branch of AMPK/Snf1-related kinases. FASEB J. 2010;24(6):1637-48. Epub 2010/01/15. doi: 10.1096/fj.09-148064. PubMed PMID: 20071654.
137. Johnson DS, Weerapana E, Cravatt BF. Strategies for discovering and derisking covalent, irreversible enzyme inhibitors. Future Med Chem. 2010;2(6):949-64. Epub 2010/07/20. PubMed PMID: 20640225; PMCID: PMC2904065.
138. Peng Y, McCorvy JD, Harpsoe K, Lansu K, Yuan S, Popov P, Qu L, Pu M, Che T, Nikolajsen LF, Huang XP, Wu Y, Shen L, Bjorn-Yoshimoto WE, Ding K, Wacker D, Han GW, Cheng J, Katritch V, Jensen AA, Hanson MA, Zhao S, Gloriam DE, Roth BL, Stevens RC, Liu ZJ. 5-HT2C Receptor Structures Reveal the Structural Basis of GPCR Polypharmacology. Cell. 2018;172(4):719-30 e14. Epub 2018/02/06. doi: 10.1016/j.cell.2018.01.001. PubMed PMID: 29398112; PMCID: PMC6309861.

139. McCloud RL, Franks CE, Campbell ST, Purow BW, Harris TE, Hsu KL. Deconstructing Lipid Kinase Inhibitors by Chemical Proteomics. Biochemistry. 2018;57(2):231-6. Epub 2017/11/21. doi: 10.1021/acs.biochem.7b00962. PubMed PMID: 29155586; PMCID: PMC5771882.
140. Olmez I, Love S, Xiao A, Manigat L, Randolph P, McKenna BD, Neal BP, Boroda S, Li M, Brenneman B, Abounader R, Floyd D, Lee J, Nakano I, Godlewski J, Bronisz A, Sulman EP, Mayo M, Gioeli D, Weber M, Harris TE, Purow B. Targeting the mesenchymal subtype in glioblastoma and other cancers via inhibition of diacylglycerol kinase alpha. Neuro Oncol. 2018;20(2):192-202. Epub 2017/10/20. doi: 10.1093/neuonc/nox119. PubMed PMID: 29048560; PMCID: PMC5777487.
141. Knight ZA, Lin H, Shokat KM. Targeting the cancer kinome through polypharmacology. Nat Rev Cancer. 2010;10(2):130-7. Epub 2010/01/23. doi: 10.1038/nrc2787. PubMed PMID: 20094047; PMCID: PMC2880454.
142. Edgar RC. MUSCLE: a multiple sequence alignment method with reduced time and space complexity. BMC Bioinformatics. 2004;5:113. Epub 2004/08/21. doi: 10.1186/1471-2105-5-113. PubMed PMID: 15318951; PMCID: PMC517706.
143. Rice P, Longden I, Bleasby A. EMBOSS: the European Molecular Biology Open Software Suite. Trends Genet. 2000;16(6):276-7. Epub 2000/05/29. PubMed PMID: 10827456.
144. Kepp O, Galluzzi L, Lipinski M, Yuan J, Kroemer G. Cell death assays for drug discovery. Nat Rev Drug Discov. 2011;10(3):221-37. Epub 2011/03/02. doi: 10.1038/nrd3373. PubMed PMID: 21358741.
145. Bartling B, Yang JY, Michod D, Widmann C, Lewensohn R, Zhivotovsky B. RasGTPase-activating protein is a target of caspases in spontaneous apoptosis of lung carcinoma cells and in response to etoposide. Carcinogenesis. 2004;25(6):909-21. Epub 2004/01/27. doi: 10.1093/carcin/bgh075. PubMed PMID: 14742324.
146. Wang Y, Yang H, Liu H, Huang J, Song X. Effect of staurosporine on the mobility and invasiveness of lung adenocarcinoma A549 cells: an in vitro study. BMC Cancer. 2009;9:174. Epub 2009/06/09. doi: 10.1186/1471-2407-9-174. PubMed PMID: 19500428; PMCID: PMC2702389.
147. Shin M, Franks CE, Hsu KL. Isoform-selective activity-based profiling of ERK signaling. Chem Sci. 2018;9(9):2419-31. Epub 2018/05/08. doi: 10.1039/c8sc00043c. PubMed PMID: 29732117; PMCID: PMC5909473.
148. Agarwal A, Das K, Lerner N, Sathe S, Cicek M, Casey G, Sizemore N. The AKT/I kappa B kinase pathway promotes angiogenic/metastatic gene expression in colorectal cancer by activating nuclear factor-kappa B and beta-catenin. Oncogene. 2005;24(6):1021-31. Epub 2004/12/14. doi: 10.1038/sj.onc.1208296. PubMed PMID: 15592509.
149. Castellano E, Sheridan C, Thin MZ, Nye E, Spencer-Dene B, Diefenbacher ME, Moore C, Kumar MS, Murillo MM, Gronroos E, Lassailly F, Stamp G, Downward J. Requirement for interaction of PI3-kinase p110alpha with RAS

in lung tumor maintenance. Cancer Cell. 2013;24(5):617-30. Epub 2013/11/16. doi: 10.1016/j.ccr.2013.09.012. PubMed PMID: 24229709; PMCID: PMC3826036.

150. Sanclemente M, Francoz S, Esteban-Burgos L, Bousquet-Mur E, Djurec M, Lopez-Casas PP, Hidalgo M, Guerra C, Drosten M, Musteanu M, Barbacid M. c-RAF Ablation Induces Regression of Advanced Kras/Trp53 Mutant Lung Adenocarcinomas by a Mechanism Independent of MAPK Signaling. Cancer Cell. 2018;33(2):217-28 e4. Epub 2018/02/06. doi: 10.1016/j.ccell.2017.12.014. PubMed PMID: 29395869.
151. Blackford AN, Jackson SP. ATM, ATR, and DNA-PK: The Trinity at the Heart of the DNA Damage Response. Mol Cell. 2017;66(6):801-17. Epub 2017/06/18. doi: 10.1016/j.molcel.2017.05.015. PubMed PMID: 28622525.
152. Graziano SL, Pfeifer AM, Testa JR, Mark GE, Johnson BE, Hallinan EJ, Pettengill OS, Sorenson GD, Tatum AH, Brauch H, et al. Involvement of the RAF1 locus, at band 3p25, in the 3p deletion of small-cell lung cancer. Genes Chromosomes Cancer. 1991;3(4):283-93. Epub 1991/07/01. PubMed PMID: 1683566.
153. Morrow AA, Alipour MA, Bridges D, Yao Z, Saltiel AR, Lee JM. The lipid kinase PI4KIIIbeta is highly expressed in breast tumors and activates Akt in cooperation with Rab11a. Mol Cancer Res. 2014;12(10):1492-508. Epub 2014/06/26. doi: 10.1158/1541-7786.MCR-13-0604. PubMed PMID: 24962317.
154. Cheng Y, Ren X, Yuan Y, Shan Y, Li L, Chen X, Zhang L, Takahashi Y, Yang JW, Han B, Liao J, Li Y, Harvey H, Ryazanov A, Robertson GP, Wan G, Liu D, Chen AF, Tao Y, Yang JM. eEF-2 kinase is a critical regulator of Warburg effect through controlling PP2A-A synthesis. Oncogene. 2016;35(49):6293-308. Epub 2016/05/18. doi: 10.1038/onc.2016.166. PubMed PMID: 27181208.
155. Ye J, Kumanova M, Hart LS, Sloane K, Zhang H, De Panis DN, Bobrovnikova-Marjon E, Diehl JA, Ron D, Koumenis C. The GCN2-ATF4 pathway is critical for tumour cell survival and proliferation in response to nutrient deprivation. EMBO J. 2010;29(12):2082-96. Epub 2010/05/18. doi: 10.1038/emboj.2010.81. PubMed PMID: 20473272; PMCID: PMC2892366.
156. Kim JA, Anurag M, Veeraraghavan J, Schiff R, Li K, Wang XS. Amplification of TLK2 Induces Genomic Instability via Impairing the G2-M Checkpoint. Mol Cancer Res. 2016;14(10):920-7. Epub 2016/08/05. doi: 10.1158/1541-7786.MCR-16-0161. PubMed PMID: 27489360; PMCID: PMC5065758.
157. Lewis TS, Shapiro PS, Ahn NG. Signal transduction through MAP kinase cascades. Adv Cancer Res. 1998;74:49-139. Epub 1998/04/30. PubMed PMID: 9561267.
158. Pearson G, Robinson F, Beers Gibson T, Xu BE, Karandikar M, Berman K, Cobb MH. Mitogen-activated protein (MAP) kinase pathways: regulation and physiological functions. Endocr Rev. 2001;22(2):153-83. Epub 2001/04/11. doi: 10.1210/edrv.22.2.0428. PubMed PMID: 11294822.

159. Seger R, Krebs EG. The MAPK signaling cascade. FASEB J. 1995;9(9):726-35. Epub 1995/06/01. PubMed PMID: 7601337.
160. Simanshu DK, Nissley DV, McCormick F. RAS Proteins and Their Regulators in Human Disease. Cell. 2017;170(1):17-33. Epub 2017/07/01. doi: 10.1016/j.cell.2017.06.009. PubMed PMID: 28666118; PMCID: PMC5555610.
161. Dhillon AS, Hagan S, Rath O, Kolch W. MAP kinase signalling pathways in cancer. Oncogene. 2007;26(22):3279-90. Epub 2007/05/15. doi: 10.1038/sj.onc.1210421. PubMed PMID: 17496922.
162. Griner EM, Kazanietz MG. Protein kinase C and other diacylglycerol effectors in cancer. Nat Rev Cancer. 2007;7(4):281-94. Epub 2007/03/27. doi: 10.1038/nrc2110. PubMed PMID: 17384583.
163. Wu P, Nielsen TE, Clausen MH. FDA-approved small-molecule kinase inhibitors. Trends Pharmacol Sci. 2015;36(7):422-39. Epub 2015/05/16. doi: 10.1016/j.tips.2015.04.005. PubMed PMID: 25975227.
164. Hatzivassiliou G, Song K, Yen I, Brandhuber BJ, Anderson DJ, Alvarado R, Ludlam MJ, Stokoe D, Gloor SL, Vigers G, Morales T, Aliagas I, Liu B, Sideris S, Hoeflich KP, Jaiswal BS, Seshagiri S, Koeppen H, Belvin M, Friedman LS, Malek S. RAF inhibitors prime wild-type RAF to activate the MAPK pathway and enhance growth. Nature. 2010;464(7287):431-5. Epub 2010/02/05. doi: 10.1038/nature08833. PubMed PMID: 20130576.
165. Heidorn SJ, Milagre C, Whittaker S, Nourry A, Niculescu-Duvas I, Dhomen N, Hussain J, Reis-Filho JS, Springer CJ, Pritchard C, Marais R. Kinase-dead BRAF and oncogenic RAS cooperate to drive tumor progression through CRAF. Cell. 2010;140(2):209-21. Epub 2010/02/10. doi: 10.1016/j.cell.2009.12.040. PubMed PMID: 20141835; PMCID: PMC2872605.
166. Poulikakos PI, Zhang C, Bollag G, Shokat KM, Rosen N. RAF inhibitors transactivate RAF dimers and ERK signalling in cells with wild-type BRAF. Nature. 2010;464(7287):427-30. Epub 2010/02/25. doi: 10.1038/nature08902. PubMed PMID: 20179705; PMCID: PMC3178447.
167. Borst J, Ahrends T, Babala N, Melief CJM, Kastenmuller W. CD4(+) T cell help in cancer immunology and immunotherapy. Nat Rev Immunol. 2018;18(10):635-47. Epub 2018/07/31. doi: 10.1038/s41577-018-0044-0. PubMed PMID: 30057419.
168. Xing Y, Hogquist KA. T-cell tolerance: central and peripheral. Cold Spring Harb Perspect Biol. 2012;4(6). Epub 2012/06/05. doi: 10.1101/cshperspect.a006957. PubMed PMID: 22661634; PMCID: PMC3367546.
169. Matsuzaki J, Tsuji T, Luescher IF, Shiku H, Mineno J, Okamoto S, Old LJ, Shrikant P, Gnjatic S, Odunsi K. Direct tumor recognition by a human CD4(+) T-cell subset potently mediates tumor growth inhibition and orchestrates anti-tumor immune responses. Sci Rep. 2015;5:14896. Epub 2015/10/09. doi: 10.1038/srep14896. PubMed PMID: 26447332; PMCID: PMC4597193.
170. Tran E, Turcotte S, Gros A, Robbins PF, Lu YC, Dudley ME, Wunderlich JR, Somerville RP, Hogan K, Hinrichs CS, Parkhurst MR, Yang JC, Rosenberg SA.

Cancer immunotherapy based on mutation-specific CD4+ T cells in a patient with epithelial cancer. Science. 2014;344(6184):641-5. Epub 2014/05/09. doi: 10.1126/science.1251102. PubMed PMID: 24812403.

171. Abe BT, Macian F. Uncovering the mechanisms that regulate tumor-induced T-cell anergy. Oncoimmunology. 2013;2(2):e22679. Epub 2013/03/26. doi: 10.4161/onci.22679. PubMed PMID: 23524444; PMCID: PMC3601153.
172. Kerr WG, Chisholm JD. The Next Generation of Immunotherapy for Cancer: Small Molecules Could Make Big Waves. J Immunol. 2019;202(1):11-9. Epub 2018/12/28. doi: 10.4049/jimmunol.1800991. PubMed PMID: 30587569; PMCID: PMC6330242.
173. Oh YM, Park HB, Shin JH, Lee JE, Park HY, Kho DH, Lee JS, Choi H, Okuda T, Kokame K, Miyata T, Kim IH, Lee SH, Schwartz RH, Choi K. Ndrg1 is a T-cell clonal anergy factor negatively regulated by CD28 costimulation and interleukin-2. Nat Commun. 2015;6:8698. Epub 2015/10/29. doi: 10.1038/ncomms9698. PubMed PMID: 26507712; PMCID: PMC4846325.
174. Appleman LJ, Tzachanis D, Grader-Beck T, van Puijenbroek AA, Boussiotis VA. Helper T cell anergy: from biochemistry to cancer pathophysiology and therapeutics. J Mol Med (Berl). 2001;78(12):673-83. Epub 2001/07/04. PubMed PMID: 11434720.
175. Sekar RB, Periasamy A. Fluorescence resonance energy transfer (FRET) microscopy imaging of live cell protein localizations. J Cell Biol. 2003;160(5):629-33. Epub 2003/03/05. doi: 10.1083/jcb.200210140. PubMed PMID: 12615908; PMCID: PMC2173363.
176. Rappsilber J. The beginning of a beautiful friendship: cross-linking/mass spectrometry and modelling of proteins and multi-protein complexes. J Struct Biol. 2011;173(3):530-40. Epub 2010/10/30. doi: 10.1016/j.jsb.2010.10.014. PubMed PMID: 21029779; PMCID: PMC3043253.